Lehrstuhl für Bauinformatik
Fakultät für Bauingenieur- und Vermessungswesen
Technische Universität München

An anisotropic p-adaptive method for linear elastostatic and elastodynamic analysis of thin-walled and massive structures

Dominik Nikolaus Scholz

Vollständiger Abdruck der von der Fakultät für Bauingenieur- und Vermessungswesen der Technischen Universität München zur Erlangung des akademischen Grades eines

Doktor-Ingenieurs

genehmigten Dissertation.

Vorsitzender: Univ.-Prof. Dr.-Ing., Dr.-Ing. habil. G. H. Müller

Prüfer der Dissertation:

1. Univ.-Prof. Dr.rer.nat. E. Rank
2. Associate Prof. Z. Yosibash, D. Sc.
   Ben-Gurion University of The Negev / Israel

Die Dissertation wurde am 17.11.2005 bei der Technischen Universität München eingereicht und durch die Fakultät für Bauingenieur- und Vermessungswesen am 27.01.2006 angenommen.

Zusammenfassung

Basierend auf einer Hexaederelement-Formulierung, die eine anisotrope Wahl der Polynomgrade für die lokalen Richtungen sowie die Komponenten des kartesischen Verschiebungsvektors erlaubt, wird in dieser Arbeit eine p-adaptive Methode für linear elastostatische sowie linear elastodynamische Probleme vorgeschlagen. Die p-adaptive Methode für statische Probleme wird durch einen anisotropen, hierarchischen Fehlerindikator gesteuert, der auf einer lokalen Projektion der Lösung aus einem gegebenen Ansatzraum in einen reduzierten, hierarchisch eingebetteten Raum beruht, wobei die Differenz in der Dehnungsenergie minimiert wird. Die p-adaptive Methode für dynamische Problemstellungen basiert auf der Anpassung der Polynomgrade mit dem Ziel, die dominanten Eigenfrequenzen genau darzustellen, die aus einer transienten Vorabrechnung mit grober Diskretisierung erhalten werden. Der hierfür entwickelte p-adaptive Eigenwertlöser wird durch einen analog konstruierten, lokal berechneten, anisotropen, hierarchischen Fehlerindikator kontrolliert, um somit den Rayleigh Quotienten zu minimieren. Für alle in dieser Arbeit untersuchten Beispiele zeigen die p-adaptiven Diskretisierungen im Vergleich zu uniformer p-Verfeinerung eine deutlich höhere Effizienz sowie höhere asymptotische Konvergenzraten. Daher kann die Methode als Abhilfe von einer wesentlichen Schwäche uniformer h- und p-Versionen gesehen werden, nämlich den oftmals geringen Konvergenzraten im asymptotischen Bereich, im Besonderen bei irregulären Lösungen. Somit können äußerst effiziente, strikt drei-dimensionale Diskretisierungen für Strukturen gefunden werden, die sowohl aus dünnwandigen als auch massiven Teilen bestehen.

Abstract

An anisotropic p-adaptive method for linear elastostatic and linear elastodynamic problems is proposed, based on a high-order hexahedral element formulation allowing for an independent adjustment of the polynomial degrees for different local directions and different components of the cartesian displacement vectors. The p-adaptive method for static problems is driven by an anisotropic hierarchic error indicator based on the idea of locally projecting the solution from a given Ansatz space to a reduced, hierarchically nested space, minimizing the difference in strain energy. The p-adaptive method for dynamic problems is based on adjusting the polynomial degrees to achieve an optimal representation of the dominant eigenfrequencies, obtained from an initial transient computation with a coarse discretization. The p-adaptive eigensolver required for this purpose is driven by an analogously constructed, locally computed, anisotropic hierarchic error indicator, thus minimizing the Rayleigh quotient. For all numerical examples investigated herein, the p-adaptive discretizations show a considerably higher efficiency and higher rates of convergence compared to uniform p-refinement. This method can accordingly be understood as a remedy for one basic problem of uniform h- and p-versions, i.e. the possibly poor asymptotic behavior, especially in presence of any irregularities in the solution. As a result, it is possible to obtain an efficient, fully three-dimensional discretization of both thin-walled and compact parts of structures.

Vorwort

Die vorliegende Arbeit entstand während meiner Tätigkeit als wissenschaftlicher Mitarbeiter am Lehrstuhl für Bauinformatik der Fakultät Bauingenieur- und Vermessungswesen der Technischen Universität München (2000 – 2005). Die Ideen zur Arbeit wurden in dem Projekt *Fluid-Struktur-Wechselwirkungen im Bauwesen — Numerische Simulation mit Höchstleistungsrechnern* (FLUSIB) des *Kompetenznetzwerkes für wissenschaftliches Hoch- und Höchstleistungsrechnen in Bayern* (KONWIHR) und dem Projekt *Elemente hoher Ordnung zur Struktursimulation in der Fluid-Struktur-Wechselwirkung* der DFG-Forschergruppe 493 (*Fluid-Struktur-Wechselwirkung: Modellierung, Simulation, Optimierung*) entwickelt und umgesetzt.

An erster Stelle möchte ich mich bei meinem Doktorvater Prof. Ernst Rank bedanken, bei dem ich beobachten und lernen durfte, wie er Probleme ganzheitlich und umfassend betrachtet und diese dabei trotzdem auf das Wesentliche reduziert, und ich bewunderte stets seinen Ideenreichtum bei der Problemlösung. Begeistert war ich von seiner großen Begeisterungsfähigkeit. Trotz seines vollen Terminkalenders schaffte er immer Freiräume zur ausführlichen und konstruktiven Diskussion, wenn Ziele wieder einmal unerreichbar schienen.

Bei Prof. Zohar Yosibash möchte ich mich bedanken für die Übernahme des Zweitgutachtens. Die Gespräche mit ihm und seine kritischen und detaillierten Anmerkungen haben einen signifikanten Gewinn für diese Arbeit bedeutet.

Prof. Gerhard Müller hat auf unkomplizierte Art den Vorsitz der Prüfung übernommen und während dieser eine angenehme Atmosphäre geschaffen.

Mein besonderer Dank gilt Alexander Düster für die ausgezeichnete wissenschaftliche und überaus geduldige Betreuung. Er hat diese Arbeit wesentlich mit definiert.

Bei Roland Krause möchte ich mich bedanken, der mich während meines Auslandaufenthalts zur Diplomarbeit in St. Louis, Missouri, USA für das Gebiet der mechanischen Simulation begeistern konnte und mich dort wie ein Familienmitglied aufgenommen hat.

Bei allen Kolleginnen und Kollegen — Hanne Cornils eingeschlossen — möchte ich mich bedanken für das ausgesprochen freundschaftliche Lehrstuhlklima und die zahlreichen Diskussionen. Zu groß war bei manchen der Beitrag zum Gelingen dieser Arbeit, dass sie nicht zu erwähnen sträflich wäre: Besonderer Dank geht daher (in alphabetischer Reihenfolge) an Ansgar Halfmann, Ulrich Heißerer, Stefan Kollmannsberger, Alexander Muthler, Andreas Niggl, Andreas Rabold, Matthias Schleinkofer, Christian Sorger und Christoph van Treeck.

Meine Eltern Gabriele und Uwe und meine Geschwister Annette und Johannes haben mir immer gezeigt, wo ich gut aufgehoben bin.

Bei Vera möchte ich mich für die vielen wertvollen Ratschläge und auch für ihre Zuwendung bedanken, beides machte die Mühen des Zusammenschreibens erträglich.

Contents

Chapter 1

Introduction

Although this thesis deals with efficient spatial discretization of pure elastostatic and elastodynamic problems, the motivation for this work arose from two projects concerned with *fluid-structure interaction* (FSI): the FLUSIB project within the *Competence Network for Technical, Scientific High Performance Computing* (KONWIHR) and a project within the research unit *Fluid-Structure Interaction — Modeling, Simulation, Optimization* funded by the *German Research Foundation* (DFG). Our approach in both projects is based on the application of high order solid elements to describe the behavior of structures interacting with fluids — e.g. thin-walled, wind-loaded plates and shells. High order solid elements can provide a fully three-dimensional solution that also includes arbitrary three-dimensional stress states while nevertheless being able to cope with high aspect ratios of thin-walled structures and being less prone to locking effects. Thus, a single type of element is sufficient for both thin-walled and thick-walled structures, without any need for transition elements between thin-walled and massive parts of the structure, see, for example, Figures 5.13 and 5.15 on pages 103 and 105, respectively, showing a thin hemispherical shell connected to a compact stiffener ring. A detailed discussion of the advantages of high order solid elements for thin-walled nonlinear continua can be found in DÜSTER [47].

For fluid-structure interaction problems, there is another obvious advantage of three-dimensional models, i.e. the inherently correct representation of the *wet surface* being in contact with the fluid without the necessity of reconstructing this skin surface from the middle surface and certain kinematic assumptions, which is the usual approach for dimensionally reduced plate and shell models.

An example by way of illustration is the plate with a re-entrant corner depicted in Figure 1.1 (left), being discretized using 16 high-order hexahedral elements, see Figure 1.1 (right). The interaction of the plate with a fluid flow in x-direction perpendicular to the plate ($\mathrm{Re} = 50$) was computed by coupling with a finite volume based CFD (*Computational Fluid Dynamics*) code provided by a project partner, see SCHOLZ et al. [123, 124], for instance. The transient response of the plate is plotted in Figure 1.2, showing the displacement of Point A, see Figure 1.1 (left), in x-direction. The amplitudes of the plate's vibration decrease over time due to the damping influence of the surrounding fluid. Taking geometric nonlinearities into account for large displacements, the structure was computed with *anisotropic* high order hexahedral elements, i.e. the polynomial degrees of the hexahedrals can be chosen independently for the

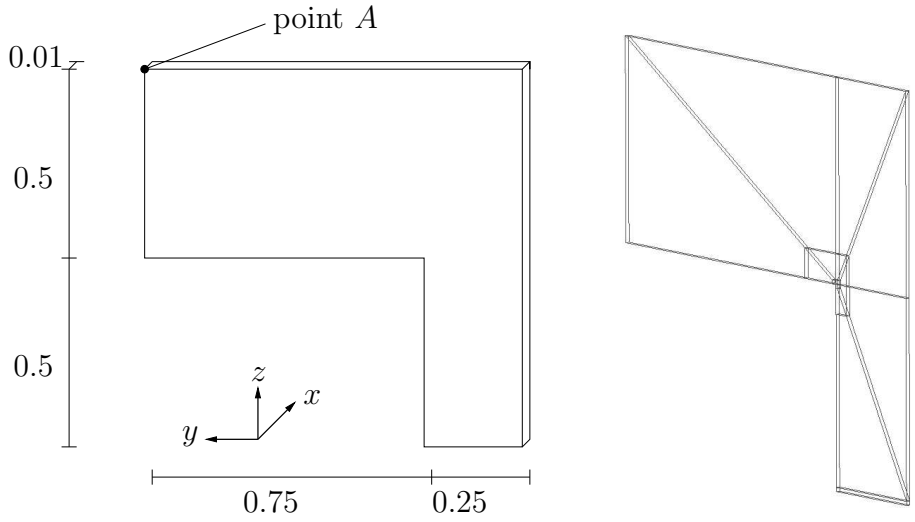

Figure 1.1: System of plate with re-entrant corner (left), hexahedral mesh (right)

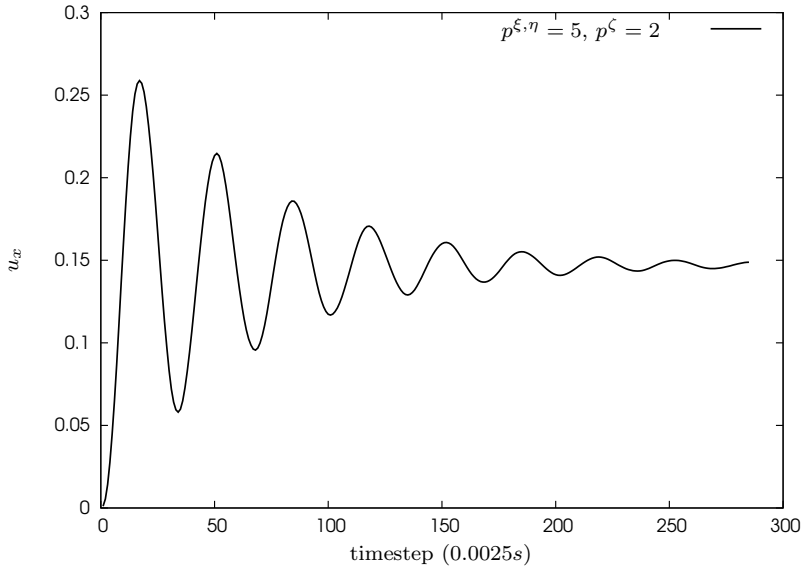

Figure 1.2: Displacement u_x of point A over time (FSI)

three local directions of the elements. In this fluid-structure interaction example, the *in-plane* polynomial degrees were chosen to be $p^{\xi,\eta} = 5$, whereas the *transversal* polynomial degree corresponding to the thickness direction has been set to $p^{\zeta} = 2$ for *all* elements.

However, this choice was not in the least arbitrary. The following sequences of computations for a simplified problem were performed in order to determine a reasonable choice for $p^{\xi,\eta}$ and p^{ζ}. Instead of computing the fluid-structure interaction problem, the fluid load was substituted by a similar uniform surface traction that remained constant in time.

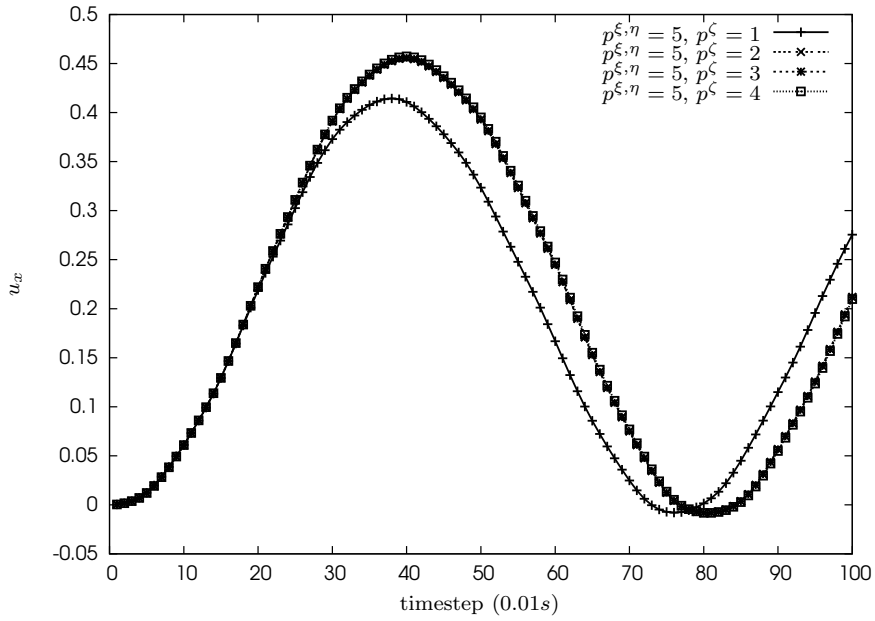

Figure 1.3: Displacement u_x of point A over time for varying p^{ζ}

In a first sequence of runs, the in-plane polynomial degrees were fixed at $p^{\xi,\eta} = 5$ and the transversal polynomial degree was varied, $p^{\zeta} = 1, ..., 4$. The corresponding displacements in x-direction of point A for approximately one period of vibration is plotted in Figure 1.3. It is evident from these results that $p^{\zeta} = 1$ leads to considerable deviations from the reference solution. However, with $p^{\zeta} = 2$, the reference deflection is already represented satisfyingly. In a second sequence of runs, the transversal polynomial degree was fixed, $p^{\zeta} = 2$ and the in-plane polynomial degree was varied, $p^{\xi,\eta} = 3, ..., 7$, see Figure 1.4. Here, $p^{\xi,\eta} = 5$ is required to approximate the reference solution sufficiently. Judging from these results, the choice of $p^{\xi,\eta} = 5$ and $p^{\zeta} = 2$ is reasonable for this system.

Although this approach yields accurate results for the investigated example, it has many disadvantages. Two sequences of computations are necessary merely to adjust two global discretization parameters, $p^{\xi,\eta}$ and p^{ζ} for *all* elements. The approach only makes sense for strictly thin-walled structures, where orientations like "in-plane directions" and "transversal direction" are reasonable. On the other hand, no use is made of local, element-wise selection of polynomial degrees. In this thesis, a local anisotropic p-adaptive method is proposed for linear elastostatic and elastodynamic problems, in order to overcome the above mentioned

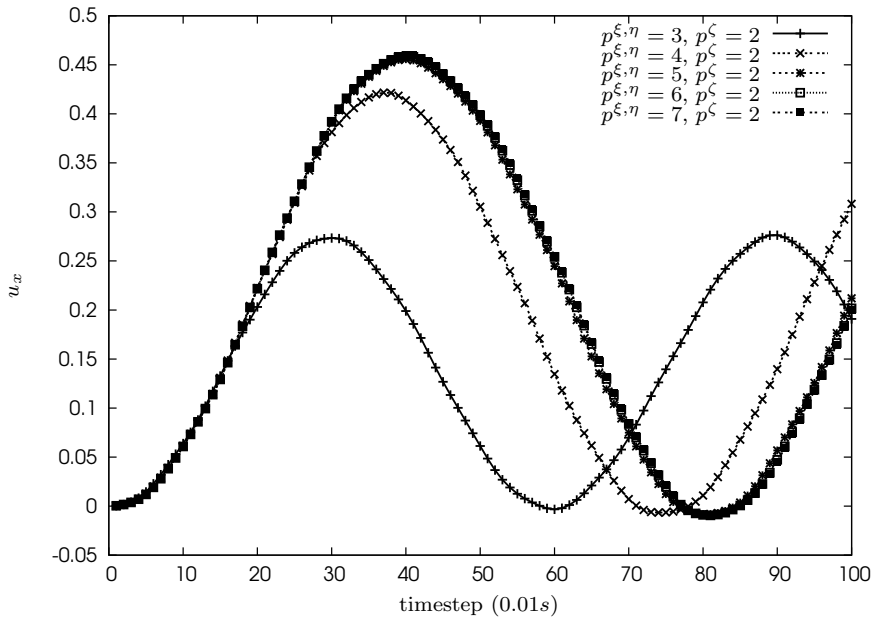

Figure 1.4: Displacement u_x of point A over time for varying $p^{\xi,\eta}$

deficiencies.

The outline of this thesis is as follows: **Chapter 2** describes the basic continuum mechanics setting including simplifications of the nonlinear equations of motion: linearization, linear elastostatic problems, harmonic vibrations, dimensional reduction of thin-walled structures using plate or shell models.

Chapter 3 introduces the discretization tools used in this thesis. For spatial discretization, high-order anisotropic hexahedral elements are described, and for time discretization the generalized α-method is recalled. The chapter concludes with a numerical example, the elastodynamic computation of a thin-walled clamped plate. The results for geometric linear and geometric nonlinear computations using hexahedral elements are compared to solutions from literature based on a two-dimensional spectral element approach in order to verify the code.

Chapter 4 provides — without claiming to be complete — an overview of existing adaptive approaches for static and dynamic structural problems.

In **Chapter 5** a local anisotropic p-adaptive method based on a hierarchic anisotropic error estimator is proposed for linear elastostatic problems. Several numerical examples are included to prove the efficiency of the approach.

The method is extended to linear elastodynamics in **Chapter 6**, involving a p-adaptive eigensolver. Again, various numerical examples are used to confirm the efficiency of the method.

Chapter 7 contains conclusions and gives an outlook for future work.

Chapter 2

Basic continuum mechanics

This chapter constitutes a short summary of the physical and mathematical models of continuum mechanics required for the subsequent finite element formulations described in Chapter 3. Here, a continuum is assumed to be a set of material particles continuously filling space, or part of a space, at every instance in time t. Every particle is characterized by physical properties, such as speed, density, etc. The following description is based on the works of Bonet and Wood [33], Wriggers [148], Altenbach [6], Szabó and Babuška [136] and Bathe [26].

2.1 Kinematics

The description of the motion and deformation of a body is referred to as its *kinematics*. An observer can use different perspectives to describe the motion of a body, resulting in different formulations.

- Using an Eulerean formulation, the observer is connected to a spatially fixed location. Changes in the configuration of the continuum are perceived as changes of physical properties at this fixed location, i.e. different particles are observed at different time instances t, when the continuum is in motion. The changed physical properties of one specific particle are not described directly using an Eulerean formulation.

- In a Lagrangean formulation, the observer is connected to a specific particle. It is possible to perceive the transient variation of physical properties of this particle directly.

Fluid mechanics problems are usually described by means of an Eulerean formulation, whereas structural mechanics problems are mainly described with a Lagrangean formulation, which is also employed in this thesis.

A particle in a body can be uniquely identified by its position vector $\mathbf{X} \in \Omega_0$, where Ω_0 denotes the *reference* — also called *material* or *initial* — configuration of the body. Thus, in the following no distinction is made between the particle and its position. In this thesis the position $\mathbf{X}$ in three-dimensional Euclidean space $\mathbb{R}^3$ is defined with respect to a orthonormal basis with origin O. The boundary of the reference configuration is denoted by $\partial\Omega_0$. The

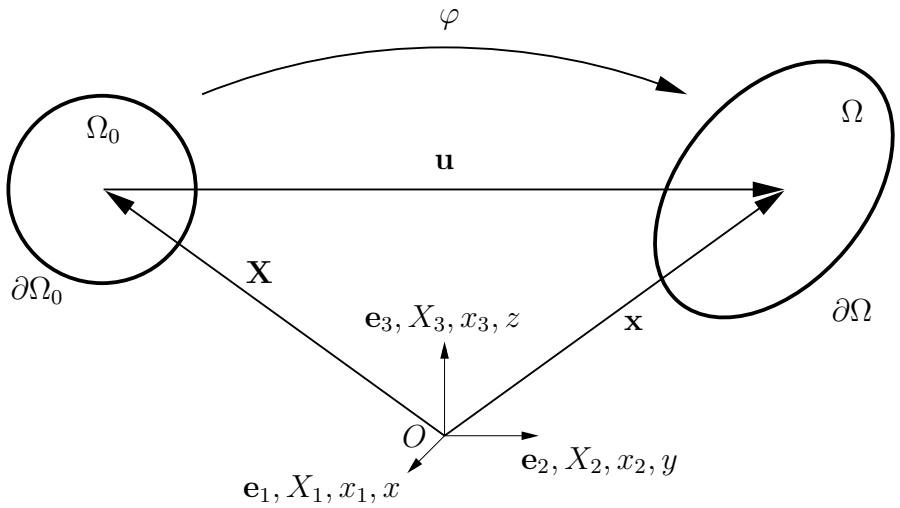

Figure 2.1: Motion of a particle

current — or *spatial* — position of a particle is denoted by $\mathbf{x} \in \Omega$ where Ω is the current — or spatial — configuration with the boundary $\partial\Omega$. The motion can be described by the mapping

$$\mathbf{x}(t) \;=\; \varphi(\mathbf{X}, t), \tag{2.1}$$

see Figure 2.1. For a fixed value of t, Equation (2.1) represents a mapping between the undeflected and the deflected body. On the other hand, for a fixed particle $\mathbf{X}$, it describes the motion in space of this particle as a function of time. The displacement of a particle can be written as

$$\mathbf{u} \;=\; \mathbf{x} - \mathbf{X}. \tag{2.2}$$

In order to describe the deformation locally, the deformation gradient $\mathbf{F}$ is introduced,

$$d\mathbf{x} \;=\; \mathbf{F}\, d\mathbf{X} \tag{2.3}$$

expressing the relative spatial position d$\mathbf{x}$ of two particles after deformation using their relative material position $d\mathbf{X}$ before deformation. $\mathbf{F}$ is the gradient of the mapping φ

$$\mathbf{F} \;=\; \frac{d\mathbf{x}}{d\mathbf{X}} = \operatorname{Grad}\mathbf{x} = \operatorname{Grad}\varphi = \operatorname{Grad}\mathbf{u} + \mathbf{I} \tag{2.4}$$

The transformation between reference and spatial area elements and reference and spatial volume elements can be derived using the deformation gradient

$$J = \det \mathbf{F}, \tag{2.5}$$
$$d\mathbf{a} = J\,\mathbf{F}^{-T}\,d\mathbf{A}, \tag{2.6}$$
$$dv = J\,dV, \tag{2.7}$$

with

$$d\mathbf{a} = \mathbf{n}\,da, \tag{2.8}$$
$$d\mathbf{A} = \mathbf{N}\,dA. \tag{2.9}$$

As mentioned above, the deformation gradient describes the local deformation including rigid body motion. Therefore, $\mathbf{F}$ is not well suited to serve as a strain measure, since a strain measure should vanish for pure translation and rotation. An obvious approach to neglect the rigid body motion is relating the *squares* of the line segments $d\mathbf{x}$ and $d\mathbf{X}$, respectively,

$$\begin{aligned} d\mathbf{x}^T\,d\mathbf{x} - d\mathbf{X}^T\,d\mathbf{X} &= (\mathbf{F}d\mathbf{X})^T\,\mathbf{F}d\mathbf{X} - d\mathbf{X}^T\,d\mathbf{X} \\ &= d\mathbf{X}^T\,(\mathbf{F}^T\mathbf{F})\,d\mathbf{X} - d\mathbf{X}^T\,\mathbf{I}\,d\mathbf{X} \\ &= d\mathbf{X}^T\,(\mathbf{F}^T\mathbf{F} - \mathbf{I})\,d\mathbf{X} \qquad =: \quad d\mathbf{X}^T\,(2\,\mathbf{E})\,d\mathbf{X}. \end{aligned} \tag{2.10}$$

The symmetric strain measure $\mathbf{E}$ is called the Green-Lagrangean strain tensor

$$\mathbf{E} = \frac{1}{2}\,(\,\mathbf{F}^T\mathbf{F} - \mathbf{I}\,), \tag{2.11}$$

where $\mathbf{I}$ is the unity tensor.

2.2 Stress and equilibrium

The basic equations of continuum mechanics are balance equations for mass, momentum and energy conservation. Appropriate measures for stress states are required to set up the momentum equations which describe global and local equilibrium.

The Cauchy stress tensor $\boldsymbol{\sigma}$ is introduced in order to set up the balance equations in the spatial configuration. Consider the surface of a general deformable body or a cut surface in its interior. The spatial traction vector

$$\hat{\mathbf{t}}(\mathbf{x}, t) = \frac{d\mathbf{f}}{da} \tag{2.12}$$

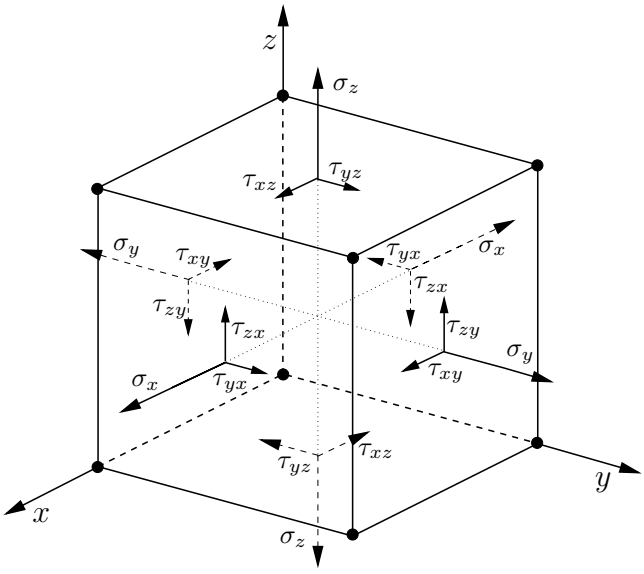

Figure 2.2: Definition of positive stress directions

is defined as the differential cutting force $d\mathbf{f}$ related to the size da of the spatial differential surface element $d\mathbf{a}$. The CAUCHY theorem gives the relation between the spatial traction vector $\hat{\mathbf{t}}$, the CAUCHY stress tensor and the normal unity vector $\mathbf{n} = \dfrac{d\mathbf{a}}{da}$

$$\hat{\mathbf{t}} = \boldsymbol{\sigma}\mathbf{n}. \tag{2.13}$$

Figure 2.2 depicts the sign convention for stresses. The *nominal* traction vector can be defined by relating the spatial differential force vector $d\mathbf{f}$ to a surface element $d\mathbf{A} = \mathbf{N}dA$ of the reference configuration

$$\mathbf{t} = \frac{d\mathbf{f}}{dA}, \tag{2.14}$$

and the corresponding stress tensor is the *first* PIOLA-KIRCHHOFF stress tensor $\mathbf{P}$.

$$\mathbf{t} = \mathbf{P}\mathbf{N}. \tag{2.15}$$

Furthermore, the *second* PIOLA-KIRCHHOFF stress tensor $\mathbf{S}$ can be introduced

$$\mathbf{S} \;=\; \mathbf{F}^{-1}\mathbf{P} = J\,\mathbf{F}^{-1}\boldsymbol{\sigma}\mathbf{F}^{-T}. \tag{2.16}$$

Once these stress measures have been established, it is possible to formulate the spatial and material balance equations of momentum. At a certain time t in the spatial configuration, the rate of change in total momentum during deformation equals the sum of all the surface and volume forces acting on the body

$$\frac{\partial}{\partial t}\int\limits_{\Omega}\rho\dot{\mathbf{u}}dv \;=\; \int\limits_{\partial\Omega}\hat{\mathbf{t}}d\mathbf{a}+\int\limits_{\Omega}\rho\mathbf{b}dv. \tag{2.17}$$

The differential relations of Equations (2.6) and (2.7) in conjunction with the nominal stress vector $\mathbf{t}$ allow the spatial momentum equation (2.17) to be transferred to the reference configuration

$$\frac{\partial}{\partial t}\int\limits_{\Omega_0}\rho_0\dot{\mathbf{u}}dV \;=\; \int\limits_{\partial\Omega_0}\mathbf{t}d\mathbf{A}+\int\limits_{\Omega_0}\rho_0\mathbf{b}dV. \tag{2.18}$$

Applying the Cauchy theorem (2.13), Equation (2.14) and the Gauss divergence theorem yields the first Cauchy equation of motion in spatial and reference configuration

$$\begin{aligned} \mathrm{div}\boldsymbol{\sigma}+\rho\mathbf{b} &= \rho\ddot{\mathbf{u}}, \quad \forall(\mathbf{x},t)\in\Omega\times(0,T], && (2.19)\\ \mathrm{Div}\mathbf{P}+\rho_0\mathbf{b} &= \rho_0\ddot{\mathbf{u}}, \quad \forall(\mathbf{X},t)\in\Omega_0\times(0,T], && (2.20) \end{aligned}$$

with:

ρ	density in spatial configuration
ρ_0	density in reference configuration
$\dot{\mathbf{u}}$	velocity
$\ddot{\mathbf{u}}$	acceleration
$\mathbf{b}$	mass related gravity force
$\hat{\mathbf{t}}$	traction vector acting on surface $\partial\Omega$
$\mathbf{t}$	nominal traction vector acting on surface $\partial\Omega_0$
div	divergence operator with respect to spatial configuration
Div	divergence operator with respect to reference configuration

The spatial momentum balance (2.20) can also be expressed using the second Piola-Kirchhoff stress tensor (2.16)

$$\mathrm{Div}\mathbf{F}\mathbf{S}+\rho_0\mathbf{b} \;=\; \rho_0\ddot{\mathbf{u}}, \quad \forall(\mathbf{X},t)\in\Omega_0\times(0,T]. \tag{2.21}$$

Important energy quantities used in this thesis are the strain energy in a system

$$E_{str}=\frac{1}{2}\int\limits_{\Omega_0}\mathbf{S}:\mathbf{E}\,dV \tag{2.22}$$

and the kinetic energy in the system

$$E_{kin}=\frac{1}{2}\int\limits_{\Omega_0}\rho_0\dot{\mathbf{u}}\cdot\dot{\mathbf{u}}\,dV. \tag{2.23}$$

The energy norm is then

$$\|\mathbf{u}\|_E = \sqrt{E_{str} + E_{kin}}. \tag{2.24}$$

2.3 Material models

The kinematic equations and balance equations discussed in Sections 2.1 and 2.2 are not sufficient to solve continuum mechanics problems. A knowledge of the behavior of the material is required as well. In the case of *elastic* materials, deformations occurring during a loading process are completely reversible, i.e. deformations vanish completely after unloading. *Plastic* material behavior results in irreversible deformations. Material models describe the relation between deformation (and deformation history, if relevant) and stresses. Throughout this thesis, linear elastic material behavior is assumed, as described by the St. Venant-Kirchhoff material model

$$\mathbf{S} = \mathbb{C}\mathbf{E}, \tag{2.25}$$

where $\mathbb{C}$ is the constant material tensor. Equation (2.25) is the generalization of Hooke's law for Green-Lagrange strain.

2.4 Boundary and initial conditions

To guarantee a unique solution, the momentum equations have to be supplied with appropriate boundary and initial conditions,

$$\begin{aligned} \mathbf{u} &= \bar{\mathbf{u}} \quad \text{on} \quad \partial_D\Omega \quad \times \quad (0,T], \\ \boldsymbol{\sigma}\mathbf{n} &= \hat{\mathbf{t}} \quad \text{on} \quad \partial_N\Omega \quad \times \quad (0,T], \\ \mathbf{u}(\mathbf{X}, t=0) &= \bar{\mathbf{u}}_0 \quad \text{in} \quad \Omega_0, \\ \dot{\mathbf{u}}(\mathbf{X}, t=0) &= \bar{\dot{\mathbf{u}}}_0 \quad \text{in} \quad \Omega_0, \end{aligned} \tag{2.26}$$

where the Dirichlet boundary $\partial_D\Omega$ and the Neumann boundary $\partial_N\Omega$ have to fulfill the relation $\partial_D\Omega \cup \partial_N\Omega = \partial\Omega$ and $\partial_D\Omega \cap \partial_N\Omega = 0$.

2.5 Variational formulation

A continuum mechanics problem can be described entirely in terms of kinematic relations (Section 2.1), balance equations (Section 2.2), material models (Section 2.3) and boundary and initial conditions (2.4). Unfortunately, a direct analytical solution of the problem is only possible in very few cases. However, approximate solutions can be determined using methods of variational calculus, e.g. by applying finite element methods. In the following, the variational form of the continuum mechanics problem is presented.

The momentum equation (2.21)

$$\mathrm{Div}\mathbf{FS} + \rho_0\mathbf{b} \;=\; \rho_0\ddot{\mathbf{u}}, \quad \forall(\mathbf{X},t) \in \Omega_0 \times (0,T] \tag{2.27}$$

is multiplied by an arbitrary test function $\mathbf{v} \in \mathcal{V}$ with $\mathbf{v} = 0$ on the Dirichlet boundary $\partial_D\Omega$ and integrated over the domain. Here, $\mathcal{V} \in [H^1(\Omega)]^{n_{dim}}$ is a SOBOLEV space, see [16], by way of illustration. Accordingly,

$$\int_{\Omega_0} \mathrm{Div}\mathbf{FS}\cdot\mathbf{v}\,dV + \int_{\Omega_0}\rho_0\mathbf{b}\cdot\mathbf{v}\,dV \;=\; \int_{\Omega_0}\rho_0\ddot{\mathbf{u}}\cdot\mathbf{v}\,dV, \quad \forall\mathbf{v}\in\mathcal{V},\ \mathbf{v}_{\partial_D\Omega}=0. \tag{2.28}$$

Partial integration of the first term and using $\mathbf{FS} : \mathrm{Grad}\,\mathbf{v} = \mathbf{S} : \mathbf{F}^T\mathrm{Grad}\,\mathbf{v}$ yields the *weak form* of equilibrium

$$\int_{\Omega_0}\mathbf{S} : \mathbf{F}^T\,\mathrm{Grad}\,\mathbf{v}\,dV + \int_{\Omega_0}\rho_0\ddot{\mathbf{u}}\,dV \;=\; \int_{\partial_N\Omega_0}\mathbf{t}\cdot\mathbf{v}\,d\mathbf{A} + \int_{\Omega_0}\rho_0\mathbf{b}\cdot\mathbf{v}\,dV, \quad \forall\mathbf{v}\in\mathcal{V},\ \mathbf{v}_{\partial_D\Omega}=0, \tag{2.29}$$

where *weak* means that less restrictions are imposed on the solution $\mathbf{u}$ and its derivatives. Since the second PIOLA-KIRCHHOFF stress tensor $\mathbf{S}$ in the first term of (2.29) is symmetric, only the symmetric part of $\mathbf{F}^T\,\mathrm{Grad}\,\mathbf{v}$ has to be taken into consideration in the contraction operation $\bullet : \bullet$, leading to the commonly used abbreviation

$$\begin{aligned}&\int_{\Omega_0}\mathbf{S} : \overbrace{\frac{1}{2}\left(\mathbf{F}^T\,\mathrm{Grad}\,\mathbf{v} + \mathrm{Grad}^T\,\mathbf{v}\,\mathbf{F}\right)}^{\delta\mathbf{E}}\,dV + \int_{\Omega_0}\rho_0\ddot{\mathbf{u}}\cdot\mathbf{v}\,dV\\ =\;&\int_{\partial_N\Omega_0}\mathbf{t}\cdot\mathbf{v}\,d\mathbf{A} + \int_{\Omega_0}\rho_0\mathbf{b}\cdot\mathbf{v}\,dV, \quad \forall\mathbf{v}\in\mathcal{V},\ \mathbf{v}_{\partial_D\Omega}=0.\end{aligned} \tag{2.30}$$

interpreting $\delta\mathbf{E}$ as the variation of the GREEN-LAGRANGE strain $\mathbf{E}$ due to the *virtual displacement* $\mathbf{v}$. As with the momentum balance (2.27), the weak form (2.30) must be satisfied for every time instance t.

2.6 Linearization

The weak form (2.29) is generally nonlinear with respect to kinematics and material behavior. This thesis employs linear elastic material behavior described by (2.25). However, in Section 3.3 a *geometric* nonlinear numerical example is considered, i.e. the strain-displacement relation (2.11) is nonlinear. For the solution process of the weak form (2.29) a nonlinear solver, a

NEWTON-RAPHSON method, is applied which necessitates the linearization of the weak form. In the following section, the linearization for geometric nonlinearity is given.

In a first step, Equation (2.29) is rearranged as follows:

$$\begin{aligned}\mathcal{W}(\mathbf{u},\mathbf{v}) &= \int_{\Omega_0} \mathbf{S} : \mathbf{F}^T \operatorname{Grad}\mathbf{v}\, dV + \int_{\Omega_0} \rho_0 \ddot{\mathbf{u}} \cdot \mathbf{v}\, dV \\ &- \int_{\partial_N \Omega_0} \mathbf{t} \cdot \mathbf{v}\, d\mathbf{A} - \int_{\Omega_0} \rho_0 \mathbf{b} \cdot \mathbf{v}\, dV, \quad \forall \mathbf{v} \in \mathcal{V},\ \mathbf{v}_{\partial_D \Omega} = 0. \end{aligned} \tag{2.31}$$

For a trial solution $\bar{\mathbf{u}}$, the increment $\Delta\mathbf{u}$ is sought to provide the equilibrium displacement $\mathbf{u} = \bar{\mathbf{u}} + \Delta\mathbf{u}$ fulfilling the weak form (2.31). Equation (2.31) can be expanded in a TAYLOR series truncated after the linear term

$$\mathcal{W}(\mathbf{u},\mathbf{v}) = \mathcal{W}(\bar{\mathbf{u}} + \Delta\mathbf{u}, \mathbf{v}) \approx \mathcal{W}(\bar{\mathbf{u}}, \mathbf{v}) + D\mathcal{W}(\bar{\mathbf{u}}, \mathbf{v})[\Delta\mathbf{u}], \tag{2.32}$$

where $D\mathcal{W}(\bar{\mathbf{u}}, \mathbf{v})[\Delta\mathbf{u}]$ is the directional derivative of $\mathcal{W}$ at point $\bar{\mathbf{u}}$ in the direction of $\Delta\mathbf{u}$.

Let us consider the nonlinear term in Equation (2.31), $\int_{\Omega_0} \mathbf{S} : \mathbf{F}^T \operatorname{Grad}\mathbf{v}\, dV$. The linearization at point $\bar{\mathbf{u}}$ in the direction of $\Delta\mathbf{u}$ for linear elastic material is given by

$$\begin{aligned} D\int_{\Omega_0} \mathbf{S} : \mathbf{F}^T \operatorname{Grad}\mathbf{v}\, dV[\Delta\mathbf{u}] &= \int_{\Omega_0} \bar{\mathbf{S}} : \operatorname{Grad}^T \Delta\,\mathbf{u} \operatorname{Grad}\mathbf{v}\, dV \\ &+ \int_{\Omega_0} \mathbf{F}^T \operatorname{Grad}\mathbf{v} : \mathbb{C} : \bar{D}\mathbf{E}[\Delta\mathbf{u}]\, dV, \end{aligned} \tag{2.33}$$

where the directional derivative of the GREEN-LAGRANGE strain tensor in the second term on the right-hand side of (2.33) is

$$\bar{D}\mathbf{E}[\Delta\mathbf{u}] = \frac{1}{2}\left(\bar{\mathbf{F}}^T \operatorname{Grad}\Delta\mathbf{u} + \operatorname{Grad}^T \Delta\mathbf{u}\bar{\mathbf{F}}\right). \tag{2.34}$$

The bar over a quantity $(\bar{\bullet})$ denotes its evaluation at point $\bar{\mathbf{u}}$. All other terms in the weak form (2.31) are either independent of or linear in $\mathbf{u}$. Making use of the abbreviation $\delta\mathbf{E}$ according to (2.30), with the symmetry of $\mathbf{S}$, and with

$$\begin{aligned} \bar{\mathbf{S}} : \operatorname{Grad}^T \Delta\,\mathbf{u} \operatorname{Grad}\mathbf{v} &= \operatorname{tr}\left(\bar{\mathbf{S}}^T \operatorname{Grad}^T \Delta\,\mathbf{u} \operatorname{Grad}\mathbf{v}\right) \\ &= \operatorname{tr}\left(\left(\operatorname{Grad}\Delta\,\mathbf{u}\,\bar{\mathbf{S}}\right)^T \operatorname{Grad}\mathbf{v}\right) = \operatorname{Grad}\Delta\,\mathbf{u}\,\bar{\mathbf{S}} : \operatorname{Grad}\mathbf{v}, \end{aligned} \tag{2.35}$$

(2.33) can alternatively be written in the following form

$$D \int_{\Omega_0} \mathbf{S} : \delta\mathbf{E}\, dV[\Delta\mathbf{u}] = \int_{\Omega_0} \mathrm{Grad}\Delta\,\mathbf{u}\,\bar{\mathbf{S}} : \mathrm{Grad}\,\mathbf{v}\, dV + \int_{\Omega_0} \delta\mathbf{E} : \mathbb{C} : \bar{D}\mathbf{E}[\Delta\mathbf{u}]\, dV. \tag{2.36}$$

For small displacements, the current configuration and the reference configuration are identical, i.e. $\mathbf{F} = \mathbf{I}$, and from (2.16) $\mathbf{S} = \boldsymbol{\sigma}$. Hence, (2.31) reduces to the weak form of linear elastodynamics

$$\mathcal{W}(\mathbf{u},\mathbf{v}) = \int_{\Omega_0} \boldsymbol{\sigma} : \mathrm{Grad}\,\mathbf{v}\, dV + \int_{\Omega_0} \rho_0 \ddot{\mathbf{u}} \cdot \mathbf{v}\, dV - \int_{\partial_N\Omega_0} \mathbf{t}\cdot\mathbf{v}\, d\mathbf{A} - \int_{\Omega_0} \rho_0 \mathbf{b}\cdot\mathbf{v}\, dV, \quad \forall \mathbf{v}\in\mathcal{V},\ \mathbf{v}_{\partial_D\Omega} = 0 \tag{2.37}$$

with

$$\boldsymbol{\sigma} = \mathbb{C}\boldsymbol{\varepsilon} \tag{2.38}$$

and

$$\boldsymbol{\varepsilon} = \frac{1}{2}\left(\mathrm{Grad}^T\,\mathbf{u} + \mathrm{Grad}\,\mathbf{u}\right). \tag{2.39}$$

being the *small strain tensor*, also referred to as the *engineering strain*.

2.7 Important simplifications

2.7.1 Linear elastostatic problems: Equivalence to minimization of potential energy

Neglecting the inertia terms in the weak form (2.37) leads to the weak form of linear elastostatics

$$\mathcal{W}(\mathbf{u},\mathbf{v}) = \int_{\Omega_0} \boldsymbol{\varepsilon} : \mathbb{C} : \mathrm{Grad}\,\mathbf{v}\, dV - \int_{\partial_N\Omega_0} \mathbf{t}\cdot\mathbf{v}\, d\mathbf{A} - \int_{\Omega_0} \rho_0 \mathbf{b}\cdot\mathbf{v}\, d\mathbf{A}, \quad \forall \mathbf{v}\in\mathcal{V},\ \mathbf{v}_{\partial_D\Omega} = 0. \tag{2.40}$$

Using the definitions

$$\mathcal{B}(\mathbf{u},\mathbf{v}) = \int_{\Omega_0} \boldsymbol{\varepsilon} : \mathbb{C} : \mathrm{Grad}\,\mathbf{v}\, dV \tag{2.41}$$

and

$$\mathcal{F}(\mathbf{v}) = \int_{\partial_N\Omega_0} \mathbf{t}\cdot\mathbf{v}\, d\mathbf{A} + \int_{\Omega_0} \rho_0\mathbf{b}\cdot\mathbf{v}\, dV, \tag{2.42}$$

(2.40) can be compactly written, denoting $\mathbf{u}_{EX}$ its exact solution

$$\mathcal{B}(\mathbf{u}_{EX},\mathbf{v}) = \mathcal{F}(\mathbf{v}) \quad \forall\mathbf{v}\in\mathcal{V},\ \mathbf{v}_{\partial_D\Omega}=0, \tag{2.43}$$

$\mathcal{B}(\mathbf{u},\mathbf{v})$ is a *bilinear form* being symmetric, i.e. $\mathcal{B}(\mathbf{u},\mathbf{v})=\mathcal{B}(\mathbf{v},\mathbf{u})$, and positive definite when the DIRICHLET boundary conditions suppress rigid body motion, i.e. $\mathcal{B}(\mathbf{u},\mathbf{u})>0$ for all $\mathbf{u}\in\mathcal{V}$ and $\mathbf{u}\neq\mathbf{0}$. $\mathcal{F}(\mathbf{v})$ is a *linear functional* or *linear form*. The energy corresponding to a displacement function $\mathbf{u}$ can be described by means of the potential energy function

$$\Pi(\mathbf{u}) = \frac{1}{2}\mathcal{B}(\mathbf{u},\mathbf{u}) - \mathcal{F}(\mathbf{u})\,. \tag{2.44}$$

It is easy to demonstrate that the exact solution $\mathbf{u}_{EX}$ minimizes the potential $\Pi(\mathbf{u})$ with respect to all functions in $\mathbf{u}\in\mathcal{V}$. Any admissible function $\mathbf{u}\neq\mathbf{u}_{EX}$ can be represented as a sum of the exact solution $\mathbf{u}_{EX}$ and a function $\mathbf{w}\neq 0$ with $\mathbf{w}_{\partial_D\Omega}=0$,

$$\mathbf{u} = \mathbf{u}_{EX} + \mathbf{w}\,. \tag{2.45}$$

Thus, the corresponding potential is

$$\Pi(\mathbf{u}) = \Pi(\mathbf{u}_{EX}+\mathbf{w}) \tag{2.46}$$

$$= \frac{1}{2}\mathcal{B}(\mathbf{u}_{EX},\mathbf{u}_{EX}) - \mathcal{F}(\mathbf{u}_{EX}) + \frac{1}{2}\mathcal{B}(\mathbf{w},\mathbf{w}) + \underbrace{\mathcal{B}(\mathbf{u}_{EX},\mathbf{w}) - \mathcal{F}(\mathbf{w})}_{0} \tag{2.47}$$

The last two terms in (2.47) vanish thanks to (2.43), thus

$$\Pi(\mathbf{u}) = \Pi(\mathbf{u}_{EX}) + \frac{1}{2}\mathcal{B}(\mathbf{w},\mathbf{w}). \tag{2.48}$$

Due to the positive definiteness of the bilinear form, the term $\frac{1}{2}\mathcal{B}(\mathbf{w},\mathbf{w})$ is always positive and it therefore follows that

$$\Pi(\mathbf{u}_{EX}) \;<\; \Pi(\mathbf{u}_{EX}+\mathbf{w}), \tag{2.49}$$

i.e. $\mathbf{u}_{EX}$ minimizes the potential

$$\min_{\mathbf{u}\in\mathcal{V}} \Pi(\mathbf{u}) \;=\; \Pi(\mathbf{u}_{EX}). \tag{2.50}$$

The uniqueness of the solution is also ensured, since (2.49) holds for all functions $\mathbf{w} \neq 0$ with $\mathbf{w}_{\partial_D\Omega} = 0$.

2.7.2 Linear elastodynamic problems: Harmonic vibrations, minimum principle of eigenfrequencies

In the special case of homogeneous boundary conditions

$$\begin{array}{rcl} \mathbf{u} = \bar{\mathbf{u}} = \mathbf{0} & \text{on} & \partial_D\Omega \times (0,T], \\ \boldsymbol{\sigma}\mathbf{n} = \mathbf{t} = \mathbf{0} & \text{on} & \partial_N\Omega \times (0,T], \end{array} \tag{2.51}$$

the weak form of linear elastodynamics (2.37) reduces to

$$\mathcal{W}(\mathbf{u},\mathbf{v}) \;=\; \int_{\Omega_0} \boldsymbol{\varepsilon} : \mathbb{C} : \operatorname{Grad}\mathbf{v}\, dV + \int_{\Omega_0} \rho_0 \ddot{\mathbf{u}}\cdot\mathbf{v}\, dV = 0. \tag{2.52}$$

Using separation of variables for the displacements $\mathbf{u}$ with harmonic variation in time

$$\mathbf{u}(\mathbf{X},t) = \mathbf{u}_k(\mathbf{X}) e^{i\omega_k t}, \quad i=\sqrt{-1} \tag{2.53}$$

we obtain

$$\mathcal{W}(\mathbf{u},\mathbf{v}) \;=\; e^{i\omega_k t}\left(\int_{\Omega_0} \boldsymbol{\varepsilon}_k : \mathbb{C} : \operatorname{Grad}\mathbf{v}\, dV - \omega_k^2 \int_{\Omega_0} \rho_0 \mathbf{u}_k\cdot\mathbf{v}\, dV\right) = 0, \tag{2.54}$$

and since (2.54) must hold for arbitrary t, we can write

$$\int_{\Omega_0} \boldsymbol{\varepsilon}_k : \mathbb{C} : \operatorname{Grad}\mathbf{v}\, dV - \omega_k^2 \int_{\Omega_0} \rho_0 \mathbf{u}_k\cdot\mathbf{v}\, dV = 0. \tag{2.55}$$

with

$$\boldsymbol{\varepsilon}_k = \frac{1}{2}\left(\operatorname{Grad}\mathbf{u}_k^T + \operatorname{Grad}\mathbf{u}_k\right). \tag{2.56}$$

being the strain state corresponding to the k-th pair of *eigenfrequencies* and *eigenfunctions* $(\omega_k, \mathbf{u}_k)$, which are solutions of the eigenproblem (2.55). In addition to the bilinear form $\mathcal{B}(\mathbf{u}, \mathbf{u})$, (2.41), the bilinear form

$$\mathcal{D}(\mathbf{u}, \mathbf{v}) = \int_{\Omega_0} \rho_0 \mathbf{u} \cdot \mathbf{v}\, dV \tag{2.57}$$

is defined and the eigenproblem (2.55) can be compactly written as

$$\mathcal{B}(\mathbf{u}_k, \mathbf{v}) - \lambda_k \mathcal{D}(\mathbf{u}_k, \mathbf{v}) = 0 \quad \forall \mathbf{v} \in \mathcal{V},\ \mathbf{v}_{\partial_D\Omega} = 0 \tag{2.58}$$

with $\lambda_k = \omega_k^2$. The eigenfunctions are orthogonal to each other and scaled such that they fulfill the orthonormality condition

$$\mathcal{D}(\mathbf{u}_i, \mathbf{u}_j) = \delta_{ij} \tag{2.59}$$

The exact eigenfunctions and eigenfrequencies $(\mathbf{u}_i, \omega_i)$ can alternatively be defined by a minimization principle, similar to the principle stating that the potential energy function is minimized by the exact solution $\mathbf{u}_{EX}$ of the corresponding elastostatic problem. For the eigenvalue problem (2.58) the RAYLEIGH quotient

$$\rho(\mathbf{u}) = \frac{B(\mathbf{u}, \mathbf{u})}{\mathcal{D}(\mathbf{u}, \mathbf{u})} \tag{2.60}$$

is minimized by the eigenfunction $\mathbf{u}_1$ corresponding to the lowest eigenfrequency ω_1 to give the corresponding eigenvalue λ_1

$$\min_{\mathbf{u}\in\mathcal{V}} \rho(\mathbf{u}) = \rho(\mathbf{u}_1) = \lambda_1 = \omega_1^2. \tag{2.61}$$

A straightforward method of illustrating this basic principle is to develop an arbitrary function $\mathbf{u}$ into a linear combination of exact eigenfunctions of infinite number

$$\mathbf{u} = \sum_{i=1}^{\infty} \alpha_i \mathbf{u}_i. \tag{2.62}$$

Substituting (2.62) in (2.60) and subsequently using (2.58), (2.59) leads to

$$\begin{aligned}
\rho(\mathbf{u}) &= \rho(\sum_{i=1}^{\infty} \alpha_i \mathbf{u}_i) \\
&= \frac{\mathcal{B}(\sum_{i=1}^{\infty} \alpha_i \mathbf{u}_i, \sum_{j=1}^{\infty} \alpha_j \mathbf{u}_j)}{\mathcal{D}(\sum_{k=1}^{\infty} \alpha_k \mathbf{u}_k, \sum_{l=1}^{\infty} \alpha_l \mathbf{u}_l)} \\
&= \frac{\sum_{i=1}^{\infty} \alpha_i \lambda_i \mathcal{D}(\mathbf{u}_i, \sum_{j=1}^{\infty} \alpha_j \mathbf{u}_j)}{\mathcal{D}(\sum_{k=1}^{\infty} \alpha_k \mathbf{u}_k, \sum_{l=1}^{\infty} \alpha_l \mathbf{u}_l)} \\
&= \frac{\lambda_1 \alpha_1^2 + \lambda_2 \alpha_2^2 + \lambda_3 \alpha_3^2 + ...}{\alpha_1^2 + \alpha_2^2 + \alpha_3^2 + ...} \\
&= \lambda_1 \frac{\alpha_1^2 + \frac{\lambda_2}{\lambda_1} \alpha_2^2 + \frac{\lambda_3}{\lambda_1} \alpha_3^2 + ...}{\alpha_1^2 + \alpha_2^2 + \alpha_3^2 + ...}
\end{aligned} \tag{2.63}$$

With an ordered sequence of eigenvalues $\lambda_1 \leq \lambda_2 \leq \lambda_3 \leq ...$ the fraction in the last line of (2.63) is always greater than or equal to 1. Thus,

$$\min_{\mathbf{u} \in \mathcal{V}} \rho(\mathbf{u}) = \rho(\mathbf{u}_1) = \lambda_1. \tag{2.64}$$

In the same manner, higher eigenvalues λ_i, $i > 1$ fulfill the minimum equations

$$\min_{\mathbf{u} \in \mathcal{V}_{i\perp}} \rho(\mathbf{u}) = \rho(\mathbf{u}_i) = \lambda_i \tag{2.65}$$

with $\mathbf{u} \in \mathcal{V}_{i\perp}$ being orthogonal to eigenfunctions $\mathbf{u}_1$,...,$\mathbf{u}_{i-1}$.

2.7.3 Dimensional reduction: Models for plates and shells

Dimensional reduction can be interpreted as a reduction of the solution space of the three-dimensional problem to obtain efficient *structural models* for thin-walled structures. In the transversal direction of plates or shells, simplified kinematics are assumed for the displacement fields, e.g. allowing only for a linear variation in the displacement function over thickness. From a historical point of view, dimensional reduction has been an option employed to make certain classes of problems tractable for analytical or approximate solution methods. Nowadays, mechanical models are solved using numerical and computational methods, and the use of plate and shell models is a popular approach to reduce the computational complexity of structural problems.

Good overviews of the different kinds of modeling and solution techniques for plates and shells are provided, for example, in Bathe [26], Belytschko et al. [27], Bischoff [30], Bischoff and Ramm [31], Bischoff et al. [32], Crisfield [40], Eberlein [56], Hauptmann [67], Hughes [72], Wall et al. [141], Wriggers [148], Yang et al. [149], Zienkiewicz and

TAYLOR [152]. Of course, this list is by no means complete and there are a lot of other important papers contributing to this problem. In the following, a very brief description of the basic assumptions for plate and shell models is given (see, for example, BISCHOFF [32]).

The most general approach for deriving models for plate or shell structures is to begin with the three-dimensional continuum equations. The geometric description

$$\mathbf{x}(\theta^1, \theta^2, \theta^3) \;=\; \mathbf{r}(\theta^1, \theta^2) + \theta^3 \mathbf{a}_3 \tag{2.66}$$

of the shell body is idealized by a two-dimensional middle surface described by $\mathbf{r}(\theta^1, \theta^2)$ (see Figure 2.3). Points outside the mid-surface are described using $\theta^3 \neq 0$ with $\mathbf{a}_3$ as the covariant vector pointing into the thickness-direction of the shell, which is often referred to as the director.

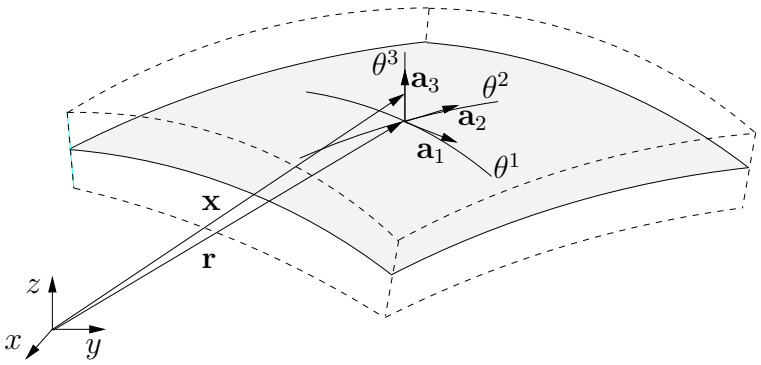

Figure 2.3: Geometric description of a shell

The displacement field is given by reducing the solution space of all admissible functions in the thickness direction

$$\mathbf{u}(\theta^1, \theta^2, \theta^3) \;=\; \mathbf{v}(\theta^1, \theta^2) + \sum_{n=1}^{n_{\max}} (\theta^3)^n \mathbf{w}_n \tag{2.67}$$

where the accuracy with respect to the three-dimensional continuum approach depends on the number $n_{\max}$.

2.7.3.1 Plate models

Plates are idealized by their *plane* middle surface. The basic assumptions of the geometric linear KIRCHHOFF and REISSNER-MINDLIN plate models read (see [119, 120, 136], for example):

- Normals to the middle surface of the plate prior to deformation are assumed to remain straight lines after deformation. While in the KIRCHHOFF theory the straight lines remain normals to the middle surface, this is not required in the REISSNER-MINDLIN theory.
- The plate has a moderate thickness t and the deflection w is independent of z, so that $u_z(x, y, z) = w(x, y)$.

- Points on the middle surface are deflected in z-direction only.
- Stresses normal to the middle surface are assumed to be negligible: $\sigma_{zz} = 0$.

The extension of the KIRCHHOFF plate model considering geometric nonlinearities is the VON KÁRMÁN plate model, see YOSIBASH and KIRBY [150], for instance. The previously mentioned plate models restrict the transversal variation of the displacement in (2.67) to be linear. It is also possible, however, to successively extend the 'kinematic' solution space leading to a hierarchy of plate models, see SCHWAB [125], for example.

2.7.3.2 Shell models

A common classification of the different shell formulations familiar from literature is based on the kinematic assumptions, i.e. the number of free parameters which are introduced when formulating the displacement field:

- **3 parameter model**
  The 3 parameter model is based on the Kirchhoff-Love theory [89] which excludes shear deformations. In this theory it is assumed that normals to the middle surface of the shell prior to deformation remain normals. Therefore, the rotation of the director is linked to the rotation of the middle surface. Furthermore, it is assumed that the length of the director does not change during deformation.
- **5 parameter model**
  The 5 parameter model is based on the theory of NAGHDI [94] and allows for shear deformation. Therefore, this theory is often referred to as the Reissner-Mindlin model. Normals to the middle surface of the plate prior to deformation are assumed to remain straight lines after deformation, but not necessarily normals. The length of the director is assumed to be constant.
- **6 parameter model**
  The 6 parameter model assumes a linear variation of all displacement components in the thickness direction and therefore allows a thickness stretch of the shell (see SIMO et al. [130]), i.e. the director of the shell may change its length. This model is the first one in this family that allows for a representation of a three-dimensional stress state, i.e. the implementation of a fully three-dimensional constitutive law.
- **7 parameter model**
  Since the 6 parameter model exhibits Poisson thickness locking, the model is extended by the enhanced assumed strain method (EAS). Poisson thickness locking is caused by an imbalance of the strains and stresses acting in the thickness direction. The additional parameter is introduced as an enhanced linear strain mode corresponding to the thickness direction (see BÜCHTER and RAMM [35] and BÜCHTER et al. [36]). Another way of avoiding Poisson thickness locking is to introduce the additional parameter via a quadratic change of the transverse displacement in thickness direction.
- **Hierarchic shell models**
  As for hierarchic plate models, it is also possible to gradually extend the kinematic assumptions (2.67) leading to a family of hierarchic shell models (see, for instance, [1]).

Chapter 3

Discretization

Instead of solving the weak form (2.29) analytically, which is intractable in most cases, approximate solutions can be found using numerical methods. The continuous problem is discretized leading to a problem with a finite number of degrees of freedom. In this thesis the spatial domain is discretized by means of the finite element method, whereas the temporal domain is discretized using a finite difference based method (the generalized α-method). Although this approach is widely used, alternative techniques are possible, for example, space-time finite elements, finite volume methods for the spatial discretization, etc.

3.1 Spatial discretization

Finite element methods begin with the weak form (2.29) of the momentum equations. Instead of weighting the weak form with *all* functions $\mathbf{v}$ in the space $\mathcal{V}$ with infinite dimensions, the general idea is to use weighting functions from a finite dimensional subspace only, $\mathbf{v} \in \mathcal{S}$. According to the Bubnov-Galerkin approach, the approximate solution $\mathbf{u}_{FE}$ is sought in the same space $\mathcal{S}$, as well.

In order to construct the finite dimensional subspace $\mathcal{S}$, the reference domain Ω_0 is subdivided — or *discretized* — into n_{el} non-overlapping subdomains — or *finite elements* — Ω_e

$$\Omega_0 \approx \bigcup_{e=1}^{n_e} \Omega_e. \tag{3.1}$$

The discretization of the domain boundary $\partial\Omega_0$ consists of the corresponding element boundary edges and faces

$$\partial\Omega_0 \approx \bigcup_{e=1}^{n_e} \partial\Omega_e \cap \partial\Omega_0. \tag{3.2}$$

Thus, the subspace S can be constructed using shape functions with local support on the elements Ω_e. In general, the exact solution $\mathbf{u}_{EX}$ is approximated by a linear combination of the corresponding element shape functions N_I

$$\mathbf{u}_{EX}(\mathbf{X}) \approx \sum_{I=1}^{n_{modes}} N_I(\mathbf{X})\mathbf{u}_I \tag{3.3}$$

where $\mathbf{u}_I$ are the amplitudes corresponding to N_I — for three-dimensional problems, for instance, $\mathbf{u}_I = (u_{1I}, u_{2I}, u_{3I})^T$. Another alternative is to sort all $\mathbf{u}_I$ corresponding to element e into one *element displacement vector* $\mathbf{d}_e$, and write

$$\mathbf{u}_e(\mathbf{X_e}) = \mathbf{N}_e(\mathbf{X_e})\mathbf{d}_e \tag{3.4}$$

It is imperative to satisfy the C_0-continuity of the function $\mathbf{u}$, in the event of element shape functions N_I not vanishing on the element boundary $\partial\Omega_e$ shared with element $\Omega_{e'}$. In this case, a corresponding shape function on element $\Omega_{e'}$ is required to ensure a continuous transition without any gaps between the two element shape functions. Element shape functions accordingly make up the shape function N_I^P defined on a *patch* of elements $\Omega^P \bigcup_{e\in P} \Omega_e$. This calls for an *assembly* process on a global level, composing quantities involving this patch function N_I^P — usually integrals over the patch — from the local element contributions, see Bathe [26], for example. The global assembly of (3.4) is then

$$\mathbf{u}(\mathbf{X}) = \mathbf{N}(\mathbf{X})\mathbf{d} \tag{3.5}$$

Throughout this thesis, only high order hierarchic shape functions are used, defined on hexahedral elements where the polynomial degrees of the shape functions can be chosen anisotropically, i.e. independently for different directions, as described in the following section.

3.1.1 Hierarchic high order anisotropic hexahedral elements

This description of high order hexahedrals is closely aligned to Düster [47]. The Ansatz functions introduced by Szabó and Babuška [136] are used. Hexahedral elements (see Figure 3.1) show some advantages when compared with their corresponding tetrahedral and pentahedral element formulations.

- Hexahedral element formulations lead to higher accuracy for low p.
- Hexahedral elements are especially well suited for thin-walled structures. One local variable can be identified to correspond with the thickness direction. It is therefore possible to choose a different polynomial degree in the thickness direction from those in the in-plane direction.
- The numerical integration of hexahedral elements can be readily performed using a Gaussian quadrature scheme.

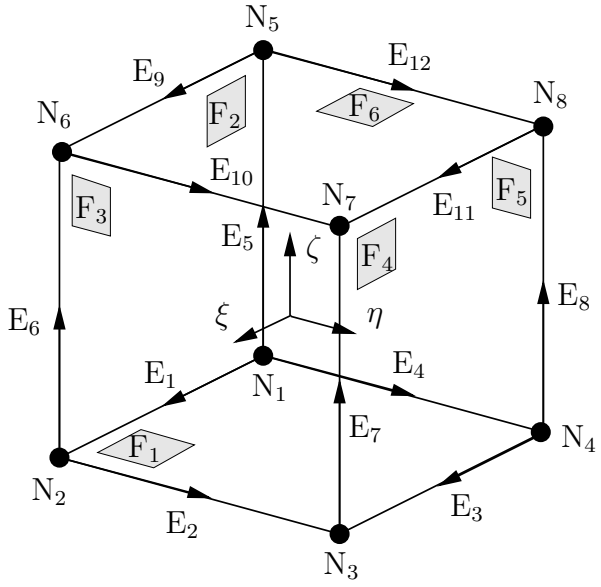

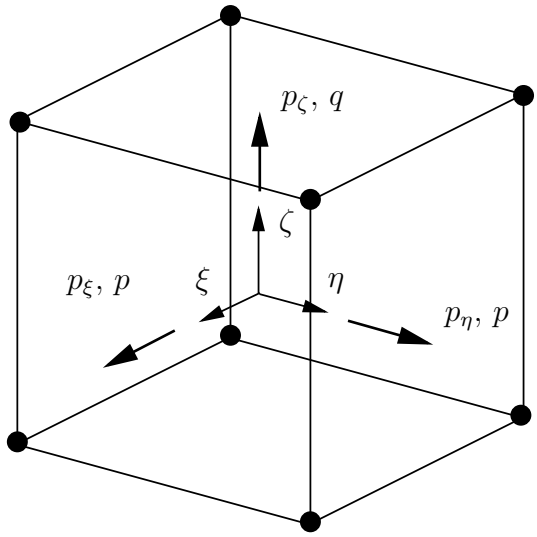

$\Omega^{\mathrm{h}}_{\mathrm{st}} = [(-1,1)\times(-1,1)\times(-1,1)]$ $\qquad$ $\mathcal{S}^{p_\xi,p_\eta,p_\zeta}_{\mathrm{ts}}(\Omega^{\mathrm{h}}_{\mathrm{st}}), \mathcal{S}^{p_\xi,p_\eta,p_\zeta}_{\mathrm{ps}}(\Omega^{\mathrm{h}}_{\mathrm{st}}), \mathcal{S}^{p,p,q}(\Omega^{\mathrm{h}}_{\mathrm{st}})$

Figure 3.1: Standard hexahedral element $\Omega^{\mathrm{h}}_{\mathrm{st}}$: definition of nodes, edges, faces and polynomial degree

An important advantage of using high order elements for plate- or shell-like structures is that they are less prone to locking effects compared to classical low order approaches, see [47], for instance.

In the following, ϕ_i denotes the integral

$$\phi_i(\xi) \;=\; \sqrt{\frac{2i-1}{2}}\int_{-1}^{\xi} L_{i-1}(x)\,dx = \frac{1}{\sqrt{4i-2}}(L_i(\xi)-L_{i-2}(\xi))\,, \quad i=2,3,... \tag{3.6}$$

of the well-known LEGENDRE polynomials L_j, which can be obtained by the RODRIGUEZ formula

$$L_j(x) \;=\; \frac{1}{2^j\,j!}\frac{d^j}{d\,x^j}\,(x^2-1)^j\,, \quad x\in(-1,1), \quad j=0,1,2,... \tag{3.7}$$

Three-dimensional shape functions can be classified into four groups:

1. **Nodal modes:** The nodal modes

$$N^{\mathrm{N}_i}_{1,1,1}(\xi,\eta,\zeta) \;=\; \frac{1}{8}\,(1+\xi_i\,\xi)(1+\eta_i\,\eta)(1+\zeta_i\zeta), \quad i=1,...,8 \tag{3.8}$$

   are the standard trilinear shape functions, familiar from the isoparametric eight-noded brick element. (ξ_i,η_i,ζ_i) are the local coordinates of the i-th node.

2. **Edge modes:** These modes are defined separately for each individual edge. If we consider, for example, edge E_1 (see Figure 3.1), the corresponding edge modes read:

$$N^{\mathrm{E}_1}_{i,1,1}(\xi,\eta,\zeta) \;=\; \frac{1}{4}\,(1-\eta)(1-\zeta)\phi_i(\xi) \tag{3.9}$$

3. **Face modes:** These modes are defined separately for each individual face. If we take a look at the face F_1, for instance, the corresponding face modes read:

$$N^{\mathrm{F}_1}_{i,j,1}(\xi,\eta,\zeta) \;=\; \frac{1}{2}\,(1-\zeta)\phi_i(\xi)\phi_j(\eta) \tag{3.10}$$

4. **Internal modes:** The internal modes

$$N^{\mathrm{int}}_{i,j,k}(\xi,\eta,\zeta) \;=\; \phi_i(\xi)\phi_j(\eta)\phi_k(\zeta) \tag{3.11}$$

   are purely local and vanish on the faces of the hexahedral element.

The indices i, j, k of the shape functions denote the polynomial degrees in the local directions ξ, η, ζ.

Three different types of Ansatz spaces have been implemented: the *trunk space* $\mathcal{S}^{p_\xi,p_\eta,p_\zeta}_{\mathrm{ts}}(\Omega^{\mathrm{h}}_{\mathrm{st}})$, the *tensor product space* $\mathcal{S}^{p_\xi,p_\eta,p_\zeta}_{\mathrm{ps}}(\Omega^{\mathrm{h}}_{\mathrm{st}})$ and the *anisotropic tensor product space* $\mathcal{S}^{p,p,q}(\Omega^{\mathrm{h}}_{\mathrm{st}})$. A detailed description of the three Ansatz spaces can be found in Appendix A and Düster [47]. For the definition of the spaces $\mathcal{S}^{p_\xi,p_\eta,p_\zeta}_{\mathrm{ts}}(\Omega^{\mathrm{h}}_{\mathrm{st}})$ and $\mathcal{S}^{p,p,q}(\Omega^{\mathrm{h}}_{\mathrm{st}})$ see also Szabó and Babuška [136]. The trunk space $\mathcal{S}^{p_\xi,p_\eta,p_\zeta}_{\mathrm{ts}}(\Omega^{\mathrm{h}}_{\mathrm{st}})$ is used throughout this thesis.

The present implementation of the p-version [54] not only allows the polynomial degree to be varied for the three different local directions but also a different degree to be chosen for each primary variable. The following example illustrates how to define a polynomial degree template $\mathbf{p}_e$ for a structural problem with three primary variables $\mathbf{u} = [u_x, u_y, u_z]^T$. Let

$$\mathbf{p}_e \;=\; \begin{array}{c} \\ \xi \\ \eta \\ \zeta \end{array} \begin{array}{c} \begin{array}{ccc} u_x & u_y & u_z \end{array} \\ \begin{pmatrix} 1 & 4 & 7 \\ 2 & 5 & 8 \\ 3 & 6 & 9 \end{pmatrix} \end{array} . \tag{3.12}$$

Taking the trunk space $\mathcal{S}^{p_\xi,p_\eta,p_\zeta}_{\mathrm{ts}}(\Omega^{\mathrm{h}}_{\mathrm{st}})$ into consideration, the polynomial degree template $\mathbf{p}$ defines the Ansatz for the displacement field

$u_x \in \mathcal{S}^{1,2,3}_{\mathrm{ts}}(\Omega^{\mathrm{h}}_{\mathrm{st}})$, $u_y \in \mathcal{S}^{4,5,6}_{\mathrm{ts}}(\Omega^{\mathrm{h}}_{\mathrm{st}})$ and $u_z \in \mathcal{S}^{7,8,9}_{\mathrm{ts}}(\Omega^{\mathrm{h}}_{\mathrm{st}})$.

The numerical examples in Sections 5 and 6, where anisotropic p-distributions are obtained by adaptation, demonstrate that anisotropic Ansatz spaces lead to efficient discretizations, such as those for thin-walled structures, as depicted in Figure 3.2. The geometric mapping used to

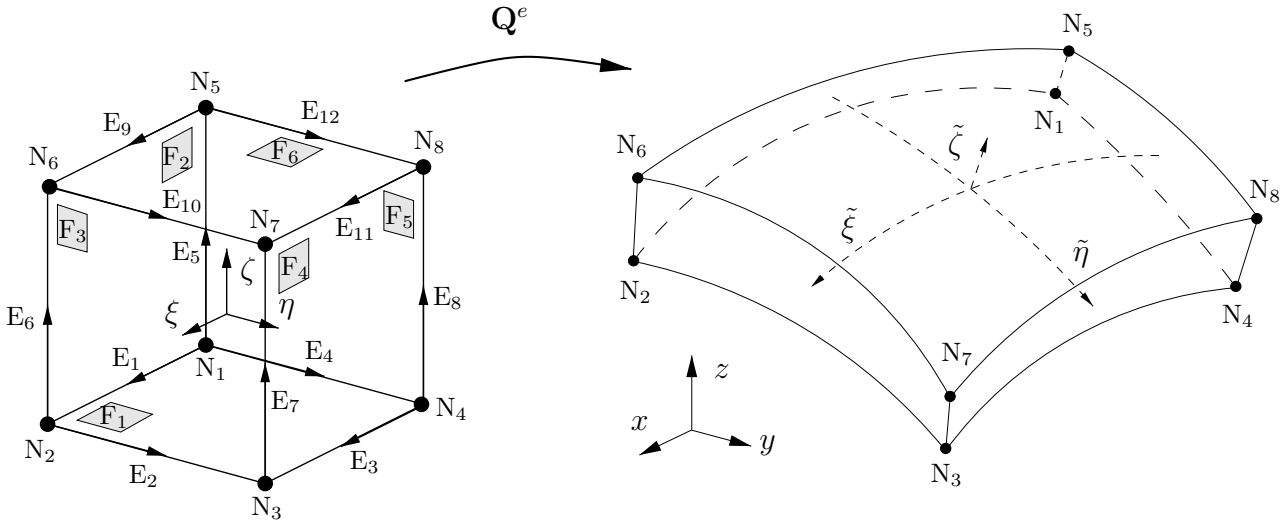

Figure 3.2: Doubly curved shell-like solid element of high order

describe the curved structure is described in Section 3.1.2.

$\mathbf{N}_e$ in (3.4) can be composed in the following manner

$$\mathbf{N}_e = \left[\mathbf{N}_e^{\mathrm{N}} \quad \mathbf{N}_e^{\mathrm{E}} \quad \mathbf{N}_e^{\mathrm{F}} \quad \mathbf{N}_e^{\mathrm{int}} \right] . \tag{3.13}$$

Condensing the internal modes in the resulting element matrices is facilitated since the internal mode matrix $\mathbf{N}^{\mathrm{int}}$ fills the end of the matrix $\mathbf{N}_e$.
The nodal modes

$$\mathbf{N}_e^{\mathrm{N}} = \begin{bmatrix} N_{1,1,1}^{\mathrm{N}_1} & & & & & & & N_{1,1,1}^{\mathrm{N}_8} & & \\ & N_{1,1,1}^{\mathrm{N}_1} & & & \ldots & & N_{1,1,1}^{\mathrm{N}_8} & & \\ & & N_{1,1,1}^{\mathrm{N}_1} & & & & & & N_{1,1,1}^{\mathrm{N}_8} \end{bmatrix} \tag{3.14}$$

are the standard trilinear shape functions familiar from the eight-noded isoparametric brick element. Note that elements not shown in matrices are zero. The edge modes

$$\mathbf{N}_e^{\mathrm{E}} = \left[\mathbf{N}_e^{\mathrm{E}_1} \quad \mathbf{N}_e^{\mathrm{E}_2} \quad \mathbf{N}_e^{\mathrm{E}_3} \quad \cdots \quad \mathbf{N}_e^{\mathrm{E}_{12}} \right] \tag{3.15}$$

are defined separately for each edge. Considering edge E_1, for example, we have

$$\mathbf{N}_e^{\mathrm{E}_1} = \begin{bmatrix} N_{2,1,1}^{\mathrm{E}_1} & & & & & & & N_{p_\xi,1,1}^{\mathrm{E}_1} & & \\ & N_{2,1,1}^{\mathrm{E}_1} & & & \cdots & & N_{p_\xi,1,1}^{\mathrm{E}_1} & & \\ & & N_{2,1,1}^{\mathrm{E}_1} & & & & & & N_{p_\xi,1,1}^{\mathrm{E}_1} \end{bmatrix} . \tag{3.16}$$

(3.16) groups all shape functions corresponding to edge E_1 for a polynomial degree up to p_ξ. Similar expressions can be obtained for $\mathbf{N}^{\mathrm{E}_2}, ..., \mathbf{N}^{\mathrm{E}_{12}}$. The face modes

$$\mathbf{N}_e^{\mathrm{F}} = \left[\mathbf{N}^{\mathrm{F}_1} \quad \mathbf{N}^{\mathrm{F}_2} \quad \mathbf{N}^{\mathrm{F}_3} \quad \cdots \quad \mathbf{N}^{\mathrm{F}_6} \right] \tag{3.17}$$

are defined separately for each face. Assuming that the tensor product space $\mathcal{S}_{\mathrm{ps}}^{p_\xi,p_\eta,p_\zeta}(\Omega_{\mathrm{st}}^{\mathrm{h}})$ is chosen, the $(p_\xi-1)(p_\eta-1)$ modes for face F_1 are collected in

$$\mathbf{N}^{\mathrm{F}_1} = \begin{bmatrix} N_{2,2,1}^{\mathrm{F}_1} & & & \cdots & N_{p_\xi,p_\eta,1}^{\mathrm{F}_1} & \\ & N_{2,2,1}^{\mathrm{F}_1} & & \cdots & & N_{p_\xi,p_\eta,1}^{\mathrm{F}_1} \\ & & N_{2,2,1}^{\mathrm{F}_1} & \cdots & & \end{bmatrix}. \tag{3.18}$$

The definition of the matrices $\mathbf{N}^{\mathrm{F}_i}, i = 2, ..., 6$ should be taken in an analogous sense. Assuming again that the tensor product space $\mathcal{S}_{\mathrm{ps}}^{p_\xi,p_\eta,p_\zeta}(\Omega_{\mathrm{st}}^{\mathrm{h}})$ is chosen, the $(p_\xi-1)(p_\eta-1)(p_\zeta-1)$ internal modes are assembled in

$$\mathbf{N}_e^{\mathrm{int}} = \begin{bmatrix} N_{2,2,2}^{\mathrm{int}} & & & \cdots & N_{p_\xi,p_\eta,p_\zeta}^{\mathrm{int}} & \\ & N_{2,2,2}^{\mathrm{int}} & & \cdots & & N_{p_\xi,p_\eta,p_\zeta}^{\mathrm{int}} \\ & & N_{2,2,2}^{\mathrm{int}} & \cdots & & \end{bmatrix}. \tag{3.19}$$

The polynomial degree templates $\mathbf{p}$ can be defined for each individual element or for a group of elements, for instance, they may be prescribed by an adaptive procedure, as proposed in Sections 5 and 6. The finite element code AdhoC [48] automatically takes care of inter-element continuity of the Ansatz. If adjacent elements have different definitions of $\mathbf{p}$, then the highest degree is always chosen for the common edge and face modes. Thus, the global Ansatz space $\mathcal{S}^{\mathcal{P}}$ is defined by the set of polynomial degree templates

$$\mathcal{P} = \{\mathbf{p_1}, ..., \mathbf{p}_{n_{el}}\}. \tag{3.20}$$

3.1.2 Geometric mapping: The blending function method

The shape functions described in the previous section were defined on the standard hexahedral element, so appropriate mapping techniques have to be used to represent the element geometry. Most finite element formulations are based on an *isoparametric mapping* employing the same shape functions to describe both the unknown displacements and the geometry. Opting for an *h*-method, i.e. increasing accuracy of the solution by decreasing the element sizes, the geometry is automatically described more accurately, as well.

By contrast, this thesis proposes a *p*-adaptive strategy in Sections 5 and 6, which means that, in order to improve the accuracy of the solution, the mesh remains fixed and only the polynomial degree templates $\mathbf{p}_e$ of the elements are adjusted. Therefore, a mapping technique has to be used to represent the geometry accurately, regardless of the element sizes. For this purpose, the blending function method, which was first proposed by Gordon and Hall [60], is used.

The corresponding formulation of the blending function method in three dimensions closely follows the work of Királyfalvi and Szabó [79]. For more information, such as further details concerning the accuracy of the method, the reader is referred to Bröker [34] and Düster [47].

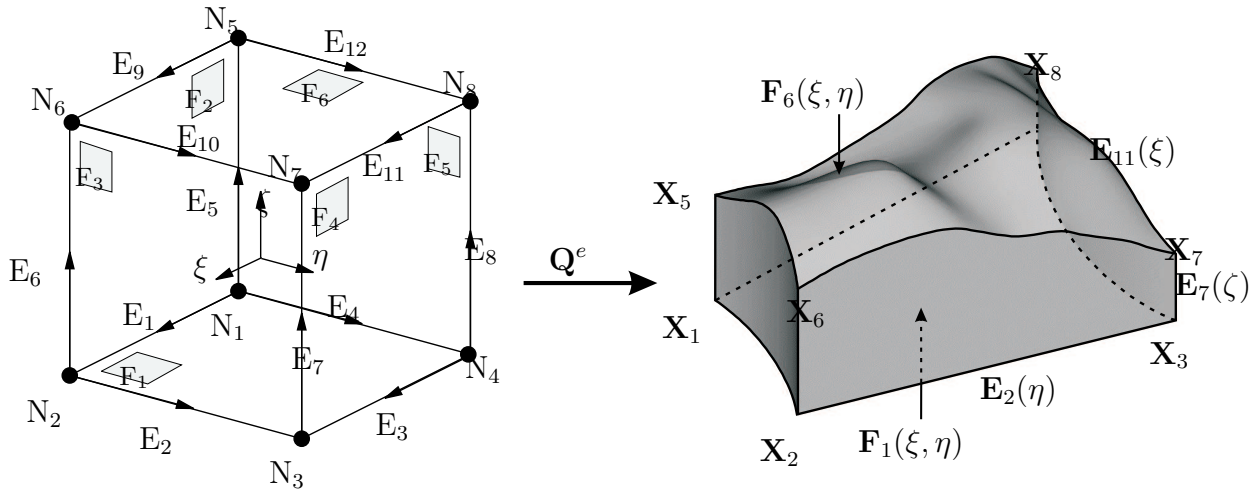

Figure 3.3: Blending function method for hexahedral elements

Let us take a look at a hexahedral element, as pictured in Figure 3.3. $\mathbf{X}_i = [X_i, Y_i, Z_i]^T$, $i = 1, ..., 8$ denote the global coordinates of the nodes. $\mathbf{E}_i = [E_{ix}, E_{iy}, E_{iz}]^T$, $i = 1, ..., 12$ are functions which depend on local coordinates (ξ, η, ζ) and describe the shape of each edge. $\mathbf{F}_i = [F_{ix}, F_{iy}, F_{iz}]^T$, $i = 1, ..., 6$ denote the functions describing the shape of each face. The mapping function $\mathbf{Q}^e(\xi, \eta, \zeta)$ from local $\boldsymbol{\xi} = [\xi, \eta, \zeta]^T$ to global coordinates $\mathbf{x} = [x, y, z]^T$ is obtained by

$$\mathbf{x} = \mathbf{Q}^e(\xi, \eta, \zeta) = \sum_{i=1}^{8} N^{\mathrm{N}_i}_{1,1,1}(\xi, \eta, \zeta)\, \mathbf{X}_i + \sum_{i=1}^{6} \mathbf{f}_i(\xi,\, \eta,\, \zeta) - \sum_{i=1}^{12} \mathbf{e}_i(\xi,\, \eta,\, \zeta)\,. \tag{3.21}$$

The first term is the standard mapping of isoparametric eight-noded hexahedral elements. The second term is referred to as face blending (see Appendix B). Consider, for example, face F_6 of the hexahedral element shown in Figure 3.3, where $\mathbf{F}_6(\xi,\, \eta)$ describes the parametric mapping of the local (ξ, η)-plane to the surface of the element:

$$\begin{aligned} \mathbf{f}_6(\xi,\, \eta,\, \zeta) \;=\; & \Big[\mathbf{F}_6(\xi, \eta) - \frac{1}{4}\big[(1-\xi)(1-\eta)\mathbf{X}_5 + (1+\xi)(1-\eta)\mathbf{X}_6 + \\ & +(1+\xi)(1+\eta)\mathbf{X}_7 + (1-\xi)(1+\eta)\mathbf{X}_8\big]\Big]\left(\frac{1+\zeta}{2}\right) \end{aligned} \tag{3.22}$$

On face F_6, where $\zeta = 1$ the blending term $\frac{1+\zeta}{2}$ equals 1 and therefore $\mathbf{f}_6(\xi,\, \eta,\, \zeta = 1)$ describes the difference between the curved and the bilinear face coordinates (ξ, η). On the other hand, the blending term guarantees that this difference (i.e. the function $\mathbf{f}_6(\xi,\, \eta,\, \zeta)$) decreases linearly to the opposite face F_1, where $\zeta = -1$ such that $\mathbf{f}_6(\xi,\, \eta,\, -1) = 0$.

The third term in Equation (3.21) corresponds to the edge blending. Considering edge E_1, for instance, we have

$$\mathbf{e}_1(\xi,\,\eta,\,\zeta) \;=\; \left[\mathbf{E}_1(\xi) - \frac{(1-\xi)\mathbf{X}_1 + (1+\xi)\mathbf{X}_2}{2}\right]\left(\frac{1-\eta}{2}\right)\left(\frac{1-\zeta}{2}\right). \tag{3.23}$$

$\mathbf{e}_i(\xi,\eta,\zeta)$, $i = 1, ..., 12$ denote the difference between the curved edge and the linear connection of the two end points, multiplied by a blending term (see Appendix B). The structure of the edge blending is similar to the face mapping, except that it now has a blending term that is linear in two variables. Since each edge belongs to two faces of a hexahedral element, a correction with respect to a straight line edge appears twice in the surface blending term (second sum) in Equation (3.21). Therefore, the corresponding edge blending term has to be subtracted.

Substituting $\mathbf{f}_i(\xi,\,\eta,\,\zeta), i = 1, ..., 6$ and $\mathbf{e}_i(\xi,\,\eta,\,\zeta), i = 1, ..., 12$ in Equation (3.21) by inserting Equations (B.2), (B.1) of Appendix B and rearranging the terms, we finally obtain

$$\begin{aligned}
\mathbf{x} \;&=\; \mathbf{Q}^e(\boldsymbol{\xi}) \qquad\qquad (3.24)\\
&=\; \frac{1}{2}\Big[(1-\zeta)\,\mathbf{F}_1(\xi,\,\eta) + (1-\eta)\,\mathbf{F}_2(\xi,\,\zeta) + (1+\xi)\,\mathbf{F}_3(\eta,\,\zeta) +\\
&\quad + (1+\eta)\,\mathbf{F}_4(\xi,\,\zeta) + (1-\xi)\,\mathbf{F}_5(\eta,\,\zeta) + (1+\zeta)\,\mathbf{F}_6(\xi,\,\eta)\Big]\\
&\quad -\frac{1}{4}\Big[(1-\zeta)\,(1-\eta)\,\mathbf{E}_1(\xi) + (1-\zeta)\,(1+\xi)\,\mathbf{E}_2(\eta) + (1-\zeta)\,(1+\eta)\,\mathbf{E}_3(\xi) +\\
&\quad + (1-\zeta)\,(1-\xi)\,\mathbf{E}_4(\eta) + (1-\xi)\,(1-\eta)\,\mathbf{E}_5(\zeta) + (1+\xi)\,(1-\eta)\,\mathbf{E}_6(\zeta) +\\
&\quad + (1+\xi)\,(1+\eta)\,\mathbf{E}_7(\zeta) + (1-\xi)\,(1+\eta)\,\mathbf{E}_8(\zeta) + (1+\zeta)\,(1-\eta)\,\mathbf{E}_9(\xi) +\\
&\quad + (1+\zeta)\,(1+\xi)\,\mathbf{E}_{10}(\eta) + (1+\zeta)\,(1+\eta)\,\mathbf{E}_{11}(\xi) + (1+\zeta)\,(1-\xi)\,\mathbf{E}_{12}(\eta)\Big]\\
&\quad + N^{\mathrm{N}_1}_{1,1,1}(\xi,\,\eta,\,\zeta)\,\mathbf{X}_1 + N^{\mathrm{N}_2}_{1,1,1}(\xi,\,\eta,\,\zeta)\,\mathbf{X}_2 + N^{\mathrm{N}_3}_{1,1,1}(\xi,\,\eta,\,\zeta)\,\mathbf{X}_3 +\\
&\quad + N^{\mathrm{N}_4}_{1,1,1}(\xi,\,\eta,\,\zeta)\,\mathbf{X}_4 + N^{\mathrm{N}_5}_{1,1,1}(\xi,\,\eta,\,\zeta)\,\mathbf{X}_5 + N^{\mathrm{N}_6}_{1,1,1}(\xi,\,\eta,\,\zeta)\,\mathbf{X}_6 +\\
&\quad + N^{\mathrm{N}_7}_{1,1,1}(\xi,\,\eta,\,\zeta)\,\mathbf{X}_7 + N^{\mathrm{N}_8}_{1,1,1}(\xi,\,\eta,\,\zeta)\,\mathbf{X}_8\,.
\end{aligned}$$

In order to compute the discretization of the weak form (2.29), integrals of functions over element domains or element boundaries and derivatives of functions with respect to global coordinates have to be evaluated. The next section describes the basic approaches. For a detailed description of the implementation of the blending function method into an existing CAD program and its loose coupling to a finite element code, the reader is referred to Bröker [34] and Düster et al. [49].

3.1.2.1 Computation of integrals

The integration of a function F over the hexahedral element domain Ω^h_e, for computing element mass or stiffness matrices or load vectors corresponding to body forces, for example, can be performed on the standard hexahedral element Ω^h_{st}.

$$\int\limits_{\Omega_e^h} F(\mathbf{X})\, dV = \iiint\limits_{\Omega_{st}^h} F(\mathbf{Q_e}(\boldsymbol{\xi}))\, \det \mathbf{J}\, d\xi\, d\eta\, d\zeta \tag{3.25}$$

The Jacobian matrix

$$\mathbf{J} \;=\; \begin{bmatrix} \dfrac{\partial x}{\partial \xi} & \dfrac{\partial y}{\partial \xi} & \dfrac{\partial z}{\partial \xi} \\ \dfrac{\partial x}{\partial \eta} & \dfrac{\partial y}{\partial \eta} & \dfrac{\partial z}{\partial \eta} \\ \dfrac{\partial x}{\partial \zeta} & \dfrac{\partial y}{\partial \zeta} & \dfrac{\partial z}{\partial \zeta} \end{bmatrix} \tag{3.26}$$

is determined by computing the derivatives of the mapping function (3.24).

Similarly, the integrals over element boundaries can be performed on the six surfaces of the standard hexahedral

$$\int\limits_{\partial\Omega_e^h} F\, d\mathbf{A} \;=\; \sum_{i=1}^{6} \iint\limits_{\partial\Omega_{\mathrm{st},i}^{\mathrm{h}} \cap \Gamma_N} F\, \sqrt{E_i\, G_i - F_i^2}\, du\, dv, \tag{3.27}$$

where

$$\begin{aligned} E_i &= \left[\frac{\partial \mathbf{F}_i}{\partial u}\right]^T \left[\frac{\partial \mathbf{F}_i}{\partial u}\right] = \left(\frac{\partial x}{\partial u}\right)^2 + \left(\frac{\partial y}{\partial u}\right)^2 + \left(\frac{\partial z}{\partial u}\right)^2, \\ G_i &= \left[\frac{\partial \mathbf{F}_i}{\partial v}\right]^T \left[\frac{\partial \mathbf{F}_i}{\partial v}\right] = \left(\frac{\partial x}{\partial v}\right)^2 + \left(\frac{\partial y}{\partial v}\right)^2 + \left(\frac{\partial z}{\partial v}\right)^2, \\ F_i &= \left[\frac{\partial \mathbf{F}_i}{\partial u}\right]^T \left[\frac{\partial \mathbf{F}_i}{\partial v}\right] = \frac{\partial x}{\partial u}\frac{\partial x}{\partial v} + \frac{\partial y}{\partial u}\frac{\partial y}{\partial v} + \frac{\partial z}{\partial u}\frac{\partial z}{\partial v} \end{aligned} \tag{3.28}$$

are defined by the first fundamental form of Gauss (see, for example, [65]). The parameters u and v coincide with the local in-plane coordinates of the corresponding face.

For the computation of both the volume integrals and the surface integrals on the standard elements, it is common practice to apply numerical integration procedures, such as the Gaussian quadrature.

3.1.2.2 Computation of derivatives

Besides integrals, the weak form (2.29) also necessitates the computation of derivatives of functions defined on the standard element Ω_{st}^h with respect to the reference coordinates, such as the gradients of $\mathbf{u}$ and $\mathbf{v}$. By means of the discretization (3.3) we can write

$$\operatorname{Grad}\mathbf{u} = \sum_{I=1}^{n} \operatorname{Grad}\mathbf{u}_I N_I = \sum_{I=1}^{n} \mathbf{u}_I \otimes \operatorname{Grad} N_I \tag{3.29}$$

with

$$\operatorname{Grad} N_I = \begin{bmatrix} \frac{\partial N_I}{\partial X} \\ \frac{\partial N_I}{\partial Y} \\ \frac{\partial N_I}{\partial Z} \end{bmatrix} = \begin{bmatrix} \frac{\partial \xi}{\partial X} & \frac{\partial \eta}{\partial X} & \frac{\partial \zeta}{\partial X} \\ \frac{\partial \xi}{\partial Y} & \frac{\partial \eta}{\partial Y} & \frac{\partial \zeta}{\partial Y} \\ \frac{\partial \xi}{\partial Z} & \frac{\partial \eta}{\partial Z} & \frac{\partial \zeta}{\partial Z} \end{bmatrix} \begin{bmatrix} \frac{\partial N_I}{\partial \xi} \\ \frac{\partial N_I}{\partial \eta} \\ \frac{\partial N_I}{\partial \zeta} \end{bmatrix} = \mathbf{J}^{-1} \begin{bmatrix} \frac{\partial N_I}{\partial \xi} \\ \frac{\partial N_I}{\partial \eta} \\ \frac{\partial N_I}{\partial \zeta} \end{bmatrix} \tag{3.30}$$

In (3.30) the chain rule has been applied. Thus, the components of $\operatorname{Grad}\mathbf{u}$ are

$$\operatorname{Grad}\mathbf{u} = \begin{bmatrix} u_{1I}\frac{\partial N_I}{\partial X} & u_{2I}\frac{\partial N_I}{\partial X} & u_{3I}\frac{\partial N_I}{\partial X} \\ u_{1I}\frac{\partial N_I}{\partial Y} & u_{2I}\frac{\partial N_I}{\partial Y} & u_{3I}\frac{\partial N_I}{\partial Y} \\ u_{1I}\frac{\partial N_I}{\partial Z} & u_{2I}\frac{\partial N_I}{\partial Z} & u_{3I}\frac{\partial N_I}{\partial Z} \end{bmatrix}. \tag{3.31}$$

3.1.3 Spatial discretization of the weak form

Having discretized the problem domain into finite elements and element-wise shape functions N_I — using high order hexahedral elements, as described in Section 3.1.1, for instance, — which are C_0-continuous across element boundaries, it is now possible to discretize the weak form (2.30)

$$\begin{aligned} &\int_{\Omega_0} \mathbf{S} : \overbrace{\frac{1}{2}\left(\mathbf{F}^T \operatorname{Grad}\mathbf{v} + \operatorname{Grad}^T \mathbf{v}\,\mathbf{F}\right)}^{\delta\mathbf{E}} dV + \int_{\Omega_0} \rho_0 \ddot{\mathbf{u}} \cdot \mathbf{v}\, dV \\ = &\int_{\partial_N \Omega_0} \mathbf{t} \cdot \mathbf{v}\, d\mathbf{A} + \int_{\Omega_0} \rho_0 \mathbf{b} \cdot \mathbf{v}\, dV, \quad \forall \mathbf{v} \in \mathcal{V},\ \mathbf{v}_{\partial_D \Omega} = 0. \end{aligned} \tag{3.32}$$

The stiffness term $\int_{\Omega_0} \mathbf{S} : \delta\mathbf{E}\, dV$ can be computed for known $\mathbf{S}$ and using for every element Ω_e (3.25), (3.29)– (3.31)

$$\delta\mathbf{E}_e = \frac{1}{2}\sum_{I=1}^{n_{modes}} \left(\mathbf{F}_e^T\left(\mathbf{v}_I \otimes \operatorname{Grad} N_I\right) + \left(\operatorname{Grad}\ N_I \otimes \mathbf{v}_I\right)\mathbf{F}_e\right) \tag{3.33}$$

with

$$\mathbf{F}_e = \operatorname{Grad}\mathbf{x}_e = \operatorname{Grad}\mathbf{u}_e + \mathbf{I} = \sum_{I=1}^{n_{modes}} \mathbf{u}_I \otimes \operatorname{Grad} N_I + \mathbf{I}. \tag{3.34}$$

The symmetric tensor $\delta\mathbf{E}_e$ can be represented in matrix notation

$$\delta\mathbf{E}_e = \begin{bmatrix} \delta E_{11} \\ \delta E_{22} \\ \delta E_{33} \\ 2\delta E_{12} \\ 2\delta E_{23} \\ 2\delta E_{31} \end{bmatrix} = \mathbf{B}_{LI}\,\mathbf{v}_I, \tag{3.35}$$

the matrix

$$\mathbf{B}_{LI} = \begin{bmatrix} F_{11}\dfrac{\partial N_I}{\partial X} & F_{21}\dfrac{\partial N_I}{\partial X} & F_{31}\dfrac{\partial N_I}{\partial X} \\ F_{12}\dfrac{\partial N_I}{\partial Y} & F_{22}\dfrac{\partial N_I}{\partial Y} & F_{32}\dfrac{\partial N_I}{\partial Y} \\ F_{13}\dfrac{\partial N_I}{\partial Z} & F_{23}\dfrac{\partial N_I}{\partial Z} & F_{33}\dfrac{\partial N_I}{\partial Z} \\ F_{11}\dfrac{\partial N_I}{\partial Y} + F_{12}\dfrac{\partial N_I}{\partial X} & F_{21}\dfrac{\partial N_I}{\partial Y} + F_{22}\dfrac{\partial N_I}{\partial X} & F_{31}\dfrac{\partial N_I}{\partial Y} + F_{32}\dfrac{\partial N_I}{\partial X} \\ F_{12}\dfrac{\partial N_I}{\partial Z} + F_{13}\dfrac{\partial N_I}{\partial Y} & F_{22}\dfrac{\partial N_I}{\partial Z} + F_{23}\dfrac{\partial N_I}{\partial Y} & F_{32}\dfrac{\partial N_I}{\partial Z} + F_{33}\dfrac{\partial N_I}{\partial Y} \\ F_{13}\dfrac{\partial N_I}{\partial X} + F_{11}\dfrac{\partial N_I}{\partial Z} & F_{23}\dfrac{\partial N_I}{\partial X} + F_{21}\dfrac{\partial N_I}{\partial Z} & F_{33}\dfrac{\partial N_I}{\partial X} + F_{31}\dfrac{\partial N_I}{\partial Z} \end{bmatrix} \tag{3.36}$$

being linear in $\mathbf{u}$ since $\mathbf{F} = \operatorname{Grad}\mathbf{u} + \mathbf{I}$. Accordingly, with the symmetric tensor $\mathbf{S}_e$ defined on element e in matrix notation

$$\mathbf{S}_e = \begin{bmatrix} S_{11} \\ S_{22} \\ S_{33} \\ S_{12} \\ S_{23} \\ S_{31} \end{bmatrix}, \tag{3.37}$$

the discretized stiffness term is expressed by

$$\begin{aligned}\int_{\Omega_0} \delta\mathbf{E} : \mathbf{S}\, dV &= \bigcup_{e=1}^{n_e} \int_{\Omega_e} \delta\mathbf{E}_e^T \mathbf{S}_e\, dV \\ &= \bigcup_{e=1}^{n_e} \sum_{I=1}^{n_{modes}} \mathbf{v}_I^T \underbrace{\int_{\Omega_e} \mathbf{B}_{LI}^T \mathbf{S}_e\, dV}_{\mathbf{q}_I(\mathbf{u}_e)} \\ &= \bigcup_{e=1}^{n_e} \sum_{I=1}^{n_{modes}} \mathbf{v}_I^T \mathbf{q}_I(\mathbf{u_e}) = \bigcup_{e=1}^{n_e} \mathbf{c}_e^T \mathbf{R}_e(\mathbf{u_e}). = \mathbf{c}^T \mathbf{R}(\mathbf{u}). \end{aligned} \tag{3.38}$$

In (3.38), the vectors $\mathbf{c}_e$ and $\mathbf{R}_e(\mathbf{u}_e)$ contain all the entries $\mathbf{v}_I$ and $\mathbf{q}_I$, respectively, of element e, whereas the vectors $\mathbf{c}$ and $\mathbf{R}(\mathbf{u})$ contain the global assemblies of the vectors $\mathbf{c}_e$ and $\mathbf{R}_e(\mathbf{u}_e)$. This assembly principle applies to all subsequent, element-wise computed quantities. Similarly, it is possible to discretize the mass term using the discretization for the acceleration

$$\ddot{\mathbf{u}} = \sum_{K=1}^{n_{modes}} N_K\, \ddot{\mathbf{u}}_K, \tag{3.39}$$

leading to

$$\int_{\Omega_0} \mathbf{v} \cdot \rho_0 \ddot{\mathbf{u}}\, dV = \bigcup_{e=1}^{n_e} \sum_{I=1}^{n_{modes}} \sum_{K=1}^{n_{modes}} \mathbf{v}_I^T \int_{\Omega_e} N_I \rho_0 N_K\, dV \ddot{\mathbf{u}}_K \tag{3.40}$$

Defining the mass matrix as

$$\mathbf{M}_{IK} \int_{\Omega_e} N_I \rho_0 N_K \mathbf{I}\, dV, \tag{3.41}$$

(3.40) leads to

$$\int_{\Omega_0} \mathbf{v} \cdot \rho_0 \ddot{\mathbf{u}}\, dV = \bigcup_{e=1}^{n_e} \sum_{I=1}^{n_{modes}} \sum_{K=1}^{n_{modes}} \mathbf{v}_I^T \mathbf{M}_{IK} \ddot{\mathbf{u}}_K = \bigcup_{e=1}^{n_e} \mathbf{c}_e^T \mathbf{M}_e \ddot{\mathbf{d}}_e = \mathbf{c}^T \mathbf{M} \ddot{\mathbf{d}}, \tag{3.42}$$

with $\mathbf{c}$, $\mathbf{M}$, $\ddot{\mathbf{d}}$ as the global assemblies of $\mathbf{v}_I$, $\mathbf{M}_{IK}$, $\ddot{\mathbf{u}}_K$, respectively. Finally, the force terms are discretized

$$\int_{\partial_N\Omega_0} \mathbf{v}\cdot\mathbf{t}\,d\mathbf{A} + \int_{\Omega_0} \mathbf{v}\cdot\rho_0\mathbf{b}\,dV$$

$$= \bigcup_{e=1}^{n_e}\sum_{I=1}^{n_{modes}} \mathbf{v}_I^T \left(\underbrace{\int_{\partial_N\Omega_e} N_I\mathbf{t}\,d\mathbf{A} + \int_{\Omega_e} N_I\rho_0\mathbf{b}\,dV}_{\mathbf{p}_I} \right) = \bigcup_{e=1}^{n_e} \mathbf{c}_e^T\mathbf{f}_e = \mathbf{c}^T\mathbf{f}. \tag{3.43}$$

Inserting the discretizations (3.38), (3.42), (3.43) into the weak form (3.32) gives

$$\mathbf{c}^T\left(\mathbf{R}(\mathbf{u}) + \mathbf{M}\ddot{\mathbf{d}} - \mathbf{f}\right) = \mathbf{0} \tag{3.44}$$

and since (3.44) must hold for arbitrary, discretized virtual displacements $\mathbf{v}$ determined by the discrete vector $\mathbf{c}$ and the discretized displacement $\mathbf{u}$ is completely described by the discrete solution vector $\mathbf{d}$,

$$\mathbf{R}(\mathbf{d}) + \mathbf{M}\ddot{\mathbf{d}} - \mathbf{f} = \mathbf{0} \tag{3.45}$$

has to be fulfilled. Equations (3.45) are called the *semidiscrete equations of motion*.

3.1.4 Important simplifications

3.1.4.1 Static equilibrium, linearization and solution procedures

For the static problems discussed in this section, the inertia terms in the equations of motion (3.45) can be disregarded, since an infinitely slow loading is assumed or a steady state is reached due to the damping of the system. Inertia terms will be taken into account for the computation of the eigenfrequencies of a system, see Section 3.1.4.3 or when (3.45) is discretized in time. To make the system (3.45) tractable for numerical solution techniques for nonlinear equations, like the NEWTON-RAPHSON method, it is necessary to provide its linearization. The linearization of the weak form of static equilibrium pertaining to a known point $\bar{\mathbf{u}}$, Equation (2.32), is expressed by

$$\begin{aligned} D\mathcal{W}(\bar{\mathbf{u}},\mathbf{v})[\Delta\mathbf{u}] &= D\int_{\Omega_0} \bar{\mathbf{S}} : \delta\bar{\mathbf{E}}\,dV[\Delta\mathbf{u}] \\ &= \int_{\Omega_0} \mathrm{Grad}\Delta\,\mathbf{u}\,\bar{\mathbf{S}} : \mathrm{Grad}\,\mathbf{v}\,dV + \int_{\Omega_0} \delta\bar{\mathbf{E}} : \mathbb{C} : \bar{D}\mathbf{E}[\Delta\mathbf{u}]\,dV. \end{aligned} \tag{3.46}$$

The bar over a quantity $\bar{\bullet}$ again denotes the evaluation of the quantity at the known point $\bar{\mathbf{u}}$. The discretization of $\mathbf{u}$, $\mathbf{v}$ in the first integral in (3.46), the so-called *initial stress* term, yields

$$
\begin{aligned}
&\int_{\Omega_0} \mathrm{Grad}\Delta\,\mathbf{u}\,\bar{\mathbf{S}} : \mathrm{Grad}\,\mathbf{v}\,dV \\
&= \bigcup_{e=1}^{n_e} \sum_{I=1}^{n_{modes}} \sum_{K=1}^{n_{modes}} \int_{\Omega_e} (\Delta\mathbf{u}_K \otimes \mathrm{Grad}\,N_K)\,\bar{\mathbf{S}}_e : (\mathbf{v}_I \otimes \mathrm{Grad}\,N_I)\;dV \\
&= \bigcup_{e=1}^{n_e} \sum_{I=1}^{n_{modes}} \sum_{K=1}^{n_{modes}} \mathbf{v}_I^T \int_{\Omega_e} \bar{G}_{IK}\mathbf{I}\,dV\,\Delta\mathbf{u}_K
\end{aligned} \tag{3.47}
$$

using the definition

$$
\bar{G}_{IK} = \mathrm{Grad}^T N_I\,\bar{\mathbf{S}}_e\,\mathrm{Grad}\,N_K \tag{3.48}
$$

or in matrix form

$$
\bar{G}_{IK} = \begin{bmatrix} \dfrac{\partial N_I}{\partial X} & \dfrac{\partial N_I}{\partial Y} & \dfrac{\partial N_I}{\partial Z} \end{bmatrix} \begin{bmatrix} \bar{S}_{11} & \bar{S}_{12} & \bar{S}_{13} \\ \bar{S}_{21} & \bar{S}_{22} & \bar{S}_{23} \\ \bar{S}_{31} & \bar{S}_{32} & \bar{S}_{33} \end{bmatrix} \begin{bmatrix} \dfrac{\partial N_K}{\partial X} \\ \dfrac{\partial N_K}{\partial Y} \\ \dfrac{\partial N_K}{\partial Z} \end{bmatrix}. \tag{3.49}
$$

The matrix defined in (3.47) is called the *initial stress matrix*. In the second term in (3.46), $\delta\bar{\mathbf{E}}$ is discretized using (3.33) and the term $\bar{D}\mathbf{E}[\Delta\mathbf{u}]$, which has the same structure as $\delta\bar{\mathbf{E}}$, is discretized by means of

$$
\begin{aligned}
\bar{D}\mathbf{E}_e[\Delta\mathbf{u}] &= \sum_{I=1}^{n_{modes}} \frac{1}{2}\left(\bar{\mathbf{F}}_e^T\,(\Delta\mathbf{u}_I \otimes \mathrm{Grad}\,N_I) + (\mathrm{Grad}\;N_I \otimes \Delta\mathbf{u}_I)\,\bar{\mathbf{F}}_e\right) \\
&= \sum_{I=1}^{n_{modes}} \bar{\mathbf{B}}_{LI}\,\Delta\mathbf{u}_I.
\end{aligned} \tag{3.50}
$$

Inserting into the second term in (3.46) yields

$$
\int_{\Omega_0} \delta\bar{\mathbf{E}} : \mathbb{C} : \bar{D}\mathbf{E}[\Delta\mathbf{u}]\,dV = \bigcup_{e=1}^{n_e} \sum_{I=1}^{n_{modes}} \sum_{K=1}^{n_{modes}} \mathbf{v}_I^T \int_{\Omega_e} \bar{\mathbf{B}}_{LI}^T : \mathbb{C} : \bar{\mathbf{B}}_{LK}\,dV\,\Delta\mathbf{u}_K. \tag{3.51}
$$

Now the discrete linearization is obtained by using (3.47) and (3.51) in (3.46)

$$
\begin{aligned}
D\mathcal{W}(\bar{\mathbf{u}}, \mathbf{v})[\Delta\mathbf{u}] &= \int_{\Omega_0} \left(\mathrm{Grad}\Delta\,\mathbf{u}\,\bar{\mathbf{S}} : \mathrm{Grad}\,\mathbf{v} + \delta\bar{\mathbf{E}} : \mathbb{C} : \bar{D}\mathbf{E}[\Delta\mathbf{u}] \right) dV \\
&= \bigcup_{e=1}^{n_e} \sum_{I=1}^{n_{modes}} \sum_{K=1}^{n_{modes}} \mathbf{v}_I^T \int_{\Omega_e} \bar{G}_{IK}\mathbf{I} + \bar{\mathbf{B}}_{LI}^T : \mathbb{C} : \bar{\mathbf{B}}_{LK}\, dV\, \Delta\mathbf{u}_K \\
&= \bigcup_{e=1}^{n_e} \sum_{I=1}^{n_{modes}} \sum_{K=1}^{n_{modes}} \mathbf{v}_I^T \bar{\mathbf{K}}_{T_{IK}}\, \Delta\mathbf{u}_K = \bigcup_{e=1}^{n_e} \mathbf{c}_e^T \bar{\mathbf{K}}_{T,e}\, \Delta\mathbf{d}_e = \mathbf{c}^T \bar{\mathbf{K}}_T\, \Delta\mathbf{d}. \quad (3.52)
\end{aligned}
$$

Once the linearization (3.52) has been established, it is possible to solve the nonlinear static equilibrium using Newton-Raphson-like methods, see for example Bonet and Wood [33], Wriggers [148]. The basic idea of such methods is first to estimate a solution $\bar{\mathbf{u}} = \mathbf{u}^{iter}$ or $\bar{\mathbf{d}} = \mathbf{d}^{iter}$ in discrete form and then to proceed to a better solution $\mathbf{u} = \mathbf{u}^{iter+1}$ or $\mathbf{d} = \mathbf{d}^{iter+1}$, respectively, in an iterative way. The discrete form of the linearization of (2.32) disregarding the inertia term is

$$
\begin{aligned}
\mathcal{W}(\mathbf{u}, \mathbf{v}) = \mathcal{W}(\bar{\mathbf{u}} + \Delta\mathbf{u}, \mathbf{v}) &\approx \mathcal{W}(\bar{\mathbf{u}}, \mathbf{v}) + D\mathcal{W}(\bar{\mathbf{u}}, \mathbf{v})[\Delta\mathbf{u}] \\
&= \mathbf{c}^T \left(\mathbf{R}(\bar{\mathbf{d}}) + \bar{\mathbf{K}}_T\, \Delta\mathbf{d} - \mathbf{f} \right) = \mathbf{0} \quad (3.53)
\end{aligned}
$$

and since (3.53) must hold for arbitrary, discretized virtual displacements $\mathbf{v}$ determined by the vector $\mathbf{c}$,

$$
\mathbf{R}(\bar{\mathbf{d}}) + \bar{\mathbf{K}}_T\, \Delta\mathbf{d} - \mathbf{f} = \mathbf{0} \quad (3.54)
$$

must be fulfilled. After solving the linear system (3.54) for $\Delta\mathbf{d}$, the improved solution $\mathbf{d}$ — or new iterate $\mathbf{d}^{iter+1}$ — is obtained by

$$
\mathbf{d} = \bar{\mathbf{d}} + \Delta\mathbf{d} \qquad \text{or} \qquad \mathbf{d}^{iter+1} = \mathbf{d}^{iter} + \Delta\mathbf{d}. \quad (3.55)
$$

3.1.4.2 Linear elastostatic problems

The linear elastostatic problem introduced in Section 2.7.1

$$
\mathcal{B}(\mathbf{u}_{EX}, \mathbf{v}) = \mathcal{F}(\mathbf{v}) \quad \forall \mathbf{v} \in \mathcal{V},\, \mathbf{v}_{\partial_D\Omega} = 0, \quad (3.56)
$$

can be discretized, i.e. the discrete solution $\mathbf{u}^{\mathcal{P}} = \mathbf{N}\mathbf{d} = \sum_J \mathbf{N}_J d_J \in \mathcal{S}^{\mathcal{P}}$ is sought, which satisfies for all functions $\mathbf{v}^{\mathcal{P}} = \mathbf{N}\mathbf{c} = \sum_I \mathbf{N}_I c_I \in \overset{\circ}{\mathcal{S}}{}^{\mathcal{P}}$

$$
\begin{aligned}
\sum_J \mathcal{B}(\mathbf{N}_J d_J, \mathbf{N}_I c_I) &= \mathcal{F}(\mathbf{N}_I c_I), \quad (3.57) \\
\Rightarrow \sum_J \mathcal{B}(\mathbf{N}_J d_J, \mathbf{N}_I) &= \mathcal{F}(\mathbf{N}_I), \quad (3.58)
\end{aligned}
$$

where $\mathbf{N}_I$ is the I-th column of $\mathbf{N}$. The space $\overset{\circ}{\mathcal{S}}{}^{\mathcal{P}}$ is the space of all functions in $\mathcal{S}^{\mathcal{P}}$ vanishing on the Dirichlet boundary. Equations (3.58) can be rewritten in matrix form

$$\underbrace{\mathbf{K}\mathbf{d}}_{\mathbf{R}(\mathbf{d})} = \mathbf{f} \tag{3.59}$$

with

$$K_{IJ} = \mathcal{B}(\mathbf{N}_I, \mathbf{N}_J), \tag{3.60}$$

$$f_I = \mathcal{F}(\mathbf{N}_I). \tag{3.61}$$

It is important to note that the stiffness matrix $\mathbf{K}$ in the linear case is independent of $\mathbf{u}$. Accordingly, standard linear equation system solvers can be used to solve for $\mathbf{d}$.

In Section 2.7.1 it was shown that the exact solution minimizes the potential energy. Accordingly, the finite element solution $\mathbf{u}^{\mathcal{P}}$ of space $\mathcal{S}^{\mathcal{P}}$ minimizes the potential with respect to all functions in $\mathcal{S}^{\mathcal{P}}$. For a function $\mathbf{u} = \mathbf{u}^{\mathcal{P}} + \mathbf{w} \in \mathcal{S}^{\mathcal{P}}$ the potential is

$$\begin{aligned}\Pi(\mathbf{u}) &= \Pi(\mathbf{u}^{\mathcal{P}} + \mathbf{w}) \\ &= \frac{1}{2}\mathcal{B}(\mathbf{u}^{\mathcal{P}}, \mathbf{u}^{\mathcal{P}}) - \mathcal{F}(\mathbf{u}^{\mathcal{P}}) + \frac{1}{2}\mathcal{B}(\mathbf{w}, \mathbf{w}) + \underbrace{\mathcal{B}(\mathbf{u}^{\mathcal{P}}, \mathbf{w}) - \mathcal{F}(\mathbf{w})}_{0} \\ &= \Pi(\mathbf{u}^{\mathcal{P}}) + \frac{1}{2}\mathcal{B}(\mathbf{w}, \mathbf{w}).\end{aligned} \tag{3.62}$$

Since $\mathcal{B}(\mathbf{w}, \mathbf{w}) > 0$ for all functions $\mathbf{w} \neq \mathbf{0}$ in $\mathcal{S}^{\mathcal{P}}$ due to the positive definiteness of the bilinear form $\mathcal{B}(\mathbf{u}, \mathbf{v})$, $\mathbf{u}^{\mathcal{P}}$ minimizes the potential with respect to all functions in $\mathcal{S}^{\mathcal{P}}$. Hence, recalling (2.50), one can write

$$\min_{\mathbf{u} \in \mathcal{S}^{\mathcal{P}}} \Pi(\mathbf{u}) = \Pi(\mathbf{u}^{\mathcal{P}}) = \Pi(\mathbf{u}_{EX} + \mathbf{e}^{\mathcal{P}}) = \Pi(\mathbf{u}_{EX}) + \frac{1}{2}\mathcal{B}(\mathbf{e}^{\mathcal{P}}, \mathbf{e}^{\mathcal{P}}) \tag{3.63}$$

with the error in energy of the finite element solution $\mathbf{e}^{\mathcal{P}} = \mathbf{u}_{EX} - \mathbf{u}^{\mathcal{P}}$. From (3.63) it is evident that $\mathbf{u}^{\mathcal{P}}$ not only minimizes the potential but also the error in *strain energy* $\frac{1}{2}\mathcal{B}(\mathbf{e}^{\mathcal{P}}, \mathbf{e}^{\mathcal{P}})$ and, equivalently, the error in *energy norm* $\|\mathbf{e}^{\mathcal{P}}\|_E$ defined as

$$\|\mathbf{e}^{\mathcal{P}}\|_E^2 = \frac{1}{2}\mathcal{B}(\mathbf{e}^{\mathcal{P}}, \mathbf{e}^{\mathcal{P}}). \tag{3.64}$$

A sequence of hierarchically nested finite element spaces $S^{\mathcal{P}_1} \subset S^{\mathcal{P}_2} \subset S^{\mathcal{P}_3} \subset ...$ results in a corresponding sequence of potentials and errors in energy norm

$$\Pi(\mathbf{u}^{\mathcal{P}_1}) \geq \Pi(\mathbf{u}^{\mathcal{P}_2}) \geq \Pi(\mathbf{u}^{\mathcal{P}_3}) \geq ... \tag{3.65}$$

$$\|\mathbf{e}^{\mathcal{P}_1}\|_E \geq \|\mathbf{e}^{\mathcal{P}_2}\|_E \geq \|\mathbf{e}^{\mathcal{P}_3}\|_E \geq ... \tag{3.66}$$

The monotone minimization of the error in strain energy norm using hierarchic spaces such as those defined in Section 3.1.1 will be exploited in Chapter 5 to serve as a basis for a p-adaptive strategy for linear elastostatic problems.

3.1.4.3 Harmonic vibrations

The discrete form of the eigenvalue problem describing harmonic vibrations (2.58) with the discretization $\mathbf{u}_k^{\mathcal{P}} = \mathbf{N}\boldsymbol{\phi}_k = \sum_J \mathbf{N}_J \phi_{k,J} \in \overset{\circ}{S}{}^{\mathcal{P}}$, $\mathbf{v}^{\mathcal{P}} = \mathbf{N}\mathbf{c} = \sum_I \mathbf{N}_I c_I \in \overset{\circ}{S}{}^{\mathcal{P}}$ is

$$\begin{aligned} \sum_J \mathcal{B}(\mathbf{N}_J\phi_{k,J}, \mathbf{N}_I c_I) - \lambda_k \mathcal{D}(\mathbf{N}_J\phi_{k,J}, \mathbf{N}_I c_I) &= 0 \\ \Rightarrow \sum_J \mathcal{B}(\mathbf{N}_J\phi_{k,J}, \mathbf{N}_I) - \lambda_k \mathcal{D}(\mathbf{N}_J\phi_{k,J}, \mathbf{N}_I) &= 0 \end{aligned} \tag{3.67}$$

Alternatively, the system can be rewritten equally well in matrix form

$$\mathbf{K}\boldsymbol{\phi}_k - \lambda_k \mathbf{M}\boldsymbol{\phi}_k = \mathbf{0} \tag{3.68}$$

with the stiffness matrix $\mathbf{K}$ defined in (3.61) and the mass matrix $\mathbf{M}$ defined in (3.41), or in the alternative notation using bilinear forms,

$$M_{IJ} = \mathcal{D}(\mathbf{N}_I, \mathbf{N}_J). \tag{3.69}$$

A block Lanczos eigensolver was implemented for solving the discrete eigenproblem (3.67), see Schwarz [127, 128] and Rabold [112].

Similarly to (2.63) and (2.65) it is evident that the finite element eigenfunction $\mathbf{u}_k^{\mathcal{P}}$ minimizes the Rayleigh quotient $\rho(\mathbf{u})$ with respect to all functions in $\overset{\circ}{S}{}^{\mathcal{P}}_{k\perp}$

$$\min_{\mathbf{u}\in\overset{\circ}{S}{}^{\mathcal{P}}_{k\perp}} \rho(\mathbf{u}) = \rho(\mathbf{u}_k^{\mathcal{P}}) = (\omega_k^{\mathcal{P}})^2 = \rho(\mathbf{u}_k + \mathbf{e}_k^{\mathcal{P}}), \tag{3.70}$$

the finite element error of the eigenfunction being $\mathbf{e}_k^{\mathcal{P}} = \mathbf{u}_k - \mathbf{u}_k^{\mathcal{P}}$. Therefore, a sequence of hierarchically nested finite element spaces $\overset{\circ}{S}{}^{\mathcal{P}_1} \subset \overset{\circ}{S}{}^{\mathcal{P}_2} \subset \overset{\circ}{S}{}^{\mathcal{P}_3} \subset ...$ results in a corresponding sequence of eigenfrequencies

$$\omega_k^{\mathcal{P}_1} \geq \omega_k^{\mathcal{P}_2} \geq \omega_k^{\mathcal{P}_3} \geq \dots . \tag{3.71}$$

The monotone minimization of the frequencies using hierarchic spaces such as those defined in Section 3.1.1 will be exploited in Chapter 6 to serve as a basis for a p-adaptive strategy for linear elastodynamic problems.

3.2 Time discretization

The semidiscrete equations of motion derived in Section 3.1.3 read

$$\mathbf{R}(\mathbf{d}) + \mathbf{M}\ddot{\mathbf{d}} - \mathbf{f} = \mathbf{0}. \tag{3.72}$$

It is known from experience that vibrations are damped as a result of friction or viscous behavior. Damping effects are frequently modeled by inserting an additional damping term $\mathbf{C}\dot{\mathbf{d}}$ with the constant damping matrix $\mathbf{C}$. In many applications the damping matrix is a linear combination of the mass and the stiffness matrix, $\mathbf{C} = a\mathbf{K} + b\mathbf{M}$, which is referred to as Rayleigh damping and has certain advantages in the modal analysis of linear elastodynamic calculations, see Bathe [26], for example. With the additional damping term the semidiscrete equations of motion are given as

$$\mathbf{R}(\mathbf{d}) + \mathbf{C}\dot{\mathbf{d}} + \mathbf{M}\ddot{\mathbf{d}} - \mathbf{f} = \mathbf{0}. \tag{3.73}$$

These equations have to be fulfilled at every time t. To complete the definition of the initial value problem, it is necessary to prescribe initial conditions at $t_0 = 0$:

$$\mathbf{d}(t_0) = \bar{\mathbf{d}}_0, \tag{3.74}$$
$$\dot{\mathbf{d}}(t_0) = \bar{\dot{\mathbf{d}}}_0. \tag{3.75}$$

Since it is not usually possible to find analytical solutions of (3.73), numerical *time integration methods* are called for. Hulbert [74] provides a very good overview of existing approaches. Again, it is possible to apply finite element techniques leading to space-time finite element formulations, see for example Hughes and Hulbert [73], Johnson [75], Li and Wiberg [86], Maute [91], Neumann [95].

However, most codes use finite difference based time integration methods. Depending on the type of problem to be solved, one may choose between either *explicit* or *implicit* methods. Explicit methods are simple to implement since the solution at timestep t_{n+1} only depends on quantities defined at t_n. Since the computation of a single timestep involves just very low computational cost, the time domain can be resolved using very small timesteps, which may possibly be necessary for problems involving impact or shock waves traveling through elastic media, for example. Unfortunately, the timestep size for explicit time integration schemes is always restricted due to stability criteria, thus making long-term integration virtually impossible.

Implicit time integration methods substitute the time derivatives in (3.73) by quantities defined at times t_n as well as t_{n+1}. Therefore, in every timestep the solution of a — possibly nonlinear — equation system is required. This additional effort can be compensated by selecting a very large timestep size and constructing unconditionally stable integration schemes is feasible.

3.2.1 Implicit time integration methods based on NEWMARK's formulae

In this work, an implicit finite difference based method, the generalized α-method, has been implemented, this being a generalization of the NEWMARK method [97], which in turn is probably the most popular time integration scheme for finite element systems of type (3.73) of the last 30 years. The NEWMARK algorithm is based on the following approximations at time t_{n+1}:

$$\mathbf{d}_{n+1} = \mathbf{d}_n + \Delta t\, \dot{\mathbf{d}}_n + \frac{\Delta t^2}{2}\left[(1-2\beta)\, \ddot{\mathbf{d}}_n + 2\beta \ddot{\mathbf{d}}_{n+1}\right], \tag{3.76}$$

$$\dot{\mathbf{d}}_{n+1} = \dot{\mathbf{d}}_n + \Delta t\left[(1-\gamma)\, \ddot{\mathbf{d}}_n + \gamma \ddot{\mathbf{d}}_{n+1}\right]. \tag{3.77}$$

These formulae can be rewritten such that $\dot{\mathbf{d}}_{n+1}$, $\ddot{\mathbf{d}}_{n+1}$ can be expressed by $\mathbf{d}_{n+1}$ being the only unknown quantity at the new timestep t_{n+1}

$$\dot{\mathbf{d}}_{n+1} = \frac{\gamma}{\beta\,\Delta t}(\mathbf{d}_{n+1} - \mathbf{d}_n) + (1 - \frac{\gamma}{\beta})\dot{\mathbf{d}}_n + (1 - \frac{\gamma}{2\beta})\Delta t \ddot{\mathbf{d}}_n, \tag{3.78}$$

$$\ddot{\mathbf{d}}_{n+1} = \frac{1}{\beta\,\Delta t^2}(\mathbf{d}_{n+1} - \mathbf{d}_n) + \frac{1}{\beta\,\Delta t}\dot{\mathbf{d}}_n + \left(\frac{1-2\beta}{2\beta}\right)\ddot{\mathbf{d}}_n \tag{3.79}$$

Inserting (3.78), (3.79) into the equations of motion (3.73) leads to the nonlinear equation system

$$\begin{aligned}\mathbf{G}(\mathbf{d}_{n+1}) &= \mathbf{M}\left[\frac{1}{\beta\,\Delta t^2}(\mathbf{d}_{n+1} - \mathbf{d}_n) + \frac{1}{\beta\,\Delta t}\dot{\mathbf{d}}_n + \left(\frac{1-2\beta}{2\beta}\right)\ddot{\mathbf{d}}_n\right] \\ &+ \mathbf{C}\left[\frac{\gamma}{\beta\,\Delta t}(\mathbf{d}_{n+1} - \mathbf{d}_n) + (1 - \frac{\gamma}{\beta})\dot{\mathbf{d}}_n + (1 - \frac{\gamma}{2\beta})\Delta t \ddot{\mathbf{d}}_n\right] \\ &+ \mathbf{R}(\mathbf{d}_{n+1}) - \mathbf{f}_{n+1} = \mathbf{0}.\end{aligned} \tag{3.80}$$

With the tangential stiffness matrix $\mathbf{K}_T(\mathbf{d}_{n+1}^{iter})$ as defined in (3.52), the linearization of (3.80) results in

$$\mathbf{K}_T^* \Delta \mathbf{d}_{n+1}^{iter+1} = -\mathbf{G}(\mathbf{d}_{n+1}^{iter}) \tag{3.81}$$

with

$$\mathbf{K}_T^* = \frac{1}{\beta\,\Delta t^2}\mathbf{M} + \frac{\gamma}{\beta\,\Delta t}\mathbf{C} + \mathbf{K}_T(\mathbf{d}_{n+1}^{iter}) \tag{3.82}$$

often called the *dynamic stiffness matrix*.

HUGHES [72] postulates the following attributes of a time integration scheme in order to be competitive:

1. Unconditionally stable when applied to linear problems
2. No more than one set of implicit equations to be solved at each timestep
3. Second order accuracy
4. Controllable algorithmic dissipation of higher modes
5. Self-starting

The NEWMARK algorithm is self-starting and only one implicit set of equations has to be solved, therefore requirements 2 and 5 are fulfilled. The attributes 1, 3 and 4 depend on the NEWMARK parameters β, γ, see [72], [26], [91], [95] for details.

For linear problems and for $2\beta \geq \gamma \geq \frac{1}{2}$, NEWMARK's algorithm is unconditionally stable. For $\gamma > \frac{1}{2}$ algorithmic dissipation is introduced, i.e. the system is damped numerically which may be desired to damp artificial higher vibration modes. However, the only combination of parameters guaranteeing second order accuracy of the integration method is $\beta = \frac{1}{4}$ in conjunction with $\gamma = \frac{1}{2}$, i.e. attributes 3 and 4 are mutually exclusive.

Many methods have been developed to overcome these difficulties. A very popular approach is the generalized α-method, see CHUNG and HULBERT [38], using the NEWMARK formulae (3.76) and (3.77) as well, but differently weighting the force terms in the equation of motion (3.73) by introducing the additional parameters α_f, α_m

$$\mathbf{M}\ddot{\mathbf{d}}_{n+1-\alpha_m} + \mathbf{C}\dot{\mathbf{d}}_{n+1-\alpha_f} + \mathbf{R}_{n+1-\alpha_f} = \mathbf{f}(t_{n+1-\alpha_f}). \tag{3.83}$$

with

$$\begin{aligned}
t_{n+1-\alpha_f} &= (1-\alpha_f)t_{n+1} + \alpha_f t_n, && (3.84)\\
\mathbf{R}_{n+1-\alpha_f} &= (1-\alpha_f)\mathbf{R}(\mathbf{d}_{n+1}) + \alpha_f \mathbf{R}(\mathbf{d}_n), && (3.85)\\
\dot{\mathbf{d}}_{n+1-\alpha_f} &= (1-\alpha_f)\dot{\mathbf{d}}_{n+1} + \alpha_f \dot{\mathbf{d}}_n, && (3.86)\\
\ddot{\mathbf{d}}_{n+1-\alpha_m} &= (1-\alpha_m)\ddot{\mathbf{d}}_{n+1} + \alpha_m \ddot{\mathbf{d}}_n. && (3.87)
\end{aligned}$$

$\mathbf{R}_{n+1-\alpha_f}$ in (3.85) is defined in analogy to CRISFIELD [41], see HEISSERER [68], for instance. An alternative option would be $\mathbf{R}_{n+1-\alpha_f} = \mathbf{R}(\mathbf{d}_{n+1-\alpha_f})$, see for example WRIGGERS [148].

The generalized α-method eliminates the mutual exclusion of second order accuracy and algorithmic damping for linear problems. An analysis of the method is given in CHUNG and HULBERT [38], for example, concluding that second order accuracy, unconditional stability and maximized algorithmic damping are achieved with

$$\gamma = \frac{1}{2} - \alpha_m + \alpha_f, \tag{3.88}$$

$$\beta = \frac{1}{4}(1 - \alpha_m + \alpha_f)^2 \tag{3.89}$$

$$\alpha_m = \frac{2\rho_\infty - 1}{\rho_\infty + 1} \tag{3.90}$$

$$\alpha_f = \frac{\rho_\infty}{\rho_\infty + 1}. \tag{3.91}$$

ρ_∞ is the user-specified value for high frequency damping. $\rho_\infty = 1$ corresponds to no algorithmic damping, $\rho_\infty = 0$ results in maximum algorithmic high frequency dissipation.

The generalized α-method reduces for $\alpha_m = 0$ to the HHT-α method proposed by Hilber, Hughes and Taylor [70] and with $\alpha_f = 0$ the WBZ-α method proposed by Wood, Bossak and Zienkiewicz [147] is obtained.

3.3 Numerical example

Although the generalized α-method has been investigated extensively for low-order finite element approximations, only little is known about its suitability to high-order elements, especially for the case of thin solid elements. To verify the p-version code and to illustrate the differences between linear and nonlinear vibrations, the transient forced response of the clamped plate depicted in Figure 3.4 is computed. The length of the quadratic plate is $L = 12$, the thickness equals to $t = 0.06$, Young's modulus is $E = 2.1 \cdot 10^{11}$, Poisson's ratio is $\nu = 0.3$ and the density is $\rho = 7850$. The uniform face load starting to act in negative z-direction on the upper surface at $t_0 = 0$ is constant over time, $t_z = -5692$.

The plate is discretized into 49 high order hexahedral elements with a uniform polynomial degree $p = 5$ in all directions for all elements. For the time discretization, the generalized α-method was used with a timestep size of $\Delta t = 0.0003375$ and $\rho_\infty = 0.8$. Both the geometric linear and geometric nonlinear behavior were taken into consideration when computing the problem and the results were compared to corresponding results obtained by Yosibash and Kirby [150] and Kirby and Yosibash [80] using a spectral element approach for solving the two-dimensional, geometric linear Kirchhoff plate model and the two-dimensional, geometric nonlinear von-Kármán plate model, see also Section 2.7.3. In Figure 3.5 the centerpoint displacement is plotted over time. The congruity between the three-dimensional and the two-dimensional approach is evident for this thin plate for both the geometrically linear and the nonlinear computation. For this example it is obvious that consideration of nonlinear effects is necessary.

No use has been made so far of anisotropic Ansatz spaces, however. Following the survey of adaptive methods in general in Chapter 4, an anisotropic p-adaptive method is proposed for linear elastostatic problems in Chapter 5 and for linear elastodynamic problems in Chapter 6.

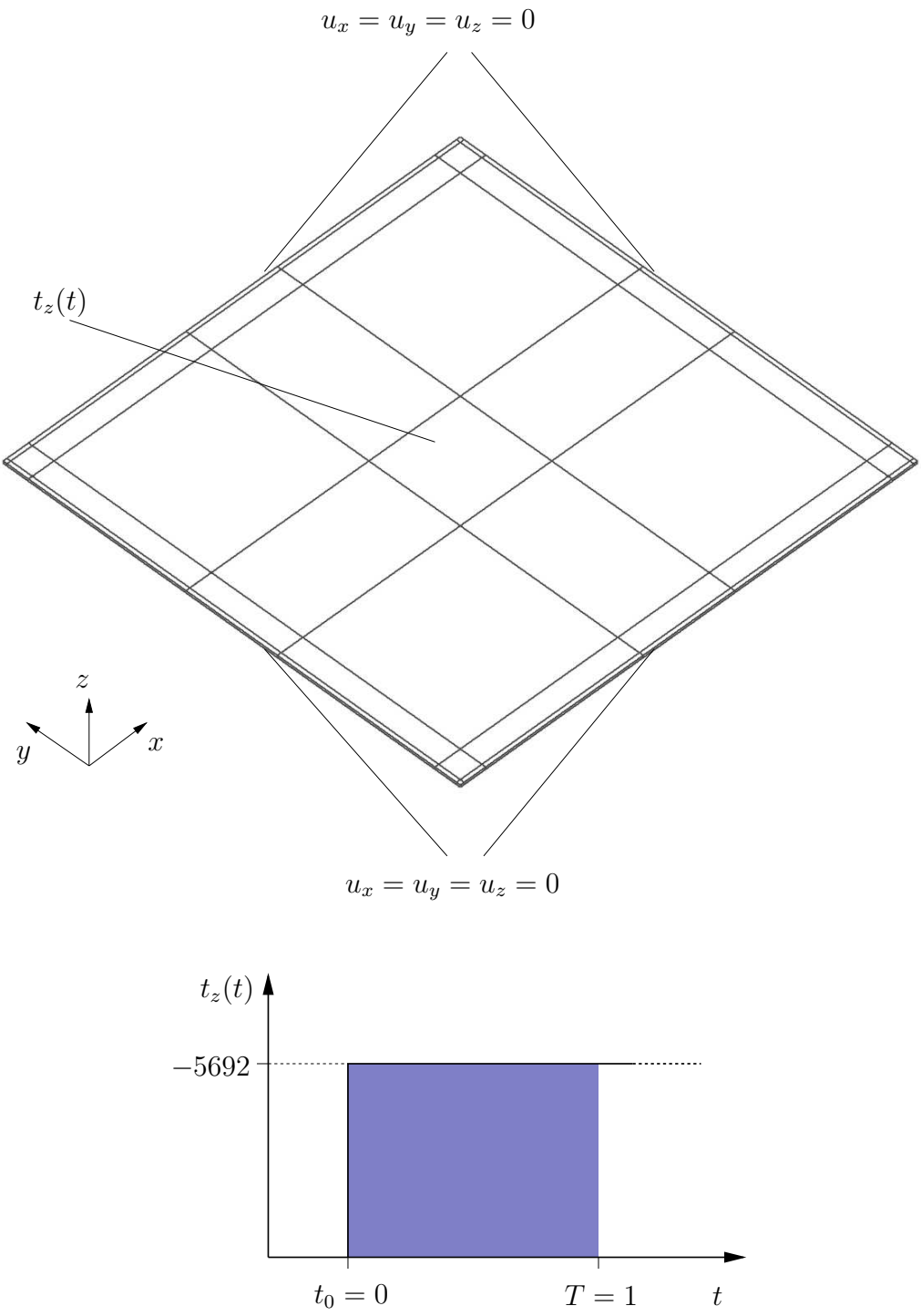

Figure 3.4: System and hexahedral mesh of clamped plate (top) and load function over time $t_z(t)$ (bottom)

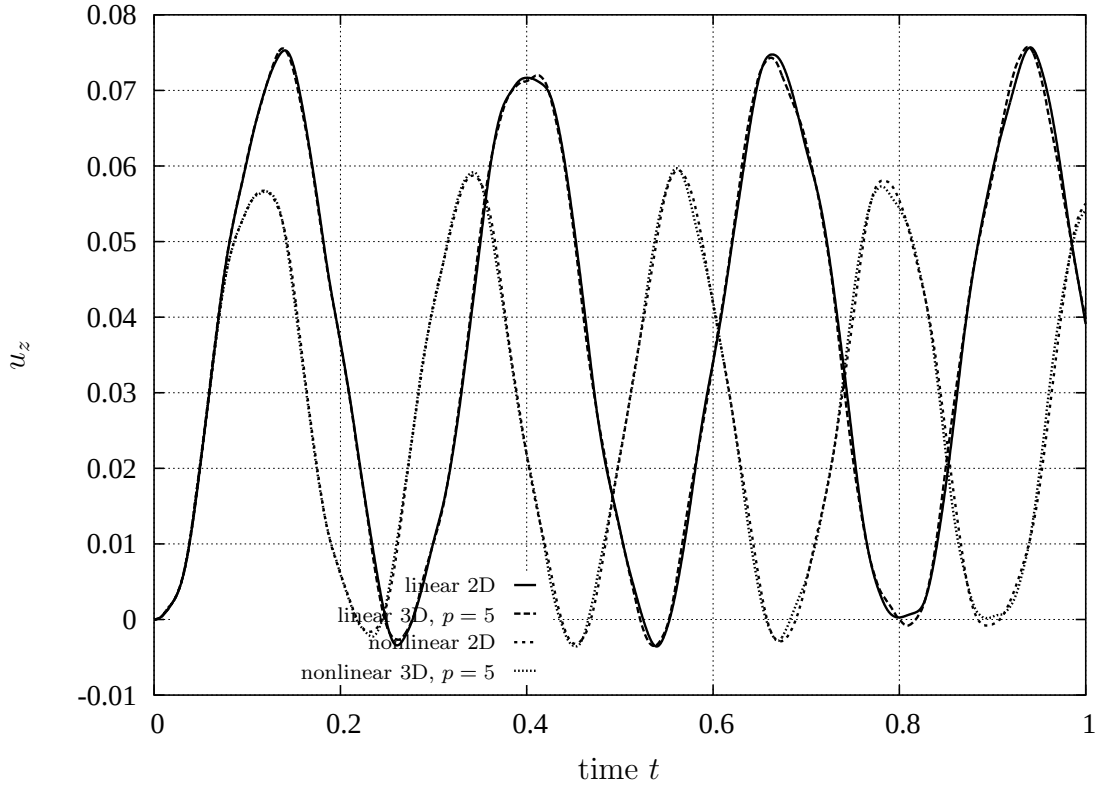

Figure 3.5: Centerpoint displacements of plate over time

Chapter 4

Error control and adaptive methods

Chapter 2 dealt with physical and mathematical models for mechanical systems which can be solved numerically using different discretization techniques, see Chapter 3. This chapter addresses the problem of how to select a model and a corresponding discretization *efficiently* and *sufficiently*. In general, a user of a simulation code has questions about the qualitative and/or quantitative behavior of a physical system under certain conditions. A *sufficient* model for this system takes all the important physical mechanisms that determine its behavior into account; a *sufficient* discretization resolves the model with the accuracy necessary to answer the user's questions, just as if he knew the exact solution. By contrast, *efficient* models and discretizations might be preferred from the point of view of computational costs, leading to savings in resources like computational time and memory usage needed for providing the desired answers. These requirements on models and discretizations give rise to *error control* and *adaptive* methods for the simulation of physical problems.

Types of error

Different types of errors can be identified during the simulation process. The first step — finding an adequate physical and mathematical model — involves a so-called *model error*. This error comes from a defect in the chosen model caused by simplifications introduced in order to make a problem more tractable. In material modeling this might be the assumption of linear material behavior instead of considering nonlinear effects, or homogenization techniques instead of resolving inhomogeneous microstructures, for concrete, composite structures or foams, for instance.

Simplified kinematic assumptions are often made for displacements in thickness direction in the case of thin-walled structures like plates and shells, i.e. displacements varying linearly over thickness only, for example. This kind of model assumption is frequently referred to as *dimensional reduction*.

Since it is not usually possible to obtain an analytical solution to the chosen mathematical model, the model is solved using numerical methods like finite difference methods or finite element methods, see Chapter 3, involving the so-called *discretization error*. Finite difference methods, for example, approximate differential terms by difference terms and the original differential equation is approximated at a finite number of points only. Finite element methods

fulfill the original differential equation in an integral sense, using a finite subspace of all admissible functions for Ansatz and test functions. In order to solve mathematical models, it is also possible to apply different discretization methods simultaneously. For instance, finite difference methods might be used for the time integration of structural dynamics problems, whereas the spatial domain is discretized by means of finite elements. Further *numerical errors* may be added by approximate solutions of resulting equation systems or eigenvalue problems.

Another source of errors is the uncertainty of data. Most physical and mathematical models fail to take the scatter of input parameters into account. Material data in particular are subject to stochastic variations and even small geometric imperfections can introduce substantial deviations in the physical model concerned. Although it is normally referred to as an extra kind of error, uncertainty can also be counted among the *model errors*, as in [103], for instance, since the stochastic variations, such as stochastic coefficients, may be included in the mathematical model. There are already several methods available for solving stochastic models. One method is to create a significant set of input data variants representing the stochastic distributions and to compute each set using standard discretization methods, followed by a post-processing step to compute corresponding sample averages, like the expected value of the solution, by means of the Monte Carlo method, for example. Another alternative is to approximate the stochastic distribution directly using numerical methods, such as the finite element method. See [19] and the literature cited therein, for instance, for an overview of solution methods for stochastic mathematical models.

All these types of errors can have a significant impact on the quality of the solution. It is therefore important that the errors are controlled, i.e. a measure for the error should be provided. Since the exact solution is usually unknown, this involves formulating error estimates, as set out in the overview of discretization error estimates contained in Sections 4.1 and 4.2. Providing a prescribable error tolerance — absolute or relative — would be a great advantage. Ideally, model and discretization should be adapted to the problem automatically, both being refined only in those areas of the domain where this is really called for, until the total model and discretization error drops below the prescribed upper limit.

Adaptivity

Model adaptivity is a relatively new concept. The basic idea is a hierarchical expansion from coarse, simplified models to finer models, through to sufficiently descriptive mathematical models. In order to estimate the error, a coarse solution is compared to a — usually locally computed — finer solution. If the difference in a certain norm is significant, the model can be expanded locally for any subsequent iteration. For model adaptivity with respect to the material, see for example, [93, 107, 108, 109, 110, 132, 134, 133, 139]. For dimensional adaptivity, i.e. adaption of kinematic assumptions over thickness for thin-walled structures, see [37, 104, 108, 125, 131, 132, 134, 133]. It should be noted that, when using a fully three dimensional model, the dimensional model error vanishes, i.e. is completely transferred to a discretization error.

Oden and Babuška [103] discuss the problem of uncertainties and propose error estimates for material data with stochastic variations. Once proper error estimates are at hand, adaptive

methods can be developed investing computational costs where the error of the computation is large, usually in areas of stochastic distributions with a strong influence on the solution. Using either Monte Carlo-like methods or a numerical approximation of the stochastic distributions, adaptive refinement in such critical areas could lead to efficient solution schemes.

Adaptive control of the discretization error is already well established for many types of problems, and it is fairly widespread for linear elastostatic problems in particular. In the following, different adaptive strategies are listed for the spatial discretization using the finite element method.

A fairly rational approach for adapting the discretization to the solution is to decrease the element sizes in areas where major errors occur, referred to as *h-adaptivity*. The element sizes can be reduced by dividing elements of the original mesh on a local level and using transition elements between unrefined and refined areas, which usually are not ideally shaped and consequently tend to cause numerical difficulties. Another option is to introduce hanging nodes which have to be coupled with the adjacent edges in order to avoid discontinuities and therefore cause additional overhead. Other approaches are based on creating a completely new mesh refined according to a density function using an adaptive, unstructured mesh generator, see SCHWEINGRUBER [129], RANK et al. [115], for instance.

Alternatively, the accuracy of the solution can be enhanced adaptively by locally increasing the polynomial degrees p of elements with major errors, called *p-adaptivity*. By increasing p, the number of degrees of freedom of the corresponding element increases accordingly. One main advantage of p-adaptive methods is that the mesh remains unchanged. A p-adaptive method is proposed in Chapters 5 and 6.

Another possibility of increasing the accuracy adaptively is by keeping the topology of the meshes but relocating the nodes and edges, referred to as *r-adaptivity*. In this way the density of elements can be adaptively increased in areas with a substantial error without introducing new elements or degrees of freedom. Moreover, irregular solutions on the domain Ω with discontinuities, like shock waves or plastic interfaces, can be divided into regular patches by relocating element boundaries onto these singularities. The drawbacks of pure r-adaptive methods are obvious: The accuracy of the method is limited for most problems since no additional degrees of freedom are introduced. In addition, the relocation of the element boundaries may lead to seriously distorted elements, causing numerical difficulties.

Each of these three basic methods for discretization adaptivity have advantages and disadvantages, which will be discussed in more detail in Section 4.1.1, where they are motivated in terms of convergence rates. In addition, important combinations like *hp-* and *rp-adaptive methods* are introduced at that point.

Error estimators

The basis of every adaptive approach is to estimate the error of a current discretization and give an indication of areas where refinement is necessary. Several terms classifying error estimates are described below.

An important distinction is made between *a priori* and *a posteriori* error estimates. A priori error estimates are based on general knowledge concerning the type of the solution to be computed, e.g. the boundedness of derivatives. They can provide information on the convergence behavior of different refinement strategies rather than presenting a reasonable indication for the areas to be refined. This type of error estimator is described in Section 4.1.1 for time-independent problems. Conversely, *a posteriori* error estimates make use of information contained in a solution that has already been computed. They can be computed explicitly by evaluating the residuals, implicitly by extending the Ansatz spaces, by recovery, i.e. by smoothing a solution, by extrapolation, etc. A posteriori error estimators for time-independent problems are described in Section 4.1.2. Some of these concepts, however, have already been applied successfully to time-dependent problems, see Section 4.2.

Another criterion distinguishes between *bounded* and *unbounded* error estimators. Upper bounds can be derived from primal variational forms, lower bounds from dual variational forms [132]. In contrast to *absolute* error estimators yielding quantitative estimates, relative estimates are computed up to an interpolation constant C, like the explicit Babuska-Miller estimator, for instance, see Section 4.1.2. Estimators predicting *global* error quantities, such as the error in energy norm, are called *global* error estimators; estimators for local quantities, like displacements or stresses in specific points or partitions, are known as *local* error estimators, which call for the solution of a dual problem, see Section 4.1.2.

Error *indicators* are local quantities indicating areas where refinement is necessary. Thus, adaptive processes can be controlled with the help of error indicators. In some citations, as well, unbounded error quantities are referred to as error indicators, e.g. [132].

The outline of the remainder of this chapter is as follows: Section 4.1 deals with a priori and a posteriori estimators for time-independent problems and proposes adaptive strategies. Some of the concepts are extended to time-dependent problems in Section 4.2 and additional topics resulting from the transient behavior are addressed, the transfer of history variables between different adaptive spatial discretizations and adaptive time integration being two cases in point. Adaptivity for eigenvalue problems will be discussed in Section 4.3 and some remarks on model adaptivity are given in Section 4.4.

4.1 Adaptivity for time-independent problems

4.1.1 A priori error estimates and convergence rates

There is a vast amount of literature and results on a priori error estimates and convergence rates for linear elliptic problems, such as [7, 16, 17, 18, 61, 62, 63, 126, 136]. In this section, an a priori estimate is derived for a simple, one-dimensional problem according to Szabó and Babuška [136], to show the principal approach. In the remainder, results of a priori estimates for two-dimensional and three-dimensional problems are summarized, as suggested in Szabó et al. [137], and adaptive h-, p- and r-methods, and hp- and rp-methods as combinations thereof, are discussed in the context of convergence rates.

Example: 1D, uniform h-refinement

An a priori error estimator shall be derived for the model problem of a one dimensional bar, given in the weak form

$$\int_0^l AE\, u'_{EX}\, v'\, dx \;=\; \int_0^l f\, v\, dx \quad \text{for all} \quad v \in \mathcal{V},\, v_{\partial\Omega_D} = 0, \tag{4.1}$$

where u_{EX} fulfills the boundary conditions. The first step is to restrict our scope to a certain class of solutions u_{EX}, i.e. AE and f are chosen for the following considerations such that

$$|u''_{EX}| \;\leq\; C, \quad 0 \leq x \leq l. \tag{4.2}$$

Our aim is to obtain an a priori estimate for a uniform h-version, therefore the bar is divided uniformly into $n_{el} = n$ elements, each element measuring $\frac{l}{n}$ in length. The piecewise linear interpolant of u_{EX} is called u_n and satisfies

$$u_n \;=\; u_{EX}(jh), \quad j = 0, ..., n. \tag{4.3}$$

The interpolation error in the kth element is

$$\bar{e}_k(x) \;=\; u_{EX}(x) - u_n(x), \quad (k-1)h \leq x \leq kh. \tag{4.4}$$

Since u_n is the interpolant of u_{EX}, $\bar{e}_k$ vanishes at the endpoints of each element, and there is a point $\bar{x}_k$ where $\bar{e}_k$ is maximum. Therefore, at this point $\bar{e}'_k = 0$, as illustrated in Figure 4.1. For this reason, and since the second derivative of the linear interpolant vanishes, $u''_n = 0$,

$$\bar{e}'_k(x) \;=\; \int_{\bar{x}_k}^x \bar{e}''_k(t)\, dt = \int_{\bar{x}_k}^x u''_{EX}(t)\, dt, \quad (k-1)h \leq x \leq kh. \tag{4.5}$$

With our assumption (4.2) with regard to the boundedness of u''_{EX}, we have

$$\max |\bar{e}'_k(x)| \;\leq\; hC, \quad (k-1)h \leq x \leq kh. \tag{4.6}$$

and accordingly

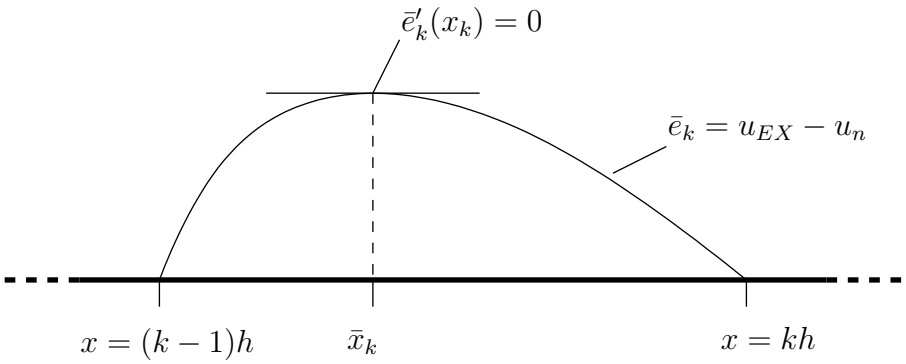

Figure 4.1: Difference $\bar{e}_k$ between exact solution u_{EX} and linear interpolant u_n between exact nodal points

$$E_{str}(\bar{e}) = \frac{1}{2}\int_0^l AE\,(\bar{e}')^2\,dx = \frac{1}{2}\sum_{k=1}^{n}\int_{(k-1)h}^{kh} AE\,(\bar{e}'_k)^2\,dx \tag{4.7}$$

$$\leq \frac{1}{2} n\,h\,K\,(C\,h)^2 = \frac{1}{2} l\,K\,C^2\,h^2 \tag{4.8}$$

with $AE(x) \leq K$. Since K and C are independent of h, and the energy of the error of the finite element solution $e = u_{EX} - u_{FE}$ is less than, or equal to that of any other piecewise linear function with the same nodal points, see Section 3.1, we can write

$$\|e\|_E = \sqrt{E_{str}(e)} \leq k\,C\,h. \tag{4.9}$$

It should be mentioned that in this special, one-dimensional example $u_{FE}(jh) = u_{EX}(jh)$, $j = 0, ..., n$. Nevertheless, this equality is not necessary for the general approach. Using $N \approx \frac{l}{h}$, (4.9) can alternatively be written as

$$\|e\|_E \leq \frac{k}{N}, \tag{4.10}$$

where k has a different value from that in Equation (4.9). Where N is large, the '$\leq$' can be substituted by '$\approx$' and we can rewrite (4.10)

$$\log \|e\|_E = \log k - \log N, \tag{4.11}$$

i.e. when plotting $\|e\|_E$ in a double logarithmic scale, we get a curve with the slope -1. In other words, for $p = 1$, uniform h-refinement and the assumption (4.2) we obtain a rate of convergence $\beta = 1$.

This simple example has been chosen to demonstrate how to obtain rates of convergence for a certain class of problems and for a specific discretization technique using the interpolation theory.

Overview of a priori error estimates in 1D

In a similar manner, it is possible to find a priori estimates for different discretization techniques, leading to the general forms for algebraic convergence

$$\|e\|_E \leq \frac{k}{N^\beta} \tag{4.12}$$

and for exponential convergence

$$\|e\|_E \leq \frac{k}{\exp(\gamma N^\theta)}. \tag{4.13}$$

Figure 4.2. shows different types of convergence curves. Curve type I corresponds to algebraic convergence, curve type II exhibits exponential convergence. Curve type III is hybrid and shows exponential behavior in the pre-asymptotic range and algebraic behavior in the asymptotic range.

The restrictions made on the polynomial degree p and the boundedness of u''_{EX}, as demonstrated in the introductory example, are dropped in the following. Accordingly, the convergence of the uniform h-version in the general case is of algebraic type (4.12) with

$$\beta = \min(p, \lambda - \frac{1}{2}). \tag{4.14}$$

In (4.14), λ is a measure for the smoothness of the solution, see [62] (where it is denoted by 'α') and [136]. According to [136], the range $\frac{1}{2} < \lambda < 2$ is representative for unsmooth solutions.

Uniform p-convergence for nonsmooth solutions containing singularities on a uniform mesh is of algebraic type (4.12), as well. For finite element meshes with nodes on all singular points, we obtain

$$\beta = 2\,\lambda - 1 \tag{4.15}$$

and

$$\beta = \lambda - \frac{1}{2} \tag{4.16}$$

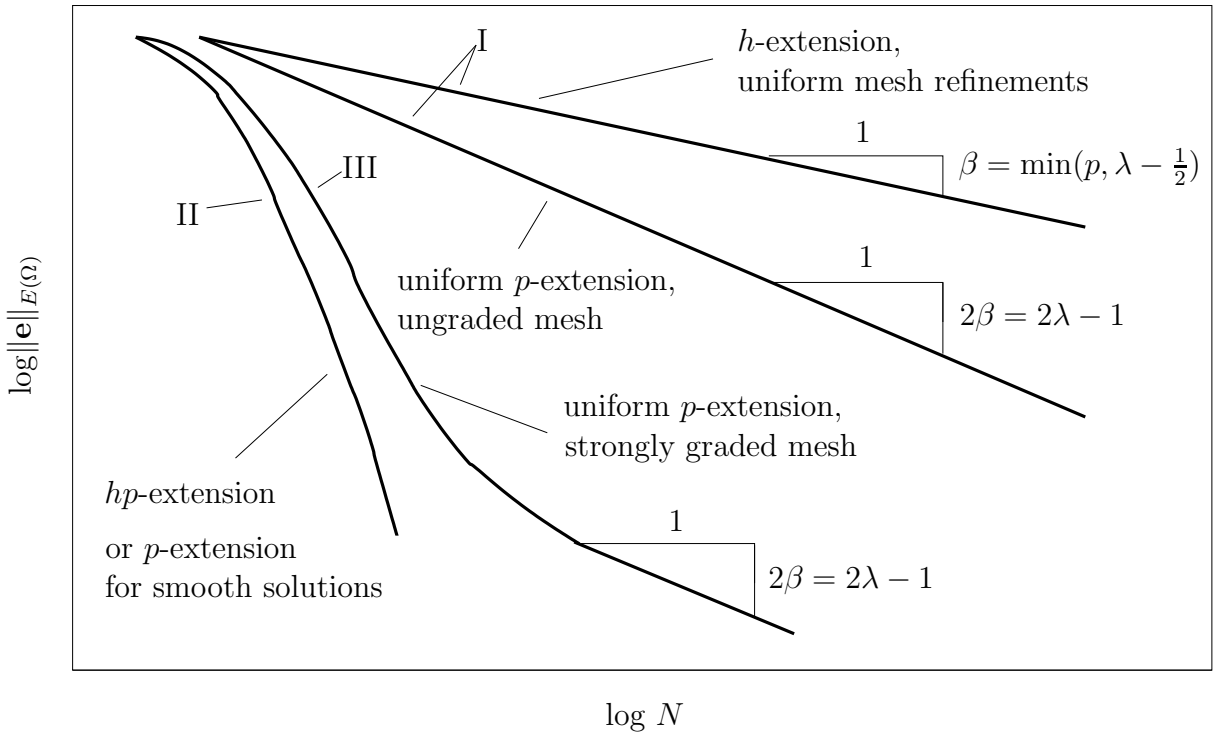

Figure 4.2: Convergence types I (algebraic), II (exponential), III (pre-asymptotic: exponential, asymptotic: algebraic)

otherwise. For smooth solutions, the convergence rate of uniform p-refinement is of exponential type (4.13).

We shall now proceed to describe a rational approach for combining the h- and the p-refinement. Assuming a singular point at $x = 0$ it is possible to construct a mesh with geometric refinement towards this singular point:

$$x_{j-1} = \begin{cases} 0 & \text{for} \quad j = 0 \\ l\, q^{n_{el}-j} & \text{for} \quad j = 1, ..., n_{el} \end{cases} , \tag{4.17}$$

q being the geometric progression, where the asymptotically ($N \to \infty$) optimal value $q = (\sqrt{2} - 1)^2 \approx 0.17$ is independent of λ. The asymptotically optimal p-distribution depends on λ and varies linearly between 1 in the smallest element and

$$p_{max} = (2\lambda - 1)(n_{el} - 1) \tag{4.18}$$

in the biggest element, rounded to the nearest integer. hp-Convergence rates are of exponential type (4.13), where $\gamma = \frac{1}{2}$ under certain conditions normally encountered in practice, see [62, 63, 136].

Uniform p-convergence on fixed meshes that are geometrically refined towards the singularity typically exhibits convergence behavior of curve type III. In the pre-asymptotic case, the rate of convergence is exponential since, for low p-values, the error stems from that part of the domain where the solution is smooth and the elements are large, so the rate of convergence equals that obtained for a smooth solution. By increasing p still further, the singularity starts to become dominant and the rate of convergence finally slows down to algebraic, usually with only a slight slope for uniform p-refinement. However, when the singularity is on a nodal point, the convergence rate is twice that of the uniform h-version.

Overview of a priori error estimates in 2D and 3D

It is possible to obtain a priori error estimates for two-dimensional and three-dimensional problems which have the same structure as (4.12) and (4.13), in a similar way. The results are summarized below according to [137]. The exact solution $\mathbf{u}_{EX}$, which can be a scalar function or a vector function, is classified into categories A, B and C on the basis of a priori information available on its regularity or its smoothness.

Category A: $\mathbf{u}_{EX}$ is analytic at all points of the solution domain, including the boundaries. By definition, a function is analytic at a certain point if it can be expanded into a Taylor series about that point. The solution is likewise in category A when analytical continuation is applicable.

Category B: $\mathbf{u}_{EX}$ is analytic at all points of the solution domain, including the boundaries, with the exception of a finite number of points (or, in 3D, a finite number of points and edges). Those locations where the exact solution is not analytic are called *singular points* or *singular edges*. The great majority of practical problems in solid mechanics fall into this category. Problems in category B are characterized by *piecewise analytic data*, i.e., the domain is bounded by piecewise analytic functions and/or the boundary conditions are piecewise analytic.

Category C: $\mathbf{u}_{EX}$ is neither in category A nor in category B.

Notes with reference to Tables 4.1 and 4.2:

Note 1: Uniform or quasi-uniform mesh refinement is assumed. In the case of optimal mesh refinement $\beta_{max} = p/2$.

Note 2: Where $\mathbf{u}_{EX}$ has a recognizable structure, then it is possible to achieve faster than algebraic rates of convergence with hp-adaptive methods.

Note 3: In the three-dimensional form, $\mathbf{u}_{EX}$ cannot be characterized by a single parameter. Nevertheless, the rate of p-convergence is at least twice the rate of h-convergence.

Note 4: It is possible to realize these convergence rates provided that all singular points lie on element vertices and edges.

Table 4.1: Asymptotic rates of convergence in two dimensions

Category	**Type of extension**		
	h	p	hp
A	algebraic $\beta = p/2$	exponential $\theta \geq 1/2$	exponential $\theta \geq 1/2$
B	algebraic Note 1 $\beta = \frac{1}{2}\min(p, \lambda)$	algebraic $\beta = \lambda$	exponential $\theta \geq 1/3$
C	algebraic $\beta > 0$	algebraic $\beta > 0$	Note 2

Table 4.2: Asymptotic rates of convergence in three dimensions

Category	**Type of extension**		
	h	p	hp
A	algebraic $\beta = p/3$	exponential $\theta \geq 1/3$	exponential $\theta \geq 1/3$
B	Note 3		exponential $\theta \geq 1/5$
C	algebraic $\beta > 0$	algebraic $\beta > 0$	Note 2

The results displayed in tables 4.1 for two-dimensional problems and 4.2 for three-dimensional problems have a similar pattern to those obtained for one-dimensional problems: again, exponential behavior is obtained for p- and hp-refinements for smooth solutions (category A). If the exact solution contains a finite number of singular points (Category B), hp-extensions with geometric refinement (now in two or three dimensions, see [137], for example) and linearly increasing polynomial degrees with increasing distance from the singular points again yield exponential rates of convergence.

Conclusions for adaptive techniques

h-adaptivity: For smooth solutions, i.e. where λ is large, the convergence rate of uniform h-refinement is controlled by the polynomial degree p of the elements, whereas for non-smooth solutions, uniform h-refinement depends on λ, if $\lambda - \frac{1}{2} < p$ for one-dimensional problems, see Equation (4.14), and if $\lambda < p$ for two-dimensional problems, see Table 4.1. In the case of strong singularities, the desired accuracy may prove to be unattainable. By constructing meshes with proper refinement, one can eliminate the dependency on λ, where the optimal refinement depends on $\mathbf{u}_{EX}$. So adaptive procedures are required

where the error is estimated from an initial computation by means of a posteriori estimates, see Section 4.1.2. It is possible to create an appropriately refined mesh based on the estimated error distribution. However, *h*-adaptive convergence rates are still restricted by the polynomial degree used, i.e. they are limited to p in one-dimensional problems, see Equation (4.14), and to $\frac{p}{2}$ in two-dimensional problems, see Table 4.1.

hp-adaptivity: The proposed, asymptotically optimal *hp*-discretizations exhibit exponential convergence rates for Categories A and B. However, this requires a knowledge of the location and strength of singularities *a priori*, which is not usually available. Therefore, *adaptive hp*-methods might be used, which seems to be the best option from all the adaptive strategies available due to their robust exponential behavior in Categories A and B. It involves finding proper mesh refinement and polynomial degree distributions using appropriate error estimators by means of an iterative approach. However, a major drawback of adaptive *hp*-methods is their extremely difficult implementation, especially for complex problems. Adaptive *hp*-methods require local mesh refinement on strongly graded meshes, for example, without necessitating the subdivision of coarse elements in "smooth areas", which is a very demanding task especially in three dimensions. The following additional reading material is recommended: Rachowicz et al. [113], Oden et al. [106], Demkowicz and Oden [43], Demkowicz et al. [46], Ainsworth and Senior [4], Melenk and Wohlmuth [92].

r-adaptivity: For several problems, it is possible to isolate singular points and edges by adaptively capturing these singularities using element boundaries, thus dividing the solution on domain Ω into regular patches, i.e. increasing the smoothness λ on the interior of the elements. For low order p, the resulting, highly distorted elements usually cause severe numerical problems [148].

rp-adaptivity: Since high order elements are not sensitive even under extreme distortions, combined *rp*-adaptive methods are clearly better suited for the relocation strategy. The efficiency was shown in Nübel et al. [101] and Nübel [100], for example, exhibiting exponential convergence rates for elastoplastic problems by adaptively approximating the plastic interface with the element boundaries being Lagrangean polynomials. Similar to *hp*-adaptive methods, the mesh handling is quite labor intensive for approaches of this nature.

p-adaptivity: Uniform *p*-refinement on strongly graded meshes is efficient in the pre-asymptotic range, but often suffers from low algebraic convergence rates in the asymptotic range (but it is still at least as good as the uniform *h*-version). A promising *p*-adaptive approach was proposed in Bertóti and Szabó [29], for instance, for two-dimensional linear elastostatic problems, where the polynomial degrees were chosen elementwise, but no use has been made so far of anisotropic Ansatz spaces. Again, for time-independent, linear elastic problems, Luo [90] uses an approach related to that proposed in Chapter 5 in a very recent work. As will be shown in Chapter 5 for linear elastostatic problems and in Chapter 6 for linear elastodynamic problems, the pre-asymptotic behavior of uniform *p*-version can be "accelerated" and the rate of convergence in the asymptotic case can be improved dramatically using an anisotropic *p*-adaptive method in three dimensions.

With this approach, the mesh is kept fixed and only the polynomial degree distribution is adjusted elementwise for the different local directions and the components of the cartesian displacement vectors according to an anisotropic error indicator, leading to very efficient discretizations, especially for three-dimensional problems.

The importance of selecting the polynomial degree p properly is demonstrated in the simple, one-dimensional example that follows. For a sequence of geometric meshes with a finite number of elements, even the asymptotically optimal p-distribution for hp-extensions described above can be substantially improved by manually adapting the polynomial degree distribution without changing the overall number of degrees of freedom N. The model problem (4.1) with $AE = l = 1$, $f(x) = \lambda(\lambda - 1)x^{\lambda-2}$ and the boundary condition $u(0) = 0$, resulting in the exact solution $u_{EX} = x^{\lambda} - x$, has to be solved numerically. λ is chosen to be 1.8, leading to a singularity in the second derivative of $\mathbf{u}_{EX}$.

A sequence of asymptotically optimal hp-discretizations for $n_{el} = 1, ..., 6$ was created with geometric refinement towards $x = 0$ and a progression factor $q = 0.17$. The asymptotically optimal linear p-distribution is given in Table 4.3 (left) according to Equation (4.18) where p_1 is the polynomial degree of the smallest element and $p_{n_{el}}$ that of the largest. The number of degrees of freedom can be obtained with $N = \sum_1^{n_{el}} p_i$.

In Table 4.3 (right) modified ("manually adapted") p-distributions with higher p at the smallest element at the singularity are shown, leading to the same number of degrees of freedom N for every mesh. They are obtained from the asymptotically optimal p-distributions by adding $\Delta p = \text{round}(0.3 p_{max})$ to p_1 corresponding to the smallest element at the singularity. Here, the operator round(x) returns the next integer to x. In order to keep the number of degrees of freedom constant, p_i is decreased by 1 for all elements $i = n_{el}, ..., n_{el} - \Delta p + 1$.

Table 4.3: Polynomial degree distributions

n_{el}	N	asympt. optimal p-distribution						adapted p-distribution					
		p_1	p_2	p_3	p_4	p_5	p_6	p_1	p_2	p_3	p_4	p_5	p_6
1	1	1						1					
2	4	1	3					2	2				
3	9	1	3	5				3	2	4			
4	18	1	3	6	8			3	3	5	7		
5	28	1	3	6	8	10		4	3	5	7	9	
6	42	1	3	6	8	11	13	5	3	5	7	10	12

Table 4.4 illustrates the errors of the two sequences of computations. For this sequence of meshes, the improvement in the finite element solution obtained by manually adapting

the asymptotically optimal p-distribution is dramatic. For $n_{el} = 4, ..., 6$, the improvement is of more than one order of magnitude. In comparison, with a uniform p-distribution on the geometric mesh with $n_{el} = 6$ and $p_i = 7$, $i = 1, ..., 6$, which also leads to a number of degrees of freedom $N = 42$, the error in energy norm can only be reduced to $\|e\|_E = 0.001387$. Of course, the performance of this refinement scheme depends on the strength of the singularity λ.

The pattern used here, where high polynomial degrees are located at the singularities, i.e. at clamped boundaries, for example, may be identified later in the p-distributions found by adaptation with the help of the anisotropic error indicator proposed in Chapters 5 and 6 for three-dimensional examples.

Table 4.4: Error in energy norm

n_{el}	$\|e\|_E$, asympt. optimal	$\|e\|_E$, adapted
1	52.704628	52.704628
2	5.271581	1.589995
3	0.526878	0.165318
4	0.052619	0.003486
5	0.005257	0.000363
6	0.000525	0.000032

4.1.2 A posteriori error estimates

Several strategies have been developed to estimate the error related to a finite element approximation *a posteriori*. There is a wealth of literature which has continued to grow during the last twenty years. No attempt is made herein to describe all the different approaches in detail but the main concepts have been included in order to provide a brief overview. For details, the reader is referred to the work of Ainsworth and Oden [3], Verfürth [140] and Wriggers [148] and the literature listed therein.

The following description of a posteriori error estimators is closely related to [3] and [47].

4.1.2.1 Explicit error estimators

Explicit error estimators, which go back to Babuška and Rheinboldt [15], Babuška and Miller [11], Kelly et al. [78], are based on a *direct* computation using only data which has already been determined by the finite element approximation. They involve the elementwise integration of residuals of the present approximation to obtain an estimate of the error in a certain norm (usually the energy norm). Two major drawbacks of explicit error estimators are that they involve unknown constants and that they are sensitive to pollution errors which may arise if singularities are not sufficiently resolved. An advantage of this class of estimators is that they are quite economical when compared to other approaches.

The approach given below is closely related to that of AINSWORTH and ODEN [3] and JOHNSON and HANSBO [76].

Suppose that $\mathbf{u}_{EX}$ is the exact solution of the variational boundary value problem

$$\mathcal{B}(\mathbf{u}_{EX}, \mathbf{v}) \;=\; \mathcal{F}(\mathbf{v}) \quad \forall \mathbf{v} \in \mathcal{V} \tag{4.19}$$

describing a linear elastic problem in $n_{\mathrm{sd}} = 2$ dimensions on a domain $\Omega \subset \mathbb{R}^{n_{\mathrm{sd}}}$ with boundary $\partial\Omega$. Then the error of a finite element approximation $\mathbf{u}_{FE}$ in a finite-dimensional space $\mathcal{S} \subset \mathcal{V}$ is defined as

$$\mathbf{e} \;=\; \mathbf{u}_{EX} - \mathbf{u}_{FE}\,. \tag{4.20}$$

An important property of the error is the so-called GALERKIN orthogonality

$$\mathcal{B}(\mathbf{e}, \mathbf{v}) \;=\; 0 \quad \forall \mathbf{v} \in \mathcal{S} \subset \mathcal{V} \tag{4.21}$$

stating that the error of a GALERKIN approximation is orthogonal to all functions in $\mathcal{S}$. Inserting (4.20) in (4.19) we obtain the following representation of the error

$$\mathcal{B}(\mathbf{e}, \mathbf{v}) \;=\; \mathcal{B}(\mathbf{u}_{\mathrm{ex}}, \mathbf{v}) - \mathcal{B}(\mathbf{u}_{FE}, \mathbf{v}) = \mathcal{F}(\mathbf{v}) - \mathcal{B}(\mathbf{u}_{FE}, \mathbf{v}) \quad \forall \mathbf{v} \in \mathcal{V} \tag{4.22}$$

which can also be expressed by the contribution of each element by splitting the integral over domain Ω into a sum of n_{el} element integrals

$$\mathcal{B}(\mathbf{e}, \mathbf{v}) \;=\; \sum_{i=1}^{n_{\mathrm{el}}} \left\{ \int_{\Omega_i} \mathbf{v} \cdot \mathbf{f}\, d\Omega + \int_{\gamma_i \cap \partial\Omega_N} \mathbf{v} \cdot \bar{\mathbf{t}}\, d\gamma - \int_{\Omega_i} \boldsymbol{\varepsilon}(\mathbf{v}) : \boldsymbol{\sigma}(\mathbf{u}_{FE})\, d\Omega \right\} \tag{4.23}$$

where γ_i denotes the boundary of element Ω_i and $\partial\Omega_N$ represents the Neumann boundary. In order to state the functional (4.23) in terms of interior and boundary residuals, we perform an integration by parts of the last term in (4.23) and obtain after rearranging

$$\mathcal{B}(\mathbf{e}, \mathbf{v}) \;=\; \sum_{i=1}^{n_{\mathrm{el}}} \int_{\Omega_i} \mathbf{r}_i \cdot \mathbf{v}\, d\Omega + \sum_{i=1}^{n_{\mathrm{ed}}} \int_{\gamma_i} \mathbf{J}_i \cdot \mathbf{v}\, d\gamma \quad \forall \mathbf{v} \in \mathcal{V} \tag{4.24}$$

where

$$\mathbf{r}_i \;=\; \operatorname{div} \boldsymbol{\sigma}(\mathbf{u}_{FE,i}) + \mathbf{f} \quad \text{on} \quad \Omega_i \tag{4.25}$$

is the interior residual of element i. In (4.24)

$$\mathbf{J}_i \;=\; \begin{cases} \boldsymbol{\sigma}(\mathbf{u}_{FE,e_1})\,\mathbf{n}_{e_1} + \boldsymbol{\sigma}(\mathbf{u}_{FE,e_2})\,\mathbf{n}_{e_2} & \text{if} \quad \gamma_i \not\subset \partial\Omega \\ \bar{\mathbf{t}} - \boldsymbol{\sigma}(\mathbf{u}_{FE})\,\mathbf{n} & \text{if} \quad \gamma_i \subset \partial\Omega_N \\ \mathbf{0} & \text{if} \quad \gamma_i \subset \partial\Omega_D \end{cases} \tag{4.26}$$

are the jumps of stresses at the n_{ed} edges of the mesh. Therefore, the stresses are transformed to the normal direction of the edge where $\mathbf{n}_{e_i}$ defines the outward normal vector of the corresponding element. If the corresponding edge γ_i is shared by two elements, say element e_1 and element e_2, then the jump is defined as the difference of the stress of both elements, whereas in the case when γ is part of a Neumann boundary $\partial\Omega_N$ the jump is given by the difference between the boundary data and the finite element approximation. On the other hand, if γ_i belongs to the Dirichlet boundary $\partial\Omega_D$, the corresponding boundary residual is set at zero.

If $\mathcal{I}_{\mathcal{S}}\mathbf{v}$ denotes the approximation to $\mathbf{v} \in \mathcal{V}$ in the finite-dimensional subspace $\mathcal{S} \subset \mathcal{V}$, then Equation (4.24) in conjunction with the Galerkin orthogonality (4.21) yields

$$0 \;=\; \sum_{i=1}^{n_{\text{el}}} \int_{\Omega_i} \mathbf{r}_i \cdot (\mathcal{I}_{\mathcal{S}}\mathbf{v})\, d\Omega + \sum_{i=1}^{n_{\text{ed}}} \int_{\gamma_i} \mathbf{J}_i \cdot (\mathcal{I}_{\mathcal{S}}\mathbf{v})\, d\gamma\,. \tag{4.27}$$

Subtracting Equation (4.27) from Equation (4.24) produces

$$\mathcal{B}(\mathbf{e},\mathbf{v}) \;=\; \sum_{i=1}^{n_{\text{el}}} \int_{\Omega_i} \mathbf{r}_i \cdot (\mathbf{v} - \mathcal{I}_{\mathcal{S}}\mathbf{v})\, d\Omega + \sum_{i=1}^{n_{\text{ed}}} \int_{\gamma_i} \mathbf{J}_i \cdot (\mathbf{v} - \mathcal{I}_{\mathcal{S}}\mathbf{v})\, d\gamma \quad \forall \mathbf{v} \in \mathcal{V}\,. \tag{4.28}$$

Applying the Cauchy-Schwarz inequality we separate both integrands such that

$$\mathcal{B}(\mathbf{e},\mathbf{v}) \;\leq\; \sum_{i=1}^{n_{\text{el}}} \|\mathbf{r}_i\|_{L_2(\Omega_i)}\, \|(\mathbf{v} - \mathcal{I}_{\mathcal{S}}\mathbf{v})\|_{L_2(\Omega_i)} + \sum_{i=1}^{n_{\text{ed}}} \|\mathbf{J}_i\|_{L_2(\gamma_i)}\, \|(\mathbf{v} - \mathcal{I}_{\mathcal{S}}\mathbf{v})\|_{L_2(\gamma_i)}\,. \tag{4.29}$$

With the estimate for the interpolation error for h-refinement

$$\|(\mathbf{v} - \mathcal{I}_{\mathcal{S}}\mathbf{v})\|_{L_2(\Omega_i)} \;\leq\; C_{1,i}\, h_i\, \|\mathbf{v}\|_{H^1(\tilde{\Omega}_i)} \tag{4.30}$$

$$\|(\mathbf{v} - \mathcal{I}_{\mathcal{S}}\mathbf{v})\|_{L_2(\partial\Omega_i)} \;\leq\; C_{2,i}\, \sqrt{h_i}\, \|\mathbf{v}\|_{H^1(\tilde{\Omega}_i)} \tag{4.31}$$

where $\tilde{\Omega}_i$ is the union of element i and its neighbors and $\|\bullet\|_{H^1(\tilde{\Omega}_i)}$ denotes the standard Sobolev norm, Equation (4.29) can be rewritten by applying the Cauchy-Schwarz inequality as

$$\mathcal{B}(\mathbf{e},\mathbf{v}) \;\leq\; \|\mathbf{v}\|_{H^1(\Omega)} \left\{ \sum_{i=1}^{n_{\text{el}}} C_{1,i}\, h_i^2\, \|\mathbf{r}_i\|^2_{L_2(\Omega_i)} + \sum_{i=1}^{n_{\text{ed}}} C_{2,i}\, h_i\, \|\mathbf{J}_i\|^2_{L_2(\gamma_i)} \right\}^{\frac{1}{2}}. \tag{4.32}$$

Estimates of the interpolation error for other refinement techniques, such as p-refinement with high order elements, can be used instead of (4.30) and (4.31), cf. KRAUSE [81], DÜSTER [53]. Because of the coercivity of the bilinear form over the global space $\mathcal{V}$ we have

$$\|\mathbf{v}\|_{H^1(\Omega)} \leq C_3 \|\mathbf{v}\|_{E(\Omega)} \tag{4.33}$$

leading to the explicit error estimator

$$\|\mathbf{e}\|^2_{E(\Omega)} \leq \sum_{i=1}^{n_{\text{el}}} \left\{ C_{4,i}\, h_i^2 \|\mathbf{r}_i\|^2_{L_2(\Omega_i)} + C_{5,i}\, h_i \|\mathbf{J}_i\|^2_{L_2(\partial\Omega_i)} \right\} \tag{4.34}$$

where the terms are regrouped. The computation of the estimated error in energy norm by applying Equation (4.34) is therefore solely based on the interior and boundary residuals. Besides the constants, all data is given by the finite element approximation.

4.1.2.2 Implicit error estimators

Implicit error estimators involve the solution of an auxiliary boundary value problem which approximates the unknown error. There are different methods:

1. **Subdomain residual method**
   The basic idea of this method proposed by BABUŠKA and RHEINBOLDT [12, 13, 14] is to decompose the global residual equation determining the error into a number of independent local problems on small subdomains with homogeneous Dirichlet boundary conditions. Using the property $\sum_{i=1}^{n_{nd}} \Theta_i(\mathbf{x}) = 1$ for all *nodal* shape functions Θ_i and $x \in \Omega$, one can write

$$\begin{aligned} \mathcal{B}(\mathbf{e}, \mathbf{v}) &= \mathcal{B}(\mathbf{e}, \mathbf{v} \sum_{i=1}^{n_{nd}} \Theta_i) = \sum_{i=1}^{n_{nd}} \mathcal{B}(\mathbf{e}, \mathbf{v}\Theta_i) \\ &= \sum_{i=1}^{n_{nd}} \left(\mathcal{F}(\mathbf{v}\Theta_i) - \mathcal{B}(\mathbf{u}_{FE}, \mathbf{v}\Theta_i)\right) = \sum_{i=1}^{n_{nd}} \left(\mathcal{F}(\mathbf{v}^{\Theta_i}) - \mathcal{B}(\mathbf{u}_{FE}, \mathbf{v}^{\Theta_i})\right) \end{aligned} \tag{4.35}$$

   for all $\mathbf{v} \in \mathcal{V}$. The test functions $\mathbf{v}^{\Theta_i} = \mathbf{v}\Theta_i$ are restricted to the patch $\tilde{\Omega}_i$ of elements containing the node i and vanish on the patch boundary $\partial\tilde{\Omega}_i$. By disregarding the mutual influence of test functions $\mathbf{v}^{\Theta_i}$, $\mathbf{v}^{\Theta_j}$ on overlapping patches $\tilde{\Omega}_i$, $\tilde{\Omega}_j$, Equation (4.35) can be decomposed into n_{nd} local equations

$$\mathcal{B}_i(\boldsymbol{\phi}_i, \mathbf{v}^{\Theta_i}) = \mathcal{F}_i(\mathbf{v}^{\Theta_i}) - \mathcal{B}_i(\mathbf{u}_{FE}, \mathbf{v}^{\Theta_i}), \tag{4.36}$$

   where $\mathcal{B}_i$, $\mathcal{F}_i$ are the restriction of $\mathcal{B}$, $\mathcal{F}$ on the nodal patch $\tilde{\Omega}_i$. The local Equation (4.36) can be solved using enhanced finite element spaces yielding the error estimator

$$\eta = \| \sum_{i=1}^{n_{nd}} \boldsymbol{\phi}_i \|_{E(\tilde{\Omega}_i)}. \tag{4.37}$$

Due to the overlapping of nodal patches, each finite element has to be considered several times, so this method is quite labor-intensive. However, BABUŠKA and MILLER [11] showed how the subdomain residual method can be improved with respect to efficiency, leading to an explicit error estimator.

2. **Element residual method**
A less time-consuming error estimator than the subdomain residual method is the so-called element residual method devised by BANK [21], BANK and WEISER [24], DEMKOWICZ et al. [44, 45] and ODEN et al. [105]. The underlying idea of this approach is to compute an approximation of the error by solving small problems defined on each individual element. Therefore, a variational problem determining the error is defined for each element

$$\mathcal{B}_e(\boldsymbol{\phi}_i, \mathbf{v}) \;=\; \mathcal{F}_e(\mathbf{v}) - \mathcal{B}_e(\mathbf{u}_{FE}, \mathbf{v}) \tag{4.38}$$

for all $\mathbf{v} \in \mathcal{V}$. $\mathcal{B}_e$, $\mathcal{F}_e$ are the restriction of $\mathcal{B}$, $\mathcal{F}$ to the element domain Ω_e. Due to the local restriction, Equation (4.38) must be supplemented by appropriate boundary conditions. For interior elements Neumann boundary conditions are applied. Since the exact boundary conditions for interior elements are unknown, an approximation is obtained by averaging the flux of adjacent elements. Unfortunately, the solvability of the corresponding boundary value problem depends heavily on the space chosen for approximating the error. It could therefore be that the local problem only provides a solution if the space is carefully chosen (see [3]). The difficulties of solving the pure Neumann problems arise from the incompatibility of the corresponding boundary data. Since the boundary data is not exact, spurious modes may arise in the solution of the local problem. To overcome this drawback, the Ansatz for the error is modified, yielding a subspace where the spurious modes are filtered out. Although adequate subspaces for first-order finite elements are familiar, the situation for high order finite elements is less clear. One way of overcoming this difficulty is to compute improved boundary data which leads to a well-posed local problem for determining the error. This approach is called the equilibrated residual method and is addressed briefly below.

3. **Equilibrated residual method**
The major drawback of the element residual method is that the local Neumann boundary value problems which determine the global error may be not well-posed. This is due to the incompatibility of the boundary data and the interior residuals. In the element residual method this problem is bypassed by selecting appropriate Ansatz spaces for the error which exclude spurious modes and therefore allow for a solution of the local

Neumann boundary value problem. The drawback of this approach is the difficulty of finding such subspaces. A different approach to this problem is the equilibrated residual method. The basic idea is to obtain well-posed problems by post-processing the fluxes, such that they are in equilibrium with the interior residual loads. AINSWORTH and ODEN [2, 3] have proved that the solution of the local Neumann boundary value problems yields an error estimator with a guaranteed upper bound if the fluxes are computed in such a way that they fulfill the equilibrium condition. For two-dimensional problems the fluxes are recomputed from the finite element solution for each edge. To avoid the necessity of solving a global problem, the degrees of freedom for the re-computed fluxes are chosen to be moments resulting from the fluxes weighted by the basis function on the corresponding edge. The introduction of moments therefore allows the global problem determining the equilibrated fluxes to be decoupled into small local problems defined on patches of elements. The idea of computing equilibrated fluxes was proposed by LADEVÈZE and LEGUILLON [83], KELLY [77] and BANK and WEISER [24].

4.1.2.3 Recovery methods

Error estimators of this type make use of the fact that the gradient of the finite element approximation is generally discontinuous across the element boundaries. Considering a pure displacement formulation for problems of plane elasticity, for example, the C^0-continuity of the Ansatz will generally cause jumps in the derivatives of the displacement field at the interelement boundaries. The underlying idea of the recovery methods is to post-process the stress field $\boldsymbol{\sigma}$ to obtain an enhanced stress field $\boldsymbol{\sigma}^*$. The approximate error $\mathbf{e}^*$ in energy norm can then be computed with

$$\|e^*\|_E = \int_\Omega (\boldsymbol{\sigma}^* - \boldsymbol{\sigma}) : \mathbb{C}^{-1} : (\boldsymbol{\sigma}^* - \boldsymbol{\sigma}) d\Omega. \tag{4.39}$$

This method was first proposed by ZIENKIEWICZ and ZHU [154] where the discontinuous stress field arising from the finite element method was smoothed by projecting it to the basis functions of the finite element approximation. An analysis of this error estimator can be found, for example, in AINSWORTH et al. [5] and RANK and ZIENKIEWICZ [116]. Similar error estimators may be derived by simply choosing different recovery methods leading to an improved stress field. A commonly used recovery procedure is the so-called superconvergent patch recovery (SPR) devised by ZIENKIEWICZ and ZHU [155, 156]. This method is based on the observation that stresses sampled at a specific set of points are more accurate then elsewhere, i.e. the stresses at these superconvergent points converge at a higher rate. These points are found to coincide with the Gauss-Legendre integration points corresponding to the polynomial used in the finite element Ansatz (see also [152]). The recovered stress field is obtained by interpolating improved nodal stresses. These improved nodal stresses are computed by applying a least squares fit to a patch of elements surrounding the corresponding node. Unfortunately, the superconvergence property is given only under very restrictive assumptions with respect to the regularity of the solution and the partition, which are not generally encountered. However, the SPR has been numerically proven to lead to an improved stress field in many applications of low order elements and therefore to provide the user with an efficient error estimator. In

the case of high order elements the SPR also seems to be a fairly effective post-processing scheme (see [25, 71, 99]).

4.1.2.4 Use of hierarchical bases for error estimation

A quite natural approach to quantify the discretization error is to enrich the current Ansatz and to estimate the error by measuring the difference between the original approximation $\mathbf{u}_\mathcal{X}$ from space $\mathcal{X}$ and the approximation $\mathbf{u}^*$ of the enriched space $\mathcal{X}^* = \mathcal{X} \oplus \mathcal{Y}$.

$$\|\mathbf{e}\|_E = \|\mathbf{u}_{EX} - \mathbf{u}_\mathcal{X}\|_E \approx \|\mathbf{u}^* - \mathbf{u}_\mathcal{X}\|_E = \|\mathbf{e}^*\|_E \tag{4.40}$$

This enrichment can be carried out either by uniform mesh refinement or by increasing the polynomial degree of the elements. The effectiveness of the approximation $\|\mathbf{e}^*\|_E$ depends on whether $\mathbf{u}^*$ is a proper improvement over the original approximation $\mathbf{u}_\mathcal{X}$. This property of $\mathbf{u}^*$ can be expressed by the saturation assumption: There is a constant $\beta \in [0, 1)$ such that

$$\|\mathbf{u}_{EX} - \mathbf{u}^*\|_E \leq \beta \|\mathbf{u}_{EX} - \mathbf{u}_\mathcal{X}\|_E. \tag{4.41}$$

Thanks to Galerkin's orthogonality $\beta \leq 1$ is always fulfilled for hierarchic extensions. The real import of (4.41) is that β is *strictly* less than unity uniformly. The major drawback of this approach is evident: since the whole problem has to be resolved with an approximation of greater complexity, the computational investment is very high.

$$\begin{aligned} \mathcal{B}(\mathbf{e}^*_\mathcal{X}, \mathbf{v}_\mathcal{X}) + \mathcal{B}(\mathbf{e}^*_\mathcal{Y}, \mathbf{v}_\mathcal{X}) &= \mathcal{F}(\mathbf{v}_\mathcal{X}) - \mathcal{B}(\mathbf{u}^*_\mathcal{X}, \mathbf{v}_\mathcal{X}) = 0, \quad \forall \mathbf{v}_\mathcal{X} \in \mathcal{X}, \\ \mathcal{B}(\mathbf{e}^*_\mathcal{X}, \mathbf{v}_\mathcal{Y}) + \mathcal{B}(\mathbf{e}^*_\mathcal{Y}, \mathbf{v}_\mathcal{Y}) &= \mathcal{F}(\mathbf{v}_\mathcal{Y}) - \mathcal{B}(\mathbf{u}^*_\mathcal{X}, \mathbf{v}_\mathcal{Y}), \quad \forall \mathbf{v}_\mathcal{Y} \in \mathcal{Y}. \end{aligned} \tag{4.42}$$

A reasonable approximation $\bar{\mathbf{e}}$ to $\mathbf{e}^*$ can be obtained by disregarding the coupling terms

$$\begin{aligned} \mathcal{B}(\bar{\mathbf{e}}_\mathcal{X}, \mathbf{v}_\mathcal{X}) &= 0, \quad \forall \mathbf{v}_\mathcal{X} \in \mathcal{X}, \\ \mathcal{B}(\bar{\mathbf{e}}_\mathcal{Y}, \mathbf{v}_\mathcal{Y}) &= \mathcal{F}(\mathbf{v}_\mathcal{Y}) - \mathcal{B}(\mathbf{u}^*_\mathcal{X}, \mathbf{v}_\mathcal{Y}), \quad \forall \mathbf{v}_\mathcal{Y} \in \mathcal{Y}. \end{aligned} \tag{4.43}$$

It is also possible to apply inexact solvers which are equivalent to the use of a modified bilinear form. An inexact solution may be performed by applying, for instance, a single Jacobian iteration corresponding to an approximate solution of the full matrix by its diagonal (see [3]). Upper and lower bounds can be derived for both additional errors caused by disregarding the coupling terms and using a modified bilinear form. For further information the reader is referred to Bank [22] and Bank and Smith [23].

In the following section a method is proposed using hierachic bases for extrapolation of the error.

4.1.2.5 Error estimation based on extrapolation methods

A very efficient global error estimate was devised by SZABÓ [135], SZABÓ and BABUŠKA [136]. This estimate is based on a hierarchic extrapolation method.

To estimate the error

$$\mathbf{e} = \mathbf{u}_{EX} - \mathbf{u}_{FE} \tag{4.44}$$

of a finite element approximation in energy norm

$$\|\mathbf{e}\|^2_{E(\Omega)} = \mathcal{B}(\mathbf{e},\mathbf{e}) = \|\mathbf{u}_{EX}\|^2_{E(\Omega)} - \|\mathbf{u}_{FE}\|^2_{E(\Omega)} \tag{4.45}$$

it is assumed that the error obeys the *a priori* estimate

$$\|\mathbf{e}\|_{E(\Omega)} \leq \frac{k}{N^\beta} \tag{4.46}$$

defining an algebraic convergence rate which is observed in h-extensions or in the case of p-extensions when singularities in the exact solution are present (see Section 4.1.1). Combining (4.45) and (4.46) yields

$$\|\mathbf{e}\|^2_{E(\Omega)} = \mathcal{B}(\mathbf{e},\mathbf{e}) = \|\mathbf{u}_{EX}\|^2_{E(\Omega)} - \|\mathbf{u}_{FE}\|^2_{E(\Omega)} \approx \frac{k^2}{N^{2\beta}}\,. \tag{4.47}$$

The underlying idea of this estimate is to compute the three unknowns $\|\mathbf{u}_{EX}\|^2_{E(\Omega)}$, k and β by applying the results of a sequence of three computations. Suppose the results of these computations are obtained by a p-extension with $p-2, p-1, p$ then N_{p-2}, N_{p-1}, N_p and $\|\mathbf{u}_{FE,p-2}\|^2_{E(\Omega)}, \|\mathbf{u}_{FE,p-1}\|^2_{E(\Omega)}, \|\mathbf{u}_{FE,p}\|^2_{E(\Omega)}$ are available and yield together with (4.47)

$$\frac{\|\mathbf{u}_{EX}\|^2_{E(\Omega)} - \|\mathbf{u}_{FE,p}\|^2_{E(\Omega)}}{\|\mathbf{u}_{EX}\|^2_{E(\Omega)} - \|\mathbf{u}_{FE,p-1}\|^2_{E(\Omega)}} \approx \left(\frac{\|\mathbf{u}_{EX}\|^2_{E(\Omega)} - \|\mathbf{u}_{FE,p-1}\|^2_{E(\Omega)}}{\|\mathbf{u}_{EX}\|^2_{E(\Omega)} - \|\mathbf{u}_{FE,p-2}\|^2_{E(\Omega)}}\right)^{\left(\frac{\log\frac{N_{p-1}}{N_p}}{\log\frac{N_{p-2}}{N_{p-1}}}\right)}. \tag{4.48}$$

To finally compute the estimate of the exact energy norm $\|\mathbf{u}_{EX}\|^2_{E(\Omega)}$ Equation (4.48) is solved by applying a NEWTON-RAPHSON scheme, for example.

A basic assumption of this estimate — besides the algebraic convergence rate (4.46) — is the monotonic convergence of the energy norm which is met when a sequence of Ansatz spaces with $\mathcal{S}^{p-2} \subset \mathcal{S}^{p-1} \subset \mathcal{S}^p$ is applied. When performing a p-extension, the basic assumption is fulfilled since the applied Ansatz spaces are hierarchic (see Chapter 3.1). To apply this approach to h-extensions as well, care must be taken to ensure that the finite element meshes are hierarchically refined, so that all functions defined on the coarser mesh can be exactly represented on the finer mesh as well, see also the discussion in Section 4.2.4. Numerous numerical examples have proved the estimate to be accurate and reliable (see [135, 136]). In this thesis, the estimate is applied as a stopping criterion for the p-adaptive procedure devised in Chapter 5 and to obtain improved values when a numerical reference solution is needed.

4.1.2.6 Estimation of the errors in quantities of interest

Most of the estimators give an approximation of the error in terms of the energy norm. This is, of course, quite a natural norm since the finite element method minimizes the error in strain energy. However, when applying the finite element analysis in a design process, the error in quantities such as displacements or stresses at specific points or integrals of such quantities over lines or areas are of even more interest. In general, the error in a linear functional of the solution extracting the quantity of interest is sought

$$\mathcal{Q}(\mathbf{e}) = \mathcal{Q}(\mathbf{u}_{EX}) - \mathcal{Q}(\mathbf{u}_{FE}). \tag{4.49}$$

A certain class of estimators is capable of approximating the error in quantities of interest $\mathcal{Q}(\mathbf{e})$. The basic idea of this approach is to introduce for the original problem, also called *primal problem*,

$$\mathcal{B}(\mathbf{u}, \mathbf{v}) = \mathcal{F}(\mathbf{v}), \quad \forall \mathbf{v} \in \mathcal{V}. \tag{4.50}$$

an *adjoint* or *dual* problem based on the same bilinear form but with a different right-hand side corresponding to the functional $\mathcal{Q}$,

$$\mathcal{B}(\mathbf{v}, \mathbf{w}^{\mathcal{Q}}) = \mathcal{Q}(\mathbf{v}), \quad \forall \mathbf{v} \in \mathcal{V}, \tag{4.51}$$

where $\mathbf{w}^{\mathcal{Q}}$ is the solution of the dual problem. Inserting $\mathbf{v} = \mathbf{e}$ in (4.51) leads to

$$\mathcal{Q}(\mathbf{e}) = \mathcal{B}(\mathbf{e}, \mathbf{w}^{\mathcal{Q}}) = \mathcal{B}(\mathbf{e}, \mathbf{w}^{\mathcal{Q}} - \mathbf{w}_{\mathcal{X}}), \tag{4.52}$$

where the second equality is valid for every $\mathbf{w}_{\mathcal{X}}$ from the finite element space $\mathcal{X}$ due to the GALERKIN orthogonality $\mathcal{B}(\mathbf{e}, \mathbf{w}_{\mathcal{X}}) = 0$. Selecting $\mathbf{w}_{\mathcal{X}}$ to be the finite element approximation of $\mathbf{w}^{\mathcal{Q}}$ then reveals

$$\mathcal{Q}(\mathbf{e}) = \mathcal{B}(\mathbf{e}, \mathbf{e}^{\mathcal{Q}}), \tag{4.53}$$

i.e., the error of the quantity of interest is determined by inserting both errors into the bilinear form, the original one and the one pertaining to the adjoint problem. To estimate the two different errors, it is possible to apply all the techniques described above, finally resulting in an error estimate for the quantity of interest.

If an adaptive procedure is based on a global error measure, such as the energy norm, then the refinement is performed in such a way that the error in the whole computational domain is reduced. When using an error estimator for a quantity of interest, then the refinement is ideal, up to a point, with respect to the chosen quantity. This, of course, leads to efficient discretizations. The drawback of this approach is that the refinement does not help to detect all critical values, such as all stress concentrations in the whole computational domain. Therefore, an adaptive refinement should also account for a global error measure. The error estimation of quantities of interest has been dealt with by various researchers, such as LOUIS [88] and BABUŠKA and MILLER [8, 9, 10]. This approach has also been applied to problems of elastoplasticity by RANNACHER and SUTTMEIER [118] and CIRAK and RAMM [39]. For a detailed literature survey see AINSWORTH and ODEN [3].

4.1.3 Notes on nonlinear problems

Error estimation for nonlinear problems is the subject-matter of current research, see for example WRIGGERS [148]. One approach, extending the error estimators for linear problems described in Section 4.1.2, is the linearization of the nonlinear problem about a known equilibrium point. An equilibrium point is a point where the difference between the generalized internal forces $\mathbf{R}(\mathbf{u})$ and the generalized external forces $\lambda\mathbf{f}$ vanishes, i.e. $\mathbf{G}(\mathbf{u}) = \mathbf{R}(\mathbf{u}) - \lambda\mathbf{f} = \mathbf{0}$. The simplified idea is illustrated in Figure 4.3.

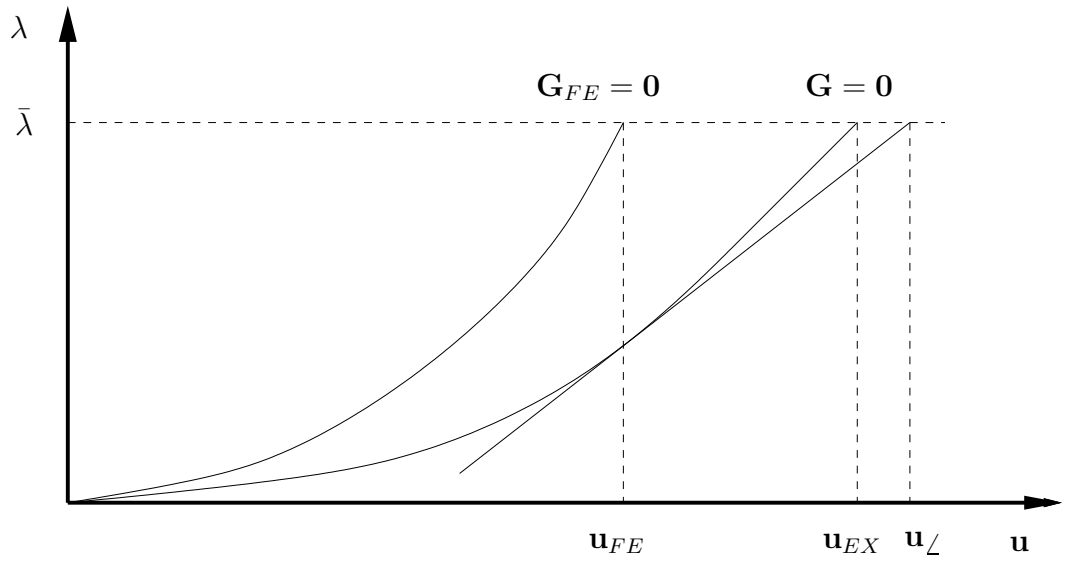

Figure 4.3: error estimation for nonlinear problems

The displacement-load function is linearized about the equilibrium point of the finite element approximation $\mathbf{u}_{FE}$ according to the load parameter λ, leading to the linearized solution $\mathbf{u}_{\angle}$. The following estimate

$$\|\mathbf{u}_{EX} - \mathbf{u}_{FE}\|(1 + c) = \|\mathbf{u}_{EX} - \mathbf{u}_{\angle}\| \tag{4.54}$$

can be derived with c depending on the nonlinear displacement function and bounded under certain circumstances, see [148], for instance. Using Equation (4.54) the error between $\mathbf{u}_{EX}$ and $\mathbf{u}_{FE}$ can be expressed by the difference between $\mathbf{u}_{FE}$ and the solution of the linearized problem $\mathbf{u}_{\angle}$ for small c. Thus, error estimators and indicators derived for the linear case can be applied.

4.1.4 Strategies for adapting the discretization

Having computed error indicators for elements or discretization parameters, a strategy has to be found to adapt the discretization accordingly. The following strategies have been proposed for h-adaptivity, see for example RANNACHER [117]:

Error balancing strategy: The local error indicators are equilibrated for all elements of the current mesh according to $\eta_e \approx TOL/n_{el}$ assuming convergence rates given by a priori estimates. This eventually leads to $\eta \approx TOL$. Since n_{el} changes when refining or coarsening the mesh, iteration with respect to n_{el} may be required.

Fixed mesh or error fraction strategy: The elements are sorted according to the element error indicators η_e and a certain percentage (e.g. 30%) of those elements corresponding to the largest η_e are refined. A strategy of this kind is useful for achieving a prescribed rate of number of degrees of freedom N per iteration or for keeping N constant, as may be desirable in time-dependent problems.

Mesh optimization strategy: The proposed approach is based on the representation

$$\eta = \sum_{e=1}^{n_{el}} \eta_e \approx \int_{\Omega} h(x)^2 \cdot \phi(x) d\Omega \tag{4.55}$$

Here, $h(x)$ is interpreted as a smoothly distributed, mesh-size function. The existence of such a representation with an h-independent error density function ϕ can only be unconditionally justified under very restrictive conditions, but is generally supported by computational experience. A representation of this kind enables the computation of an optimal $h(x)$-function. In the limit this approach leads to the *error balancing strategy* described above.

These considerations with respect to h-adaptivity can be extended to other refinement strategies. A p-adaptive strategy for time-independent problems is proposed in Chapter 5. With regard to hp-adaptive methods, the question as to whether, and where to refine the element size h or to increase the polynomial degree p in order to obtain the most efficient discretizations has not been answered completely, so far. The approach of Ainsworth and Senior [4] is based on estimating the local regularity of the solution. Melenk and Wohlmuth [92] use an extrapolation of the estimated error with respect to the previous refinement steps. Demkowicz and Oden [43] and Oden et al. [106] propose a three-step method consisting of an initial computation, the adaptation of h and finally the adaptation of p. Rachowicz et al. [113] and Demkowicz et al. [46] use a local projection of a reference solution concurrently on h- and p-refinements in order to decide which strategy is more efficient.

4.2 Adaptivity for time-dependent problems

Since the solution of transient problems has to reflect the temporal behavior of a system, a discretization of the time domain is required in numerical approaches. Therefore, in addition to the spatial error discussed in Section 4.2, a *time discretization error* is introduced. Both the temporal and the spatial error have to be controlled. For the purpose of error analysis and estimation, the total error is divided into the spatial and the temporal error, see Eriksson et al. [57]

$$\mathbf{e} = \mathbf{e}_{tot} = \mathbf{u}_{EX} - \mathbf{u}_{st} = (\mathbf{u}_{EX} - \mathbf{u}_s) + (\mathbf{u}_s - \mathbf{u}_{st}) = \mathbf{e}_s + \mathbf{e}_t. \tag{4.56}$$

In Equation (4.56), $\mathbf{u}_s$ solely contains a spatial error but no temporal error. The error in energy is decomposed into the error in strain energy and the error in kinetic energy

$$\|\mathbf{e}\|_E^2 = E_{str}(\mathbf{e}) + E_{kin}(\mathbf{e}) = \|\mathbf{e}\|_{E_{str}}^2 + \|\mathbf{e}\|_{E_{kin}}^2 \tag{4.57}$$

and it is usually assumed that the error in energy can be split into a purely spatial part and a purely temporal part, see for example Riccius [121], Maute [91], Neumann [95],

$$\|\mathbf{e}\|_E^2 = \|\mathbf{e}_s + \mathbf{e}_t\|_E^2 = \|\mathbf{e}_s\|_{E_{str}}^2 + \|\mathbf{e}_s\|_{E_{kin}}^2 + \|\mathbf{e}_t\|_{E_{str}}^2 + \|\mathbf{e}_t\|_{E_{kin}}^2 = \|\mathbf{e}_s\|_E^2 + \|\mathbf{e}_t\|_E^2, \tag{4.58}$$

i.e. the errors $\mathbf{e}_s$ and $\mathbf{e}_t$ are assumed to be orthogonal with respect to the energy.

Another distinction can be made between the global and the local error. In the discussion of the spatial errors in Section 4.2 a global spatial error was defined over the whole domain, for instance, the error in energy norm. On the other hand, local errors were defined as errors in pointwise quantities or in quantities in a partition of interest, such as pointwise displacements or stress resultants over a subdomain. These considerations for spatial errors can be transferred to the time domain. A global temporal error defines the error introduced in the complete time interval. A local temporal error is the error introduced in a certain subinterval, such as a timestep of the time discretization scheme.

Thanks to its simplicity, timestep adaptivity is a very widespread concept, since only one scalar quantity needs to be adapted. In many approaches in structural dynamics, adaptive time-stepping is coupled with Newmark-based discretization techniques, see Zienkiewicz and Xie [153], Wiberg and Li [143], Li et al. [87], Kuhl [82], Riccius et al. [121, 121], Neumann et al. [95]. A popular approach estimates the local temporal error within a timestep, i.e. the influence of previous timesteps is disregarded, by computing an improved solution, using a Taylor series expansion, for instance. Temporal error estimation is discussed in Section 4.2.1.

It is more difficult to control the spatial error adaptively, since mesh adaptation is usually called for. Therefore, spatial adaptivity is not as widespread as time adaptivity in structural dynamics. Most error estimators are based on the semi-discrete form (3.45), approximating the spatial global error in energy norm. Recovery methods are frequently employed for both the error in strain and that in kinetic energy, cf. [86, 91, 95, 121, 144]. Maute [91] and Neumann [95] propose adaptivity for local quantities based on dual methods. Existing approaches to spatial error estimation for adaptive methods in structural dynamics are described in Section 4.2.2. Adaptive strategies for temporal and spatial discretization are discussed in Section 4.2.3.

4.2.1 Error of temporal discretization

Error control of time integration has been dealt with in numerous scientific contributions. PARK [111] adjusted the timestep size to the highest frequency occurring in the whole time interval computed. BERGAN et al. [28] adapted the timestep size with respect to *currently* occurring frequencies. The differences in results due to different timestep sizes or due to time integration schemes of different order were used by THOMAS et al. [138] and KUHL [82]. However, those approaches are expensive in a computational sense, since the problem has to be solved twice or with expensive multi-step methods. Therefore, in many approaches single-step methods with inexpensive error indicators are used and the results improved using the higher order Taylor series expansion, cf. ZIENKIEWICZ [153], LI [87], WIBERG [143], RICCIUS [122].

In the following the spatial error is disregarded and a distinction is made between the global and the local temporal error estimates. The global temporal error $\mathbf{e}_{glb}$ is the difference between the approximation $\mathbf{u}_n$ computed numerically in the current timestep and the exact solution $\mathbf{u}_{EX}(t_n)$,

$$\mathbf{e}_{glb}(t_n) = \mathbf{u}_{EX} - \mathbf{u}_n, \tag{4.59}$$
$$\dot{\mathbf{e}}_{glb}(t_n) = \dot{\mathbf{u}}_{EX} - \dot{\mathbf{u}}_n. \tag{4.60}$$

The global error $\mathbf{e}_{glb}(t_n)$ measures the total temporal error of the time interval $[0, t_n]$. The local error measures the error of a single timestep $[t_{n-1}, t_n]$. It is assumed that the numerical solution at $t = t_{n-1}$ is "exact". This "exact" solution is used as the initial condition for computing the exact solution $\hat{\mathbf{u}}_{EX}$ at $t = t_n$. The local errors in displacements and velocities are given by the differences

$$\mathbf{e}_{loc}(t_n) = \hat{\mathbf{u}}_{EX} - \mathbf{u}_n, \tag{4.61}$$
$$\dot{\mathbf{e}}_{loc}(t_n) = \dot{\hat{\mathbf{u}}}_{EX} - \dot{\mathbf{u}}_n. \tag{4.62}$$

4.2.1.1 Local temporal estimates

Since neither $\hat{\mathbf{u}}_{EX}$ nor $\dot{\hat{\mathbf{u}}}_{EX}$ are known, the "exact" solutions are approximated by improved solutions $\mathbf{u}^*$ and $\dot{\mathbf{u}}^*$

$$\mathbf{e}_{loc}(t_n) \approx \mathbf{e}_n = \mathbf{u}_n^* - \mathbf{u}_n, \tag{4.63}$$
$$\dot{\mathbf{e}}_{loc}(t_n) \approx \mathbf{e}_n = \dot{\mathbf{u}}_n^* - \dot{\mathbf{u}}_n. \tag{4.64}$$

In analogy to [146, 151, 153] — computing improved displacements by means of the Taylor series of third order — a fourth order Taylor expansion is used in [86, 87, 143], where $\mathbf{d}_n^*$ denotes the improved finite element displacement vector:

$$\mathbf{d}_n^* = \mathbf{d}_{n-1} + \Delta t \dot{\mathbf{d}}_{n-1} + \frac{\Delta t^2}{2}\ddot{\mathbf{d}}_{n-1} + \frac{\Delta t^3}{6}\dddot{\mathbf{d}}_{n-1} + \frac{\Delta t^4}{24}\ddddot{\mathbf{d}}_{n-1} + \mathcal{O}(\Delta t^5) \tag{4.65}$$

In the same manner, improved velocities are given by

$$\dot{\mathbf{d}}_n^* = \dot{\mathbf{d}}_{n-1} + \Delta t \ddot{\mathbf{d}}_{n-1} + \frac{\Delta t^2}{2} \dddot{\mathbf{d}}_{n-1} + \frac{\Delta t^3}{6} \ddddot{\mathbf{d}}_{n-1} + \mathcal{O}(\Delta t^4). \tag{4.66}$$

The fourth order terms in Equations (4.65) and (4.66) are computed with difference quotients

$$\ddddot{\mathbf{d}}_{n-1} = \frac{\dddot{\mathbf{d}}_n - \dddot{\mathbf{d}}_{n-1}}{\Delta t} + \mathcal{O}(\Delta t). \tag{4.67}$$

The derivative of the accelerations $\dddot{\mathbf{d}}_n$ at the new point in time $t = t_n$ is computed from the known accelerations $\ddot{\mathbf{d}}_{n-1}$ and $\ddot{\mathbf{d}}_n$ and $\dddot{\mathbf{d}}_{n-1}$ of the last point in time $t = t_n - 1$

$$\frac{\dddot{\mathbf{d}}_n + \dddot{\mathbf{d}}_{n-1}}{2} = \frac{\ddot{\mathbf{d}}_n - \ddot{\mathbf{d}}_{n-1}}{\Delta t}. \tag{4.68}$$

At $t = 0$, the derivatives of the accelerations are computed from the derivative of the equations of motion [86]. Combining the Taylor series expansions (4.65), (4.66) with the difference quotients (4.67) and from (4.68) we obtain

$$\mathbf{d}_n^* = \mathbf{d}_{n-1} + \Delta t \dot{\mathbf{d}}_{n-1} + \frac{\Delta t^2}{2} \ddot{\mathbf{d}}_{n-1} + \frac{\Delta t^3}{24} (3\dddot{\mathbf{d}}_{n-1} + \dddot{\mathbf{d}}_{n-1}) + \mathcal{O}(\Delta t^5) \tag{4.69}$$

and

$$\dot{\mathbf{d}}_n^* = \dot{\mathbf{d}}_{n-1} + \Delta t \ddot{\mathbf{d}}_{n-1} + \frac{\Delta t^2}{6} (2\dddot{\mathbf{d}}_{n-1} + \dddot{\mathbf{d}}_{n-1}) + \mathcal{O}(\Delta t^4). \tag{4.70}$$

Using Equations (4.63) and (4.64) for the local error with the NEWMARK formulae (3.76) and (3.77) for $\mathbf{d}_n$ and Equations (4.69) and (4.70) for the improved solutions $\mathbf{d}_n^*$ results in

$$\mathbf{e}_n = \frac{\Delta t^3}{12} \left[\left(6\beta - \frac{1}{2} \right) \dddot{\mathbf{d}}_n + \left(6\beta - \frac{3}{2} \right) \dddot{\mathbf{d}}_{n-1} \right], \tag{4.71}$$

$$\dot{\mathbf{e}}_n = \frac{\Delta t^2}{6} \left[(3\gamma - 1) \dddot{\mathbf{d}}_n + (3\gamma - 2) \dddot{\mathbf{d}}_{n-1} \right]. \tag{4.72}$$

The indicators (4.71), (4.72) can be used for all admissible values of β and γ. A disadvantage of the error indicators is that the difference quotients of first order used for the higher order derivatives may be inaccurate. RICCIUS [121] computes the higher order derivatives with central difference quotients

$$\dddot{\mathbf{d}}_{n-1} = \frac{\ddot{\mathbf{d}}_n - \ddot{\mathbf{d}}_{n-2}}{2\Delta t} + \mathcal{O}(\Delta t^2), \tag{4.73}$$

$$\ddddot{\mathbf{d}}_{n-1} = \frac{\ddot{\mathbf{d}}_{n-2} - 2\ddot{\mathbf{d}}_{n-1} + \ddot{\mathbf{d}}_n}{\Delta t^2} + \mathcal{O}(\Delta t^2), \tag{4.74}$$

resulting in

$$\mathbf{e}_n = \frac{\Delta t^2}{24}\left[\ddot{\mathbf{d}}_{n-2} + (2-24\beta)\,\ddot{\mathbf{d}}_{n-1} + (24\beta-3)\,\ddot{\mathbf{d}}_n\right], \tag{4.75}$$

$$\dot{\mathbf{e}}_n = \frac{\Delta t}{12}\left[\ddot{\mathbf{d}}_{n-2} + (4-12\gamma)\,\ddot{\mathbf{d}}_{n-1} + (12\gamma-5)\,\ddot{\mathbf{d}}_n\right]. \tag{4.76}$$

For $\beta \neq \frac{1}{6}$ and $\gamma \neq \frac{1}{2}$, the simplification of indicators (4.75), (4.76) is given in [121].

Li [85], Maute [91], Neumann [95] use a discontinuous time Galerkin method for the time integration. As a consequence, the jump observed in displacements and velocities between two time intervals can serve as a local temporal error indicator.

4.2.1.2 Global temporal estimates

For the estimation of the global error in energy norm at time $t = t_n$, Zienkiewicz and Xie [153] suggest the summation of energy norms of all local errors

$$\|\mathbf{e}_{glb}(t_n)\|_E = \sum_{m=1}^{n} \|\mathbf{e}_m\|_E \tag{4.77}$$

or, alternatively,

$$\|\mathbf{e}_{glb}(t_n)\|_E = N\|\mathbf{e}_n\|_E. \tag{4.78}$$

Equation (4.78) seems to be somewhat random, but is advantageous especially for damped systems, where the error is damped in accordance with the damping of displacements, see Maute [91]. Riccius [121] uses the estimator

$$\|\mathbf{e}_{glb}(t_n)\|_E = \frac{t_n}{\Delta t}\|\mathbf{e}_n\|_E. \tag{4.79}$$

Neumann [95] proposes computing the global error estimator by introducing a dual backward problem in time based on a time discontinuous Galerkin method. However, this approach is very time-consuming, necessitating the computation of the entire backward problem, i.e. the dual solution at t_m, $m = n-1, ..., 0$ must be computed for every timestep for which the error is desired. He states that the method provides usable results for a model problem with a number of degrees of freedom in space $N = 2$ (two-mass system).

4.2.2 Spatial error

A common approach for finding error estimates for the spatial error of structural dynamics is to transfer error estimates of static problems to dynamic problems. In addition to the error in strain energy, it is also important to take the error in kinetic energy into account for structural dynamics problems. Error estimators and indicators of this kind allow an appropriate adjustment of the spatial discretization, see Section 4.2.3.1.

First approaches are already in place for estimating local spatial errors for structural dynamics problems with a view to local quantities of interest, cf. MAUTE [91], NEUMANN [95]. In the following section, only error estimators and indicators for global quantities, usually the error in energy norm, are described. As in the previous section, we now focus on the spatial error and disregard errors of time discretization.

A very popular approach involves recovery techniques based on the semi-discrete formulation of the equations of motion, see WIBERG and LI [144], WIBERG ET AL. [143], RICCIUS and SCHWEIZERHOF [122], RICCIUS [121], MAUTE [91], NEUMANN [95]. The error in strain energy is estimated by means of the same recovery techniques described in Section 4.1.2.3 for time-independent problems.

For the computation of the error in kinetic energy

$$\|\mathbf{e}\|_{E_{kin}} = \sum_{e=1}^{n_{el}} \|\mathbf{e}\|_{E_{kin}(\Omega_e)} = \sum_{i=1}^{n_{el}} \int_{\Omega_e} (\dot{\mathbf{u}}_{EX} - \dot{\mathbf{u}}_{FE}) \cdot \rho(\dot{\mathbf{u}}_{EX} - \dot{\mathbf{u}}_{FE}) d\Omega_e \tag{4.80}$$

the exact velocities $\dot{\mathbf{u}}_{EX}$ are required, but not available. Therefore, $\dot{\mathbf{u}}_{EX}$ is approximated by recovering the numerical results $\dot{\mathbf{u}}_{FE}$ to obtain improved velocities $\dot{\mathbf{u}}^*$. The recovery of velocities involves certain difficulties, since in contrast to the stresses $\boldsymbol{\sigma}_{FE}$, the velocities $\dot{\mathbf{u}}_{FE}$ are continuous and the improvement by simple smoothing is less significant. When using SPR-techniques, another problem arises. The superconvergent points are GAUSS-LOBATTO points as opposed to GAUSS-LEGENDRE points, which are superconvergent for spatial derivatives of $\mathbf{u}_{FE}$, such as stresses, and GAUSS-LOBATTO points are usually identical to the nodes of the finite element mesh. Therefore, "patch-assembly" elements are used instead of "patch-assembly" nodes (since the nodes are already superconvergent), where the improved solution is described with a polynomial consisting of terms contained in the shape functions used for the finite element approximation, plus one or two additional higher order terms. It is possible to compute the element error immediately after recovering the solution on the element patch, whereas the patches for all the element nodes have to be computed in advance when using "patch-assembly" nodes for improved stresses. For more details, the reader is referred to WIBERG and LI [145], MAUTE [91].

Another concept has been proposed by RICCIUS [121]. Instead of trying to improve the velocities, he *degenerates* them and estimates the error by the difference between $\dot{\mathbf{u}}_{FE}$ and those "degenerated" velocities, weighted by a constant correction factor. The advantages of the approach are that the solution does not necessarily need to have superconvergent points and

no equation system needs to be solved. The "degenerated" velocities are computed at nodal points by averaging the centerpoint velocities of all adjacent elements, which could be interpreted as an evaluation on a coarser grid. The correction factor bears in mind that the difference to a degenerated — not improved — solution is computed. Unfortunately, no results are available for higher order elements. It can be noted that the p-adaptive approach for dynamic problems described in Chapter 6 is a related concept, where the hierarchic solution is projected on Ansatz spaces of lower order.

Recovery-based error estimates are very popular and widespread. However, as mentioned above, for dynamic problems the mathematical basis is weak. More elaborate approaches to error estimation for hyperbolic problems of second order based on dual problems have already been discussed in Johnson [75], Eriksson et al. [57], Bangerth and Rannacher [20], Maute [91]. Only few residual based estimators were examined for problems of this type, see for example Neumann [95] and the literature listed therein.

4.2.3 Adaptive strategies

4.2.3.1 Strategies for spatial adaptivity

In structural dynamics, most approaches use h-adaptivity for adjusting the spatial discretization to control the error. For p-, hp-, r-extensions only a few adaptive approaches for structural dynamics problems are known to the author, such as Demkowicz [43] using hp-adaptivity for elastic scattering. In Chapter 6 a p-adaptive strategy is described for structural vibrations based on adapting the discretization to the eigenmodes excited most.

We shall now proceed to describe an h-adaptive strategy for linear or bilinear elements according to Maute [91] by way of an example in order to point out the basic aspects, followed by modifications of the strategy. As mentioned above, the spatial error in energy $\|\mathbf{e}_s\|_E^2$ is composed of the element contributions to strain and kinetic energy

$$\|\mathbf{e}_s\|_E^2 = \sum_{e=1}^{n_{el}} \|\mathbf{e}\|_{E(\Omega_e),s}^2 = \sum_{e=1}^{n_{el}} \|\mathbf{e}\|_{E_{str}(\Omega_e),s}^2 + \|\mathbf{e}\|_{E_{kin}(\Omega_e),s}^2. \tag{4.81}$$

The element contributions can be computed using the methods described in Sections 4.1.2 and 4.2.2, e.g. for recovery-based estimates

$$\|\mathbf{e}_s\|_{E_{str}}^2 \approx \sum_{e=1}^{n_{el}} \int_{\Omega_e} (\boldsymbol{\sigma}^* - \boldsymbol{\sigma}_{FE}) : \mathbb{C}^{-1} : (\boldsymbol{\sigma}^* - \boldsymbol{\sigma}_{FE}) d\Omega_e \tag{4.82}$$

$$\|\mathbf{e}_s\|_{E_{kin}}^2 \approx \sum_{e=1}^{n_{el}} \int_{\Omega_e} (\dot{\mathbf{u}}^* - \dot{\mathbf{u}}_{FE}) \cdot \rho (\dot{\mathbf{u}}^* - \dot{\mathbf{u}}_{FE}) d\Omega_e \tag{4.83}$$

In the following illustration, no distinction is made between the approximated and the exact error, i.e. the approximated error drives the adaptive strategy. The relative spatial error is

$$\eta_s = \frac{\|\mathbf{e}_s\|_E}{\max_{t_n} \|\mathbf{u}_{EX}\|_E} \approx \frac{\|\mathbf{e}_s\|_E}{\max_{t_n} \|\mathbf{u}_{FE}\|_E}, \tag{4.84}$$

where the error $\|\mathbf{e}_s\|_E^2$ is related to the maximum energy norm $\max_{t_n} \|\mathbf{u}_{EX}\|_E$ or $\max_{t_n} \|\mathbf{u}_{FE}\|_E$, respectively. The discretization is accepted when the relative error is within the prescribed lower and upper error bounds

$$\bar{\eta}_{s,l} \leq \eta_s \leq \bar{\eta}_{s,u} \quad \text{or} \quad \eta_s \leq \bar{\eta}_{s,u} \tag{4.85}$$

If the relative spatial error is not within the prescribed bounds, then the spatial discretization has to be adapted. Usually the lower bound is disregarded. In the case of h-adaptivity, the optimal mesh is obtained when the element errors are distributed equally over the domain Ω. The admissible total error in energy norm is computed from the relative upper limit $\bar{\eta}_{s,u}$ and the maximum energy $\max_{t_n} \|\mathbf{u}_{EX}\|_E$

$$\|\bar{\mathbf{e}}_s\|_E = \Theta_s \bar{\eta}_{s,u} \max_{t_n} \|\mathbf{u}_{EX}\|_E, \tag{4.86}$$

where Θ_s is a safety factor usually chosen to satisfy $0.8 \leq \Theta_s \leq 1.1$. Since the element errors are to be equally distributed, the admissible element error in energy can be computed

$$\|\bar{\mathbf{e}}_s\|_{E(\Omega_e)} = \frac{\|\bar{\mathbf{e}}_s\|_E}{n_{el}}, \tag{4.87}$$

where n_{el} is the number of elements of the current mesh. The local refinement indicator ξ_e is a relative measure of the element errors

$$\xi_e = \frac{\|\mathbf{e}_s\|_{E(\Omega_e)}}{\|\bar{\mathbf{e}}_s\|_{E(\Omega_e)}}, \tag{4.88}$$

The new element size h_{new} can be computed with ξ_e and the element size on the current mesh h_{old}

$$h_{new} = \frac{h_{old}}{\xi_e^{1/p}}, \tag{4.89}$$

p being the order of the spatial Ansatz. For (4.89) it was assumed that the error converges with an order $\mathcal{O}(h^p)$. In the presence of singularities, the convergence rate may be lower, see Section 4.1.1.

There are several modifications to this strategy described above. Several contributions use only the error in strain energy and neglect the kinetic portion, for example Li [85], since either no method for estimating the error in kinetic energy was available or the estimation was

problematic and insufficient.

Instead of relating the error to the maximum energy norm of all timesteps, it is possible to relate it to the energy norm of the current timestep. However, this usually results in strong fluctuations in the relative error due to the variation of the current energy. In addition, comparing the error of different timesteps is difficult.

Riccius [121] and Neumann [95] prescribe the *absolute* error, which requires careful selection. For this reason, an initial computation using a coarse mesh is suggested.

The prescribed element error in Equation (4.87) referred to the number of elements n_{el} in the *current mesh*. However, it may be justified to relate it to the number of elements in the *target mesh*, since the element error should be distributed equally, there. This calls for iteration in respect of n_{el}.

This strategy can also be used for refinement according to the error in quantities of interest, when local a posteriori error estimates computed from the solution of a dual problem are applied. This is possible even though not a strict Galerkin method is applied, as is usually required for dual problems, i.e. finite difference-based methods can be used for the time integration. Maute [91] starts with a time Galerkin method for local error estimation, which can be transferred to finite difference methods using appropriate analogies to interpret certain finite difference methods as Galerkin methods.

4.2.3.2 Strategies for temporal adaptivity

As mentioned in Section 4.2.1 adaptive time integration has been addressed in numerous scientific contributions, see the citations given there. The strategies of spatial and temporal adaptivity are analogous. However, it is clearly easier to adapt the time discretization, since usually only one value — the timestep size or the order of the integration method — has to be adjusted, instead of constructing a new adaptive mesh. For time adaptivity, an error is prescribed with either relative or absolute bounds. In the following section, local relative error bounds $\bar{\eta}_t$ are assumed and compared to the estimated global or local errors η_t computed with the methods described in Section 4.2.1.

According to Dahlquist and Björck [42], the maximum order of accuracy obtainable with an A-stable integration method is 2, from which it follows that

$$\eta_t \quad \propto \quad \Delta t^3 \tag{4.90}$$

holds for the (local) maximum rate of convergence. It is accordingly possible to choose

$$\Delta t_{new} = \Delta t \sqrt[3]{\frac{\bar{\eta}_t}{\eta_t}} \tag{4.91}$$

For instance, the rate of convergence for the error in NEWMARK based methods with $\gamma \neq \frac{1}{2}$ is lower than 3 and therefore needs to be corrected with a factor $0 \leq \kappa \leq 1$, see for example LI [85],

$$\Delta t_{new} = \Delta t \sqrt[3\kappa]{\frac{\bar{\eta}_t}{\eta_t}}. \tag{4.92}$$

Similar considerations lead to adaptive strategies for global or absolute error bounds. Since time adaptive methods have already been subject to elaborate investigation, they are not subject matter of this thesis.

4.2.3.3 Remarks

The error can be controlled in every timestep or in every nth-timestep. Alternatively, the point in error control can be coupled to the change in energy norm.

In many approaches, either the temporal or the spatial error is controlled, see RICCIUS [121], for instance. LI [85] recognizes that the temporal error is sensitive to any changes in spatial discretization. It should be noted that temporal adaptivity only changes the time integration parameters. By contrast, changes in spatial discretization lead to a change in the initial conditions for the corresponding timestep, i.e. in addition to the discretization error, an error based on the transfer of history variables is introduced. This topic is discussed below.

4.2.4 Transfer of history variables

In the event of a change in the spatial discretization, the state variables of motion — also called history variables — get a new support on new shape functions and therefore have to be transferred from the old to the new discretization. In the following timestep the displacements $\mathbf{u}$, the velocities $\dot{\mathbf{u}}$ and the accelerations $\ddot{\mathbf{u}}$ are required and so usually all three variables have to be transferred. Possibly higher time derivatives than the second are needed for the computation of the next timestep, necessary for a temporal error estimator, for instance, see Section 4.2.1.

Either bilinear or biquadratic LAGRANGEan shape functions are used in the majority of two-dimensional approaches. In this case, a popular method is to use the same interpolation (bilinear or biquadratic) for transferring data from the old mesh to the nodes of the new mesh.

The relevant time-consuming tasks include

- neighborhood search
- computation of local coordinates

Neighborhood search is necessary to determine the element e_{old} of the old mesh in which the node i_{new} of the new mesh is located. This single task has a complexity of $\mathcal{O}(n_{el_{old}})$ to $\mathcal{O}(log(n_{el_{old}}))$ and usually has to be repeated for every node $i_{new} = 1, ..., n_{nd_{new}}$ times. The

computation of the local coordinates of node i_{new} in element e_{old} can only be achieved in a closed form for bilinear elements. For elements of higher order with more complex geometries, the local coordinates have to be determined by a NEWTON-RAPHSON iteration. Once the local coordinates are available, the data can be evaluated at node i_{new} using the shape functions defined on e_{old}.

Transferring data between different discretizations introduces an error unless strictly hierarchical refinement is applied, see discussion on hierarchical refinement below. This transfer error usually leads to a change in energy in the system. This can be interpreted as a modification of the initial value problem, so the subsequent computation is inconsistent. Since the transfer error cannot be compensated, it has to be minimized and kept under control.

LI [85], RICCIUS [121], WIBERG and ABDULWAHAB [142], RICCIUS and SCHWEIZERHOF [122], NEUMANN et al. [96], MAUTE [91] suggest several methods to improve the quality of transferred data, which are described below.

A first step is to smooth the data. The smoothing techniques are similar to those used for recovery based error estimators. One possibility is to average the values of neighboring nodes. For a node i, for example, the smoothed displacement $\mathbf{u}_{i,smo}$ can be computed as

$$\mathbf{u}_{i,smo} = \frac{1}{n_{ngb}+1}\left(\mathbf{u}_{n_i} + \sum_{j=1}^{n_{ngb}} \mathbf{u}_j\right), \tag{4.93}$$

n_{ngb} being the number of neighbors of node i. One disadvantage is that the distance between the neighboring nodes and node i is not respected in Equation (4.93). One way of remedying this problem is to use the weighted L_2-projection proposed by RICCIUS [122] or a weighted, nearest neighbor interpolation, see HALFMANN [66], for instance.

The data do not generally fulfill the conservation laws for momentum and energy either before or after smoothing. Despite the fact that it is impossible to avoid solving a different initial value problem from the original one following transfer, the data can be made consistent in itself, i.e. it can be recovered to such a degree that it fulfills at least the equilibrium conditions and energy conservation.

For the sake of conserving energy, the displacement function can be scaled by means of a scalar factor before or/and after smoothing. The factor is chosen such that the total strain energy before and after transfer, or before and after smoothing, remains constant. In the same manner, it is possible to find a scaling factor for the velocities keeping the kinetic energy constant.

However, only global energy conservation is enforced with this approach. In order to account for local conservation, the local correction factors can be computed elementwise in a first step and global energy conservation can be enforced in a second step [91]. A further alternative is a local L_2-projection with constraints providing energy conservation [142].

Similarly, it is possible to compute improved velocities when conservation of kinetic momentum is prescribed. However, as described in Riccius [121], kinetic energy and momentum cannot be conserved simultaneously. He proposes a method to preserve momentum and *total* energy.

Once they have been transferred, smoothed and corrected, the data do not generally fulfill the equilibrium conditions. Li [85] computes the accelerations using the equations of motion, where the *transferred* displacements and velocities are prescribed. Maute [91] takes up this idea but prescribes the *transferred and energy corrected* displacements and velocities.

In general, it can be stated that such correction techniques may lead to a degeneration in the smoothness of the accelerations. Moreover, the numerical effort is high. From this point of view, hierarchical approaches are an interesting alternative. When working with hierarchic bases, refinement does not lead to an error, since the functions on the coarse discretization can be represented exactly on the fine discretization. Only coarsening leads to an error, which can be reduced by projection techniques. Another important aspect of hierarchic bases is that the highest hierarchic degrees of freedom may only be omitted when carrying hardly any energy. Then, the transfer error is small as well and — even more important — can be readily controlled by computing the corresponding energies. This task is particularly simple when using hierarchic shape functions, as described in Section 3.1.1, since the energy for a hierarchic degree of freedom can be obtained by multiplying its amplitude with the corresponding stiffness terms.

Riccius [121], Neumann [95] propose a h-hierarchic approach in the sense that all nodes of a coarse mesh are contained in the fine mesh following pure refinement, using bilinear quadrilateral elements. However, the basis is not hierarchic unless *all* the elements are uniformly refined, since transition elements are required for local refinement, so transfer is not exact when it follows local refinement. To illustrate this phenomenon, the point refinement of a quadrilateral element towards one node results in one "quarter" element and two distorted elements sharing the "diagonal" edge from the center point to the corner node opposite to the refined node, see Figure 4.4. After refinement, a shape function is necessarily linear along this "diagonal" edge. The original shape function on the original element, however, is generally quadratic along the same line.

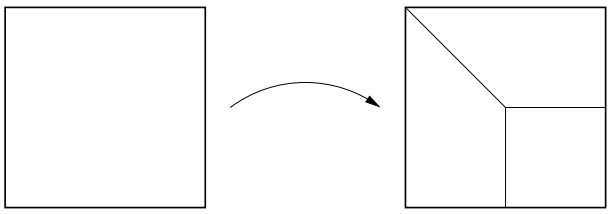

Figure 4.4: Transition between refined and unrefined areas: point refined element

By contrast, using a p-method with hierarchic shape functions as described in Section 3.1.1, refinement with *local* support on the element leads to an *exact* transfer. For the p-adaptive

method described in Chapter 6, a constant discretization is used for the time period concerned — adjusted to the frequencies excited most in an adaptive process — in order to keep the method as simple as possible. Nevertheless, an adaptation of p during the time-stepping process seems to be very profitable in the light of the arguments given above and the very promising results of the p-adaptive approach in general, as shown in Chapters 5 and 6.

4.3 Adaptivity for eigenvalue problems

Adaptive methods were described for the time-independent problems addressed in Chapter 4.1 and for transient problems in Section 4.2. There are also adaptive methods for the eigenvalue problems introduced in Sections 2.7.2 and 3.1.4.3, where the discretization is adjusted to represent the eigenmodes and corresponding frequencies in the best possible way.

In the following it is assumed that, since eigenfunctions $\mathbf{u}_k$ corresponding to the eigenvalue λ_k are determined up to a constant factor, they are scaled to satisfy

$$\int_\Omega \mathbf{u}_k^{EX} \cdot \rho \mathbf{u}_k^{EX} d\Omega \;=\; 1 = \int_\Omega \mathbf{u}_k^{FE} \cdot \rho \mathbf{u}_k^{FE} d\Omega \tag{4.94}$$

4.3.1 A priori estimates for eigenvalue problems

A priori estimates exist for eigenvalue problems. For h-extensions some results are summarized below according to Neumann [95]. For convex domains, it can be shown that the eigenfunction is in the function space H_2. A priori estimates based on this fact are provided for the error in (strain) energy norm of $\mathbf{u}_k$, see Hackbusch [64], Nystedt [102], for example.

$$\|\mathbf{u}_k^{EX} - \mathbf{u}_k^{FE}\|_{E_{str}} \leq C_{E_{str}} \frac{\lambda_k^{EX} + 2d}{d} \|hD^2\mathbf{u}_k\|_{L_2} \tag{4.95}$$

with

$$D^2\mathbf{u}_k = \left(\sum_{i=1}^{3} \sum_{j=1}^{i} \sum_{l=1}^{3} \frac{\partial^2 u_{k,l}^2}{\partial x_i \, \partial x_j} \right)^{\frac{1}{2}}, \tag{4.96}$$

or for the error in L_2-norm

$$\|\mathbf{u}_k^{EX} - \mathbf{u}_k^{FE}\|_{E_{str}} \leq C_2 \frac{\lambda_k^{EX} + 2d}{d} \|h^2 D^2\mathbf{u}_k\|_{L_2}, \tag{4.97}$$

where d is the smallest distance between the eigenvalue under consideration and all the other eigenvalues. The error in eigenvalues has the same convergence rate as the error in energy norm

$$\lambda_k^{FE} - \lambda_k^{EX} \leq C_{\lambda_k} \frac{\lambda_k + 2d}{d} \| hD^2 \mathbf{u}_k \|_{L_2}. \tag{4.98}$$

$C_{E_{str}} > 0$, $C_2 > 0$, $C_{\lambda_k} > 0$ are constants depending on the domain Ω, only. As is already evident from Equations (4.95), (4.97), (4.98) these estimates are only valid for single eigenvalues ($d > 0$). For multiple eigenvalues ($d = 0$) additional considerations are required, cf. Heuveline and Rannacher [69].

For non-convex domains, for instance, domains with re-entrant corners, the convergence rate is reduced owing to the singularity, see for example Nystedt [102].

4.3.2 A posteriori estimates for eigenvalue problems and adaptivity

There are several approaches for a posteriori error estimation. For a single eigenvalue λ_k Neumann [95] approximates the error in strain energy norm by recovering the eigenfunction $\mathbf{u}_k$. The SPR-concept devised by Zienkiewicz and Zhu [155] is applied, making use of superconvergent points for stresses in order to approximate the exact stresses. The error in L_2-norm is approximated by transferring the concept of degenerated velocities described in Chapter 4.2.2 to eigenvalue problems and thus computes degenerated rather than improved eigenfunctions. The error in L_2-norm is then approximated in a similar way using the L_2-norm of the difference between the finite element solution for the eigenfunction and its degeneration multiplied by a constant factor. The h-adaptive process, however, is driven by the SPR-based error estimator for computing the error in energy norm. It should be mentioned that it is a simplification to consider the error in strain energy only, since the mass terms are also modified by the refinement of discretization.

Residual based error estimators have been proposed by several researchers, including Nystedt [102], Larson [84]. Heuveline and Rannacher [69] propose an error estimator using a dual auxiliary problem which is accordingly able to provide estimates for arbitrary quantities of interest.

Neymeyr [98] proposes error estimates both for controlling the iteration error of the preconditioned inverse iteration, which is applied as an eigensolver, within the finite element space used, and for the actual finite element approximation itself, using hierarchical expansion. As an example, he uses the estimators for h-adapting a problem governed by the two-dimensional Laplacean Equation.

Friberg [58] and Friberg et al. [59] propose a hierarchic error estimator and a p-adaptive procedure. In the following illustration, the notation is aligned to [59]. Using a hierarchic basis leading to hierarchic stiffness and mass matrices, the discrete eigenvalue problem can be written as

$$\left(\begin{bmatrix} \mathbf{K}_{(n)} & \mathbf{K}_{(n,m)} \\ \mathbf{K}_{(m,n)} & \mathbf{K}_{(m)} \end{bmatrix} - \lambda^{(n,m)} \begin{bmatrix} \mathbf{M}_{(n)} & \mathbf{M}_{(n,m)} \\ \mathbf{M}_{(m,n)} & \mathbf{M}_{(m)} \end{bmatrix} \right) \begin{bmatrix} \mathbf{x}^{(n)} \\ \mathbf{x}^{(m)} \end{bmatrix} = \mathbf{0} \tag{4.99}$$

where (n) and (m) denote the numbers of degrees of freedom for a current level of discretization and a possible hierarchical refinement, respectively. By definition, $\boldsymbol{\phi}_k^{(n)}, k = 1, ...n$, are the true eigenmodes obtained from (4.99) with all components $\mathbf{x}^{(m)}$ restrained to zero, whereas $\boldsymbol{\psi}_k^{(n+m)}, k = 1, ..., (n+m)$ represents the solution of the complete system. Eigenvalues $\lambda_k^{(n)}$, $\lambda_k^{(n+m)}$ are defined corresponding to $\boldsymbol{\phi}_k^{(n)}$ and $\boldsymbol{\psi}_k^{(n+m)}$. The basic idea in FRIBERG [58] is to assume for computed eigenpairs $(\lambda_k^{(n)}, \boldsymbol{\phi}_k^{(n)})$ that $\boldsymbol{\phi}_k^{(n)} \approx \boldsymbol{\psi}_k^{(n)}$ and $\lambda_k^{(n+m)} \approx \lambda_k^{(n)}$ such that $\boldsymbol{\psi}_k^{(n)}$ can be computed from (4.99). Using a Taylor series expansion for the RAYLEIGH quotient, an error indicator for $m = 1$ ($\mathbf{K}_{(m,m)} = K_{(n+1,n+1)}$, $\mathbf{M}_{(m,m)} = M_{(n+1,n+1)}$) is found to be

$$\eta_k^{(n+1)} = \frac{1}{k_k^{(n)}} \cdot \frac{([\mathbf{K}_{(n+1,n)} - \lambda_k^{(n)} \mathbf{M}_{(n+1,n)}] \boldsymbol{\phi}_k^{(n)})^2}{K_{(n+1,n+1)} - \lambda_k^{(n)} M_{(n+1,n+1)}}, \tag{4.100}$$

For further details on the derivation see [58]. This error indicator can be computed for every degree of freedom to be added. One drawback of the estimator is that, when $\lambda_k^{(n)}$ is in the vicinity of $K_{(n+1,n+1)}/M_{(n+1,n+1)}$, the estimator tends to infinity. Another drawback is that a large set of computationally costly stiffness terms of higher order has to be computed although they may not be needed in a subsequent adaptive computation. In FRIBERG et al. [59] the error indicator is used to hierarchically refine the discretization of a rectangular two-dimensional structure in a p-adaptive approach. Unfortunately, the adaptation is restricted to a maximum polynomial degree $p = 3$ and an asymptotic range could not be reached to evaluate the rate of convergence of the method.

The hierarchic anisotropic error indicator for eigenvalue problems described in Chapter 6 is based on *reduction* rather than *expansion* and accordingly involves a lower computational investment. The local polynomial degrees of the hierarchical p-refinements shown in the numerical examples in Section 6.3 are quasi unlimited (up to $p = 20$, for instance).

4.4 Model adaptivity

The concept of model adaptivity is relatively new. The underlying idea is to set up a sequence from coarse to finer physical and mathematical models. The model error of the model locally in use has to be estimated and the model can be adjusted accordingly. *Material* model adaptivity is based on refinement of models describing material behavior from simplified linear elastic material to nonlinear hyperelastic or plastic material or considering inhomogeneities in the microstructure of the material. For further information on material model adaptivity, the reader is referred to [93, 107, 108, 109, 110, 132, 134, 133, 139].

Some of the approaches to *dimensional* adaptivity already cited at the beginning of this chapter are presented below. A hierarchy of models is necessary to describe kinematic behavior ranging from the most simple to the most complex kinematic behavior. One approach is to use a hierarchy of models, each representing a spatial dimension. The resulting coarse-to-fine sequence $1D \rightarrow 2D \rightarrow 3D$ would consist of three models. Moreover, the "dimensional steps", i.e. $1D \rightarrow 2D$ and $2D \rightarrow 3D$, can be further subdivided, for example, by using hierarchical

plate or shell models, as described in Section 2.7.3 for the transition $2D \rightarrow 3D$.

Schwab [125] proposes a posteriori estimates of the modeling error for hierarchic plate models. The error estimators are based on the residual tractions on the plate surfaces. The residual tractions are the difference between the external tractions due to the applied load and the internal tractions according to the deformation computed with the model level under consideration.

Stein et al. [132] propose directional, or anisotropic, estimators using an equilibrated residual method, which they refer to as the "Posterior Equilibrium Method", where the estimator is computed on an extended model using extended test spaces. These estimators allow for adaptivity of the mathematical model — for example from the two-dimensional plate theory to the three-dimensional continuum theory — and discretization adaptivity in thickness direction of the full model, which they refer to as "dimensional adaptivity".

Oden and Cho [104] describe an *hpq*-adaptive approach for thin-walled structures. The adaptive approach is based on a hierarchical model for plates and shells, where q denotes the hierarchic level of the model. The total error can be decomposed orthogonally into a model and a discretization error. The total error is computed with the aid of an a posteriori error estimator, also solving local three dimensional problems based on an equilibrated residual approach. The basic idea of this *hpq*-adaptive method is that the ratio of model error and total error is assumed to be equally distributed over the domain. The error is reduced using a four-step strategy:

1. Compute problem on initial mesh with initial h_0, p_0, q_0. Compute error indicators and estimator (sum).

2. Find quasi optimal q-refined hierarchical model q_f elementwise with rationale of reducing model portion of total error computed in step 1 by increasing the element model level assuming convergence rates given by a priori estimates [104]. Compute solution with h_0, p_0, q_f and compute error indicators and estimator.

3. Accordingly, compute number of new elements per element for optimal h-refined mesh (equidistributed error) assuming a priori h-convergence for intermediate mesh. Compute solution and error indicators and estimator with h_f, p_0, q_f.

4. Finally, compute final p-distribution necessary to fall below target error assuming a priori p-convergence. Compute solution with h_f, p_f, q_f and estimate error. If necessary, repeat steps 2–4.

As a result, it was noted that the q-convergence was limited by the approximation error, and the *hp*-convergence was bounded by the model level q.

Düster and Scholz [55] proposed a *pq*-adaptive approach for thin-walled structures, which is actually a pure discretization adaptive approach, but closely related to model adaptivity. The basic idea is to use a fully three-dimensional model, i.e. the model error completely turns into a discretization error. Two discretization parameters — p and q— can be chosen per high order hexahedral element. p is the in-plane polynomial degree of the element, and

q the transversal polynomial degree, which can be related to the model level of hierarchic shell or plate models. An important advantage of this approach is that no different types of models — or elements — have to be implemented and managed, since a single flexible and efficient element type is sufficient for the entire model. An error indicator compares hierarchic sequences of computations. A two-step approach is used, the first step serving to adapt the transversal polynomial degree, and the second step adjusting the in-plane polynomial degree. If the estimated error in the final model fails to drop below the target error, the procedure has to be repeated.

From this point of view, the p-adaptive approach proposed in Chapters 5 and 6 of this thesis is a one-step approach, with concurrent estimation and adaptation of the transversal and in-plane polynomial degrees.

Chapter 5

An anisotropic p-adaptive method for elastostatic problems

After surveying different adaptive methods for structures in general and for thin-walled plates and shells in particular in the preceding Chapter 4, this chapter proposes a new p-adaptive method for linear elastostatic problems. This method is extended to linear elastodynamic problems in Chapter 6.

The goal of a p-adaptive method can be formulated as an optimization problem:

For a fixed mesh Δ dividing the domain Ω into n_{el} elements with fixed mapping $\mathcal{Q} = \{\mathbf{Q}_1, ..., \mathbf{Q}_{n_{el}}\}$, find a set of polynomial degree templates

$$\mathcal{P} \;=\; \{\mathbf{p_1}, ..., \mathbf{p}_{n_{el}}\} \tag{5.1}$$

for which the error in a specific norm $\| \bullet \|$ is smaller than a prescribed tolerance TOL and the costs in terms of computational resources are minimal.

Remarks:

1. The polynomial degree template for a hexahedral element e described in Section 3.1.1 is defined as

$$\mathbf{p}_e \;=\; \begin{matrix} \\ \xi \\ \eta \\ \zeta \end{matrix} \begin{matrix} \begin{matrix} u_x & u_y & u_z \end{matrix} \\ \begin{pmatrix} p_e^{1,1} & p_e^{1,2} & p_e^{1,3} \\ p_e^{2,1} & p_e^{2,2} & p_e^{2,3} \\ p_e^{3,1} & p_e^{3,2} & p_e^{3,3} \end{pmatrix} \end{matrix} , \tag{5.2}$$

   i.e. every element has 9 polynomial degrees as parameters to be selected in the adaptive process.

2. It is possible to select from various norms for quantifying the error. However, the energy norm $\| \bullet \|_E$ is a natural choice for the finite element method and will therefore be used in the adaptive approach discussed here.

3. The types of costs in terms of computational resources can be manifold. Obviously, the most restricting resources are computation time, measured in CPU time, for instance, and memory usage. For both the computation time and the memory usage the number of degrees of freedom N of a system seems to be a reasonable indicator for the computational demand. In the case of p-adaptivity, i.e. a fixed mesh is used, N is a function that depends solely on the set of polynomial degrees $\mathcal{P}$. Nevertheless, it is important to note that N is only a rough estimate for the resources needed, which of course also depend on such aspects as the data structures and algorithms used or on which architecture the computations are performed.

There are two requirements for setting up a p-adaptive method: firstly, a global stopping criterion is needed. Secondly, speaking in terms of optimization, we need a sensitivity analysis describing which polynomial degrees exert a strong influence on the error of the solution and which do not, i.e. we need an error indicator.

5.1 The stopping criterion: Hierarchy-based extrapolation

The extrapolation technique based on hierarchic extension of the finite element spaces, described in Section 4.1.2.5, will be used by way of a stopping criterion. Let us recall the error $\mathbf{e}$ of an approximate finite element solution $\mathbf{u}^{\mathcal{P}} \in \mathcal{S}^{\mathcal{P}}$ which represents the difference between the exact solution $\mathbf{u}_{EX} \in \mathcal{V}$ and its approximation

$$\mathbf{e} \;=\; \mathbf{u}_{EX} - \mathbf{u}^{\mathcal{P}}, \quad \mathbf{u}^{\mathcal{P}} \in \mathcal{S}^{\mathcal{P}}. \tag{5.3}$$

Having a sequence of hierarchically nested approximation spaces constructed by hierarchic p-extensions

$$\mathcal{S}^{\mathcal{P}_1} \subset \mathcal{S}^{\mathcal{P}_2} \subset \mathcal{S}^{\mathcal{P}_3} \subset ... \tag{5.4}$$

we can write

$$\mathcal{S}^{\mathcal{P}_2} = \mathcal{S}^{\mathcal{P}_1 + \Delta\mathcal{P}^{+}_{1\to 2}}, \quad \mathcal{S}^{\mathcal{P}_3} = \mathcal{S}^{\mathcal{P}_2 + \Delta\mathcal{P}^{+}_{2\to 3}}, ... \tag{5.5}$$

with the *set of difference polynomial degree templates* $\Delta\mathcal{P}^{+}_{k\to k+1}$ with entries

$$\Delta p_e^{i,j} \;\geq\; 0, \tag{5.6}$$

where the strict inequality

$$\Delta p_{\bar{e}}^{\bar{i},\bar{j}} \;>\; 0 \tag{5.7}$$

must be fulfilled, at least for one specific combination $\bar{e}$, $\bar{i}$, $\bar{j}$. The operator

$$\mathcal{P} + \Delta\mathcal{P} \;=\; p_e^{i,j} + \Delta p_e^{i,j} \tag{5.8}$$

was used in Equation (5.5). Hence, the errors in energy norm of the finite element approximations $\mathbf{u}^{\mathcal{S}^{\mathcal{P}_1}}$, $\mathbf{u}^{\mathcal{S}^{\mathcal{P}_2}}$, $\mathbf{u}^{\mathcal{S}^{\mathcal{P}_3}}$ are connected by the following inequality, see also Section 3.1.4.2:

$$\|\mathbf{u}_{EX} - \mathbf{u}^{\mathcal{P}_1}\|_E \geq \|\mathbf{u}_{EX} - \mathbf{u}^{\mathcal{P}_2}\|_E \geq \|\mathbf{u}_{EX} - \mathbf{u}^{\mathcal{P}_3}\|_E \tag{5.9}$$

A necessary condition for achieving accurate results with this extrapolation method is that the saturation assumption (4.41) described in Section 4.1.2.4 holds, i.e. we can replace the *greater equal* sign in inequality (5.9) with a strict *greater* sign. In other words, it is important to choose the hierarchic refinement $\Delta\mathcal{P}^{+}_{k\to k+1}$ reasonably so as to ensure a real improvement. Starting from an initial approximation space $\mathcal{S}^{\mathcal{P}_1}$, the question arises how to construct the hierarchic refinement $\Delta\mathcal{P}^{+}_{k\to k+1}$ accounting for both the saturation assumption and minimum costs, as claimed at the beginning of this chapter. An error indicator fulfilling this requirement is suggested in the following section.

5.2 An anisotropic hierarchic error indicator

Hierarchic Ansatz spaces can serve as a powerful basis for examining the sensitivity of the approximation error to the discretization parameters representing this hierarchy. The quantity of interest is the change of error $\Delta\mathbf{e}$ when varying the discretization parameters, i.e. the set of polynomial degree templates $\mathcal{P}$, by a set of difference templates $\Delta\mathcal{P}$:

$$\Delta\mathbf{e} \;=\; \mathbf{e}^{\mathcal{P}} - \mathbf{e}^{\mathcal{P}\pm\Delta\mathcal{P}} = \mathbf{u}_{EX} - \mathbf{u}^{\mathcal{P}} - \mathbf{u}_{EX} + \mathbf{u}^{\mathcal{P}\pm\Delta\mathcal{P}} = -\mathbf{u}^{\mathcal{P}} + \mathbf{u}^{\mathcal{P}\pm\Delta\mathcal{P}}, \tag{5.10}$$

or, using the Galerkin orthogonality, in energy norm:

$$\|\Delta\mathbf{e}\|_E \;=\; \|\mathbf{u}^{\mathcal{P}} - \mathbf{u}^{\mathcal{P}\pm\Delta\mathcal{P}}\|_E = \left|\|\mathbf{u}^{\mathcal{P}}\|_E - \|\mathbf{u}^{\mathcal{P}\pm\Delta\mathcal{P}}\|_E\right| \tag{5.11}$$

$$\;=\; \frac{1}{2}\left|\mathcal{B}(\mathbf{u}^{\mathcal{P}},\mathbf{u}^{\mathcal{P}}) - \mathcal{B}(\mathbf{u}^{\mathcal{P}\pm\Delta\mathcal{P}},\mathbf{u}^{\mathcal{P}\pm\Delta\mathcal{P}})\right|^{\frac{1}{2}} \tag{5.12}$$

For a systematic analysis all entries $p_e^{i,j}$ of the set of polynomial degree templates have to be examined. For one specific entry $p_{\bar{e}}^{\bar{i},\bar{j}}$ we can set

$$\Delta\mathcal{P}_{\bar{e}}^{\bar{i},\bar{j}} = \begin{cases} \Delta p_{\bar{e}}^{\bar{i},\bar{j}} \;>\; 0 \\ \Delta p_e^{i,j} \;=\; 0 \quad \text{for} \quad \{e,i,j\} \neq \{\bar{e},\bar{i},\bar{j}\} \end{cases} \tag{5.13}$$

and accordingly define a hierarchic error indicator based on *extension* marked by $\hat{}$

$$\begin{aligned}\hat{\lambda}_{\bar{e}}^{\bar{i},\bar{j}} &= \|\mathbf{u}^{\mathcal{P}} - \mathbf{u}^{\mathcal{P}+\Delta\mathcal{P}_{\bar{e}}^{\bar{i},\bar{j}}}\|_E \\ &= \frac{1}{2}\left|\mathcal{B}(\mathbf{u}^{\mathcal{P}},\mathbf{u}^{\mathcal{P}}) - \mathcal{B}(\mathbf{u}^{\mathcal{P}+\Delta\mathcal{P}_{\bar{e}}^{\bar{i},\bar{j}}},\mathbf{u}^{\mathcal{P}+\Delta\mathcal{P}_{\bar{e}}^{\bar{i},\bar{j}}})\right|^{\frac{1}{2}} \\ &= \frac{1}{2}\left|\mathcal{B}(\mathbf{u}^{\mathcal{P}},\mathbf{u}^{\mathcal{P}}) - \mathcal{B}(\mathbf{u}^{\mathcal{P}+},\mathbf{u}^{\mathcal{P}+})\right|^{\frac{1}{2}}\end{aligned} \tag{5.14}$$

or a hierarchic error indicator based on *reduction* marked by $\check{}$

$$\begin{aligned}\check{\lambda}_{\bar{e}}^{\bar{i},\bar{j}} &= \|\mathbf{u}^{\mathcal{P}} - \mathbf{u}^{\mathcal{P}-\Delta\mathcal{P}_{\bar{e}}^{\bar{i},\bar{j}}}\|_E \\ &= \frac{1}{2}\left|\mathcal{B}(\mathbf{u}^{\mathcal{P}},\mathbf{u}^{\mathcal{P}}) - \mathcal{B}(\mathbf{u}^{\mathcal{P}-\Delta\mathcal{P}_{\bar{e}}^{\bar{i},\bar{j}}},\mathbf{u}^{\mathcal{P}-\Delta\mathcal{P}_{\bar{e}}^{\bar{i},\bar{j}}})\right|^{\frac{1}{2}} \\ &= \frac{1}{2}\left|\mathcal{B}(\mathbf{u}^{\mathcal{P}},\mathbf{u}^{\mathcal{P}}) - \mathcal{B}(\mathbf{u}^{\mathcal{P}-},\mathbf{u}^{\mathcal{P}-})\right|^{\frac{1}{2}}.\end{aligned} \tag{5.15}$$

In Equations (5.14) and (5.15) , the *expanded/reduced* polynomial degree templates $\mathcal{P} \pm \Delta\mathcal{P}_{\bar{e}}^{\bar{i},\bar{j}}$ were alternatively written in abbreviated form as $\mathcal{P}\pm$. The error indicator of type (5.14) is closely related to the error estimator described in Section 4.1.2.4, where the difference between two hierarchical solutions approximates the error of the complete system. By contrast, the indicators (5.14) and (5.15) are also intended to provide information on the *direction* of the error. Therefore, (5.14) is also comparable to directional error estimators like those suggested by STEIN [132], recalled in Section 4.4, where anisotropic error estimation is also based on an expansion strategy.

The case of symmetric or antisymmetric modes playing a dominant role in the solution of a mechanical system should be taken into account when choosing a value for $\Delta p_{\bar{e}}^{\bar{i},\bar{j}}$. If the exact solution features such a characteristic, then the error may be significantly reduced at either the even or the odd polynomial degree steps during p-refinement, only. For the indicators (5.14) and (5.15) to yield reliable results, regardless of whether $p_{\bar{e}}^{\bar{i},\bar{j}}$ is even or odd, it is appropriate to choose $\Delta p_{\bar{e}}^{\bar{i},\bar{j}} \geq 2$.

Besides the computation of $\mathbf{u}^{\mathcal{P}}$, the original solution, $\mathbf{u}^{\mathcal{P}\pm}$ also has to be determined for both indicators. This *reduced/expanded* solution can be computed from the weak form of equilibrium (2.43)

$$\mathcal{B}(\mathbf{u},\mathbf{v}) = \mathcal{F}(\mathbf{v}) \tag{5.16}$$

with

$$\mathbf{u} \in \mathcal{S}^{\mathcal{P}\pm} \tag{5.17}$$

satisfying the Dirichlet boundary conditions and for all

$$\mathbf{v} \in \overset{\circ}{S}{}^{\mathcal{P}\pm} \tag{5.18}$$

vanishing at the Dirichlet boundaries. In discrete form according to (3.58) we can write

$$\sum_J \mathcal{B}(\mathbf{N}_J d_J, \mathbf{N}_I a_I) = \mathcal{F}(\mathbf{N}_I a_I) \tag{5.19}$$

$$\Rightarrow \sum_J \mathcal{B}(\mathbf{N}_J d_J, \mathbf{N}_I) = \mathcal{F}(\mathbf{N}_I) \tag{5.20}$$

with

$$\mathbf{N}_J d_J \in \mathcal{S}^{\mathcal{P}\pm} \tag{5.21}$$

and for all

$$\mathbf{N}_I a_I \in \overset{\circ}{S}{}^{\mathcal{P}\pm}. \tag{5.22}$$

There is another possible interpretation for the indicator by *reduction* (5.15): the computation of $\mathbf{u}^{\mathcal{P}-}$ can be considered as the finite element projection of $\mathbf{u}^{\mathcal{P}}$ onto the Ansatz space $\mathcal{S}^{\mathcal{P}-}$, in the sense that $\mathbf{u}^{\mathcal{P}-}$ minimizes the strain energy of the difference between $\mathbf{u}^{\mathcal{P}}$ and any function in $\mathcal{S}^{\mathcal{P}-}$:

$$\begin{aligned}
&\mathcal{B}(\mathbf{u}^{\mathcal{P}} - \mathbf{u}^{\mathcal{P}-}, \mathbf{u}^{\mathcal{P}} - \mathbf{u}^{\mathcal{P}-}) \\
&= \min_{\mathbf{u}\in\mathcal{S}^{\mathcal{P}-}} \mathcal{B}(\mathbf{u}^{\mathcal{P}} - \mathbf{u}, \mathbf{u}^{\mathcal{P}} - \mathbf{u}) \\
&= \min_{\mathbf{u}\in\mathcal{S}^{\mathcal{P}-}} \big(\mathcal{B}(\mathbf{u}^{\mathcal{P}}, \mathbf{u}^{\mathcal{P}}) + 2\mathcal{B}(\mathbf{u}^{\mathcal{P}}, \mathbf{u}) + \mathcal{B}(\mathbf{u}, \mathbf{u})\big)
\end{aligned} \tag{5.23}$$

In order to find a rule for computing $\mathbf{u}^{\mathcal{P}-}$ in analogy to (5.16) we use the discretization

$$\mathbf{u} = \sum_J \mathbf{N}_J d_J, \tag{5.24}$$

$$\mathbf{N}_I \in \mathcal{S}^{\mathcal{P}-}, \tag{5.25}$$

requiring that the partial derivatives of the function to be minimized with respect to d_I must vanish:

$$\underbrace{\frac{\partial \mathcal{B}(\mathbf{u}^{\mathcal{P}}, \mathbf{u}^{\mathcal{P}})}{\partial d_I}}_{0} - 2\frac{\partial \mathcal{B}(\mathbf{u}^{\mathcal{P}}, \sum_J \mathbf{N}_J d_J)}{\partial d_I} + \frac{\partial \mathcal{B}(\sum_J \mathbf{N}_J d_J, \sum_K \mathbf{N}_K d_K)}{\partial d_I} = 0 \tag{5.26}$$

$$\Longleftrightarrow \sum_J \sum_K \frac{\partial \mathcal{B}(\mathbf{N}_J d_J, \mathbf{N}_K d_K)}{\partial d_I} = 2 \sum_J \frac{\partial \mathcal{B}(\mathbf{u}^{\mathcal{P}}, \mathbf{N}_J d_J)}{\partial d_I} \tag{5.27}$$

$$\Longleftrightarrow \sum_J \mathcal{B}(\mathbf{N}_J d_J, \mathbf{N}_I) = \mathcal{B}(\mathbf{u}^{\mathcal{P}}, \mathbf{N}_I) \tag{5.28}$$

From the equivalent representations (5.20) and (5.28) it is, of course, evident that

$$\mathcal{F}(\mathbf{N}_I) = \mathcal{B}(\mathbf{u}^{\mathcal{P}}, \mathbf{N}_I), \tag{5.29}$$

Equation (5.28) will gain in importance as an alternative way of computing $\mathbf{u}^{\mathcal{P}^-}$ in the context of local error indication, when the finite element projection is reduced on a local level, i.e. on an element's domain.

The indicators (5.14) and (5.15) require a *global* solution of a problem of the same order in size as the original problem for every polynomial degree of freedom, i.e. for hexahedral elements with polynomial degree templates of type (5.2) $n_{pdof} = n_{el} \cdot 9$ global solutions would be necessary. It is therefore necessary to markedly reduce the complexity of the problem in order to compute the indicators with reasonable effort. The following sections describe approximations of the error indicators of type (5.15).

5.2.1 An implicit anisotropic hierarchical error indicator on element level

Since a direct computation of (5.15) for every polynomial degree is computationally too demanding, a reasonable, i.e. cheaper but still reliable, approximation to (5.15) has to be found. The basic idea behind the error indicator computed on element level, as proposed in this section, is that it may be assumed that the effects of cutting degrees of freedom in a specific element $\bar{e}$ on the global solution can be reduced to this element's domain.

With regard to the finite element projection (5.28), $\mathbf{u}^{\mathcal{P}}$ is not projected globally but elementwise, satisfying the Dirichlet boundary conditions

$$\sum_J \mathcal{B}(\mathbf{N}_{e,J} d_J, \mathbf{N}_{e,I}) = \mathcal{B}(\mathbf{u}^{\mathcal{P}}, \mathbf{N}_{e,I}), \tag{5.30}$$

where $\mathbf{N}_{e,I}$ are the element basis functions of element e. If insufficient boundary conditions are prescribed, resulting in a singular problem, the corresponding rigid body modes have to be suppressed. The right-hand side of (5.30) is, of course, not the element load vector in general, but it can be considered as the *equilibrated* element load vector which is in equilibrium with the internal forces of the element.

In order to illustrate the idea of elementwise projection, we consider the simple one-dimensional model problem of a linear elastic bar clamped at one end and subjected to a distributed traction, see Figure 5.1, with $EA = L = 1$, $f(x) = sin(2\pi x/L)$, $F = 0$, $u(0) = 0$. A closed form

exists for this problem, so that the finite element approximations can be compared to the exact solution. Moreover, the nodal values of finite element approximations match the analytical solution to the problem exactly. It should be noted that for one-dimensional examples the set of polynomial degree templates $\mathcal{P}$ is reduced to the element polynomial degrees p_e. The finite element mesh used here has four elements with equidistant nodes.

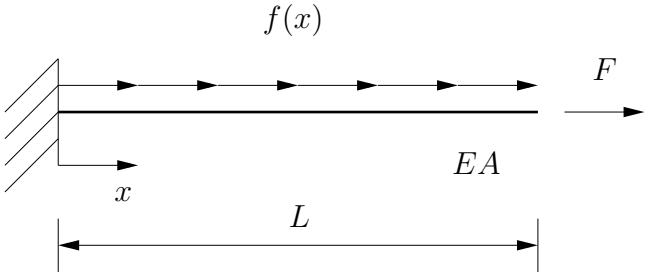

Figure 5.1: Linear elastic bar

We compare finite element solutions computed directly on a global level for uniform $p_{red} = 1, ..., 7$ with approximations obtained by elementwise finite element projections of a hierarchically higher-order, finite element solution computed with $p = 8$ onto Ansatz spaces corresponding to p_{red}, using the projection (5.30). In order to suppress the rigid body mode in longitudinal direction, the displacement of the node with the lower x-coordinate is prescribed for every element according to the solution obtained with $p = 8$.

In Figure 5.2 the global error in energy norm of the direct computations is compared to the corresponding error of the solution obtained by elementwise projection. The values of both methods are in the same order of magnitude for all polynomial degrees. Since the projection is intended to be applied as an error indicator providing reliable local information, the elementwise differences in strain energy of both approaches are plotted in Figure 5.3. It is clear from Figure 5.3 that the strain energy computed directly can be very accurately approximated by elementwise projection.

For this one-dimensional model problem the elementwise projection matches the directly computed solution very well. It also performs well for complex three-dimensional examples as a reliable error indicator, as will be shown in Section 5.4.

The general computation of the error indicator can be sketched using the following steps:

1. Compute solution of original global problem

$$\mathbf{K}^{\mathcal{P}}\mathbf{d}^{\mathcal{P}} = \mathbf{f}^{\mathcal{P}}. \tag{5.31}$$

2. Compute the right-hand side of (5.30), the equilibrated element load vector $\breve{\mathbf{f}}_{\bar{e}}$, using the element stiffness matrix $\mathbf{K}^{\mathcal{P}}_{\bar{e}}$ and the element solution vector $\mathbf{d}^{\mathcal{P}}_{\bar{e}}$

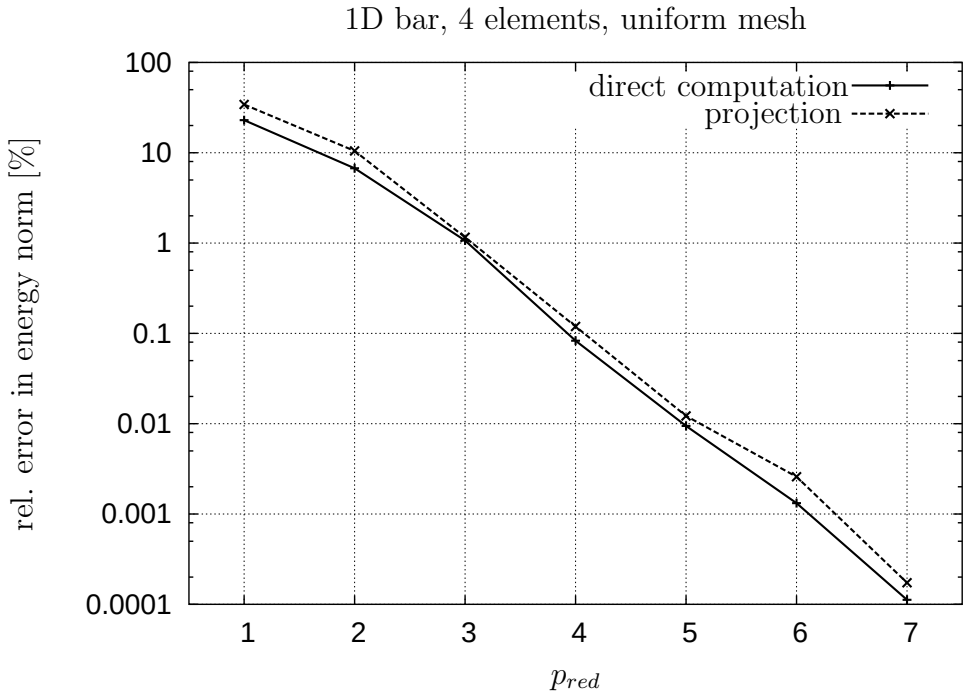

Figure 5.2: Relative error in energy norm for $p_{red} = 1, ..., 7$: directly computed solution and corresponding elementwise projection from $p = 8$ onto p_{red}

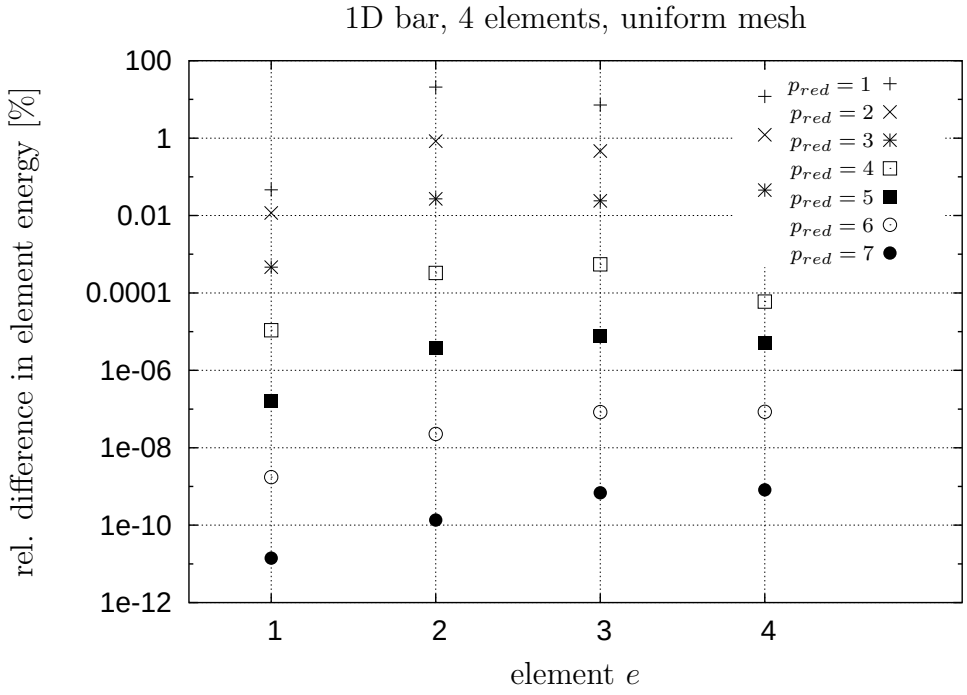

Figure 5.3: Elementwise relative difference in strain energy between directly computed solution with $p_{red} = 1, ..., 7$ and corresponding elementwise projection from $p = 8$ onto p_{red}

$$\breve{\mathbf{f}}_{\bar{e}}^{\mathcal{P}} = \mathbf{K}_{\bar{e}}^{\mathcal{P}} \mathbf{d}_{\bar{e}}^{\mathcal{P}} \tag{5.32}$$

In contrast to the element load vector $\mathbf{f}_{\bar{e}}$ representing the external loads applied to the element's domain and Neumann boundaries, the equilibrated element load also accounts for the loads on the inter-element boundaries, which can only be determined by global equilibrium.

3. Set Dirichlet boundary conditions and, if necessary, suppress rigid body modes of reduced element stiffness matrix $\mathbf{K}_{\bar{e}}^{\mathcal{P}-}$ and compute $\tilde{\mathbf{d}}_{\bar{e}}^{\mathcal{P}-}$ using

$$\mathbf{K}_{\bar{e}}^{\mathcal{P}-} \tilde{\mathbf{d}}_{\bar{e}}^{\mathcal{P}-} = \breve{\mathbf{f}}_{\bar{e}}^{\mathcal{P}-}, \tag{5.33}$$

where $\breve{\mathbf{f}}_{\bar{e}}^{\mathcal{P}-}$ is the subvector of $\breve{\mathbf{f}}_{\bar{e}}$ and $\mathbf{K}_{\bar{e}}^{\mathcal{P}-}$ is a submatrix of $\mathbf{K}^{\mathcal{P}}$ after cutting the corresponding degrees of freedom. $\tilde{\mathbf{d}}_{\bar{e}}^{\mathcal{P}-}$ is the approximation of the displacement vector computed with the reduced space $\mathbf{d}_{\bar{e}}^{\mathcal{P}-}$ obtained by local projection.

4. Compute

$$\begin{aligned} \breve{\lambda}_{\bar{e}}^{\bar{i},\bar{j}} &\approx \left| \frac{1}{2}\mathcal{B}(\mathbf{u}_{\bar{e}}^{\mathcal{P}}, \mathbf{u}_{\bar{e}}^{\mathcal{P}}) - \frac{1}{2}\mathcal{B}(\tilde{\mathbf{u}}_{\bar{e}}^{\mathcal{P}-}, \tilde{\mathbf{u}}_{\bar{e}}^{\mathcal{P}-}) \right|^{\frac{1}{2}} \\ &= \left| \frac{1}{2}\mathbf{d}_{\bar{e}}^{\mathcal{P}T} \mathbf{K}_{\bar{e}}^{\mathcal{P}} \mathbf{d}_{\bar{e}}^{\mathcal{P}} - \frac{1}{2}\tilde{\mathbf{d}}_{\bar{e}}^{\mathcal{P}-T} \mathbf{K}_{\bar{e}}^{\mathcal{P}-} \tilde{\mathbf{d}}_{\bar{e}}^{\mathcal{P}-} \right|^{\frac{1}{2}} \end{aligned} \tag{5.34}$$

The local indicator (5.34) is already a significant reduction of the system to be solved. Nevertheless, solving the element level Equation Systems (5.33) might prove to be very costly, especially when considering element matrices corresponding to polynomial degree templates of high order. It is with this in mind that two ways of approximating (5.33) with *explicit* expressions, i.e. without solution of an equation system, are proposed in Section 5.2.2.

5.2.2 Explicit anisotropic hierarchical error indicators on element level

In order to find explicit approximations to the local implicit error indicator (5.34), the equation system $\mathbf{K}_{\bar{e}}^{\mathcal{P}} \mathbf{d}_{\bar{e}}^{\mathcal{P}} = \breve{\mathbf{f}}_{\bar{e}}^{\mathcal{P}}$ is written in block matrix form

$$\overbrace{\begin{bmatrix} \mathbf{K}_{\bar{e}}^{11} & \mathbf{K}_{\bar{e}}^{12} \\ \mathbf{K}_{\bar{e}}^{21} & \mathbf{K}_{\bar{e}}^{22} \end{bmatrix}}^{\mathbf{K}_{\bar{e}}^{\mathcal{P}}} \overbrace{\begin{bmatrix} \tilde{\mathbf{d}}_{\bar{e}}^{1} + \Delta\mathbf{d}_{\bar{e}}^{1} \\ \mathbf{d}_{\bar{e}}^{2} \end{bmatrix}}^{\mathbf{d}_{\bar{e}}^{\mathcal{P}}} = \overbrace{\begin{bmatrix} \breve{\mathbf{f}}_{\bar{e}}^{1} \\ \breve{\mathbf{f}}_{\bar{e}}^{2} \end{bmatrix}}^{\breve{\mathbf{f}}_{\bar{e}}^{\mathcal{P}}}, \tag{5.35}$$

with

$$\mathbf{K}_{\bar{e}}^{11} = \mathbf{K}_{\bar{e}}^{\mathcal{P}-\Delta\mathcal{P}_{\bar{e}}^{\bar{i},\bar{j}}}, \tag{5.36}$$
$$\tilde{\mathbf{d}}_{\bar{e}}^{1} = \tilde{\mathbf{d}}_{\bar{e}}^{\mathcal{P}-}, \tag{5.37}$$
$$\breve{\mathbf{f}}_{\bar{e}}^{1} = \breve{\mathbf{f}}_{\bar{e}}^{\mathcal{P}-}. \tag{5.38}$$

Using GALERKIN orthogonality

$$\mathcal{B}(\tilde{\mathbf{u}}_{\bar{e}}^{\mathcal{P}-}, \tilde{\mathbf{u}}_{\bar{e}}^{\mathcal{P}-}) = \mathcal{B}(\mathbf{u}_{\bar{e}}^{\mathcal{P}}, \tilde{\mathbf{u}}_{\bar{e}}^{\mathcal{P}-}), \tag{5.39}$$

we can rewrite the second term in (5.34):

$$\frac{1}{2}\tilde{\mathbf{d}}_{\bar{e}}^{1^T}\mathbf{K}_{\bar{e}}^{11}\tilde{\mathbf{d}}_{\bar{e}}^{1} = \mathbf{d}_{\bar{e}}^{\mathcal{P}^T}\mathbf{K}_{\bar{e}}^{\mathcal{P}}\begin{bmatrix}\tilde{\mathbf{d}}_{\bar{e}}^{1}\\ \mathbf{0}\end{bmatrix} = \mathbf{d}_{\bar{e}}^{\mathcal{P}^T}\begin{bmatrix}\mathbf{K}_{\bar{e}}^{11}\tilde{\mathbf{d}}_{\bar{e}}^{1}\\ \mathbf{K}_{\bar{e}}^{21}\tilde{\mathbf{d}}_{\bar{e}}^{1}\end{bmatrix}, \tag{5.40}$$

and with the equilibrium condition for the reduced local problem and the hierarchy of the corresponding load vector

$$\mathbf{K}_{\bar{e}}^{11}\tilde{\mathbf{d}}_{\bar{e}}^{1} = \breve{\mathbf{f}}_{\bar{e}}^{1} = \mathbf{K}_{\bar{e}}^{11}\left(\tilde{\mathbf{d}}_{\bar{e}}^{1} + \Delta\mathbf{d}_{\bar{e}}^{1}\right) + \mathbf{K}_{\bar{e}}^{12}\mathbf{d}_{\bar{e}}^{2} \tag{5.41}$$

we obtain from (5.40)

$$\frac{1}{2}\tilde{\mathbf{d}}_{\bar{e}}^{1^T}\mathbf{K}_{\bar{e}}^{11}\tilde{\mathbf{d}}_{\bar{e}}^{1} = \mathbf{d}_{\bar{e}}^{\mathcal{P}}\begin{bmatrix}\mathbf{K}_{\bar{e}}^{11}\left(\tilde{\mathbf{d}}_{\bar{e}}^{1} + \Delta\mathbf{d}_{\bar{e}}^{1}\right) + \mathbf{K}_{\bar{e}}^{12}\mathbf{d}_{\bar{e}}^{2}\\ \mathbf{K}_{\bar{e}}^{21}\tilde{\mathbf{d}}_{\bar{e}}^{1}\end{bmatrix}. \tag{5.42}$$

The approximation introduced for computing (5.42) knowing $\mathbf{d}_{\bar{e}}^{\mathcal{P}}$, only, is for the lower entry of the second vector

$$\mathbf{K}_{\bar{e}}^{21}\tilde{\mathbf{d}}_{\bar{e}}^{1} \approx \mathbf{K}_{\bar{e}}^{21}\left(\tilde{\mathbf{d}}_{\bar{e}}^{1} + \Delta\mathbf{d}_{\bar{e}}^{1}\right) \tag{5.43}$$

This is justifiable since the changes $\Delta\mathbf{d}_{\bar{e}}^{1}$ should be small and the off-diagonal terms $\mathbf{K}_{\bar{e}}^{21}$ are not dominant in a positive definite matrix. Accordingly, (5.40) can be written as

$$\frac{1}{2}\tilde{\mathbf{d}}_{\bar{e}}^{1^T}\mathbf{K}_{\bar{e}}^{11}\tilde{\mathbf{d}}_{\bar{e}}^{1} \approx \frac{1}{2}\mathbf{d}_{\bar{e}}^{\mathcal{P}^T}\begin{bmatrix}\mathbf{K}_{\bar{e}}^{11}\left(\tilde{\mathbf{d}}_{\bar{e}}^{1} + \Delta\mathbf{d}_{\bar{e}}^{1}\right) + \mathbf{K}_{\bar{e}}^{12}\mathbf{d}_{\bar{e}}^{2}\\ \mathbf{K}_{\bar{e}}^{21}\left(\tilde{\mathbf{d}}_{\bar{e}}^{1} + \Delta\mathbf{d}_{\bar{e}}^{1}\right)\end{bmatrix} \tag{5.44}$$

This type of approximation is referred to as *version 1* in Section 5.4.

A second approximation method based on the plain cut-off of the corresponding degrees of freedom is referred to as the approximation of *version 2*:

$$\frac{1}{2}\tilde{\mathbf{d}}_{\bar{e}}^{1^T}\mathbf{K}_{\bar{e}}^{11}\tilde{\mathbf{d}}_{\bar{e}}^{1} \approx \frac{1}{2}\left(\tilde{\mathbf{d}}_{\bar{e}}^{1} + \Delta\mathbf{d}_{\bar{e}}^{1}\right)^T\mathbf{K}_{\bar{e}}^{11}\left(\tilde{\mathbf{d}}_{\bar{e}}^{1} + \Delta\mathbf{d}_{\bar{e}}^{1}\right) \tag{5.45}$$

5.3 The p-adaptive strategy

With the stopping criterion described in Section 5.1 and one of the local error indicators defined both in Section 5.2.1 and 5.2.2 we are now in a position to set up a p-adaptive algorithm. Sophisticated optimization schemes suggesting p-refinements and coarsenings of the set of polynomial degree templates $\mathcal{P}$ could be applied here. For instance, it is possible to choose the incremental step size in the p-discretization not only depending on the sensitivities provided by the error indicator but also on the basis of additional information, such as feedback of the improvements in the global optimization variable, i.e. the error in strain energy during the adaptive iterations. Instead, we intentionally employ a very straightforward adaptive procedure where changes in the polynomial degree templates are based on the error indicator, only.

The p-adaptive procedure used here sorts the polynomial degrees of freedom according to their sensitivity with respect to the error in strain energy estimated with the error indicator and simply refines a fixed proportion of the polynomial degrees of freedom, which also allows a staggering of the step sizes of p-changes.

Before choosing the adaptive polynomial degree templates, it is necessary to set a few parameters with respect to the error indicator and the optimization strategy. The difference polynomial degree $\Delta p_{\bar{e}}^{\bar{i},\bar{j}} = 2$, representing the number of polynomial degrees the indicator 'looks back', is chosen for the error indicator, according to the recommendations given in Section 5.2. It is also necessary to select one of the three element level types of error indicators — implicit, explicit *version 1* or *version 2*.

For the p-adaptive procedure, it is either possible to select the tolerance TOL for the stopping criterion or to define a maximum number of iterations $maxiter$. In addition, it is necessary to stipulate the proportions for the staggered refinement and coarsening. Therefore, the polynomial degrees of freedom $p_e^{i,j}$ are sorted according to their error indicator $\check{\lambda}_e^{i,j}$ in increasing order, resulting in the sequence

$$\lambda_1 < \lambda_2 < ... < \lambda_{n_{pdof}}, \tag{5.46}$$

where n_{pdof} is the number of polynomial degrees of freedom. Using the proportional error limits

$$\lambda_{r\%} = \lambda_{\mathrm{int}(\frac{r}{100}(n_{pdof}-1))+1} \tag{5.47}$$

meaning that approximately $r\%$ of the polynomial degrees of freedom have *smaller or equal* error indicators than $\lambda_{r\%}$ and approximately $(100-r)\%$ have larger error indicators, it is possible to define a proportionally staggered refinement strategy. In (5.47) the operator $\mathrm{int}(x)$ returns the integer part of the floating point number x. The staggered refinement scheme suggested here can be written as

$$\Delta\mathcal{P}_{iter+1} = \Delta p_{e,iter+1}^{i,j} = \begin{cases} 0 & \text{for} & & \check{\lambda}_e^{i,j} & < & \lambda_{70\%} \\ 1 & \text{for} & \lambda_{70\%} & \leq \check{\lambda}_e^{i,j} & < & \lambda_{90\%} \\ 2 & \text{for} & \lambda_{90\%} & \leq \check{\lambda}_e^{i,j} & & \end{cases} \tag{5.48}$$

In order to allow for the symmetric refinement of those polynomial degrees, which correspond to exactly equal (or due to round-off errors slightly different) error indicators as a result of the symmetry of the system, the refinement ranges are extended by proportional distortion of the absolute values of the limits $\lambda_{70\%}$, $\lambda_{90\%}$ by a factor ε. A choice of $\varepsilon = 0.01$ is used for the numerical examples.

Although only refinement is used in the following, coarsening can also be introduced in a similar way for polynomial degrees with low error indicators. In fact, coarsening has already been applied successfully for several examples, but it is not proposed to discuss this aspect here in order to keep the adaptive strategy as simple as possible.

In order to start the procedure, it is necessary to choose an initial set of polynomial degree templates $\mathcal{P}_0$. Here, a uniform set of $p_{e,0}^{i,j} = 4$ is recommended in order to avoid locking effects.

Having computed three sequential adaptive iterations, the aforementioned increments of polynomial degrees provide sufficient discretization improvement at every step for the hierarchic extrapolation to yield results accurate enough to be used as a stopping criterion. When the solution has *even/odd*-mode characteristics, as described in Section 5.2, the improvement in the solution is assumed to be substantial as well, since the polynomial degrees are increased by odd *and* even increments.

If any of the parameters specified above are changed in one of the subsequent examples, for investigating purposes of the robustness of the procedure against changes of this parameter, for instance, this will be clearly pointed out.

The p-adaptive strategy can be sketched as shown in Algorithm A-1. This algorithm will be applied on four examples in the following section: a clamped plate, a cylindrical shell with a clamped boundary, a hemispherical shell with a stiffener and the spring-back analysis of a thin metal sheet after the deep drawing process. Since the main objective of the next section is to analyze the refinement strategy based on the proposed error indicators, use is made of even more accurate reference solutions than those obtained from extrapolation from the current and the last two iterations. Such reference solutions may be obtained not only by higher hierarchic Ansatz spaces but also by mesh refinement.

5.4 Numerical examples

For all numerical examples in this section, the trunk space $\mathcal{S}_{\text{ts}}^{\mathcal{P}}$ is used for the discretization with hexahedral elements, see Section 3.1.1.

5.4.1 Clamped plate

The first example under consideration is a quadratic plate clamped at all boundaries which is subjected to a uniform load on the upper surface. Since the system is symmetric, only one quarter of the plate is modeled, resulting in the boundary conditions $u_x = u_y = u_z = 0$ at the

Algorithm A-1 p-Adaptive strategy

set $iter = 0$, $\mathcal{P}_{iter}$ **uniformly to** $p^{i,j}_{e,iter} = 4$
repeat
  compute $\mathbf{u}^{\mathcal{P}_{iter}}$
  for all $\{e, i, j\}$ **compute** $\check{\lambda}^{i,j}_e$
  sort all $\check{\lambda}^{i,j}_e$ **and find** $\lambda_{70\%}$, $\lambda_{90\%}$
  set

$$\Delta\mathcal{P}_{iter+1} = \Delta p^{i,j}_{e,iter+1} = \begin{cases} 0 & \text{for} \quad \check{\lambda}^{i,j}_e < \lambda_{70\%}(1-\varepsilon) \\ 1 & \text{for} \quad \lambda_{70\%}(1-\varepsilon) \leq \check{\lambda}^{i,j}_e < \lambda_{90\%}(1-\varepsilon) \\ 2 & \text{for} \quad \lambda_{90\%}(1-\varepsilon) \leq \check{\lambda}^{i,j}_e \end{cases}$$

  set $\mathcal{P}_{iter+1} = \mathcal{P}_{iter} + \Delta\mathcal{P}_{iter+1}$
  if $(iter \geq 2)$ **then**
    compute $\eta = \|\mathbf{e}\|_E$ **using hierarchic extrapolation**
  else
    set $\eta = TOL + \varepsilon$ *(stopping criterion not fulfilled yet)*
  end if
  $iter = iter + 1$
until $(\eta < TOL)$ OR $(iter > maxiter)$

two clamped boundaries and $u_x = 0$ and $u_y = 0$, respectively, at the symmetric boundaries, see Figure 5.4.

One quarter of the plate has a length $L = 6$ with a thickness $t = 0.35$. The plate is uniformly loaded with $t_z = -100$. The material is assumed to be linear elastic with YOUNG's modulus $E = 300\,000$ and $\nu = 0.2$ being POISSON's ratio.

The system is discretized with one element layer over the thickness using nine hexahedral elements, where the mesh is refined to the clamped boundaries in order to resolve the boundary layer, see Figure 5.4.

In order to evaluate the performance of the p-adaptive strategy, it was compared to a uniform p-refinement. A reference strain energy was computed by hierarchic extrapolation (see Section 4.1.2.5) of a sequence of three adaptively chosen, hierarchic p-discretizations to be $E_{str} = 13.27485483$. The reason for using an adaptive sequence instead of the uniform results is the higher accuracy which can be achieved. Higher accuracy is easy to recognize considering the fact that the strain energy is maximized in a sequence of hierarchically improved discretizations applying homogeneous displacement boundary conditions. The largest values for the strain energy, obtained by the adaptive procedure, could therefore be assumed to be the most accurate ones.

In Figure 5.5 the error in energy norm $\|\mathbf{e}\|_E = |E_{str} - E^{FE}_{str}|^{\frac{1}{2}}$ is plotted against the total number of degrees of freedom N. The sequence of uniform p-refinement $p = 2, ..., 16$ reveals the typical S-shape of the p-version type of convergence. The convergence is exponential in

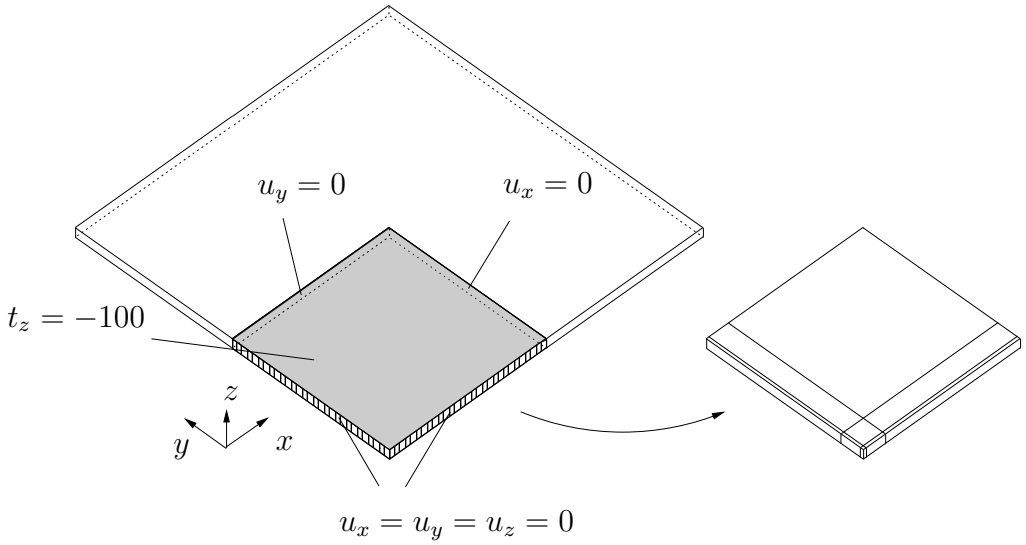

Figure 5.4: System of clamped plate (left) and hexahedral mesh (right)

the pre-asymptotic range, where the error is dominated by the polynomial degree of the approximating functions. The slope of the curve is subsequently reduced dramatically, and the algebraic convergence in the asymptotic range is reached. This range is usually dominated by singularities, in this case resulting from the clamped boundaries. The order of convergence in the asymptotic part is often very poor compared to the exponential pre-asymptotic range.

The adaptive curve shown in Figure 5.5 starting from a uniform polynomial degree distribution $p_{e,0}^{i,j} = p_0 = 4$ was obtained using the implicit local error indicator introduced in Section 5.2.1. Evidently, the adaptive sequence is more efficient since it is always below the uniform curve. The advantage of the adaptive approach is obvious even in the exponential preasymptotic range of the uniform curve, although this is the inherent strength of uniform p-version. However, the real impact of the p-adaptive approach is to be found in the asymptotic range, where the uniform curve shows poor asymptotic behavior and the adaptive curve has an immediately apparent, higher order of convergence.

Figure 5.6 demonstrates the robustness of the p-adaptive method against the starting polynomial degree $p_0 = 3, ..., 7$. The minimum polynomial degree in this sequence is 3, since the error indicator uses the 'look back' difference polynomial degree $\Delta p_{\bar{e}}^{\bar{i},\bar{j}} = 2$ and the minimum polynomial degree on which the solution can be projected (in this approach) is linear corresponding to the nodal shape functions. Again, all adaptive curves are below the uniform curve and exhibit approximately the same — clearly higher than uniform — order of convergence in the asymptotic range.

The performance of the explicit local error indicators of *version 1* and *version 2* proposed in Section 5.2.2 are compared to the uniform curve and the local implicit error indicator in Figure 5.7. Of all adaptive curves, the implicit curve appears to be the smoothest. However, the explicit indicator of *version 1* only slightly deviates from the implicit curve in the pre-asymptotic range. In the asymptotic range it has a similar order of convergence. The error

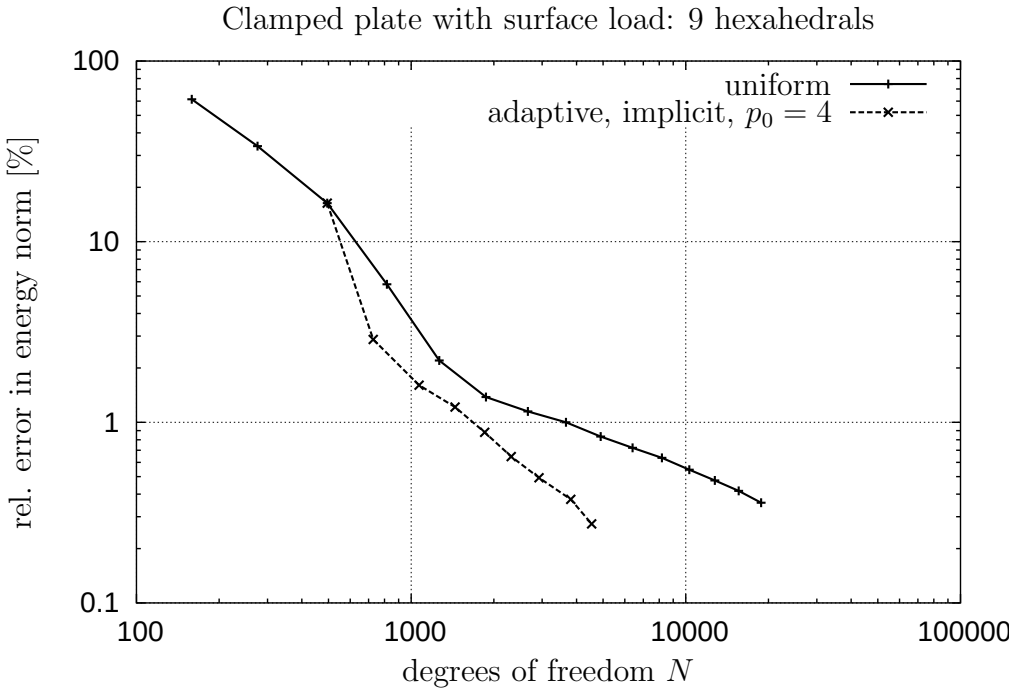

Figure 5.5: Convergence of uniform and adaptive p-refinement using local implicit error indicator

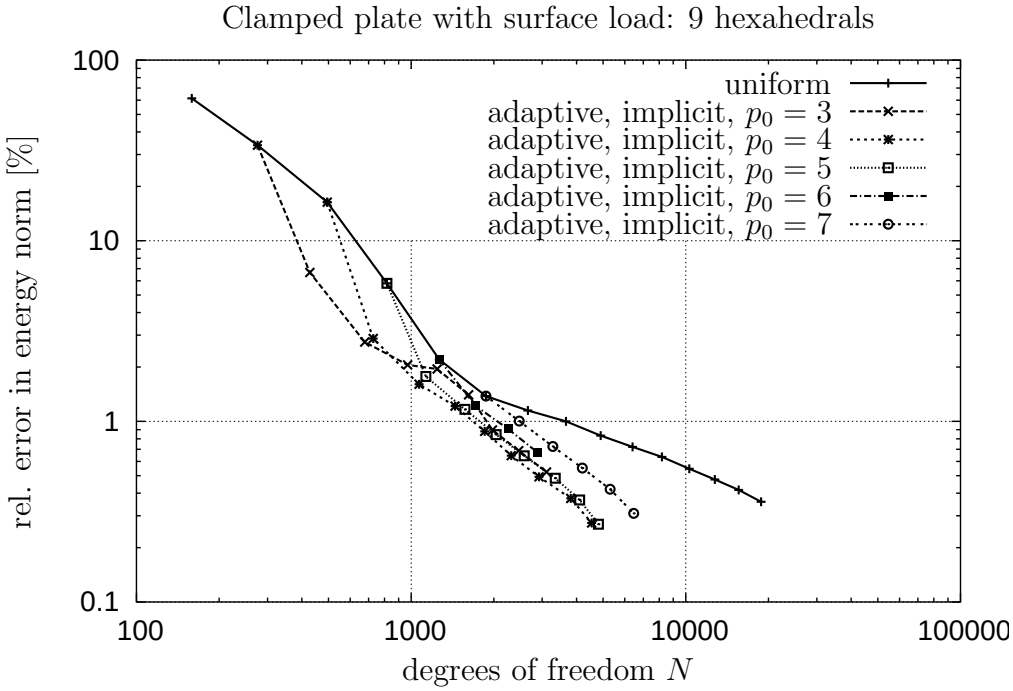

Figure 5.6: Convergence of uniform and adaptive p-refinement using local implicit error indicator and different starting polynomial degrees

indicator of *version 2* shows significant deviation from the implicit curve at the transition between the pre-asymptotic range and the asymptotic range. Nevertheless, following some 'adaptive searching' it finds an efficient path as well. Once again, one aspect that all three adaptive curves have in common is that they are clearly superior to the uniform curve.

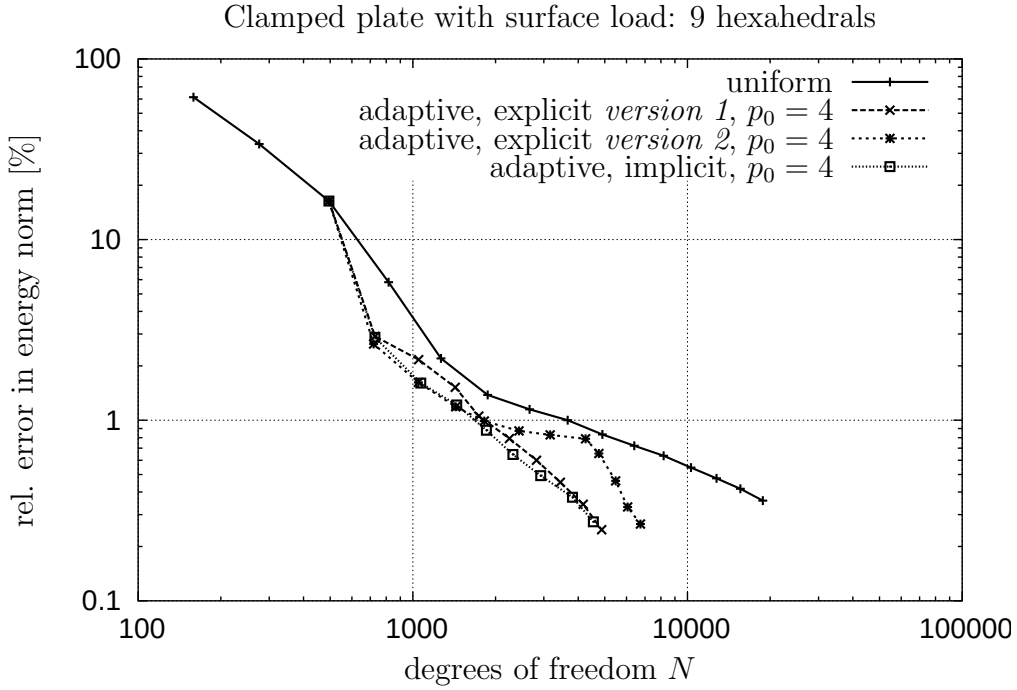

Figure 5.7: Convergence of uniform and adaptive p-refinement using local implicit error indicator and local explicit error indicators of *version 1* and *version 2*

The relative error in energy norm is plotted versus the elapsed CPU time (1.3 GHz standard PC) in Figure 5.8. In the first few iterations, the adaptive runs do not seem to be superior due to the adaptive overhead. However, in order to provide an accuracy of approximately 1% in energy norm it takes 117s for uniform $p = 9$ and only 44s for an adaptive discretization. Again, the real impact of the adaptive approach becomes evident for higher accuracies. Of course, the question may arise if the accuracies in the range of 0.3% in energy norm as obtained in Figure 5.8 make any sense for practical considerations. Nevertheless, for investigation purposes of the method the sum of the CPU times of all adaptive runs including computation of error indicators, 2805s, may be compared to the CPU time for a single uniform run with corresponding accuracy using $p = 18$, 26536s, yielding a speed-up factor of 9.46.

A graphical representation of the polynomial degree templates is plotted in Figure 5.9. It can be observed that high polynomial degrees occur at the largest element, whereas low polynomial degrees are adaptively chosen for the small elements at the corner. The largest polynomial degrees appear in thickness direction ζ at the boundary layer elements, since complex three dimensional stress states have to be described at the clamped supports. Here, the high polynomial degrees indicate that further mesh refinement of the boundary layers could improve

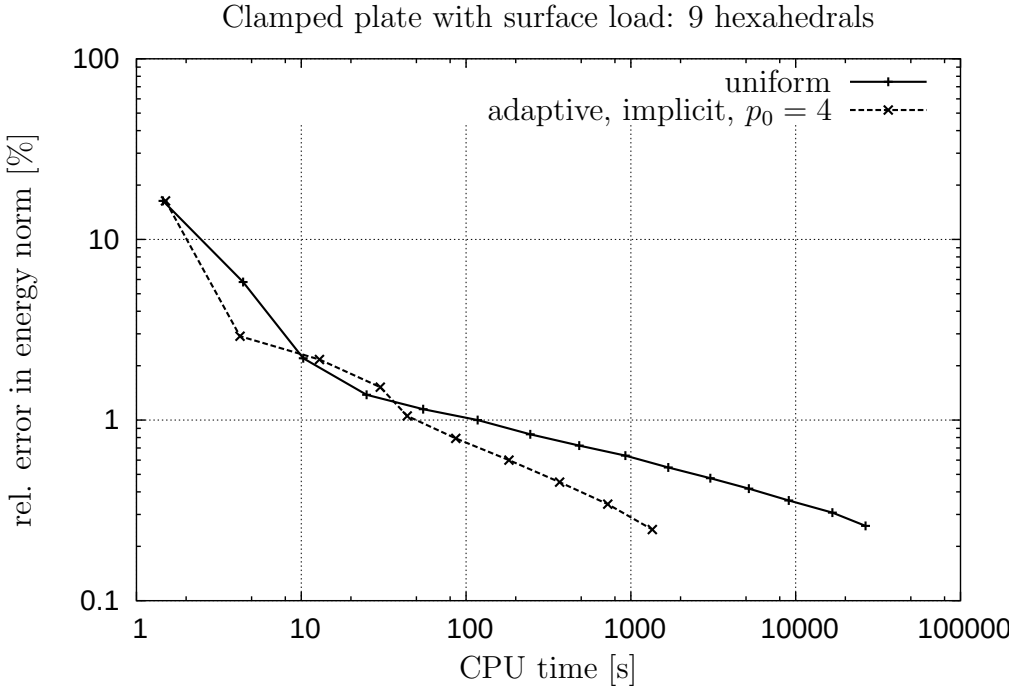

Figure 5.8: Convergence of uniform and adaptive p-refinement using local explicit error indicator of *version 1* plotted versus CPU time (1.3 GHz standard PC)

the convergence of uniform p-version. Moreover, the symmetry of the polynomial degree templates in Figure 5.9 is noteworthy. The polynomial degree template p^{ζ,u_z} is symmetric to the bisecting line spanned by the clamped corner point and the center of the plate. When mirroring the polynomial degree template p^{ξ,u_x} with respect to the bisecting line, the resulting template is p^{η,u_y}. The other pairs fulfilling this symmetry are $\{p^{\eta,u_x}, p^{\xi,u_y}\}$, $\{p^{\xi,u_z}, p^{\eta,u_z}\}$ and $\{p^{\zeta,u_x}, p^{\zeta,u_y}\}$.

5.4.2 Cylindrical shell

The p-adaptive approach has been proved to be efficient for a plate-like structure in Section 5.4.1. In the following section, the method is applied to shell-like structures. As a first example, a cylindrical shell clamped at one boundary and loaded with a bending moment at the opposite boundary will be considered, see Figure 5.10. The material is assumed to be linear elastic with YOUNG's modulus $E = 1.0 \cdot 10^7$ and $\nu = 0.3$ being POISSON's ratio. The mesh consists of nine hexahedral elements that have been distorted in order to demonstrate the robustness of the elements against locking, see Figure 5.10.

In order to account for a correct representation of the curved geometry, the blending function method is used for the mapping between the local coordinates of the standard hexahedral element and the corresponding global coordinates, see Section 3.1.2. In this example, the reference solution was computed in advance using a sequence of solutions on a different, undistorted mesh consisting of 121 hexahedral elements with refinements to the boundary. This was nec-

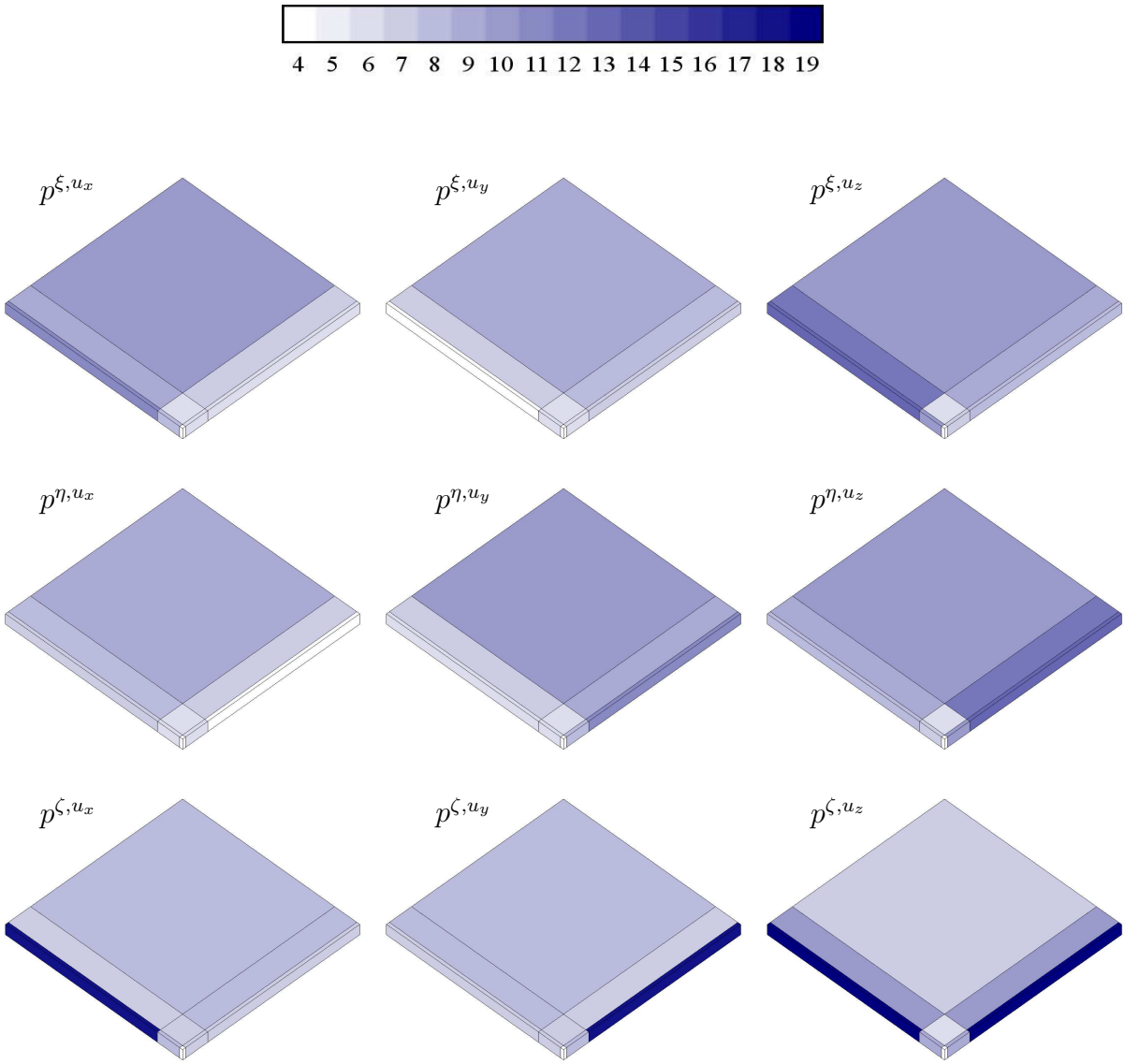

Figure 5.9: Graphical representation of polynomial degree templates corresponding to iteration 9 of adaptive procedure using the explicit error indicator of *version 1* for plate

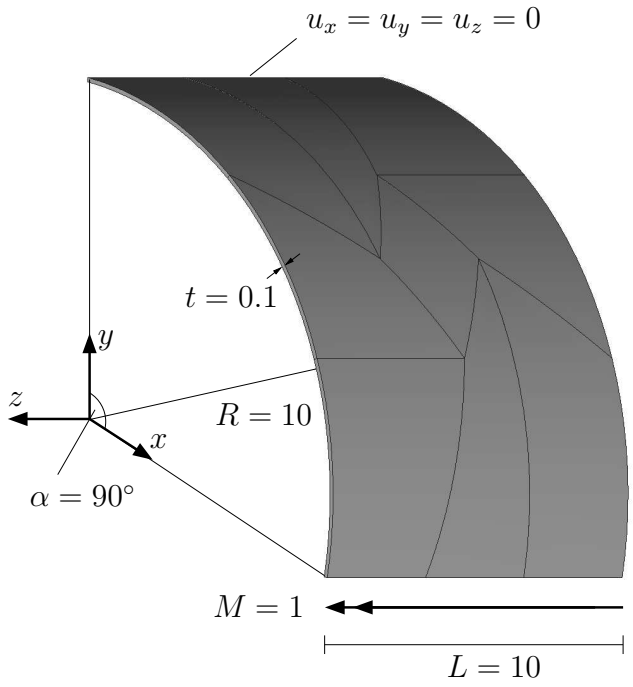

Figure 5.10: System and hexahedral mesh of a cylindrical shell

essary in order to exclude a wrong reference solution due to poor convergence resulting from a possibly bad resolution of boundary layer effects with the given nine-element-mesh.

In Figure 5.11 the relative errors in energy norm

- for uniform refinement,
- for anisotropic refinements with constant polynomial degree $p^\zeta = 1, 2, 3, 4$ over thickness and uniform refinement of in-plane polynomial degrees, only, and
- for adaptive refinement starting from initial polynomial degree $p_0 = 4$

are plotted versus the corresponding number of equations.

Quasi horizontal asymptotic slope can be observed for the anisotropic curves corresponding to the polynomial degrees $p^\zeta = 1, 2, 3$ in thickness direction. This is due to the dominant discretization error resulting from the restriction to low polynomial degrees over the thickness, which makes the corresponding sequences converge to the wrong solution. As already mentioned in Sections 2.7.3 and 4.4 such restrictions can be related to the model assumptions of plate or shell theories where fixed kinematic behavior over the thickness is prescribed. Instead, by using a transversal polynomial degree of $p^\zeta = 4$ a very efficient discretization, showing a clearly higher rate of convergence than the uniform sequence, is obtained.

However, the most efficient method is, again, the p-adaptive approach converging with a significantly steeper slope than all other curves. Moreover, the adaptive sequence was found in an *automatic* way without the need for 'model decisions' for a rational choice of the thickness

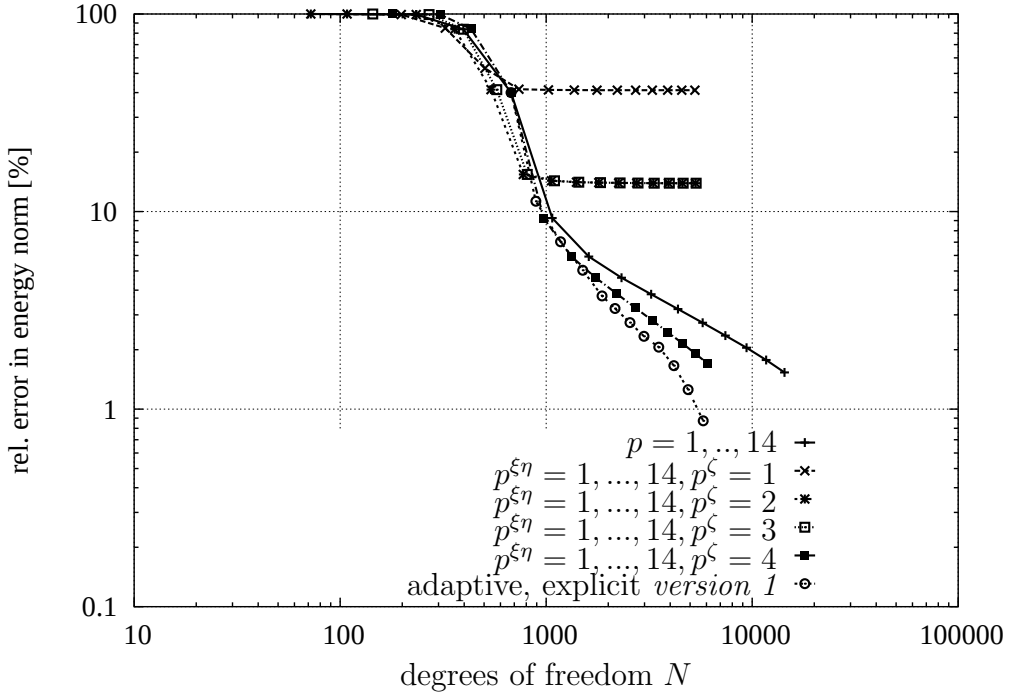

Figure 5.11: Convergence of uniform, anisotropic and adaptive p-refinements for a cylindrical shell

polynomial degree. For example, in the case of anisotropic refinement with constant thickness polynomial degree, the choice of $p^{\zeta} = 3$ would have resulted in convergence to an incorrect solution, where the next polynomial degree step, $p^{\zeta} = 4$, already performs very well. In other words, a deeper insight into the behavior of the system is necessary in order to trust the results using a fixed polynomial degree over the thickness, where the p-adaptive procedure suggests an appropriate choice of $\mathcal{P}$ in an automatic and reliable way.

Another interesting aspect is that, although the mesh being used is not at all an optimally a priori refined mesh resolving the singularities at the clamped boundary, the convergence rate of the p-adaptive procedure towards the reference solution is highly satisfactory. Once more, the p-adaptive approach seems to be an appropriate means to overcome the poor asymptotic behavior of uniform p-version in the presence of singularities.

The graphical representation of the polynomial degree templates in Figure 5.12 shows large polynomial degrees at the clamped boundary where a complex stress state is to be expected. The lowest polynomial degrees were chosen for p^{ζ,u_z}, since ζ corresponds to the thickness of the shell, which is very small compared to the other dimensions and the displacement component u_z in cylinder axis direction is also small in relation to the components perpendicular to the axis.

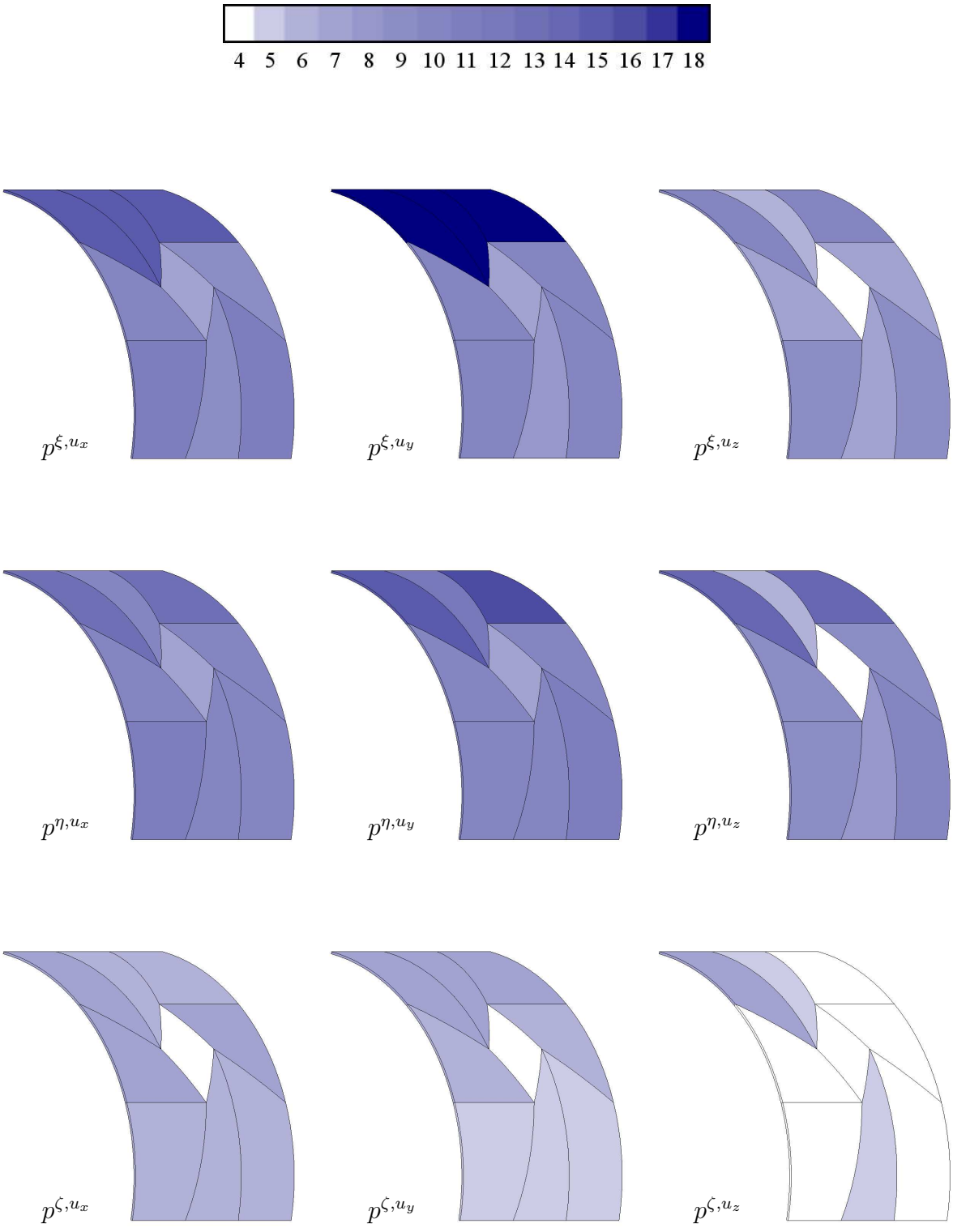

Figure 5.12: Graphical representation of polynomial degree templates corresponding to iteration 11 of adaptive procedure using the explicit error indicator of *version 1* for a cylindrical shell

5.4.3 Hemispherical shell with stiffener

Whereas the previous examples were dealing exclusively with thin-walled structures, the structure investigated in this section is a construction consisting of a hemispherical shell connected to a stiffener, i.e. it is composed of thin-walled and compact parts, see Figure 5.13. This serves to illustrate one major advantage of the entirely three-dimensional approach. A dimensionally reduced theory for the thin-walled part of the structure would lead to a dimensional transition at the joint between the two-dimensional shell and the stiffener which is obviously subjected to an arbitrary three-dimensional stress state. Since only three-dimensional elements are used, no dimensional transition elements are required at the connection, see also RANK et al. [114].

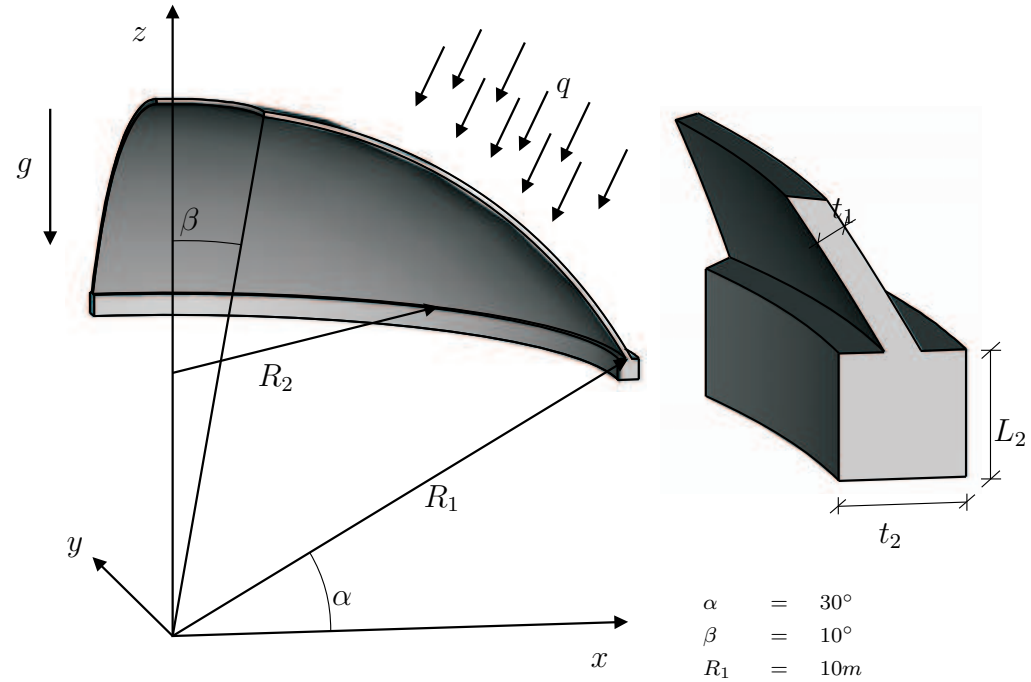

Symmetry to x-z-plane:
$u_y = 0$

Symmetry to y-z-plane:
$u_x = 0$

Boundary conditions:
$u_z = 0$

α	=	$30°$
β	=	$10°$
R_1	=	$10m$
R_2	=	$5\sqrt{3}m$
t_1	=	$0.1m$
t_2	=	$0.4m$
L_2	=	$0.4m$
E	=	$6.825 \cdot 10^7 \frac{kN}{m^2}$
ν	=	0.3
ρ	=	$500 \frac{kg}{m^3}$
g	=	$10.0 \frac{m}{S^2}$
q	=	$100.0 \frac{kN}{m^2}$

Figure 5.13: Hemispherical shell with stiffener

In Figure 5.14 the relative errors in energy norm are plotted versus the number of degrees of freedom for uniform and adaptive p-refinement using initial polynomial degrees $p_0 = 4, 5, 6$. Again, all adaptive curves are below the uniform curve, i.e. are clearly more efficient, and the adaptive curves have similar slopes in the asymptotic range yielding a significantly higher rate of convergence compared to the uniform refinement. A single run with adaptive discretization (obtained with $p_0 = 4$) resulting in less than 1% error in energy norm takes 154s on a 1.4 GHz

PC, a corresponding uniform run needs 390s. In order to achieve an accuracy of approximately 0.75% in energy norm, an adaptive run takes 310s, a uniform run 1574s.

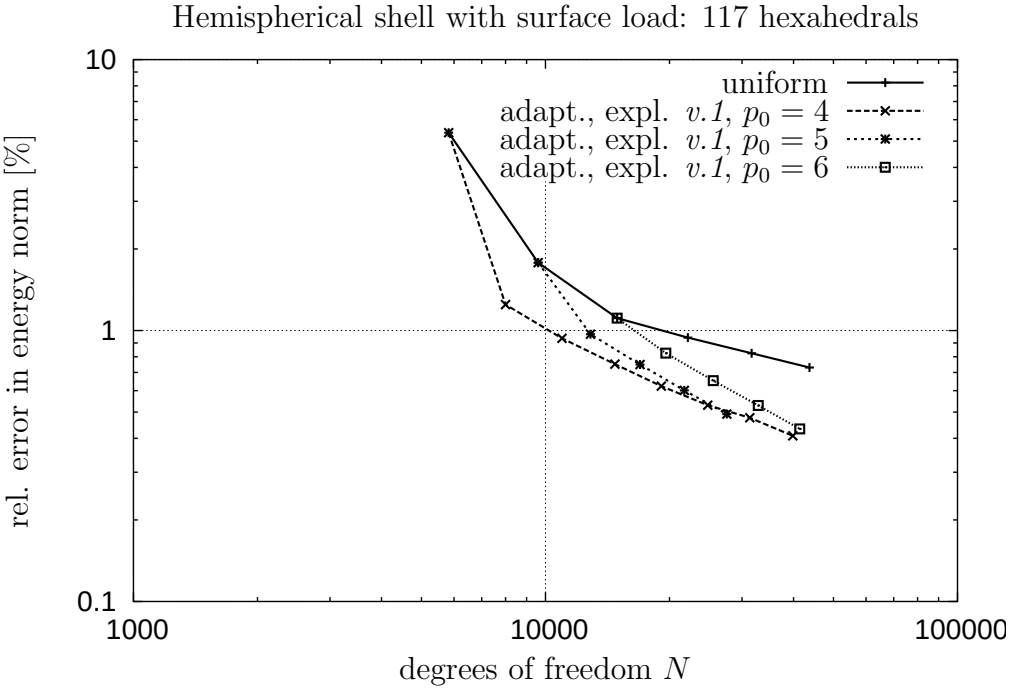

Figure 5.14: Convergence of uniform and adaptive p-refinement using local explicit error indicator of *version 1* and different starting polynomial degrees for a hemispherical shell with stiffener

The polynomial degree templates visualized in Figure 5.15 show graded polynomial degrees of the shell-like elements, where the polynomial degrees of the elements close to the joint with the stiffener reveal the largest degrees decaying with the distance to the joint. The polynomial degrees of the 'needle' elements modeling the stiffener are depicted in Figure 5.16.

5.4.4 Spring-back analysis of thin metal sheet (S-rail)

The following example analyzes the spring-back properties of a thin metal sheet following the deep drawing process. Figure 5.17 depicts a schematic sketch of the deep drawing process, where a thin metal sheet clamped in the blank holder is pressed into a die by means of a punch. After the deep-drawing process, as long as the sheet is clamped between the punch and the die, the geometry of the sheet is approximately the same as that of the tool. Once the punch is released and the blank has been removed from the tool, however, the residual elastic stresses in the material cause an elastic spring-back. Since the geometry of the sheet before and after the spring back may differ significantly, and due to the fact that the exact final geometry is of interest, an accurate simulation of this effect is important.

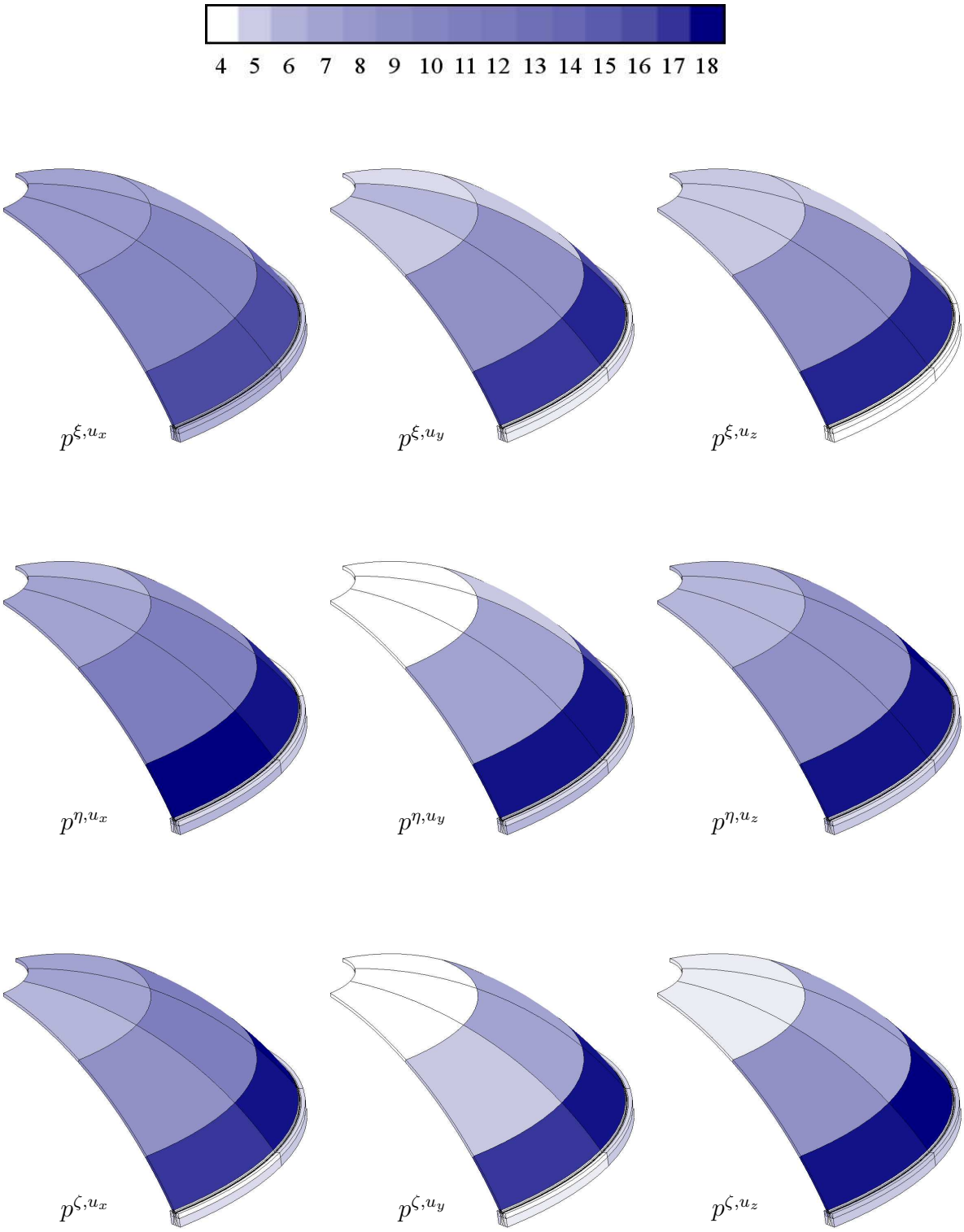

Figure 5.15: Graphical representation of polynomial degree templates corresponding to iteration 7 of adaptive procedure using the explicit error indicator of *version 1* for a hemispherical shell with stiffener

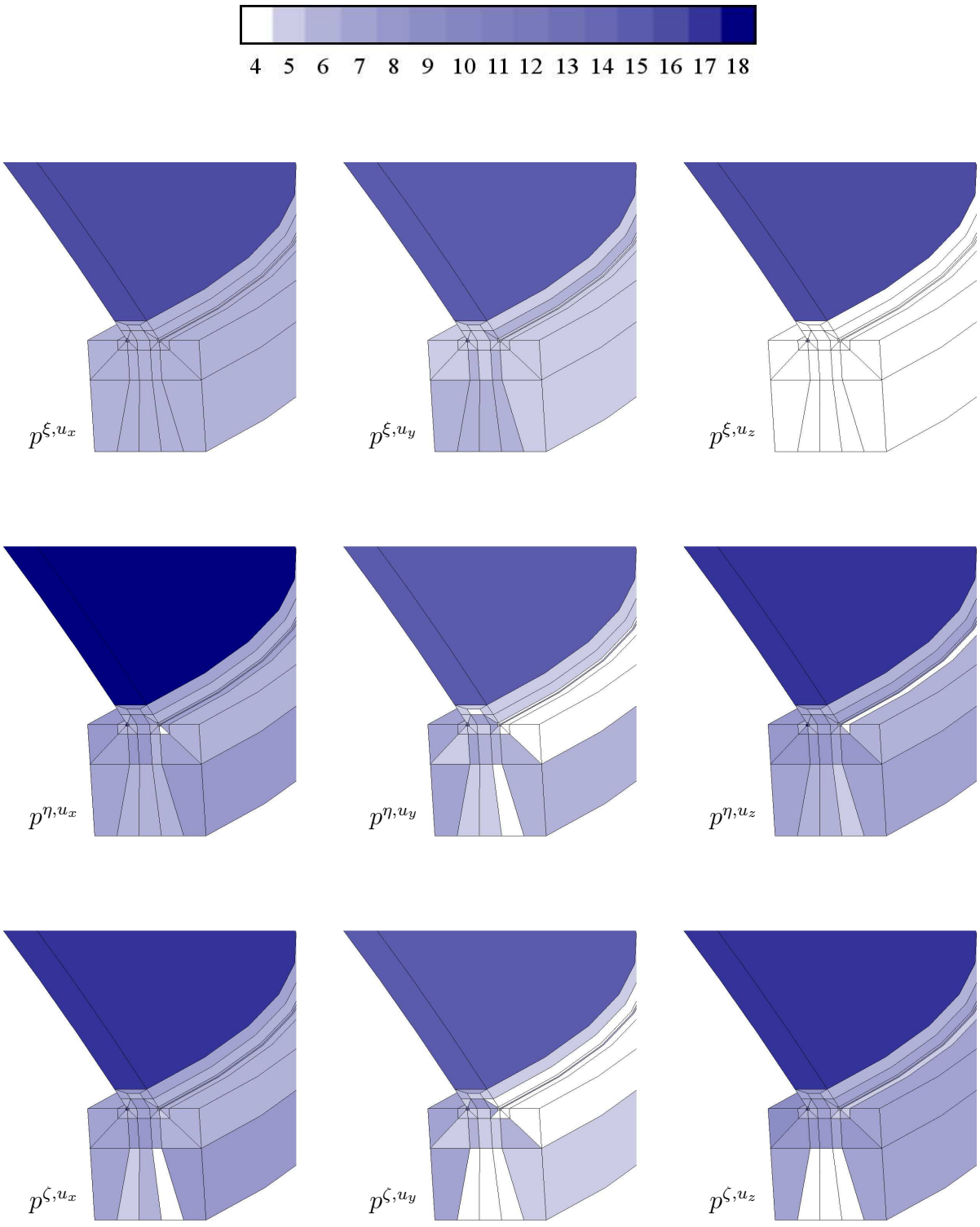

Figure 5.16: Graphical representation of polynomial degree templates corresponding to iteration 7 of adaptive procedure using the explicit error indicator of *version 1* for a hemispherical shell with stiffener (zoom-in)

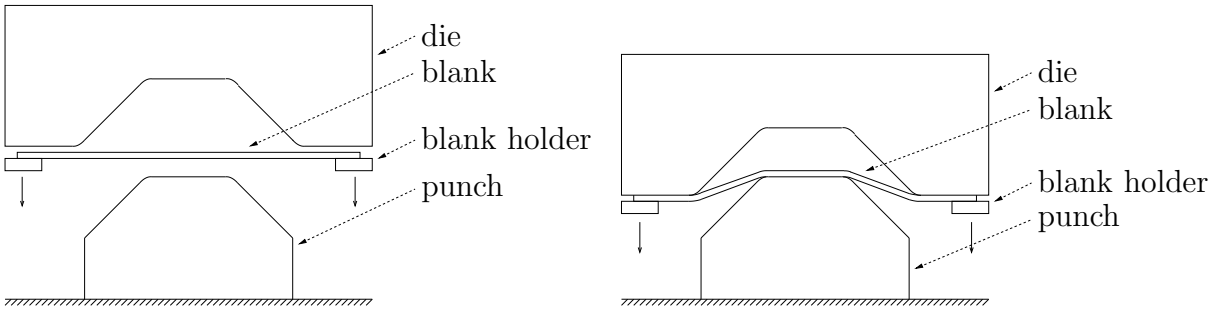

Figure 5.17: Schematic sketch of deep-drawing process

The S-rail formed by deep drawing a thin aluminum sheet, as depicted in Figure 5.18, is a benchmark problem introduced at the conference *NUMISHEET 1996*. The material behavior governing the spring-back is assumed to be linear elastic with a YOUNG's modulus $E = 70000$ and $\nu = 0.33$ being POISSON's ratio. The kinematic behavior is assumed to be geometrically linear.

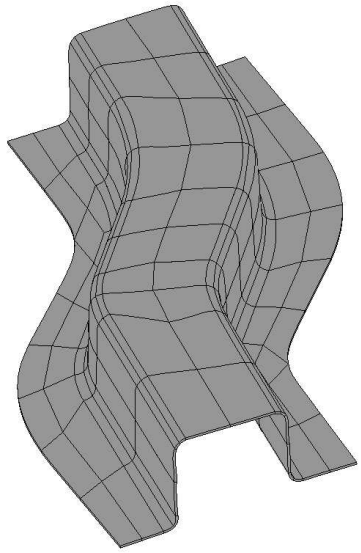

Figure 5.18: Hexahedral mesh of S-rail

The geometry of the S-rail is quite smooth except for the small radii which are accordingly resolved using thin stripes of elements. The S-rail is neither clamped nor otherwise constrained in any way: only the rigid body modes are fixed. Thus, geometry, boundary conditions and loading by elastic residual stresses lack singularities and therefore the system and mesh in Figure 5.18 are more or less optimal.

It is, however, evident from Figure 5.19 that the p-adaptive approach is again clearly more

efficient than the uniform p-refinement, and an (admittedly very slightly) different order of convergence can be observed in the asymptotic range. The anisotropic curve $p^\zeta = 4$ and uniform refinement of the in-plane polynomial degrees p^ξ and p^η, only, reveals how crucial a 'good' choice of the thickness polynomial degree p^ζ is. The anistropic discretization converges to the wrong solution due to the dominant discretization error over the thickness. As already mentioned in Section 5.4.2, this discretization error can be compared with the model error of shell and plate theories with fixed kinematic assumptions.

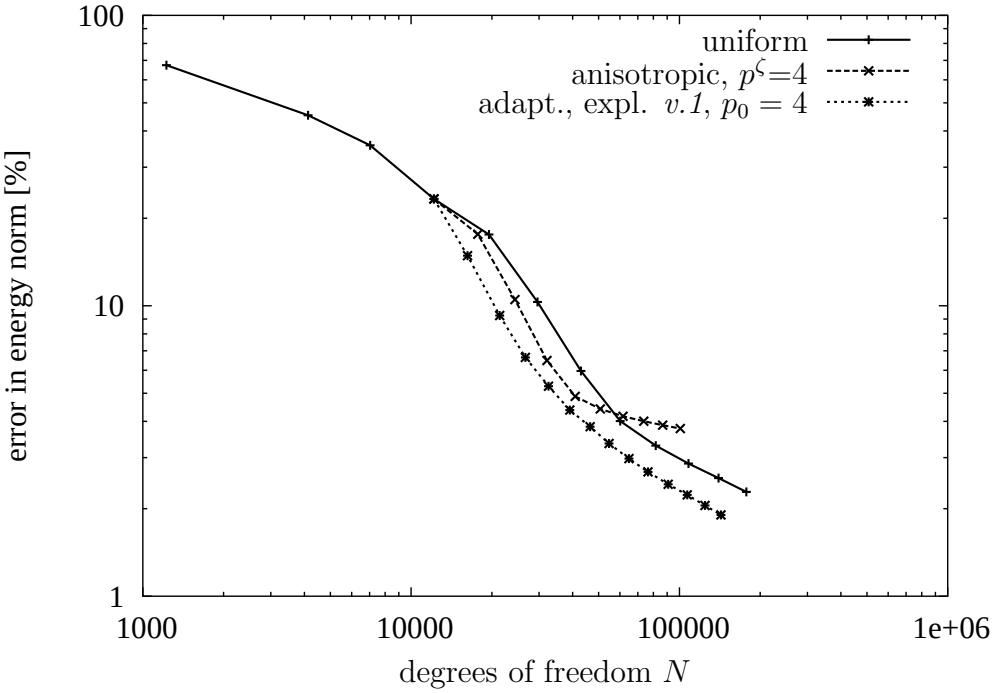

Figure 5.19: Convergence of uniform p-refinement, anisotropic p-refinement and adaptive p-refinement using local explicit error indicator of *version 1* for S-rail

Figure 5.20 illustrates the polynomial degree templates elementwise. It is apparent that the in-plane polynomial degrees p^ξ and p^η are of significantly higher order than the thickness polynomial degrees p^ζ and distributed 'relatively uniformly'. The thickness polynomial degrees are minimal at the free boundaries, since the corresponding elements are less constrained by residual stresses in connection with small radii in a doubly curved geometry than those elements in the interior. Hence, a dimensional reduction might be allowed for these boundary elements.

5.4.5 Remarks

In all the examples under consideration, the p-adaptive curves were clearly more efficient, i.e. higher accuracy with the number of degrees of freedom in the same order of magnitude, than those corresponding to uniform p-refinement. Moreover, in every example, a higher rate of convergence was observed in the asymptotic range. Therefore, this method can be regarded as

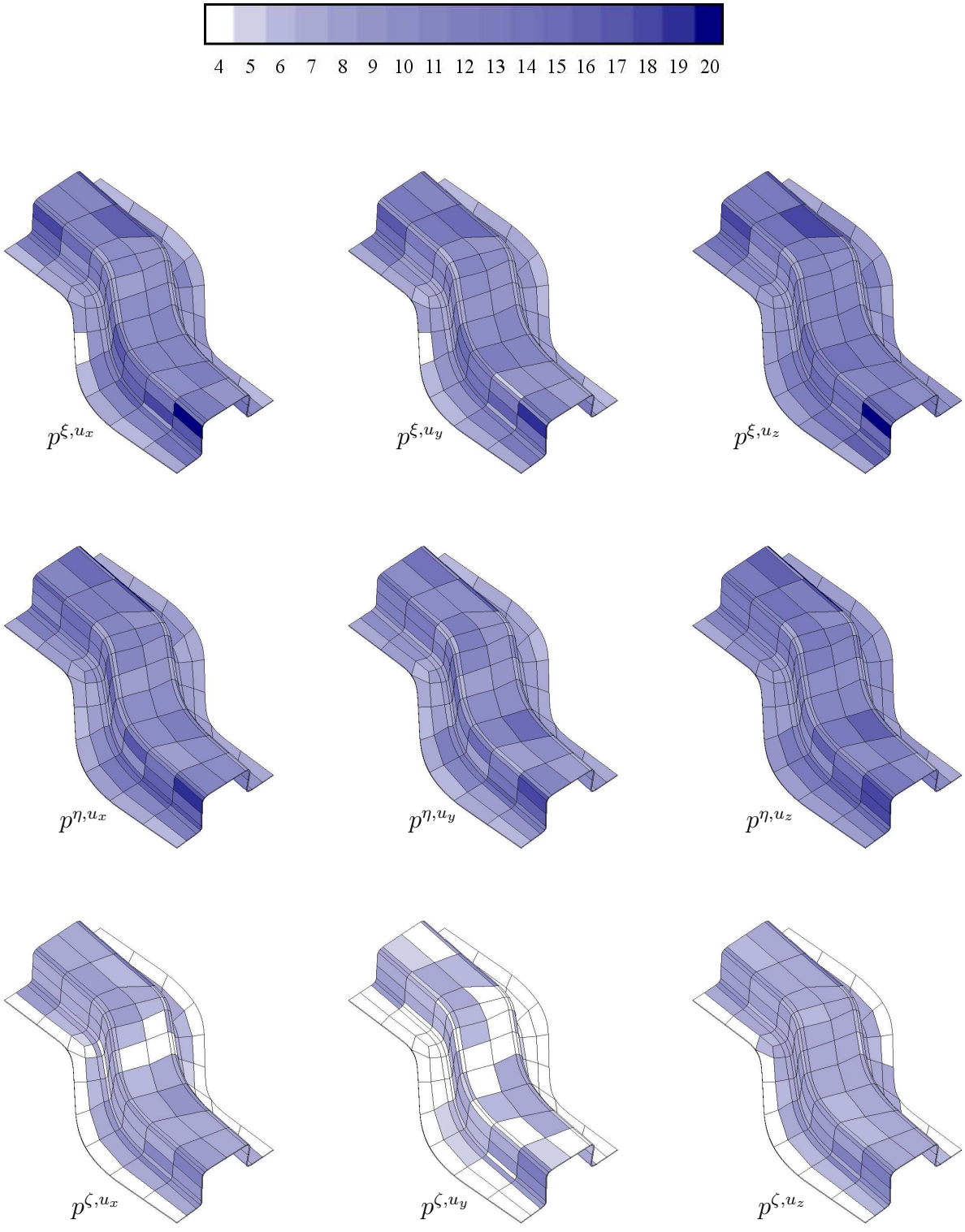

Figure 5.20: Graphical representation of polynomial degree templates corresponding to iteration 7 of adaptive procedure using the explicit error indicator of *version 1* for *S*-rail

a remedy for one basic problem of uniform p-version, i.e. the often poor asymptotic behavior, particularly in the presence of irregularities in the solution.

This p-adaptive method controls the 3D-discretization error. However, for thin-walled structures, p^ζ corresponds to the model error of plate and shell theories. Therefore, this p-adaptive method includes model adaptivity as it automatically chooses p^ζ which corresponds to the kinematic model assumptions of dimensionally reduced theories.

Chapter 6

An anisotropic p-adaptive method for elastodynamic problems

The p-adaptive method for elastostatic problems proposed in Chapter 5 is extended to problems of linear elastodynamics below. Since both the basic principles and the notation adhere closely to those conceived for the p-adaptivity for elastostatics, a knowledge of Chapter 5 is recommended. The subject of this section is adaptivity in the *spatial* domain, whereas the *temporal* domain is assumed to be discretized accurately enough. It is, however, possible to apply time-step adaptivity in a fairly straightforward manner, as suggested in Section 4.2.

A time integration method is called for to solve time-dependent problems, as described in Section 3.2. Time integration methods can be categorized into *direct* and *indirect* schemes. When using *direct* time integration, the time-integration scheme is applied directly to the semidiscrete, coupled system of ordinary differential equations

$$\mathcal{B}(\mathbf{u},\mathbf{v}) + \mathcal{C}(\dot{\mathbf{u}},\mathbf{v}) + \mathcal{D}(\ddot{\mathbf{u}},\mathbf{v}) \;=\; \mathcal{F}(\mathbf{v}), \quad \mathbf{v} \in \mathcal{S} \tag{6.1}$$

with $\mathcal{S}$ being the finite element space, or in matrix notation

$$\mathbf{K}\mathbf{d}(t) + \mathbf{C}\dot{\mathbf{d}}(t) + \mathbf{M}\ddot{\mathbf{d}}(t) = \mathbf{F}(t). \tag{6.2}$$

Usually, direct time integration requires the solution of a linear equation system. For time integration schemes of the NEWMARK family or related schemes, direct time integration requires the solution of systems with the same number of degrees of freedom N at every timestep.

When the eigenvectors $\boldsymbol{\phi}_k$ associated with the eigenfrequencies ω_k of the system are not only $\mathbf{K}$- and $\mathbf{M}$-orthogonal but also $\mathbf{C}$-orthogonal, as in case of RAYLEIGH damping, or $\mathbf{C} = \mathbf{0}$, the system (6.2) can be completely decoupled using modal analysis. Integrating these decoupled, ordinary differential equations is referred to as *indirect* time integration. This requires the solution of the eigenvalue problem corresponding to (6.2) with $\mathbf{F} = \mathbf{0}$

$$\mathbf{K}\boldsymbol{\phi}_k = \omega_k^2 \mathbf{M}\boldsymbol{\phi}_k, \tag{6.3}$$

see Section 2.7.2. The main computational effort in direct time integration involves the repeated solution of the linear equation system depending on the integration scheme, whereas in the case of indirect time integration the predominant task is to solve the eigenvalue problem (6.3).

In most applications, specific frequencies and corresponding eigenvectors dominate the solution of the time dependent problem, such as that resulting from a specific spatial distribution of the load, a specific load frequency, resonance effects, etc. There are usually only a few dominating frequencies compared to the number of spatial degrees of freedom of the system. Moreover, for many practical problems only the lowest frequencies are of interest. Figure 6.1 (left) plots the internal energy $E_{kin} + E_{str}$ of a clamped square plate subjected to a sudden, uniform surface load, whereas Figure 6.1 (right) shows the decomposition of $E_{kin} + E_{str}$ into the proportions associated to the lowest five eigenfrequencies. It is evident that in this case the first eigenfrequency clearly dominates the dynamic behavior of the plate. The plate example will be investigated in further detail in Section 6.3. These facts can be exploited using indirect time integration schemes by only computing those eigenfrequencies and eigenvectors dominating the problem in an accurate and computationally economic way. In the case of direct integration schemes, spatial discretizations are sought, which are able to *represent* these dominating eigenfrequencies and eigenvectors *efficiently*.

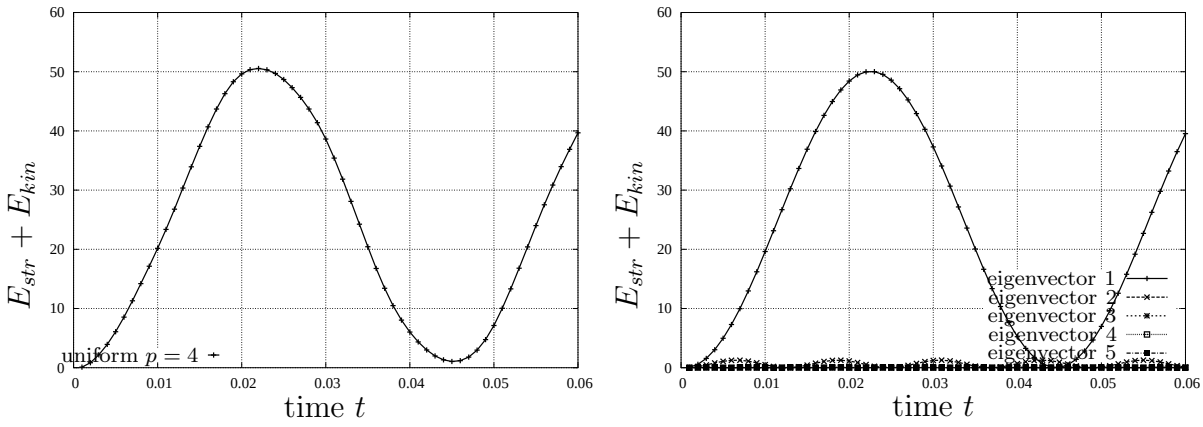

Figure 6.1: Internal energy $E_{str} + E_{kin}$ of clamped plate subjected to sudden surface load over time (left) and decomposition of $E_{kin} + E_{str}$ into the proportions associated to the lowest five eigenfrequencies

Regardless of which time integration method being used, direct or indirect, the objective is to find an efficient spatial discretization for the solution of (6.3), which can be obtained by means of an adaptive eigensolver that provides an accurate representation of the important eigenfrequencies and the corresponding eigenvectors with adaptive refinements to save computational resources.

6.1 An anisotropic p-adaptive hierarchic eigensolver

In analogy to the p-adaptivity for elastostatic problems described in Chapter 5, a p-adaptive eigensolver adapts the finite element discretization determined by the polynomial degrees of the shape functions $\mathcal{P}$, the mesh Δ and the mapping $\mathcal{Q}$

$$\mathcal{S} = \mathcal{S}(\mathcal{P}, \Delta, \mathcal{Q}), \tag{6.4}$$

simply by varying the set of polynomial degree templates

$$\mathcal{P} = \{\mathbf{p_1}, ..., \mathbf{p}_{n_{el}}\} \tag{6.5}$$

with

$$\mathbf{p}_e = \begin{array}{c} \\ \xi \\ \eta \\ \zeta \end{array} \begin{array}{c} \begin{array}{ccc} u_x & u_y & u_z \end{array} \\ \begin{pmatrix} p_e^{1,1} & p_e^{1,2} & p_e^{1,3} \\ p_e^{2,1} & p_e^{2,2} & p_e^{2,3} \\ p_e^{3,1} & p_e^{3,2} & p_e^{3,3} \end{pmatrix} \end{array} . \tag{6.6}$$

Therefore, for a fixed mesh and fixed mapping, the finite element discretization can be written as

$$\mathcal{S} = \mathcal{S}^{\mathcal{P}} \tag{6.7}$$

Similar to the approach in Chapter 5, the sensitivity of the solution of the eigenvalue problem (6.3) has to be analyzed with respect to changes of the discretization $\mathcal{S}^{\mathcal{P}}$ in order to be in a position to set up a p-adaptive procedure.

6.1.1 An anisotropic hierarchic error indicator

In Chapter 5, the change in strain energy was used for quantifying the sensitivity of the solution to the change in a specific $p_{\bar{e}}^{\bar{i},\bar{j}}$. For the dynamic eigenvalue problem, a reasonable measure has turned out to be the RAYLEIGH quotient ρ, which is related to the lowest circular frequency ω_1, as follows:

$$\omega_1^2 = \min_{\mathbf{u}\in\mathcal{V}} \rho(\mathbf{u}) = \min_{\mathbf{u}\in\mathcal{V}} \frac{\mathcal{B}(\mathbf{u},\mathbf{u})}{\mathcal{D}(\mathbf{u},\mathbf{u})} = \frac{\mathcal{B}(\mathbf{u}_1,\mathbf{u}_1)}{\mathcal{D}(\mathbf{u}_1,\mathbf{u}_1)}, \tag{6.8}$$

i.e. the eigenfunction $\mathbf{u}_1$ corresponding to ω_1 is that function $\mathbf{u} \in \mathcal{V}$ minimizing the RAYLEIGH quotient ρ. The higher frequencies ω_k are obtained by searching for the eigenfunctions $\mathbf{u}_k$ in the space $\mathcal{V}_{k\perp}$ restricted to being orthogonal to the eigenfunctions $\mathbf{u}_1, ..., \mathbf{u}_{k-1}$ that have already been found

$$\omega_k^2 = \min_{\mathbf{u}\in\mathcal{V}_{k\perp}} \rho(\mathbf{u}) = \min_{\mathbf{u}\in\mathcal{V}_{k\perp}} \frac{\mathcal{B}(\mathbf{u},\mathbf{u})}{\mathcal{D}(\mathbf{u},\mathbf{u})} = \frac{\mathcal{B}(\mathbf{u}_k,\mathbf{u}_k)}{\mathcal{D}(\mathbf{u}_k,\mathbf{u}_k)}. \tag{6.9}$$

Since only finite dimensional Ansatz spaces $\mathcal{S}^{\mathcal{P}}$, $\mathcal{S}^{\mathcal{P}}_{k\perp}$ are used rather than $\mathcal{V}$, $\mathcal{V}_{k\perp}$, respectively, we obtain the approximations $\omega_1^{\mathcal{P}}$ with

$$\omega_1^2 \approx \min_{\mathbf{u}\in\mathcal{S}^{\mathcal{P}}} \rho(\mathbf{u}) = \frac{\mathcal{B}(\mathbf{u}_1^{\mathcal{P}},\mathbf{u}_1^{\mathcal{P}})}{\mathcal{D}(\mathbf{u}_1^{\mathcal{P}},\mathbf{u}_1^{\mathcal{P}})} = \frac{\boldsymbol{\phi}_1^T\mathbf{K}\boldsymbol{\phi}_1}{\boldsymbol{\phi}_1^T\mathbf{M}\boldsymbol{\phi}_1} = (\omega_1^{\mathcal{P}})^2 \tag{6.10}$$

and $\omega_k^{\mathcal{P}}$ with

$$\omega_k^2 \approx \min_{\mathbf{u}\in\mathcal{S}^{\mathcal{P}}_{k\perp}} \rho(\mathbf{u}) = \frac{\mathcal{B}(\mathbf{u}_k^{\mathcal{P}},\mathbf{u}_k^{\mathcal{P}})}{\mathcal{D}(\mathbf{u}_k^{\mathcal{P}},\mathbf{u}_k^{\mathcal{P}})} = \frac{\boldsymbol{\phi}_k^T\mathbf{K}\boldsymbol{\phi}_k}{\boldsymbol{\phi}_k^T\mathbf{M}\boldsymbol{\phi}_k} = (\omega_k^{\mathcal{P}})^2. \tag{6.11}$$

A sequence of hierarchically nested finite element spaces

$$\mathcal{S}^{\mathcal{P}_1} \subset \mathcal{S}^{\mathcal{P}_2} \subset \mathcal{S}^{\mathcal{P}_3} \subset ... \tag{6.12}$$

results in the sequence of approximations

$$\omega_k^{\mathcal{P}_1} \geq \omega_k^{\mathcal{P}_2} \geq \omega_k^{\mathcal{P}_3} \geq ..., \tag{6.13}$$

see Section 3.1.4.3. In the same manner as that used for the p-adaptive approach for elastostatic problems discussed in Chapter 5, two hierarchic spaces $\mathcal{S}^{\mathcal{P}}$ and $\mathcal{S}^{\mathcal{P}^-}$ are constructed by varying one specific entry $p_{\bar{e}}^{\bar{i},\bar{j}}$ in the set of polynomial degree templates in order to obtain sensitivity information,

$$\mathcal{S}^{\mathcal{P}} \supset \mathcal{S}^{\mathcal{P}^-} = \mathcal{S}^{\mathcal{P}-\Delta\mathcal{P}_{\bar{e}}^{\bar{i},\bar{j}}} \tag{6.14}$$

with

$$\Delta\mathcal{P}_{\bar{e}}^{\bar{i},\bar{j}} = \begin{cases} \Delta p_{\bar{e}}^{\bar{i},\bar{j}} > 0 \\ \Delta p_e^{i,j} = 0 \quad \text{for} \quad \{e,i,j\} \neq \{\bar{e},\bar{i},\bar{j}\} \end{cases} \tag{6.15}$$

An anisotropic hierarchic error indicator for the entry $p_{\bar{e}}^{\bar{i},\bar{j}}$ based on reduction can be written as

$$\lambda_{\bar{e},k}^{\bar{i},\bar{j}} = \rho(\mathbf{u}^{\mathcal{P}^-}) - \rho(\mathbf{u}^{\mathcal{P}}) \geq 0 \tag{6.16}$$

6.1.1.1 An anisotropic, hierarchic error indicator computed on element level

Since, as in the elastostatic case, the global computation of $\rho(\mathbf{u}^{\mathcal{P}^-})$ for every combination of $\{e,i,j\}$ is prohibitively expensive, the costs are, again, reduced by an approximation, which can be computed locally on element level and explicitly, i.e. without solving an equation system.

The two assumptions for computing the local, explicit approximation of (6.16) are

- that the influence of varying $p_{\bar{e}}^{\bar{i},\bar{j}}$ may be reduced to the domain of element $\bar{e}$, and
- that $\boldsymbol{\phi}_{\bar{e},k}^{\mathcal{P}^-}$ can be approximated by simply omitting those entries of $\boldsymbol{\phi}_{\bar{e},k}^{\mathcal{P}}$ corresponding to the difference template $\Delta\mathcal{P}_{\bar{e}}^{\bar{i},\bar{j}}$

$$\tilde{\boldsymbol{\phi}}_{\bar{e}}^{\mathcal{P}^-} = \pi\boldsymbol{\phi}_{\bar{e}}^{\mathcal{P}}, \tag{6.17}$$

with π being the cut-off operator.

Based on these assumptions, the anisotropic, hierarchic error indicator computed on element level can be written as

$$\begin{aligned}
\lambda_{\bar{e}}^{\bar{i},\bar{j}} &= \rho(\mathbf{u}^{\mathcal{P}^-}) - \rho(\mathbf{u}^{\mathcal{P}}) \\
&= \frac{\boldsymbol{\phi}_{1,k}^{\mathcal{P}^-{}^T}\mathbf{K}_1\boldsymbol{\phi}_{1,k}^{\mathcal{P}^-} + ... + \boldsymbol{\phi}_{\bar{e},k}^{\mathcal{P}^-{}^T}\mathbf{K}_{\bar{e}}\boldsymbol{\phi}_{\bar{e},k}^{\mathcal{P}^-} + ... + \boldsymbol{\phi}_{n_{el},k}^{\mathcal{P}^-{}^T}\mathbf{K}_{n_{el}}\boldsymbol{\phi}_{n_{el},k}^{\mathcal{P}^-}}{\boldsymbol{\phi}_{1,k}^{\mathcal{P}^-{}^T}\mathbf{M}_1\boldsymbol{\phi}_{1,k}^{\mathcal{P}^-} + ... + \boldsymbol{\phi}_{\bar{e},k}^{\mathcal{P}^-{}^T}\mathbf{M}_{\bar{e}}\boldsymbol{\phi}_{\bar{e},k}^{\mathcal{P}^-} + ... + \boldsymbol{\phi}_{n_{el},k}^{\mathcal{P}^-{}^T}\mathbf{M}_{n_{el}}\boldsymbol{\phi}_{n_{el},k}^{\mathcal{P}^-}} - \rho(\mathbf{u}^{\mathcal{P}}) \\
&\approx \left| \frac{\boldsymbol{\phi}_{1,k}^{\mathcal{P}^T}\mathbf{K}_1\boldsymbol{\phi}_{1,k2}^{\mathcal{P}} + ... + \tilde{\boldsymbol{\phi}}_{\bar{e},k}^{\mathcal{P}^-{}^T}\mathbf{K}_{\bar{e},k}\tilde{\boldsymbol{\phi}}_{\bar{e},k}^{\mathcal{P}^-} + ... + \boldsymbol{\phi}_{n_{el},k}^{\mathcal{P}^T}\mathbf{K}_{n_{el}}\boldsymbol{\phi}_{n_{el},k}^{\mathcal{P}}}{\boldsymbol{\phi}_{1,k}^{\mathcal{P}^T}\mathbf{M}_1\boldsymbol{\phi}_{1,k}^{\mathcal{P}} + ... + \tilde{\boldsymbol{\phi}}_{\bar{e},k}^{\mathcal{P}^-{}^T}\mathbf{M}_{\bar{e}}\tilde{\boldsymbol{\phi}}_{\bar{e},k}^{\mathcal{P}^-} + ... + \boldsymbol{\phi}_{n_{el},k}^{\mathcal{P}^T}\mathbf{M}_{n_{el}}\boldsymbol{\phi}_{n_{el},k}^{\mathcal{P}}} - \rho(\mathbf{u}^{\mathcal{P}}) \right|.
\end{aligned} \tag{6.18}$$

In (6.18) the terms $\boldsymbol{\phi}_{e,k}^{\mathcal{P}^T}\mathbf{K}_e\boldsymbol{\phi}_{e,k}^{\mathcal{P}}$ and $\boldsymbol{\phi}_{e,k}^{\mathcal{P}^T}\mathbf{M}_e\boldsymbol{\phi}_{e,k}^{\mathcal{P}}$ are required for all elements $e = 1, ..., n_{el}$ such that computations on all elements seem to be necessary for this approximation of $\lambda_{\bar{e}}^{\bar{i},\bar{j}}$. However, these element contributions have to be computed only once and may be stored temporarily. Therefore, for all subsequent computations, only element level calculations are needed.

6.1.2 A p-adaptive strategy for the eigenvalue problem

The strategy proposed here is analogous to that of Section 5.3. As a stopping criterion, again, a hierarchic extrapolation may be used to compute a reference solution ω_k^{ref} to be compared to a prescribed tolerance TOL. Alternatively, a maximum number of iterations may be stipulated, or a maximum number of degrees of freedom N_{max}, for instance, when an efficient discretization for a time-stepping scheme is sought, where the transient problem is dominated by specific frequencies, see Section 6.2, and computational time is limited. The number of degrees of freedom in a direct time integration scheme is, of course, even more crucial than in

the static case, since a system of order N equations has to be solved at every time step.

The error indicator used for obtaining the sensitivity of the frequency ω_k to the variation of a specific entry $p_{\bar{e}}^{\bar{i},\bar{j}}$ is the explicit error indicator computed on element level (6.18), where a 'look back' difference polynomial degree $\Delta p_{\bar{e}}^{\bar{i},\bar{j}} = 2$ is used, as in Section 5.3.

As in the static case, the error indicators $\lambda_{e,k}^{i,j}$ corresponding to the entries $p_e^{i,j}$ are sorted and fixed proportions are refined according to the same staggered scheme as in Section 5.3, see algorithm A-2.

One difference between the algorithm in this section and that given in Section 5.3 is that, since adaptation to more than one eigenfrequency, ω_k, $k = k_1, ..., k_n$ may be desired, where $k_1, ..., k_n$ do not necessarily have to be sequential integers, it is recommended to choose the new polynomial degree template to be the maximum hull of the templates $\mathcal{P}_{iter+1,k}$ suggested for adaptation to all frequencies ω_k

$$\mathcal{P}_{iter+1} = \max_{k=k_1,...,k_n} p_{e,iter+1,k}^{i,j} \,, \tag{6.19}$$

see the inner loop over k in the following algorithm. Alternatively, an outer loop over the number of frequencies to be adapted to, n, could be used to call the eigensolver for every frequency ω_k separately. However, this might be less efficient depending on the eigensolver employed, for example, the LANCZOS based eigensolver used here computes all frequencies in one run much more efficiently than in separate runs for every ω_k, see SCHWARZ [127, 128] and RABOLD [112].

6.2 A p-adaptive strategy for time-dependent problems

The p-adaptive strategy for solving time-dependent, elastodynamic problems suggested here consists of the following, principle steps:

1. Find frequencies dominating the problem by initial computation of the transient problem with coarse spatial discretization,
2. find discretization adapted to dominating frequencies and
3. recompute problem of interest using discretization found by adaptation.

The following section describes the task of identifying the dominating frequencies. The p-adaptive eigensolver of Section 6.1 is used for an adaptive computation of the governing frequencies. The initial time-dependent computation described below and the recomputation with the adaptively chosen discretization may be computed using an arbitrary time integration scheme. The numerical examples discussed in Section 6.3 were computed applying members of the generalized-α-family of algorithms, see Section 3.2.1.

Algorithm A-2 p-Adaptive strategy for eigenvalue problem

set $iter = 0$, $\mathcal{P}_{iter}$ **uniformly to** $p^{i,j}_{e,iter} = 4$
repeat
  compute $\omega_k^{\mathcal{P}_{iter}}$, $k = k_1, ..., k_n$
  for $k = k_1, ..., k_n$ **do**
    for all $\{e, i, j\}$ **compute** $\lambda^{i,j}_{e,k}$ **using** (6.18)
    sort all $\lambda^{i,j}_{e,k}$ **and find** $\lambda_{70\%}$, $\lambda_{90\%}$
    set

$$\Delta\mathcal{P}_{iter+1,k} = \Delta p^{i,j}_{e,iter+1,k} = \begin{cases} 0 & \text{for} & & \check{\lambda}^{i,j}_e & < & \lambda_{70\%}(1-\varepsilon) \\ 1 & \text{for} & \lambda_{70\%}(1-\varepsilon) & \check{\lambda}^{i,j}_e & < & \lambda_{90\%}(1-\varepsilon) \\ 2 & \text{for} & \lambda_{90\%}(1-\varepsilon) & \check{\lambda}^{i,j}_e & & \end{cases}$$

    set $\mathcal{P}_{iter+1,k} = \mathcal{P}_{iter} + \Delta\mathcal{P}_{iter+1,k}$
    if $(iter \geq 2)$ **then**
      compute $\eta_k = \omega_k^{\mathcal{P}_{iter}} - \omega_k^{ref}$ **using hierarchic extrapolation for** ω_k^{ref}
    else
      set $\eta_k = TOL + \varepsilon$ *(stopping criterion not fullfilled yet)*
    end if
  end for
  set

$$\mathcal{P}_{iter+1} = \max_{k=k_1,...,k_n} p^{i,j}_{e,iter+1,k}\,,$$

$$\eta = \max_{k=k_1,...,k_n} \eta_k\,,$$

$$iter = iter + 1$$

until $(\eta < TOL)$ OR $(iter > maxiter)$ OR $(N_{iter} > N_{max})$

In order to recognize the dominating frequencies, an initial solution of the structural dynamic problem (6.2) is computed with an initial, uniform polynomial degree distribution $p_e^{i,j} = 4$, where $\mathbf{d}(t)$, $\dot{\mathbf{d}}(t)$ are subsequently needed to extract the prevailing frequencies. In addition, the eigenvalue problem (6.3) has to be solved, yielding the eigenfrequencies $\omega_1, ..., \omega_{n_{eigen}}$ with $n_{eigen} \ll N$, again using an initial uniform p-distribution $p_e^{i,j} = 4$.

Once the approximations of eigenvectors $\boldsymbol{\phi}_k$ are known, the approximations $\mathbf{d}(t)$, $\dot{\mathbf{d}}(t)$ can be projected onto the corresponding eigenvector space spanned by $\boldsymbol{\phi}_k$. If all N eigenvectors were known, the amplitudes $\mathbf{x}(t)$ associated with the eigenvectors $\boldsymbol{\phi}_k$ would have to fulfill the relation

$$\mathbf{d}(t) = \boldsymbol{\Phi}\mathbf{x}(t) \tag{6.20}$$

in order to fully describe the displacement vector $\mathbf{d}(t)$ with

$$\boldsymbol{\Phi} = [\boldsymbol{\phi}_1, ..., \boldsymbol{\phi}_N] \tag{6.21}$$

and

$$\mathbf{x}(t) = [x_1(t), ..., x_N(t)]^T. \tag{6.22}$$

Multiplying (6.20) with $\boldsymbol{\Phi}^T\mathbf{M}$ from the left we obtain

$$\boldsymbol{\Phi}^T\mathbf{M}\mathbf{d}(t) = \boldsymbol{\Phi}^T\mathbf{M}\boldsymbol{\Phi}\mathbf{x}(t) = \mathbf{x}(t), \tag{6.23}$$

using the $\mathbf{M}$-orthogonality

$$\boldsymbol{\phi}_i^T\mathbf{M}\boldsymbol{\phi}_j = \delta_{ij} \tag{6.24}$$

of the eigenvectors, or

$$x_k(t) = \boldsymbol{\phi}_k^T\mathbf{M}\mathbf{d}(t). \tag{6.25}$$

Accordingly, in order to project the velocity vector $\dot{\mathbf{d}}(t)$ onto the eigenvector space, we can differentiate (6.25) with respect to time, to get

$$\dot{x}_k(t) = \boldsymbol{\phi}_k^T\mathbf{M}\dot{\mathbf{d}}(t). \tag{6.26}$$

It is apparent that only the eigenvector $\boldsymbol{\phi}_k$ is needed to compute (6.25) and (6.26), not the complete set of N eigenvectors, as required first in Equation (6.20). Once x_k, $\dot{x}_k$, $k = 1, ..., n_{eigen}$ are known, it is easy to compute the strain energy associated with eigenvector $\boldsymbol{\phi}_k$ as

$$
\begin{aligned}
E_{str,k}(t) &= \frac{1}{2}(\boldsymbol{\phi}_k x_k(t))^T \mathbf{K} \boldsymbol{\phi}_k x_k(t) && (6.27)\\
&= \frac{1}{2} x_k^2(t) \boldsymbol{\phi}_k^T \mathbf{K} \boldsymbol{\phi}_k && (6.28)\\
&= \frac{1}{2} x_k^2(t) \omega_k^2 && (6.29)
\end{aligned}
$$

using the $\mathbf{K}$-orthogonality of eigenvectors

$$\boldsymbol{\phi}_i^T \mathbf{K} \boldsymbol{\phi}_j = \delta_{ij} \omega_i^2, \tag{6.30}$$

and, again using (6.24), the kinetic energy associated with $\boldsymbol{\phi}_k$ as

$$
\begin{aligned}
E_{kin,k}(t) &= \frac{1}{2}(\boldsymbol{\phi}_k \dot{x}_k(t))^T \mathbf{M} \boldsymbol{\phi}_k \dot{x}_k(t) && (6.31)\\
&= \frac{1}{2} \dot{x}_k^2(t) \boldsymbol{\phi}_k^T \mathbf{M} \boldsymbol{\phi}_k && (6.32)\\
&= \frac{1}{2} \dot{x}_k^2(t). && (6.33)
\end{aligned}
$$

Finally, a reasonable measure is needed to decide which eigenfrequencies dominate the solution of the transient problem and, since only n_{eigen} eigenfrequencies are taken into consideration instead of N eigenfrequencies existing for the spatially discrete system, whether this reduction is justified, i.e. whether n_{eigen} is large enough.

To identify the prevailing frequencies, it is possible to use the *mean internal energy* of the system

$$\bar{E}_{int} = \frac{1}{T} \int_T E_{str}(t) + E_{kin}(t) dt \tag{6.34}$$

to compare its proportions

$$\bar{E}_{int,k} = \frac{1}{T} \int_T E_{str,k}(t) + E_{kin,k}(t) dt \tag{6.35}$$

contributed by the different eigenfrequencies ω_k. A frequency ω_k can be regarded as dominant when its proportion of the overall mean internal energy exceeds a certain limit

$$\frac{\bar{E}_{int,k}}{\bar{E}_{int}} > r_1, \tag{6.36}$$

where r_1 can be chosen according to the accuracy desired, for example, r_1=0.05.

In addition, care should be taken to ensure that energies of the chosen frequencies represent a sufficient proportion of the overall mean internal energy, i.e.

$$\frac{\sum_{k=k_1}^{k_n} \bar{E}_{int,k}}{\bar{E}_{int}} > r_2, \tag{6.37}$$

with r_2 again to be chosen to yield a desired accuracy, $r_2 = 0.95$, for example. If this criterion cannot be fulfilled, frequencies not satisfying (6.36) have to be included or the number of computed eigenfrequencies n_{eigen} has to be increased.

It is accordingly possible to select the n dominant eigenfrequencies ω_k, $k = k_1, ..., k_n$, where the $k_1, ..., k_n$ in increasing order do not necessarily have to be consecutive integers, and the transient problem can be recomputed using the adapted p-discretization.

The proposed p-adaptive strategy is summarized in algorithm A-3. Of course, it is possible to repeat algorithm A-3 if necessary.

6.3 Numerical examples

For all numerical examples in this section, the trunk space $\mathcal{S}_{\text{ts}}^{\mathcal{P}}$ is used for the spatial discretization with hexahedral elements, see Section 3.1.1.

6.3.1 Clamped plate

As a first example, the clamped quadratic plate already discussed in Section 5.4.1, where it is subjected to a static, i.e. an infinitely slowly applied load, is investigated. This section proceeds to analyze the transient behavior. Thus, the uniform surface load will not be applied statically, but suddenly at time $t = t_0 = 0$, acting then at least until $t = T = 0.05$, the end of the time period of interest, which is slightly larger than the maximum eigenperiod of the system. The system, mesh and load function over time are depicted in Figure 6.2. The material of the plate is assumed to be linear elastic described by YOUNG's modulus of elasticity $E = 30000000$, POISSON's ratio $\nu = 0.2$ and density $\rho = 1.0$.

An initial solution of the transient problem 6.2 is computed using a uniform polynomial degree $p_e^{i,j} = 4$ (according to steps 1, 2 of algorithm A-3). As a time integration scheme, the *trapezoidal rule* is used ($\alpha_m = \alpha_f = 0, \beta = 0.25, \gamma = 0.5$), see Section 3.2.1, and a time-step size of $\Delta t = 0.001$.

The strain and kinetic energies are evaluated at every time-step (necessary for step 3), as depicted in Figure 6.3.

Algorithm A-3 p-Adaptive strategy for transient problems

1: **set** $p_e^{i,j} = 4$
2: **solve transient problem**

$$\mathbf{K}\mathbf{d}(t) + \mathbf{C}\dot{\mathbf{d}}(t) + \mathbf{M}\ddot{\mathbf{d}}(t) = \mathbf{F}(t) \quad \text{for} \quad t \in [0, T]$$

3: **compute**

$$\bar{E}_{int} = \frac{1}{T} \int_T E_{str}(t) + E_{kin}(t) dt$$

4: **solve eigenvalue problem**

$$\mathbf{K}\boldsymbol{\phi}_k = \omega_k^2 \mathbf{M}\boldsymbol{\phi}_k \quad \text{with} \quad k = 1, ..., n_{eigen},\ n_{eigen} \ll N$$

5: **project** $\mathbf{d}$, $\dot{\mathbf{d}}$ on eigenvectors $\boldsymbol{\phi}_1, ..., \boldsymbol{\phi}_{n_{eigen}}$:

$$\begin{aligned} x_k(t) &= \boldsymbol{\phi}_k^T \mathbf{M}\mathbf{d}(t) \\ \dot{x}_k(t) &= \boldsymbol{\phi}_k^T \mathbf{M}\dot{\mathbf{d}}(t) \end{aligned}$$

6: **compute proportions of** $\bar{E}_{int}$ **associated with** ω_k

$$\bar{E}_{int,k} = \frac{1}{T} \int_T \frac{1}{2} x_k^2(t) \omega_k^2 + \frac{1}{2} \dot{x}_k^2(t) dt$$

7: **select dominant frequencies** ω_k**,** $k = k_1, ..., k_n$ **fulfilling**

$$\frac{\bar{E}_{int,k}}{\bar{E}_{int}} > r_1$$

8: **if** $(\frac{\sum_{k=k_1}^{k_n} \bar{E}_{int,k}}{\bar{E}_{int}} \leq r_2)$ **then**
9: **include non-dominant frequencies until** $(\frac{\sum_{k=k_1}^{k_n} \bar{E}_{int,k}}{\bar{E}_{int}} \geq r_2)$ **if possible**
10: **end if**
11: **if** $(\frac{\sum_{k=k_1}^{k_n} \bar{E}_{int,k}}{\bar{E}_{int}} \leq r_2)$ **then**
12: **increase** n_{eigen}
13: **goto step** 4
14: **end if**
15: **apply** p**-adaptive eigensolver (Section 6.1) for** ω_k**,** $k = k_1, ..., k_n$
16: **recompute transient problem (step 2) using adaptively selected discretization**

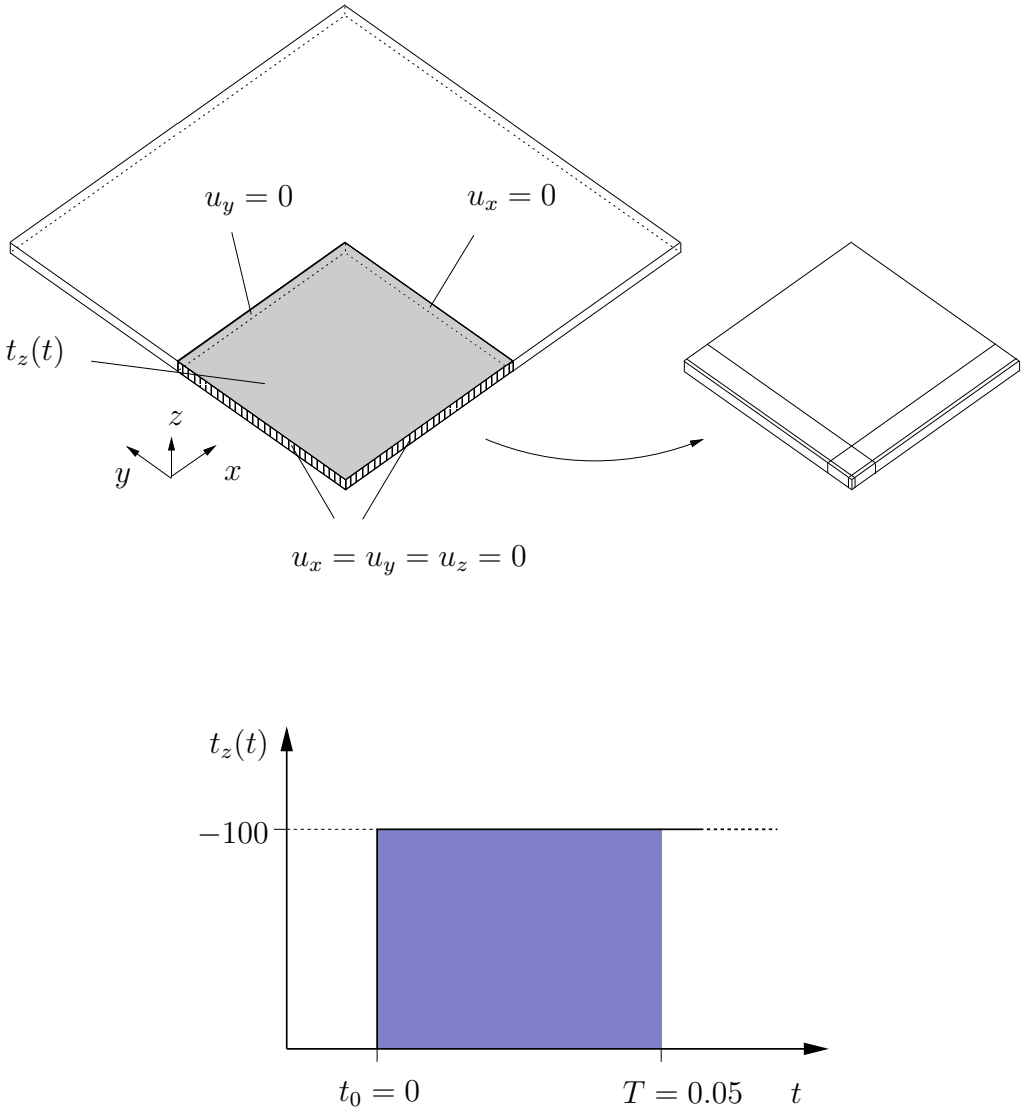

Figure 6.2: System of clamped plate (top left) and hexahedral mesh (top right) and load function over time $t_z(t)$ (bottom)

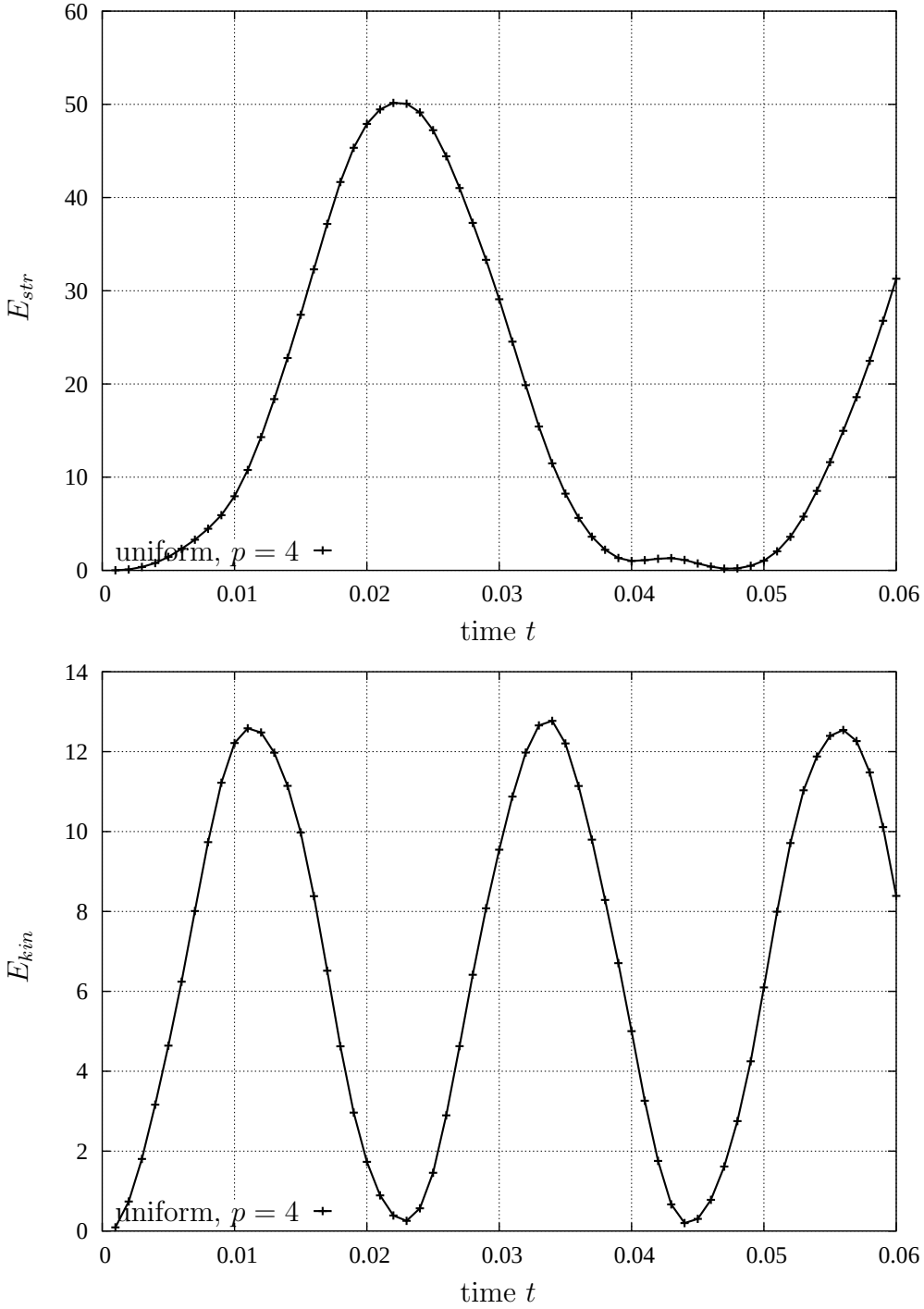

Figure 6.3: Strain energy E_{str} and kinetic energy E_{kin} of clamped plate subjected to sudden surface load over time

In order to find the dominant frequencies of the problem, the eigenvalue problem (6.3) is solved, and $n_{eigen} = 5$ eigenfrequencies and eigenvectors are computed (step 4). Both here and in the following adaptive iterations for specific eigenfrequencies, the LANCZOS eigensolver is applied. The displacement and velocity vectors $\mathbf{d}$, $\dot{\mathbf{d}}$ are projected onto the eigenvector space (step 5) and the strain and kinetic energies associated with the eigenvectors $\boldsymbol{\phi}_1, ..., \boldsymbol{\phi}_5$ are evaluated (necessary for step 6). The decomposition is plotted in Figure 6.4 from which it is evident that the dominant frequency is ω_1. For ω_1 we obtain $\frac{\bar{E}_{int,1}}{\bar{E}_{int}} = 0.970$, thus, using $r_1 = 0.05$ and $r_2 = 0.95$ as suggested in Section 6.2, both criteria (6.36) and (6.37) are fulfilled (steps 7 and 8).

For ω_1 the adaptive eigensolver is applied (step 15) with a stopping criterion $N_{max} = 2500$ resulting in five adaptive runs, see Figure 6.5. A hierarchically refined, higher order solution was used by way of a reference solution. As in the convergence surveys for elastostatic problems in Section 5.4, the adaptive convergence curve is always below the curve corresponding to uniform p-refinement, i.e. it is more efficient, and, interestingly, also shows a clearly higher rate of convergence in the asymptotic range, where uniform p-refinement shows poor behavior.

The set of polynomial degree templates $\mathcal{P}_5$ corresponding to the iteration $iter = 5$ is visualized in Figure 6.6, revealing similar characteristics to those in the elastostatic case: large polynomial degrees on the largest element, low polynomial degrees at the small, corner elements and the largest polynomial degrees on the long, boundary layer elements around the clamped support, indicating that further mesh refinement would be reasonable for the uniform p-version. The same symmetries can be observed as described in Section 5.4.1.

For analysis purposes, the discretizations of all the iterative steps of the p-adaptive eigensolver are used for recomputing the transient problem (step 16). In order to compare the efficiency of the adaptive and uniform p-discretizations, the error measure

$$\eta(t) = \left(\frac{|\Delta E_{str}(t)| + |\Delta E_{kin}(t)|}{E_{max}} \right)^{\frac{1}{2}} \tag{6.38}$$

is introduced. Figure 6.7 plots the maximum error and the mean error over time

$$\eta_{max} = \max_t \eta(t), \tag{6.39}$$

$$\bar{\eta} = \frac{\int_{\Delta t} \eta(t)\, dt}{\Delta t}. \tag{6.40}$$

From both plots it is obvious that the adaptive refinements show a markedly higher efficiency than uniform p-refinements.

6.3.2 Cantilever

As a second example, a cantilever clamped at one side is investigated. Although subjected to a loading similar to the plate in Section 6.3.1 and despite the fact that again only one — the lowest — frequency is dominant, it is necessary to adjust the discretization to optimally

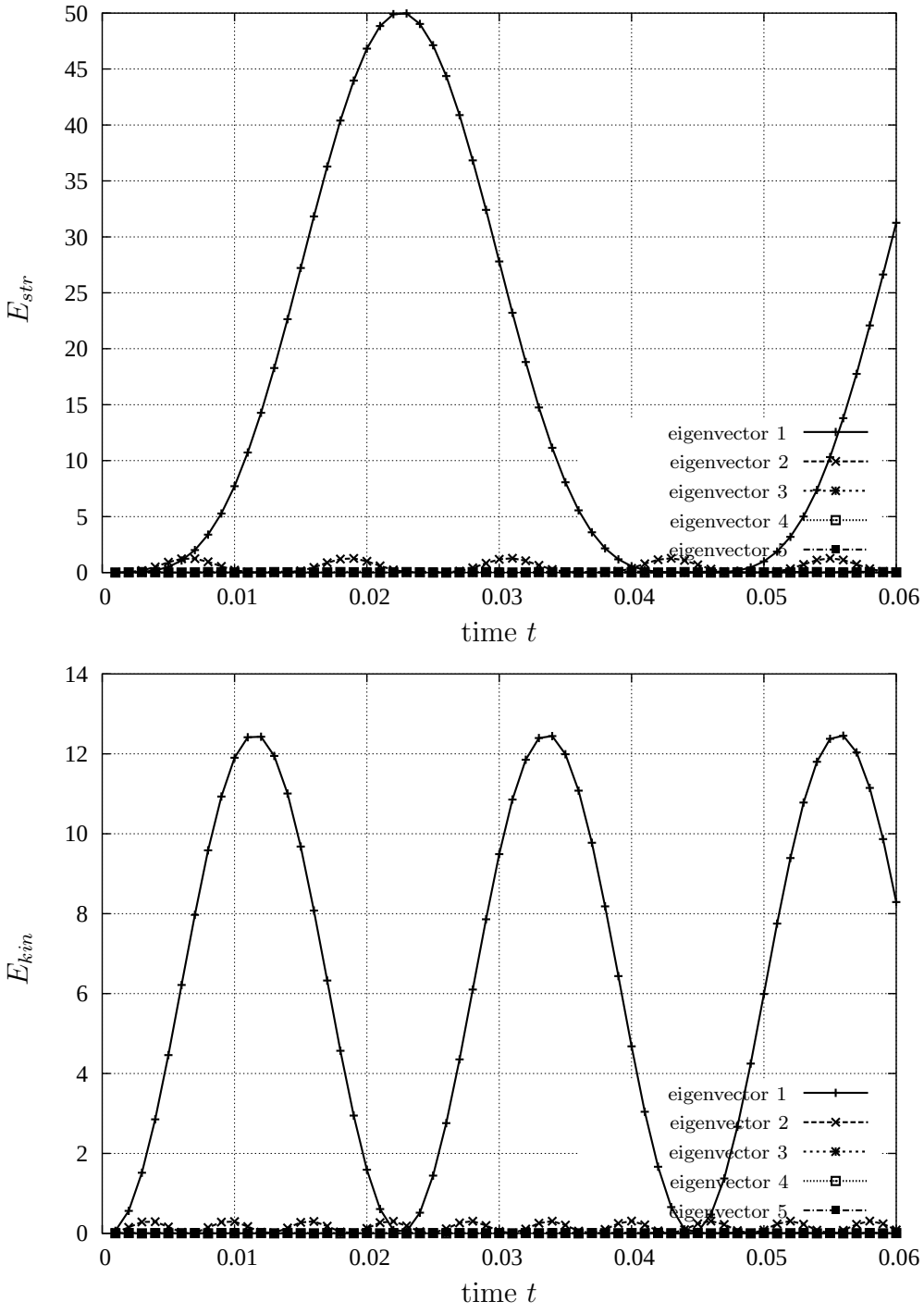

Figure 6.4: Decomposition of strain energy E_{str} and kinetic energy E_{kin} into the proportions associated with the lowest five eigenfrequencies

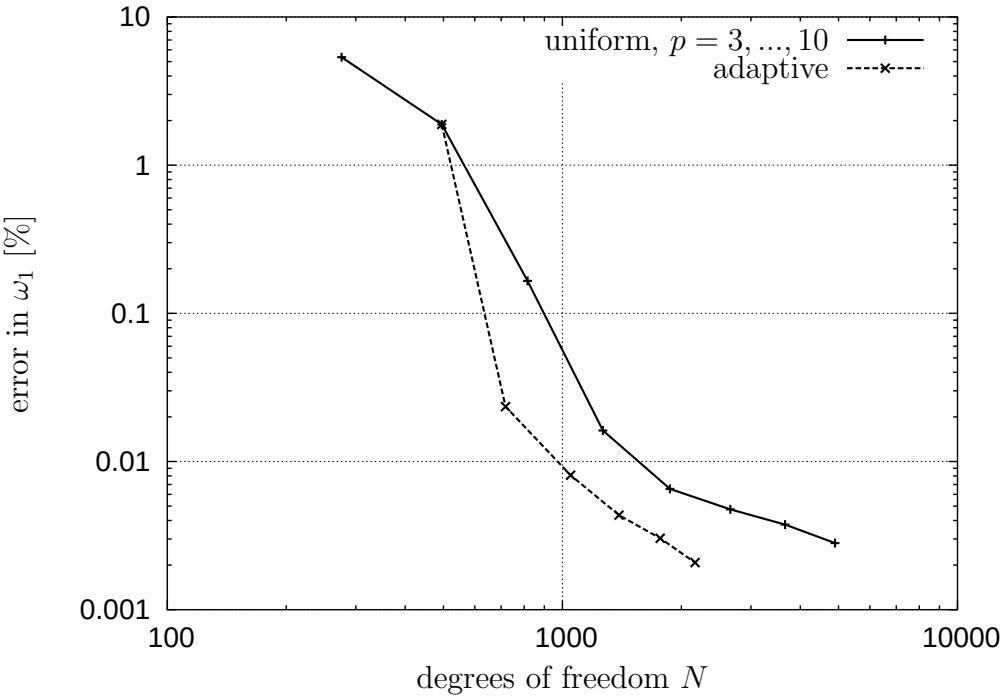

Figure 6.5: Convergence of eigenfrequency ω_1 for plate

represent *two* eigenmodes due to the multiplicity of the first eigenfrequency, as explained below.

For this example, YOUNG's modulus of elasticity has been chosen to be $E = 2.1 \cdot 10^{11}$, the density to be $\rho = 7.85 \cdot 10^3$ and POISSON's ratio to be $\nu = 0.3$. The face load is applied suddenly at time $t_0 = 0$, acting until the end of the time period of interest $T = 0.3$, see Figure 6.8.

The time discretization using the generalized α-method with a numerical high frequency damping $\rho_\infty = 0.8$ and a time-step size of $\Delta t = 0.005$ is assumed to be sufficiently accurate.

The fixed mesh used for the p-adaptive spatial error control consists of 54 elements, composed of six layers in length-, i.e. x-direction, where every layer consists of 3×3 elements aligned to give a refinement towards the corners of the cross-section. The different lengths of the layers result in a refinement towards the clamped boundary, see Figure 6.8.

The following investigation is along the same lines as Algorithm A-3 or the example illustrated in Section 6.3.1, respectively. The initial coarse computation with uniform $p_e^{i,j} = 4$ of the time period of interest yields the strain and kinetic energies plotted over time in Figure 6.9.

The dominant eigenfrequency for this system is the multiple frequency $\omega_{1/2} = \omega_1 = \omega_2 \approx 4.18$, once again approximated using $p_e^{i,j} = 4$. The multiplicity of the eigenfrequency results directly from the symmetry of the cross-section. In Figure 6.10 the dominant eigenvector is clearly the second one, $\boldsymbol{\phi}_2$. However, since $\boldsymbol{\phi}_1$ and $\boldsymbol{\phi}_2$ correspond to the same frequency, arbitrary linear combinations of both are also potential eigenvectors, i.e. $\boldsymbol{\phi}_1$ and $\boldsymbol{\phi}_2$ are not uniquely defined.

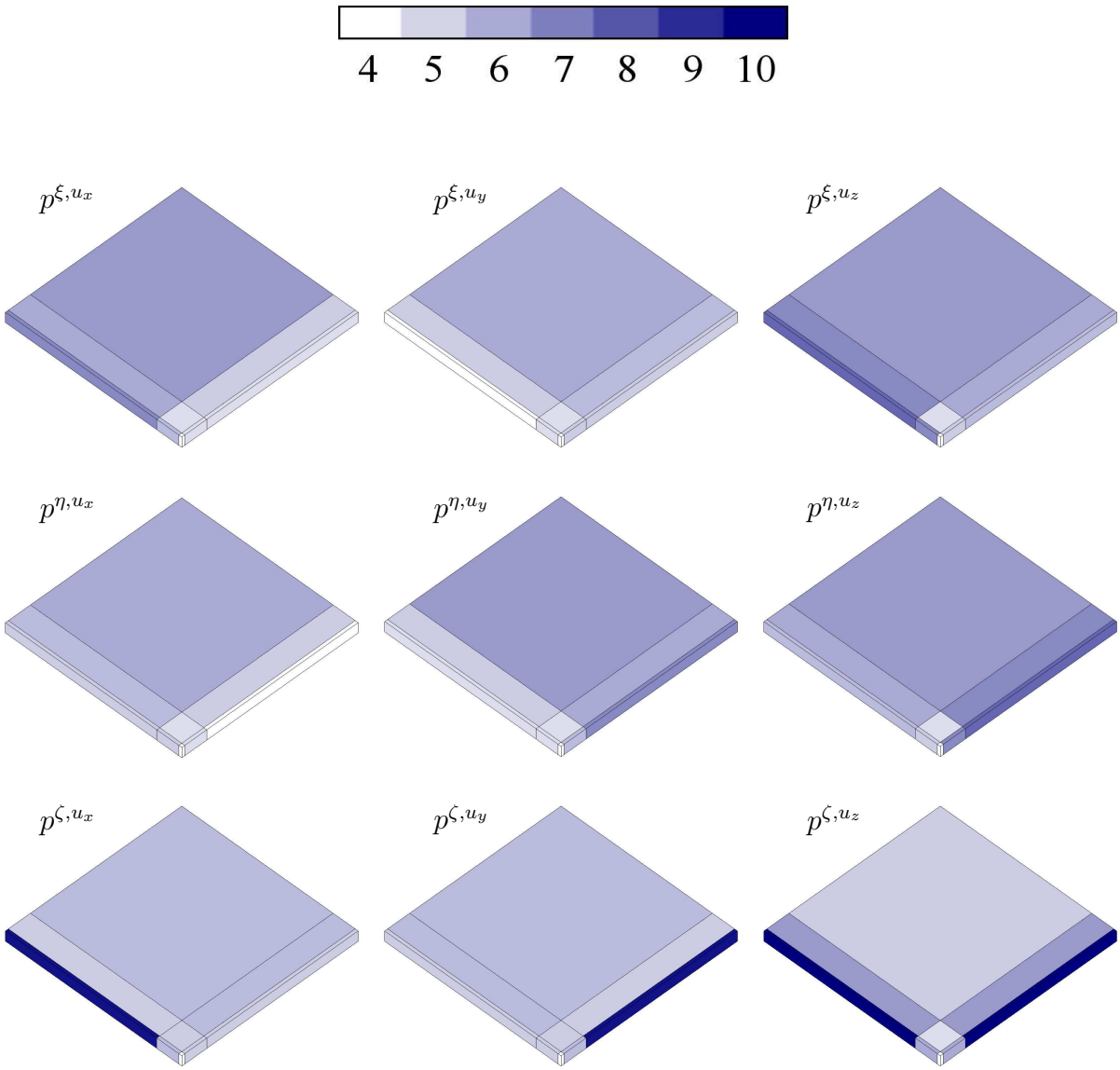

Figure 6.6: Graphical representation of polynomial degree templates corresponding to iteration 5 of the adaptive eigensolver using the explicit error indicator of *version 1* for a 3D plate

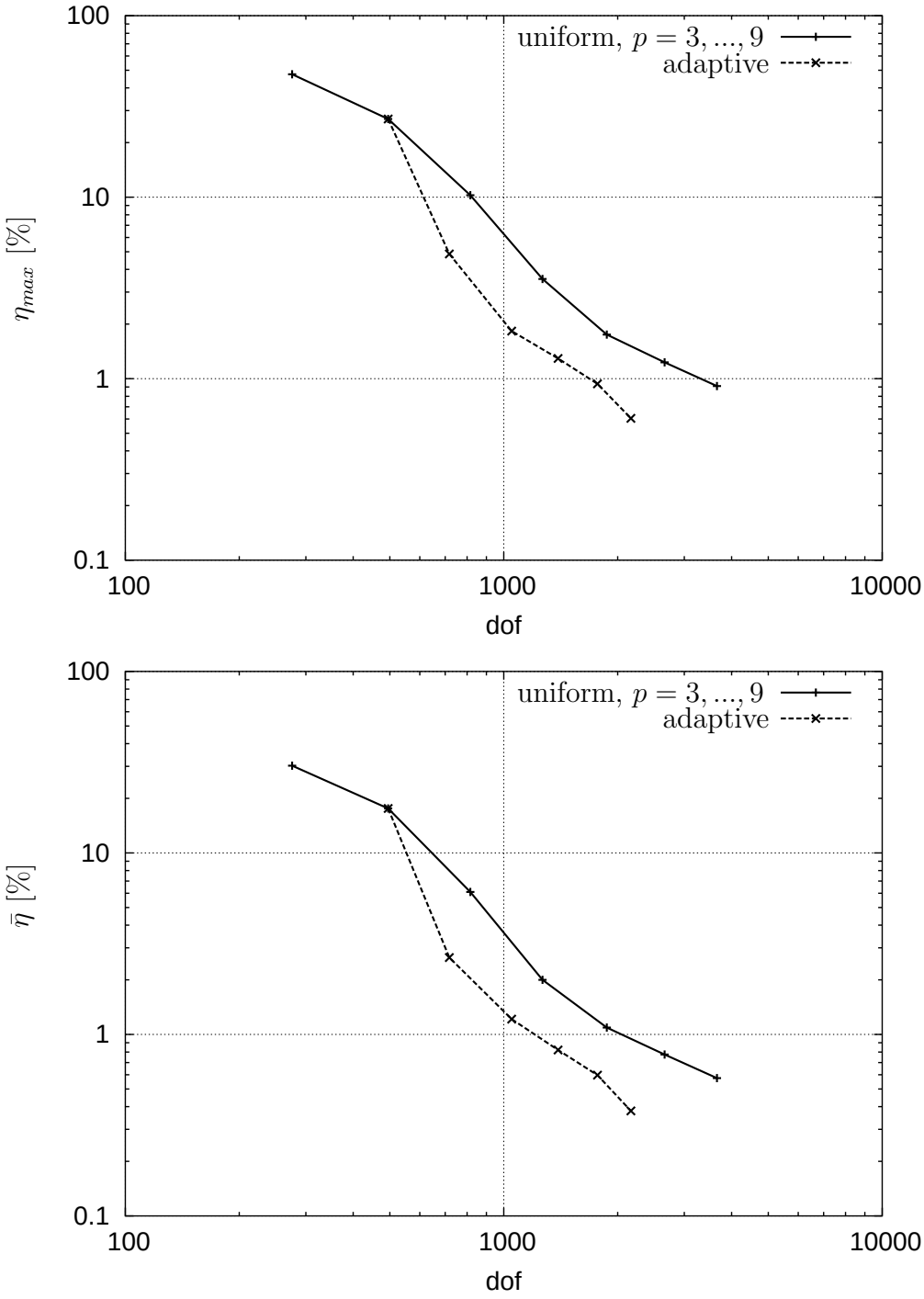

Figure 6.7: Maximum error η_{max} and mean error $\bar{\eta}$ for transient computation of plate

Thus, it makes no sense to adapt for either $\boldsymbol{\phi}_1$ or $\boldsymbol{\phi}_2$, since the result would be arbitrary. One possible way of overcoming this problem is to make the p-adaptive eigensolver find a discretization to optimally represent the *space spanned by* $\boldsymbol{\phi}_1$ *and* $\boldsymbol{\phi}_2$. Therefore, we adapt both for $\boldsymbol{\phi}_1$ and $\boldsymbol{\phi}_2$ simultaneously, choosing the maximum entries of the polynomial degree templates suggested by the adaptive procedure for either $\boldsymbol{\phi}_1$ or $\boldsymbol{\phi}_2$.

The convergence of the double eigenfrequency $\omega_{1/2}$ for uniform p-refinement is compared to adaptive p-refinement with the goal of efficiently describing $\boldsymbol{\phi}_1$ and $\boldsymbol{\phi}_2$ in Figure 6.11. The adaptive curve shows a considerably higher convergence rate, especially in the accuracy range where poor asymptotic behavior can be observed for the uniform curve.

The recomputation of the time period in question using the discretizations found by adaptation also represents the enormous gain in efficiency by p-adaptivity, which is evident from the maximum error over time η_{max} and the mean error over time $\bar{\eta}$ according to Equations (6.38)–(6.40) plotted in Figure 6.12.

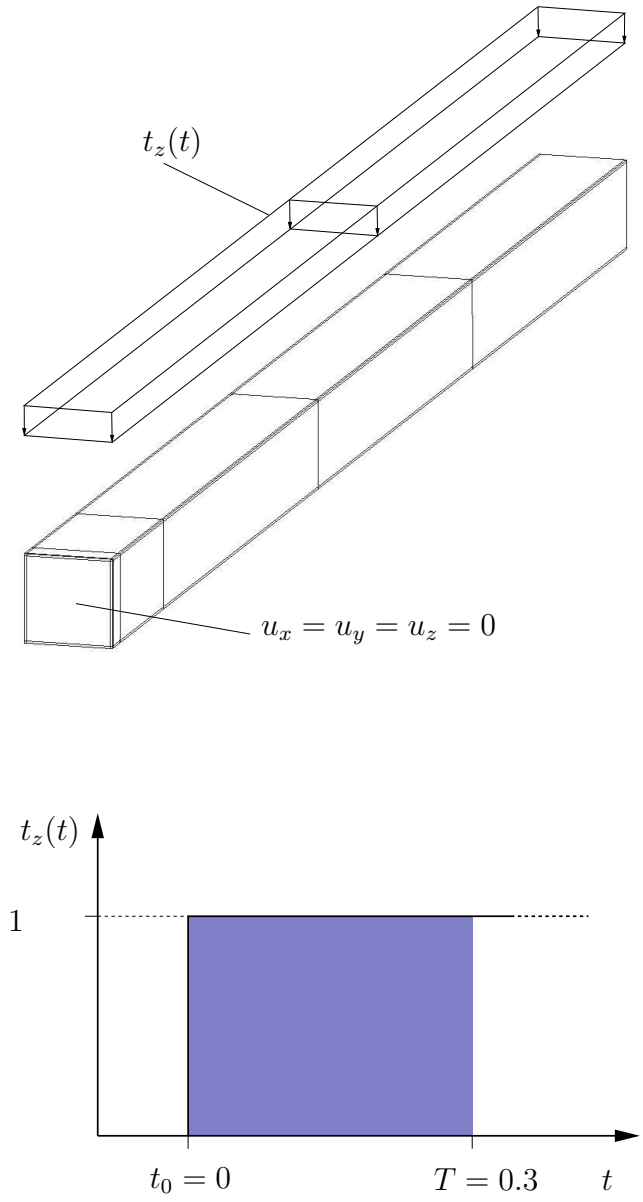

Figure 6.8: System and hexahedral mesh of cantilever (top) and load function over time $t_z(t)$ (bottom)

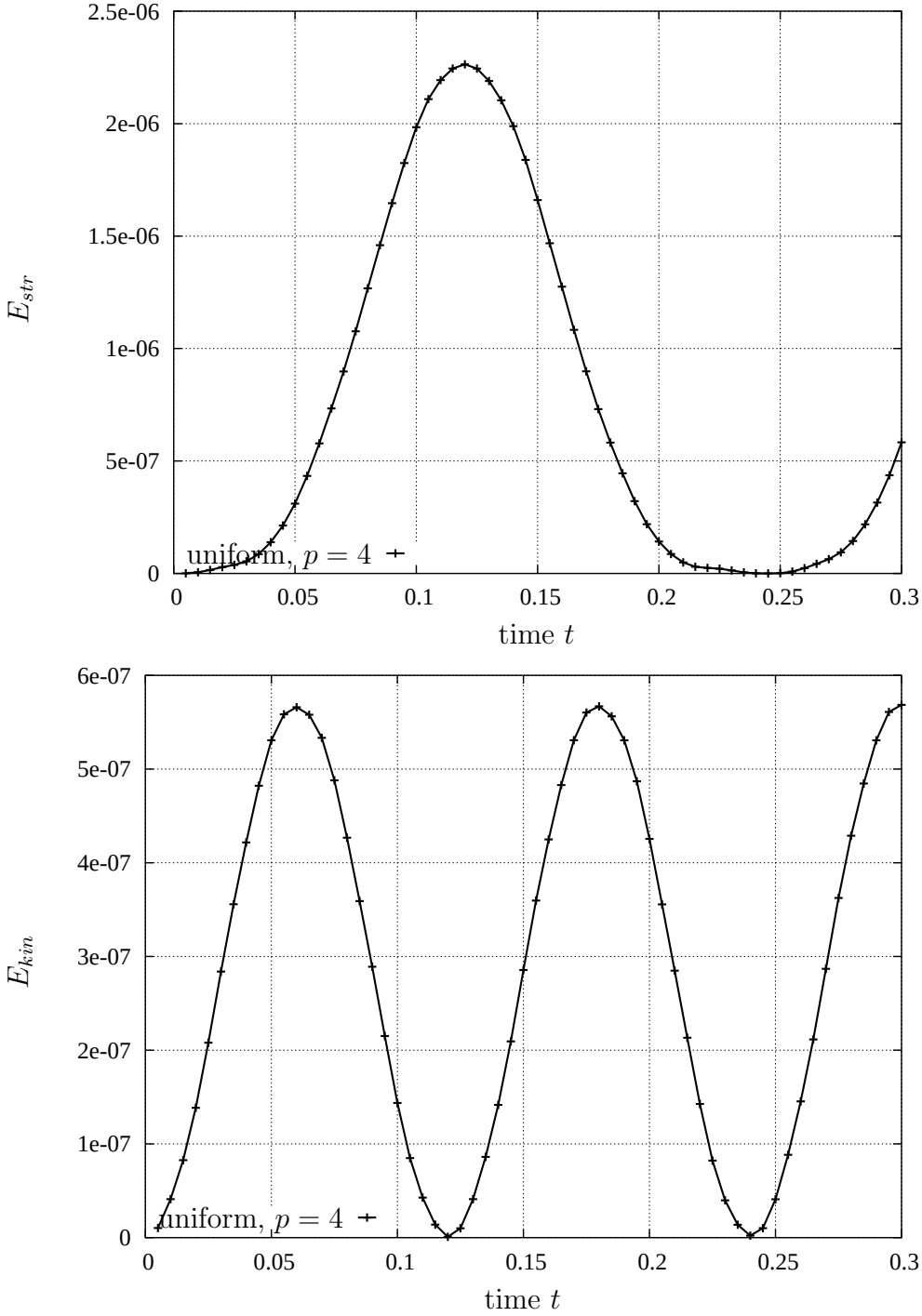

Figure 6.9: Strain energy E_{str} and kinetic energy E_{kin} of cantilever subjected to sudden surface load over time

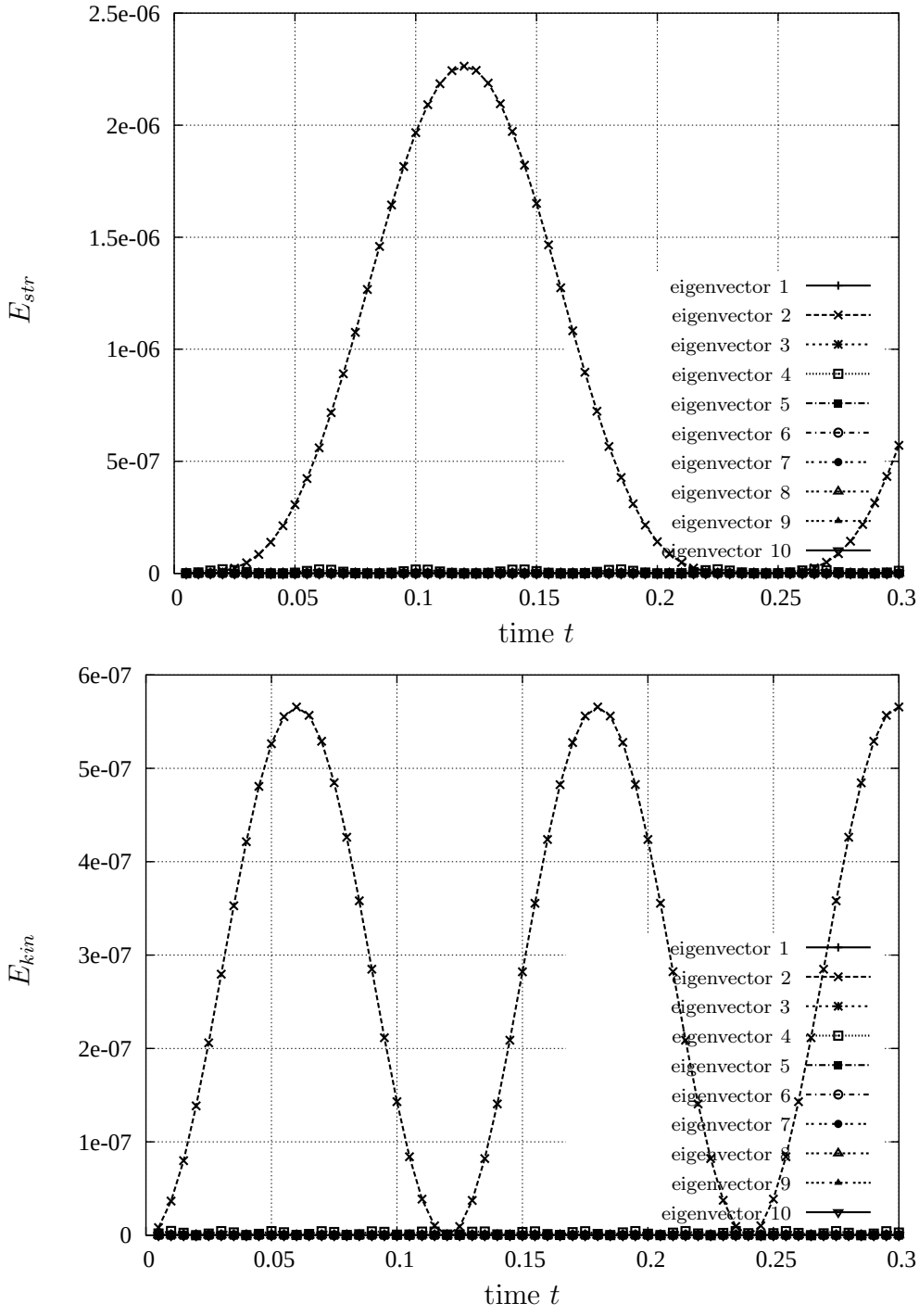

Figure 6.10: Decomposition of strain energy E_{str} and kinetic energy E_{kin} into the proportions associated with the lowest ten eigenfrequencies over time

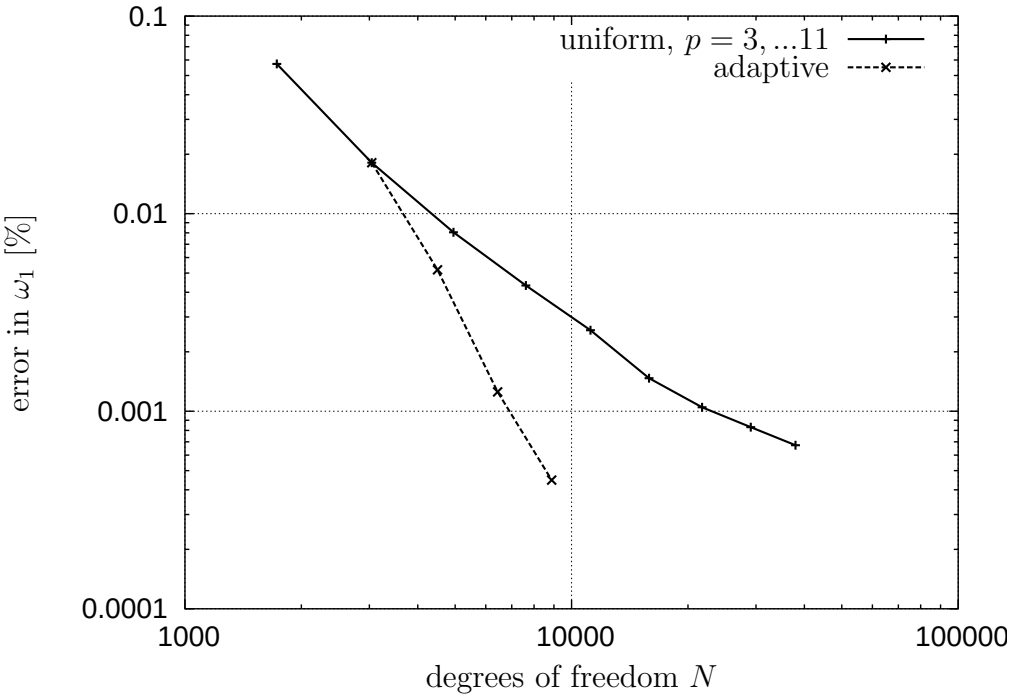

Figure 6.11: Convergence of eigenfrequency $\omega_{1/2}$ for cantilever

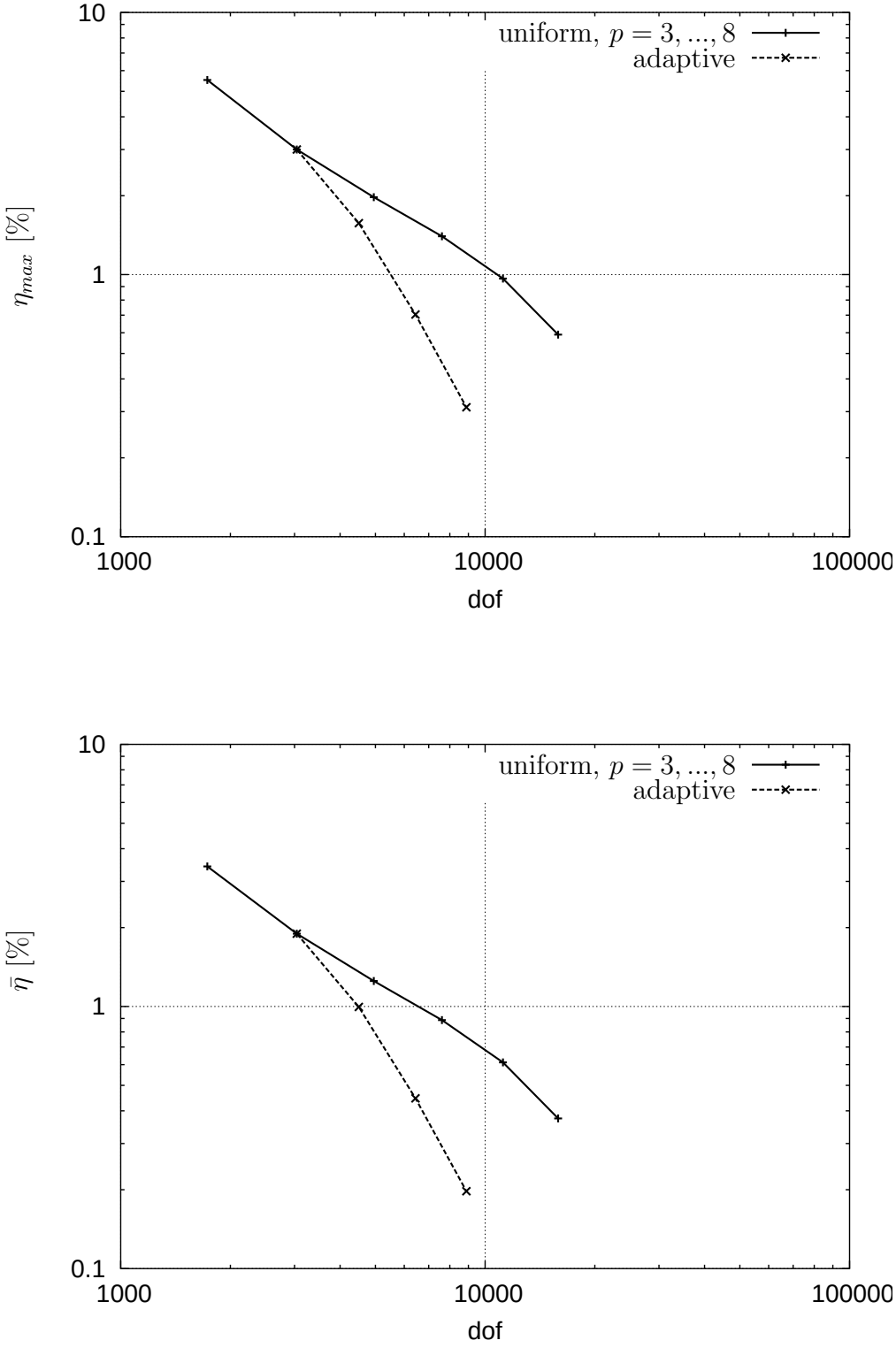

Figure 6.12: Maximum error η_{max} and mean error $\bar{\eta}$ for the transient computation of cantilever

Chapter 7

Summary

Based on a high-order hexahedral element formulation allowing for the independent adjustment of polynomial degrees for different local directions and displacement fields, this thesis proposes an anisotropic p-adaptive method for linear elastostatic and linear elastodynamic problems.

The p-adaptive method for static problems is driven by an anisotropic hierarchic error indicator based on the idea of locally projecting the solution from a given Ansatz space to a reduced, hierarchically nested space, minimizing the difference in strain energy. For all numerical examples under consideration, the anisotropic p-adaptive discretizations are clearly more efficient than a uniform p-refinement. In addition, a higher rate of convergence is observed in the asymptotic range in each of the examples.

The p-adaptive method for dynamic problems is based on adjusting the polynomial degrees in order to optimally represent the dominant eigenfrequencies, obtained from an initial transient computation with a coarse discretization. The p-adaptive eigensolver required for this purpose involves a similarly constructed, locally computed, anisotropic hierarchic error indicator, thus minimizing the RAYLEIGH quotient. For the numerical examples investigated here, the p-adaptive discretizations again show a markedly higher efficiency and higher asymptotic rates of convergence for both the eigenfrequencies and the errors in the transient computations, compared to the uniform p-refinement.

This method can therefore be regarded as a remedy for one basic problem encountered in uniform h- and p-versions, namely their possibly poor asymptotic behavior, especially in presence of irregularities of the solution. This accordingly allows for an efficient, fully three-dimensional discretization of both thin-walled and compact parts of structures.

These results offer several interesting options for future developments:

- Although the strict hierarchy of the finite element matrices is lost for nonlinear problems, the approach presented here should also work for moderate nonlinear behavior. Modified error indicators could be developed, taking nonlinear effects into account, which would apply to a more general class of nonlinearities.
- An extension of the proposed method to adaptivity with respect to local quantities based

on the solution of dual problems could be highly interesting. The user could be provided with very intuitive error measures, like the errors in pointwise displacements or stresses or in stress resultants over specified areas.

- For dynamic computations, the adaptation of the polynomial degrees during the transient computation seems to be a promising approach. Due to the strictly hierarchic Ansatz spaces, no transfer error between two discretizations is introduced by refinement. Only coarsening, i.e. the reduction of polynomial degrees related to cutting off hierarchic modes, leads to transfer errors which, however, can readily be controlled by observing the corresponding loss in energy.

- This thesis proposes an adaptive strategy for controlling the spatial error. Adaptive methods could be applied for time integration as well. Moreover, a correlation of the accuracy of time integration to that of the spatial discretization would be advantageous.

Appendix A

Ansatz spaces for high order elements

A.1 The trunk space $\mathcal{S}_{\mathbf{ts}}^{p_\xi,p_\eta,p_\zeta}(\Omega_{\mathbf{st}}^{\mathbf{h}})$ for hexahedral elements

8 **nodal modes**

$$N_{1,1,1}^{\mathrm{N}_i}(\xi,\eta,\zeta) = \tfrac{1}{8}(1+\xi_i\,\xi)(1+\eta_i\,\eta)(1+\zeta_i\zeta), \quad i=1,...,8 \tag{A.1}$$

$4((p_\xi-1)+(p_\eta-1)+(p_\zeta-1))$ **edge modes**
$4(p_\xi-1)$ edge modes in ξ-direction

$$\begin{aligned}
N_{i,1,1}^{\mathrm{E}_1}(\xi,\eta,\zeta) &= \tfrac{1}{4}(1-\eta)(1-\zeta)\phi_i(\xi)\,, \quad i=2,...,p_\xi\\
N_{i,1,1}^{\mathrm{E}_3}(\xi,\eta,\zeta) &= \tfrac{1}{4}(1+\eta)(1-\zeta)\phi_i(\xi)\,, \quad i=2,...,p_\xi\\
N_{i,1,1}^{\mathrm{E}_9}(\xi,\eta,\zeta) &= \tfrac{1}{4}(1-\eta)(1+\zeta)\phi_i(\xi)\,, \quad i=2,...,p_\xi\\
N_{i,1,1}^{\mathrm{E}_{11}}(\xi,\eta,\zeta) &= \tfrac{1}{4}(1+\eta)(1+\zeta)\phi_i(\xi)\,, \quad i=2,...,p_\xi
\end{aligned} \tag{A.2}$$

$4(p_\eta-1)$ edge modes in η-direction

$$\begin{aligned}
N_{1,j,1}^{\mathrm{E}_2}(\xi,\eta,\zeta) &= \tfrac{1}{4}(1+\xi)(1-\zeta)\phi_j(\eta)\,, \quad j=2,...,p_\eta\\
N_{1,j,1}^{\mathrm{E}_4}(\xi,\eta,\zeta) &= \tfrac{1}{4}(1-\xi)(1-\zeta)\phi_j(\eta)\,, \quad j=2,...,p_\eta\\
N_{1,j,1}^{\mathrm{E}_{10}}(\xi,\eta,\zeta) &= \tfrac{1}{4}(1+\xi)(1+\zeta)\phi_j(\eta)\,, \quad j=2,...,p_\eta\\
N_{1,j,1}^{\mathrm{E}_{12}}(\xi,\eta,\zeta) &= \tfrac{1}{4}(1-\xi)(1+\zeta)\phi_j(\eta)\,, \quad j=2,...,p_\eta
\end{aligned} \tag{A.3}$$

$4(p_\zeta-1)$ edge modes in ζ-direction

$$\begin{aligned}
N_{1,1,k}^{\mathrm{E}_5}(\xi,\eta,\zeta) &= \tfrac{1}{4}(1-\xi)(1-\eta)\phi_k(\zeta)\,, \quad k=2,...,p_\zeta\\
N_{1,1,k}^{\mathrm{E}_6}(\xi,\eta,\zeta) &= \tfrac{1}{4}(1+\xi)(1-\eta)\phi_k(\zeta)\,, \quad k=2,...,p_\zeta\\
N_{1,1,k}^{\mathrm{E}_7}(\xi,\eta,\zeta) &= \tfrac{1}{4}(1+\xi)(1+\eta)\phi_k(\zeta)\,, \quad k=2,...,p_\zeta\\
N_{1,1,k}^{\mathrm{E}_8}(\xi,\eta,\zeta) &= \tfrac{1}{4}(1-\xi)(1+\eta)\phi_k(\zeta)\,, \quad k=2,...,p_\zeta
\end{aligned} \tag{A.4}$$

face modes

$$
\begin{aligned}
N^{\mathrm{F}_1}_{i,j,1}(\xi,\eta,\zeta) &= \frac{1}{2}(1-\zeta)\phi_i(\xi)\phi_j(\eta), \\
&\quad i=2,...,p_\xi-2, j=2,...,p_\eta-2, i+j=4,...,\max\{p_\xi,p_\eta\} \\
N^{\mathrm{F}_2}_{i,1,k}(\xi,\eta,\zeta) &= \frac{1}{2}(1-\eta)\phi_i(\xi)\phi_k(\zeta), \\
&\quad i=2,...,p_\xi-2, k=2,...,p_\zeta-2, i+k=4,...,\max\{p_\xi,p_\zeta\} \\
N^{\mathrm{F}_3}_{1,j,k}(\xi,\eta,\zeta) &= \frac{1}{2}(1+\xi)\phi_j(\eta)\phi_k(\zeta), \\
&\quad j=2,...,p_\eta-2, k=2,...,p_\zeta-2, j+k=4,...,\max\{p_\eta,p_\zeta\}
\end{aligned}
$$

continued

$$
\begin{aligned}
N^{\mathrm{F}_4}_{i,1,k}(\xi,\eta,\zeta) &= \frac{1}{2}(1+\eta)\phi_i(\xi)\phi_k(\zeta), \\
&\quad i=2,...,p_\xi-2, k=2,...,p_\zeta-2, i+k=4,...,\max\{p_\xi,p_\zeta\} \\
N^{\mathrm{F}_5}_{1,j,k}(\xi,\eta,\zeta) &= \frac{1}{2}(1-\xi)\phi_j(\eta)\phi_k(\zeta), \\
&\quad j=2,...,p_\eta-2, k=2,...,p_\zeta-2, j+k=4,...,\max\{p_\eta,p_\zeta\} \\
N^{\mathrm{F}_6}_{i,j,1}(\xi,\eta,\zeta) &= \frac{1}{2}(1+\zeta)\phi_i(\xi)\phi_j(\eta), \\
&\quad i=2,...,p_\xi-2, j=2,...,p_\eta-2, i+j=4,...,\max\{p_\xi,p_\eta\}
\end{aligned}
\tag{A.5}
$$

internal modes

$$
\begin{aligned}
N^{\mathrm{int}}_{i,j,k}(\xi,\eta,\zeta) &= \phi_i(\xi)\phi_j(\eta)\phi_k(\zeta), \\
&\quad i=2,...,p_\xi-4,\ j=2,...,p_\eta-4,\ k=2,...,p_\zeta-4, \\
&\quad i+j+k=6,...,\max\{p_\xi,p_\eta,p_\zeta\}
\end{aligned}
\tag{A.6}
$$

A.2 The tensor product space $\mathcal{S}^{p_\xi,p_\eta,p_\zeta}_{\mathbf{ps}}(\Omega^{\mathbf{h}}_{\mathbf{st}})$ for hexahedral elements

nodal and edge modes as in Equations (A.1)–(A.4)

$2\left[(p_\xi-1)(p_\eta-1)+(p_\xi-1)(p_\zeta-1)+(p_\eta-1)(p_\zeta-1)\right]$ **face modes**

$$
\begin{aligned}
N^{\mathrm{F}_1}_{i,j,1}(\xi,\eta,\zeta) &= \tfrac{1}{2}(1-\zeta)\phi_i(\xi)\phi_j(\eta), \quad i=2,...,p_\xi, \quad j=2,...,p_\eta \\
N^{\mathrm{F}_2}_{i,1,k}(\xi,\eta,\zeta) &= \tfrac{1}{2}(1-\eta)\phi_i(\xi)\phi_k(\zeta), \quad i=2,...,p_\xi, \quad k=2,...,p_\zeta \\
N^{\mathrm{F}_3}_{1,j,k}(\xi,\eta,\zeta) &= \tfrac{1}{2}(1+\xi)\phi_j(\eta)\phi_k(\zeta), \quad j=2,...,p_\eta, \quad k=2,...,p_\zeta \\
N^{\mathrm{F}_4}_{i,1,k}(\xi,\eta,\zeta) &= \tfrac{1}{2}(1+\eta)\phi_i(\xi)\phi_k(\zeta), \quad i=2,...,p_\xi, \quad k=2,...,p_\zeta \\
N^{\mathrm{F}_5}_{1,j,k}(\xi,\eta,\zeta) &= \tfrac{1}{2}(1-\xi)\phi_j(\eta)\phi_k(\zeta), \quad j=2,...,p_\eta, \quad k=2,...,p_\zeta \\
N^{\mathrm{F}_6}_{i,j,1}(\xi,\eta,\zeta) &= \tfrac{1}{2}(1+\zeta)\phi_i(\xi)\phi_j(\eta), \quad i=2,...,p_\xi, \quad j=2,...,p_\eta
\end{aligned}
\tag{A.7}
$$

$(p_\xi - 1)(p_\eta - 1)(p_\zeta - 1)$ **internal modes**

$$N^{\text{int}}_{i,j,k}(\xi,\eta,\zeta) \;=\; \phi_i(\xi)\phi_j(\eta)\phi_k(\zeta)\,, \quad i = 2,...,p_\xi, \quad j = 2,...,p_\eta, \quad k = 2,...,p_\zeta \tag{A.8}$$

A.3 The anisotropic tensor product space $\mathcal{S}^{p,p,q}(\Omega^{\mathbf{h}}_{\mathbf{st}})$ for hexahedral elements

nodal modes as in (A.1)

8(p-1) + 4(q-1) edge modes

8(p-1) edge modes in ξ-η plane

$$\begin{aligned}
N^{\mathrm{E}_1}_{i,1,1}(\xi,\eta,\zeta) &= \tfrac{1}{4}(1-\eta)(1-\zeta)\phi_i(\xi) \quad i=2,...,p\\
N^{\mathrm{E}_2}_{1,j,1}(\xi,\eta,\zeta) &= \tfrac{1}{4}(1+\xi)(1-\zeta)\phi_j(\eta) \quad j=2,...,p\\
N^{\mathrm{E}_3}_{i,1,1}(\xi,\eta,\zeta) &= \tfrac{1}{4}(1+\eta)(1-\zeta)\phi_i(\xi) \quad i=2,...,p\\
N^{\mathrm{E}_4}_{1,j,1}(\xi,\eta,\zeta) &= \tfrac{1}{4}(1-\xi)(1-\zeta)\phi_j(\eta) \quad j=2,...,p\\
N^{\mathrm{E}_9}_{i,1,1}(\xi,\eta,\zeta) &= \tfrac{1}{4}(1-\eta)(1+\zeta)\phi_i(\xi) \quad i=2,...,p\\
N^{\mathrm{E}_{10}}_{1,j,1}(\xi,\eta,\zeta) &= \tfrac{1}{4}(1+\xi)(1+\zeta)\phi_j(\eta) \quad j=2,...,p\\
N^{\mathrm{E}_{11}}_{i,1,1}(\xi,\eta,\zeta) &= \tfrac{1}{4}(1+\eta)(1+\zeta)\phi_i(\xi) \quad i=2,...,p\\
N^{\mathrm{E}_{12}}_{1,j,1}(\xi,\eta,\zeta) &= \tfrac{1}{4}(1-\xi)(1+\zeta)\phi_j(\eta) \quad j=2,...,p
\end{aligned} \tag{A.9}$$

4(q-1) edge modes in ζ-direction

$$\begin{aligned}
N^{\mathrm{E}_5}_{1,1,k}(\xi,\eta,\zeta) &= \tfrac{1}{4}(1-\xi)(1-\eta)\phi_k(\zeta) \quad k=2,...,q\\
N^{\mathrm{E}_6}_{1,1,k}(\xi,\eta,\zeta) &= \tfrac{1}{4}(1+\xi)(1-\eta)\phi_k(\zeta) \quad k=2,...,q\\
N^{\mathrm{E}_7}_{1,1,k}(\xi,\eta,\zeta) &= \tfrac{1}{4}(1+\xi)(1+\eta)\phi_k(\zeta) \quad k=2,...,q\\
N^{\mathrm{E}_8}_{1,1,k}(\xi,\eta,\zeta) &= \tfrac{1}{4}(1-\xi)(1+\eta)\phi_k(\zeta) \quad k=2,...,q
\end{aligned} \tag{A.10}$$

4(p-1)(q-1) + (p-2)(p-3) face modes

face modes in ξ-η plane

$$\begin{aligned}
N^{\mathrm{F}_1}_{i,j,1}(\xi,\eta,\zeta) &= \tfrac{1}{2}(1-\zeta)\phi_i(\xi)\phi_j(\eta), \quad i,j=2,...,p-2, \quad i+j=4,...,p\\
N^{\mathrm{F}_6}_{i,j,1}(\xi,\eta,\zeta) &= \tfrac{1}{2}(1+\zeta)\phi_i(\xi)\phi_j(\eta), \quad i,j=2,...,p-2, \quad i+j=4,...,p
\end{aligned} \tag{A.11}$$

face modes in ξ-ζ and η-ζ plane

$$\begin{aligned}
N^{\mathrm{F}_2}_{i,1,k}(\xi,\eta,\zeta) &= \tfrac{1}{2}(1-\eta)\phi_i(\xi)\phi_k(\zeta), \quad i=2,...,p, \quad k=2,...,q\\
N^{\mathrm{F}_3}_{1,j,k}(\xi,\eta,\zeta) &= \tfrac{1}{2}(1+\xi)\phi_j(\eta)\phi_k(\zeta), \quad j=2,...,p, \quad k=2,...,q\\
N^{\mathrm{F}_4}_{i,1,k}(\xi,\eta,\zeta) &= \tfrac{1}{2}(1+\eta)\phi_i(\xi)\phi_k(\zeta), \quad i=2,...,p, \quad k=2,...,q\\
N^{\mathrm{F}_5}_{1,j,k}(\xi,\eta,\zeta) &= \tfrac{1}{2}(1-\xi)\phi_j(\eta)\phi_k(\zeta), \quad j=2,...,p, \quad k=2,...,q
\end{aligned} \tag{A.12}$$

(p-3)(p-2)(q-1)/2 internal modes

$$N^{\mathrm{int}}_{i,j,k}(\xi,\eta,\zeta) = \phi_i(\xi)\phi_j(\eta)\phi_k(\zeta),\ i,j=2,...,p-2,\ i+j=4,...,p,\ k=2,...,q \tag{A.13}$$

Appendix B

The blending function method for hexahedral elements

B.1 Edge blending (from [79])

$$
\begin{aligned}
\mathbf{e}_1(\xi,\eta,\zeta) &= \left[\mathbf{E}_1(\xi) - \frac{(1-\xi)\mathbf{X}_1 + (1+\xi)\mathbf{X}_2}{2}\right]\left(\frac{1-\eta}{2}\right)\left(\frac{1-\zeta}{2}\right)\\
\mathbf{e}_2(\xi,\eta,\zeta) &= \left[\mathbf{E}_2(\eta) - \frac{(1-\eta)\mathbf{X}_2 + (1+\eta)\mathbf{X}_3}{2}\right]\left(\frac{1+\xi}{2}\right)\left(\frac{1-\zeta}{2}\right)\\
\mathbf{e}_3(\xi,\eta,\zeta) &= \left[\mathbf{E}_3(\xi) - \frac{(1-\xi)\mathbf{X}_4 + (1+\xi)\mathbf{X}_3}{2}\right]\left(\frac{1+\eta}{2}\right)\left(\frac{1-\zeta}{2}\right)\\
\mathbf{e}_4(\xi,\eta,\zeta) &= \left[\mathbf{E}_4(\eta) - \frac{(1-\eta)\mathbf{X}_1 + (1+\eta)\mathbf{X}_4}{2}\right]\left(\frac{1-\xi}{2}\right)\left(\frac{1-\zeta}{2}\right)\\
\mathbf{e}_5(\xi,\eta,\zeta) &= \left[\mathbf{E}_5(\zeta) - \frac{(1-\zeta)\mathbf{X}_1 + (1+\zeta)\mathbf{X}_5}{2}\right]\left(\frac{1-\xi}{2}\right)\left(\frac{1-\eta}{2}\right)\\
\mathbf{e}_6(\xi,\eta,\zeta) &= \left[\mathbf{E}_6(\zeta) - \frac{(1-\zeta)\mathbf{X}_2 + (1+\zeta)\mathbf{X}_6}{2}\right]\left(\frac{1+\xi}{2}\right)\left(\frac{1-\eta}{2}\right)\\
\mathbf{e}_7(\xi,\eta,\zeta) &= \left[\mathbf{E}_7(\zeta) - \frac{(1-\zeta)\mathbf{X}_3 + (1+\zeta)\mathbf{X}_7}{2}\right]\left(\frac{1+\xi}{2}\right)\left(\frac{1+\eta}{2}\right)\\
\mathbf{e}_8(\xi,\eta,\zeta) &= \left[\mathbf{E}_8(\zeta) - \frac{(1-\zeta)\mathbf{X}_4 + (1+\zeta)\mathbf{X}_8}{2}\right]\left(\frac{1-\xi}{2}\right)\left(\frac{1+\eta}{2}\right)\\
\mathbf{e}_9(\xi,\eta,\zeta) &= \left[\mathbf{E}_9(\xi) - \frac{(1-\xi)\mathbf{X}_5 + (1+\xi)\mathbf{X}_6}{2}\right]\left(\frac{1-\eta}{2}\right)\left(\frac{1+\zeta}{2}\right)
\end{aligned}
\tag{B.1}
$$

continued

$$\mathbf{e}_{10}(\xi,\eta,\zeta) = \left[\mathbf{E}_{10}(\eta) - \frac{(1-\eta)\mathbf{X}_6 + (1+\eta)\mathbf{X}_7}{2}\right]\left(\frac{1+\xi}{2}\right)\left(\frac{1+\zeta}{2}\right)$$

$$\mathbf{e}_{11}(\xi,\eta,\zeta) = \left[\mathbf{E}_{11}(\xi) - \frac{(1-\xi)\mathbf{X}_8 + (1+\xi)\mathbf{X}_7}{2}\right]\left(\frac{1+\eta}{2}\right)\left(\frac{1+\zeta}{2}\right)$$

$$\mathbf{e}_{12}(\xi,\eta,\zeta) = \left[\mathbf{E}_{12}(\eta) - \frac{(1-\eta)\mathbf{X}_5 + (1+\eta)\mathbf{X}_8}{2}\right]\left(\frac{1-\xi}{2}\right)\left(\frac{1+\zeta}{2}\right)$$

B.2 Face blending (from [79])

$$\begin{aligned}
\mathbf{f}_1(\xi,\eta,\zeta) = &\left[\mathbf{F}_1(\xi,\,\eta) - \frac{1}{4}\Big[(1-\xi)(1-\eta)\mathbf{X}_1 + (1+\xi)(1-\eta)\mathbf{X}_2 + \right.\\
&\left.(1+\xi)(1+\eta)\mathbf{X}_3 + (1-\xi)(1+\eta)\mathbf{X}_4\Big]\right]\left(\frac{1-\zeta}{2}\right)\\
\mathbf{f}_2(\xi,\eta,\zeta) = &\left[\mathbf{F}_2(\xi,\,\zeta) - \frac{1}{4}\Big[(1-\xi)(1-\zeta)\mathbf{X}_1 + (1+\xi)(1-\zeta)\mathbf{X}_2 + \right.\\
&\left.(1+\xi)(1+\zeta)\mathbf{X}_6 + (1-\xi)(1+\zeta)\mathbf{X}_5\Big]\right]\left(\frac{1-\eta}{2}\right)\\
\mathbf{f}_3(\xi,\eta,\zeta) = &\left[\mathbf{F}_3(\eta,\,\zeta) - \frac{1}{4}\Big[(1-\eta)(1-\zeta)\mathbf{X}_2 + (1+\eta)(1-\zeta)\mathbf{X}_3 + \right.\\
&\left.(1+\eta)(1+\zeta)\mathbf{X}_7 + (1-\eta)(1+\zeta)\mathbf{X}_6\Big]\right]\left(\frac{1+\xi}{2}\right)\\
\mathbf{f}_4(\xi,\eta,\zeta) = &\left[\mathbf{F}_4(\xi,\,\zeta) - \frac{1}{4}\Big[(1-\xi)(1-\zeta)\mathbf{X}_4 + (1+\xi)(1-\zeta)\mathbf{X}_3 + \right.\\
&\left.(1+\xi)(1+\zeta)\mathbf{X}_7 + (1-\xi)(1+\zeta)\mathbf{X}_8)\Big]\right]\left(\frac{1+\eta}{2}\right)\\
\mathbf{f}_5(\xi,\eta,\zeta) = &\left[\mathbf{F}_5(\eta,\,\zeta) - \frac{1}{4}\Big[(1-\eta)(1-\zeta)\mathbf{X}_1 + (1+\eta)(1-\zeta)\mathbf{X}_4 + \right.\\
&\left.(1+\eta)(1+\zeta)\mathbf{X}_8 + (1-\eta)(1+\zeta)\mathbf{X}_5\Big]\right]\left(\frac{1-\xi}{2}\right)\\
\mathbf{f}_6(\xi,\eta,\zeta) = &\left[\mathbf{F}_6(\xi,\,\eta) - \frac{1}{4}\Big[(1-\xi)(1-\eta)\mathbf{X}_5 + (1+\xi)(1-\eta)\mathbf{X}_6 + \right.\\
&\left.(1+\xi)(1+\eta)\mathbf{X}_7 + (1-\xi)(1+\eta)\mathbf{X}_8\Big]\right]\left(\frac{1+\zeta}{2}\right)
\end{aligned} \tag{B.2}$$

Appendix C

Definition of tangential and normal vectors for hexahedral elements

The tangential vectors

$$\mathbf{t}_1 = [t_{1x}, t_{1y}, t_{1z}]^T = \frac{\mathbf{t}_1^*}{\|\mathbf{t}_1^*\|} \quad , \quad \mathbf{t}_2 = [t_{2x}, t_{2y}, t_{2z}]^T = \frac{\mathbf{t}_2^*}{\|\mathbf{t}_2^*\|} \quad \text{with} \quad \mathbf{t}_1 \cdot \mathbf{t}_2 = 0 \tag{C.1}$$

are defined for each separate face of the hexahedral element:
Face 3 and 5 ($\xi = \pm 1$)

$$\begin{aligned} \mathbf{t}_1^* &= \left[\frac{\partial x}{\partial \eta}, \frac{\partial y}{\partial \eta}, \frac{\partial z}{\partial \eta}\right]^T \quad , \quad \mathbf{t}_2^* = \left[\frac{\partial x}{\partial \zeta}, \frac{\partial y}{\partial \zeta}, \frac{\partial z}{\partial \zeta}\right]^T \\ \mathbf{t}_1^* &= \left[\frac{\partial x}{\partial \zeta}, \frac{\partial y}{\partial \zeta}, \frac{\partial z}{\partial \zeta}\right]^T \quad , \quad \mathbf{t}_2^* = \left[\frac{\partial x}{\partial \eta}, \frac{\partial y}{\partial \eta}, \frac{\partial z}{\partial \eta}\right]^T \end{aligned} \tag{C.2}$$

Face 4 and 2 ($\eta = \pm 1$)

$$\begin{aligned} \mathbf{t}_1^* &= \left[\frac{\partial x}{\partial \zeta}, \frac{\partial y}{\partial \zeta}, \frac{\partial z}{\partial \zeta}\right]^T \quad , \quad \mathbf{t}_2^* = \left[\frac{\partial x}{\partial \xi}, \frac{\partial y}{\partial \xi}, \frac{\partial z}{\partial \xi}\right]^T \\ \mathbf{t}_1^* &= \left[\frac{\partial x}{\partial \xi}, \frac{\partial y}{\partial \xi}, \frac{\partial z}{\partial \xi}\right]^T \quad , \quad \mathbf{t}_2^* = \left[\frac{\partial x}{\partial \zeta}, \frac{\partial y}{\partial \zeta}, \frac{\partial z}{\partial \zeta}\right]^T \end{aligned} \tag{C.3}$$

Face 6 and 1 ($\zeta = \pm 1$)

$$\begin{aligned} \mathbf{t}_1^* &= \left[\frac{\partial x}{\partial \xi}, \frac{\partial y}{\partial \xi}, \frac{\partial z}{\partial \xi}\right]^T \quad , \quad \mathbf{t}_2^* = \left[\frac{\partial x}{\partial \eta}, \frac{\partial y}{\partial \eta}, \frac{\partial z}{\partial \eta}\right]^T \\ \mathbf{t}_1^* &= \left[\frac{\partial x}{\partial \eta}, \frac{\partial y}{\partial \eta}, \frac{\partial z}{\partial \eta}\right]^T \quad , \quad \mathbf{t}_2^* = \left[\frac{\partial x}{\partial \xi}, \frac{\partial y}{\partial \xi}, \frac{\partial z}{\partial \xi}\right]^T \end{aligned} \tag{C.4}$$

The positive (outward) normal vector is computed via the cross-product:

$$\mathbf{n} = [n_x, n_y, n_z]^T = \frac{\mathbf{t}_1 \times \mathbf{t}_2}{\|\mathbf{t}_1 \times \mathbf{t}_2\|} \tag{C.5}$$

Bibliography

[1] R.L. Actis, B.A. Szabó, and Ch. Schwab. Hierarchic models for laminated plates and shells. *Computer Methods in Applied Mechanics and Engineering*, 172:79–107, 1999.

[2] M. Ainsworth and J.T. Oden. A unified approach to a posteriori error estimation based on element residual methods. *Numerische Mathematik*, 65:23–50, 1993.

[3] M. Ainsworth and J.T. Oden. *A posteriori error estimation in finite element analysis*. John Wiley & Sons, 2000.

[4] M. Ainsworth and B. Senior. Aspects of an adaptive *hp*-finite element method: Adaptive strategy, conforming approximation and efficient solvers. *Computer Methods in Applied Mechanics and Engineering*, 150:65–87, 1997.

[5] M. Ainsworth, J.Z. Zhu, A.W. Craig, and O.C. Zienkiewicz. Analysis of the Zienkiewicz-Zhu a-posteriori error estimator in the finite element method. *International Journal for Numerical Methods in Engineering*, 28:2161–2174, 1989.

[6] J. Altenbach and H. Altenbach. *Einführung in die Kontinuumsmechanik*. Teubner-Verlag, 1994.

[7] I. Babuška and B.Q. Guo. Approximation properties of the hp-version of the finite element method. *Computer Methods in Applied Mechanics and Engineering*, 133:319–346, 1996.

[8] I. Babuška and A. Miller. The post-processing approach in the finite element method. Part 1. Calculation of displacements, stresses and other higher derivatives of the displacements. *International Journal for Numerical Methods in Engineering*, 20:1085–1109, 1984.

[9] I. Babuška and A. Miller. The post-processing approach in the finite element method. Part 2. The calculation of stress intensity factors. *International Journal for Numerical Methods in Engineering*, 20:1111–1129, 1984.

[10] I. Babuška and A. Miller. The post-processing approach in the finite element method. Part 3. A posteriori error estimates and adaptive mesh selection. *International Journal for Numerical Methods in Engineering*, 20:2311–2324, 1984.

[11] I. Babuška and A. Miller. A feedback finite element method with a posteriori error estimation: Part 1. *Computer Methods in Applied Mechanics and Engineering*, 61:1–40, 1987.

[12] I. Babuška and W.C. Rheinboldt. A posteriori error estimates for the finite element method. *International Journal for Numerical Methods in Engineering*, 12:1597–1615, 1978.

[13] I. Babuška and W.C. Rheinboldt. Error estimates for adaptive finite element computations. *SIAM Journal on Numerical Analysis*, 18:736–754, 1978.

[14] I. Babuška and W.C. Rheinboldt. Adaptive approaches and reliability estimations in finite element analysis. *Computer Methods in Applied Mechanics and Engineering*, 17:519–540, 1979.

[15] I. Babuška and W.C. Rheinboldt. Analysis of optimal finite element meshes in R^1. *Mathematics of Computation*, 33:435–463, 1979.

[16] I. Babuška and T. Strouboulis. *The finite element method and its reliability.* Oxford University Press, 2001.

[17] I. Babuška and M. Suri. The optimal convergence rate of the p-version of the finite element method. *SIAM Journal on Numerical Analysis*, 24:750–776, 1987.

[18] I. Babuška and M. Suri. The p- and hp-versions of the finite element method. An overview. *Computer Methods in Applied Mechanics and Engineering*, 80:5–26, 1990.

[19] I. Babuška, R. Tempone, and G. Zouraris. Galerkin finite element approximations of stochastic elliptic partial differential equations. *SIAM Journal on Numerical Analysis*, 42(2):800–825, 2004.

[20] W. Bangerth and R. Rannacher. Finite element approximation of the acoustic wave equation: Error control and mesh adaption. *East-West Journal of Numerical Mathematics*, 7(4):263–282, 1999.

[21] R.E. Bank. Analysis of a local a posteriori error estimate for elliptic equations. In I. Babuška, O.C. Zienkiewicz, J. Gago, and E.R. de A. Olivera, editors, *Accuracy estimates and adaptive refinements in finite element computations*, pages 119–128. John Wiley & Sons, 1986.

[22] R.E. Bank. Hierarchical bases and the finite element method. *Acta Numerica*, 5:1–45, 1996.

[23] R.E. Bank and R.K. Smith. A posteriori error-estimates based on hierarchical bases. *SIAM Journal on Numerical Analysis*, 30:921–935, 1993.

[24] R.E. Bank and A. Weiser. Some a posteriori error estimators for elliptic partial differential equations. *Mathematics of Computation*, 44:283–301, 1985.

[25] S. Bartels and C. Carstensen. Each averaging technique yields reliable a posteriori error control in FEM on unstructured grids. Part II: Higher order FEM. Preprint, Mathematisches Seminar, Christian-Albrechts-Universität zu Kiel, 2000.

[26] K.J. Bathe. *Finite element procedures.* Prentice Hall, 1996.

[27] T. Belytschko, W.K. Liu, and B. Moran. *Nonlinear finite elements for continua and structures*. John Wiley & Sons, 2000.

[28] P. Bergan and E. Mollestad. An automatic time-stepping algorithm for dynamic problems. *Computer Methods in Applied Mechanics and Engineering*, 49:299–318, 1985.

[29] E. Bertóti and B. Szabó. Adaptive selection of polynomial degrees on a finite element mesh. *International Journal for Numerical Methods in Engineering*, 42:561–578, 1998.

[30] M. Bischoff. *Theorie und Numerik einer dreidimensionalen Schalenformulierung*. PhD thesis, Institut für Baustatik, Universität Stuttgart, 1999.

[31] M. Bischoff and E. Ramm. Solid-like shell or shell-like solid formulation? A personal view. In *Proceedings of ECCM '99, European Conference on Computational Mechanics*, München, Germany, 1999.

[32] M. Bischoff, W.A. Wall, K.-U. Bletzinger, and E. Ramm. Models and Finite Elements for Thin-walled Structures. In E. Stein, R. de Borst, and T.J.R. Hughes, editors, *Encyclopedia of Computational Mechanics*, volume 2, chapter 3, pages 59–137. John Wiley & Sons, 2004.

[33] J. Bonet and R.D. Wood. *Nonlinear continuum mechanics for finite element analysis*. Cambridge University Press, New York, 1997.

[34] H. Bröker. *Integration von geometrischer Modellierung und Berechnung nach der p-Version der FEM*. PhD thesis, Lehrstuhl für Bauinformatik, Fakultät für Bauingenieur- und Vermessungswesen, Technische Universität München, 2001.

[35] N. Büchter and E. Ramm. 3d-extension of nonlinear shell equations based on the enhanced assumed strain concept. *Computational Methods in Applied Sciences*, pages 39–59, 1992.

[36] N. Büchter, E. Ramm, and D. Roehl. Three-dimensional extension of nonlinear shell formulation based on the enhanced assumed strain concept. *International Journal for Numerical Methods in Engineering*, 37:2551–2568, 1994.

[37] J.R. Cho and J.T. Oden. A priori modeling error estimations of hierarchical models for elasticity problems for plate- and shell-like structures. *Mathematical and Computer Modeling*, 23(10):117–133, 1996.

[38] J. Chung and G.M. Hulbert. A time integration algorithm for structural dynamics with improved numerical dissipation: the generalized-α method. *Computer Methods in Applied Mechanics and Engineering*, 149:33–48, 1997.

[39] F. Cirak and E. Ramm. A posteriori error estimation and adaptivity for elastoplasticity using the reciprocal theorem. *International Journal for Numerical Methods in Engineering*, 47:379–393, 2000.

[40] M.A. Crisfield. *Non-linear finite element analysis of solids and structures, Volume 1*. John Wiley & Sons, 1991.

[41] M.A. Crisfield. *Non-linear finite element analysis of solids and structures, Volume 2*. John Wiley & Sons, 1997.

[42] G. Dahlquist and A. Björck. *Numerical methods*. Prentice-Hall, Englewood-Cliffs, N.Y., 1974.

[43] L. Demkowicz and J.T. Oden. Application of *hp*-adaptive BE/FE methods to elastic scattering. *Computer Methods in Applied Mechanics and Engineering*, 133:287–318, 1996.

[44] L. Demkowicz, J.T. Oden, and T Strouboulis. Adaptive finite elements for flow problems with moving boundaries. Part 1: Variational principles and a posteriori error estimates. *Computer Methods in Applied Mechanics and Engineering*, 46:217–251, 1984.

[45] L. Demkowicz, J.T. Oden, and T. Strouboulis. An adaptive p-version finite element method for transient flow problems with moving boundaries. In R.H. Gallagher, editor, *Finite Elements in Fluids VI*, pages 291–305. John Wiley, 1985.

[46] L. Demkowicz, W. Rachowicz, and P. Devloo. A fully automatic *hp*-adaptivity. *Journal of Scientific Computing*, 17:127–155, 2002.

[47] A. Düster. *High order finite elements for three-dimensional, thin-walled nonlinear continua*. PhD thesis, Lehrstuhl für Bauinformatik, Fakultät für Bauingenieur- und Vermessungswesen, Technische Universität München, http://www.inf.bv.tum.de/~duester, 2001.

[48] A. Düster, H. Bröker, H. Heidkamp, U. Heißerer, S. Kollmannsberger, R. Krause, A. Muthler, A. Niggl, V. Nübel, M. Rücker, and D. Scholz. *AdhoC^4 – User's Guide*. Lehrstuhl für Bauinformatik, Technische Universität München, 2004.

[49] A. Düster, H. Bröker, and E. Rank. The p-version of the finite element method for three-dimensional curved thin walled structures. *International Journal for Numerical Methods in Engineering*, 52:673–703, 2001.

[50] A. Düster, S. Hartmann, and E. Rank. p-fem applied to finite isotropic hyperelastic bodies. *Computer Methods in Applied Mechanics and Engineering*, 192:5147–5166, 2003.

[51] A. Düster, A. Niggl, V. Nübel, and E. Rank. A numerical investigation of high-order finite elements for problems of elasto-plasticity. *Journal of Scientific Computing*, 17:429–437, 2002.

[52] A. Düster and E. Rank. The p-version of the finite element method compared to an adaptive h-version for the deformation theory of plasticity. *Computer Methods in Applied Mechanics and Engineering*, 190:1925–1935, 2001.

[53] A. Düster and E. Rank. A p-version finite element approach for two- and three-dimensional problems of the J_2 flow theory with non-linear isotropic hardening. *International Journal for Numerical Methods in Engineering*, 53:49–63, 2002.

[54] A. Düster and M. Rücker. *AdhoC^3 – User's Guide*. Lehrstuhl für Bauinformatik, Technische Universität München, 2001.

[55] A. Düster, D. Scholz, and E. Rank. *pq*-Adaptive solid finite elements for three-dimensional plates and shells. *submitted to Computer Methods in Applied Mechanics and Engineering*, 2005.

[56] R. Eberlein. *Finite-Elemente-Konzepte für Schalen mit großen elastischen und plastischen Verzerrungen*. PhD thesis, Institut für Mechanik, Technische Hochschule Darmstadt, 1997.

[57] K. Eriksson, D. Estep, P. Hansbo, and C. Johnson. Introduction to adaptive methods for differential equations. *Acta Numerica*, pages 105–158, 1995.

[58] P.O. Friberg. An error indicator for the generalized eigenvalue problem using the hierarchical finite element method. *International Journal for Numerical Methods in Engineering*, 23:91–98, 1986.

[59] P.O. Friberg, D. Makovička, and N.-E. Wiberg. An adaptive procedure for eigenvalue problems using the hierarchical finite element method. *International Journal for Numerical Methods in Engineering*, 24:319–335, 1987.

[60] W.J. Gordon and Ch.A. Hall. Construction of curvilinear co-ordinate systems and applications to mesh generation. *International Journal for Numerical Methods in Engineering*, 7:461–477, 1973.

[61] W. Gui and I. Babuška. The h-, p- and hp-versions of the finite element method in one dimension. Part I: The error analysis of the p-version. *Numerische Mathematik*, 49:577–612, 1986.

[62] W. Gui and I. Babuška. The h-, p- and hp-versions of the finite element method in one dimension. Part II: The error analysis of the h- and hp-versions. *Numerische Mathematik*, 49:613–657, 1986.

[63] W. Gui and I. Babuška. The h-, p- and hp-versions of the finite element method in one dimension. Part III: The adaptive hp-version. *Numerische Mathematik*, 49:659–683, 1986.

[64] W. Hackbusch. *Theorie und Numerik elliptischer Differentialgleichungen*. B.G. Teubner, Stuttgart, 1996.

[65] W. Hackbusch, H.R. Schwarz, and E. Zeidler. *Taschenbuch der Mathematik*. B.G. Teubner, 25. edition, 1996.

[66] A. Halfmann. *Ein geometrisches Modell zur numerischen Simulation der Fluid-Struktur-Interaktion windbelasteter, leichter Flächentragwerke*. PhD thesis, Lehrstuhl für Bauinformatik, Fakultät für Bauingenieur- und Vermessungswesen, Technische Universität München, 2002.

[67] R. Hauptmann. *Strukturangepaßte geometrisch nichtlineare Finite Elemente für Flächentragwerke*. PhD thesis, Institut für Mechanik, Universität Fridericiana Karlsruhe, 1997.

[68] U. Heißerer. Solution of the semidiscrete equations of structural dynamics by the generalized-alpha method and its implementation in a p-fem code. Diploma thesis, Lehrstuhl für Bauinformatik, Fakultät für Bauingenieurwesen, TU München, 2001.

[69] V. Heuveline and R. Rannacher. A posteriori error control for finite element approximations of elliptic eigenvalue problems. *acm*, 15(6):107–138, 2001.

[70] H.M. Hilber, T.J.R Hughes, and R.L. Taylor. Improved numerical dissipation for time integration algorithms in structural dynamics. *Earthquake Engineering & Structural Dynamics*, 5:283–292, 1977.

[71] S.M. Holzer. Implementing advanced finite element methods. In W.A. Wall, K.-U. Bletzinger, and K. Schweizerhof, editors, *Trends in computational structural mechanics*, CIMNE, Barcelona, Spain, 2001.

[72] T.J.R. Hughes. *The finite element method*. Dover Publications, 2000.

[73] T.J.R Hughes and G.M. Hulbert. Space-time finite element methods for elastodynamics. formulations and error estimates. *Computer Methods in Applied Mechanics and Engineering*, 62:339–363, 1988.

[74] G.M. Hulbert. Computational structural dynamics. In E. Stein, R. de Borst, and T.J.R. Hughes, editors, *Encyclopedia of Computational Mechanics*, volume 2, chapter 5, pages 169–193. John Wiley & Sons, 2004.

[75] C. Johnson. Discontinuous Galerkin finite element methods for second order hyperbolic problems. *Computer Methods in Applied Mechanics and Engineering*, 84:117–129, 1993.

[76] C. Johnson and P. Hansbo. Adaptive finite element methods in computational mechanics. *Computer Methods in Applied Mechanics and Engineering*, 101:143–181, 1992.

[77] D.W. Kelly. The self-equilibration of residuals and complementary a posteriori error estimates in the finite element method. *International Journal for Numerical Methods in Engineering*, 20:1491–1506, 1984.

[78] D.W. Kelly, J.P. Gago, O.C. Zienkiewicz, and I. Babuška. A posteriori error analysis and adaptive processes in the finite element method: Part I - Error analysis. *International Journal for Numerical Methods in Engineering*, 19:1593–1619, 1983.

[79] G. Királyfalvi and B.A. Szabó. Quasi-regional mapping for the p-version of the finite element method. *Finite Elements in Analysis and Design*, 27:85–97, 1997.

[80] R.M. Kirby and Z. Yosibash. Solution of von-Kármán dynamic non-linear plate equations using a pseudo-spectral method. *Computer Methods in Applied Mechanics and Engineering*, 193:575–599, 2004.

[81] R. Krause. *Multiscale computations with a combined h- and p-version of the finite-element method*. PhD thesis, Fach Numerische Methoden und Informationsverarbeitung, Universität Dortmund, 1996.

[82] D. Kuhl. *Stabile Zeitintegrationsalgorithmen in der nichtlinearen Elastodynamik dünnwandiger Tragwerke*. PhD thesis, Institut für Baustatik, Universität Stuttgart, 1996.

[83] P. Ladevèze and D. Leguillon. Error estimate procedure in the finite element method and applications. *SIAM Journal on Numerical Analysis*, 20:485–509, 1983.

[84] M.G. Larson. A posteriori and a priori error analysis for finite element approximations of selfadjoint elliptic eigenvalue problems. *SIAM Journal on Numerical Analysis*, 38(2):608–625, 2000.

[85] X. Li. *Adaptive finite element procedures in structural dynamics*. PhD thesis, Chalmers University of Technology, Göteborg, 1996.

[86] X. Li and N.-E. Wiberg. Structural dynamics analysis by time-discontinuous Galerkin finite element method. *International Journal for Numerical Methods in Engineering*, 39:2131–2152, 1996.

[87] X. Li, L. Zeng, and N.-E. Wiberg. A simple local error estimator and adaptive time-stepping procedure for direct integration method in dynamical analysis. *Communications in Numerical Methods in Engineering*, 9:273–292, 1993.

[88] A. Louis. Acceleration of convergence for finite element solutions of the Poisson equation. *Numerische Mathematik*, 33:43–53, 1979.

[89] A.E.H. Love. On the small vibrations and deformations of thin elastic shells. *Philosophical Transactions of the Royal Society*, 179:491, 1888.

[90] X.J. Luo. *An automatic adaptive directional variable p-version method in 3D curved domains*. PhD thesis, Rensselaer Polytechnic Institute, Troy, New York, 2005.

[91] A. Maute. *Fehlerkontrolle bei Finite-Element-Methoden in der linearen Strukturdynamik*. Dissertation, Institut für Baustatik, Universität Stuttgart, 2001.

[92] J.M. Melenk and B.I. Wohlmuth. On residual-based a posteriori error estimation in *hp*-FEM. *Advances in Computational Mechanics*, 15:311–331, 2001.

[93] N. Moës, J.T. Oden, K. Vemaganti, and J.-F. Remacle. Simplified methods and a posteriori error estimation for the homogenization of representative volume elements (REV). *Computer Methods in Applied Mechanics and Engineering*, 176:265–278, 1999.

[94] P.M. Naghdi. The theory of shells. In S. Flügge, editor, *Handbuch der Physik*, volume VIa/2, pages 425–640. Springer, 1972.

[95] J. Neumann. *Anwendung von adaptiven Finite Element Algorithmen auf Probleme der Strukturdynamik*. Dissertation, Institut für Mechanik, Universität Karlsruhe, 2004.

[96] J. Neumann, J. Riccius, and K. Schweizerhof. Adaptive analysis of dynamically loaded shell structures. In S. Idelsohn, E. Oñate, and E. Dvorkin, editors, *Comp. Mech. New Trends & Applications*, CIMNE, Barcelona, Spain, 1998.

[97] N.M. Newmark. A numerical method for structural dynamics. *Journal of Engineering Mechanics (ASCE)*, 85:67–94, 1959.

[98] K. Neymeyr. A posteriori error estimation for elliptic eigenproblems. *Numerical Linear Algebra with Applications*, 9:263–279, 2002.

[99] A. Niggl. *Ein Fehlerindikator für elastoplastische Materialprobleme bei Verwendung der p-Version der FEM.* Diploma thesis, Lehrstuhl für Bauinformatik, TU München, 2001.

[100] V. Nübel. *Die adaptive rp-Methode für elastoplastische Probleme.* PhD thesis, Lehrstuhl für Bauinformatik, Technische Universität München, 2005.

[101] V. Nübel, A. Düster, and E. Rank. An *rp*-adaptive finite element method for the deformation theory of plasticity. *submitted to Computational Mechanics*, 2004.

[102] C. Nystedt. A priori and a posteriori error estimates and adaptive finite element methods for a model eigenvalue problem. Technical report, Department of Mathematics, Chalmers University of Technology, Göteborg, 1995.

[103] J.T. Oden, I. Babuška, F. Nobile, Y. Feng, and R. Tempone. Theory and methodology for estimation and control of errors due to modeling, approximation, and uncertainty. *Computer Methods in Applied Mechanics and Engineering*, 194:195–204, 2005.

[104] J.T. Oden and J.R. Cho. Adaptive *hpq*-finite element methods of hierarchical models for plate- and shell-like structures. *Computer Methods in Applied Mechanics and Engineering*, 136:317–345, 1996.

[105] J.T. Oden, L. Demkowicz, T. Strouboulis, and P. Devloo. Adaptive methods for problems in solid and fluid mechanics. In I. Babuška, O.C. Zienkiewicz, J. Gago, and E.R. de A. Olivera, editors, *Accuracy estimates and adaptive refinements in finite element computations*, pages 249–280. John Wiley & Sons, 1986.

[106] J.T. Oden, A. Patra, and Y. Feng. An *hp*-adaptive strategy. In A.K. Noor, editor, *Adaptive Multilevel and Hierarchical Computational Strategies*, pages 23–46. ASME Publication, 1992.

[107] J.T. Oden and S. Prudhomme. Estimation of modeling error in computational mechanics. *Journal of Computational Physics*, 182:486–515, 2002.

[108] J.T. Oden, S. Prudhomme, D.C. Hammerand, and M.S. Kuczma. Modelling error and adaptivity in nonlinear continuum mechanics. *Computer Methods in Applied Mechanics and Engineering*, 190:6663–6684, 2001.

[109] J.T. Oden and K. Vemaganti. Adaptive hierarchical modeling of heterogeneous structures, predictability: quantifying uncertainty in models of complex phenomena. *Physica D*, 133:404–415, 1999.

[110] J.T. Oden and K. Vemaganti. Estimation of local modeling error and goal-oriented modeling of heterogeneous materials; part I: error estimates and adaptive algorithms. *Journal of Computational Physics*, 164:22–47, 2001.

[111] K. Park and P. Underwood. A variable central difference method for structural dynamic analysis — part I: Theoretical aspects. *Computer Methods in Applied Mechanics and Engineering*, 22:241–258, 1980.

[112] A. Rabold. *Vorbereitende Arbeiten zur Berechnung der Trittschalldämmung von Holzbalkendecken anhand der Finiten Elemente Methode*. Diploma thesis, Lehrstuhl für Bauinformatik, TU München, 2004.

[113] W. Rachowicz, J.T. Oden, and L. Demkowicz. Toward a universal h-p adaptive finite element strategy, part 3. Design of h-p meshes. *Computer Methods in Applied Mechanics and Engineering*, 77:181–212, 1989.

[114] E. Rank, A. Düster, V. Nübel, K. Preusch, and O.T. Bruhns. High order finite elements for shells. *Computer Methods in Applied Mechanics and Engineering*, 194:2494–2512, 2005.

[115] E. Rank, R. Krause, and M. Schweingruber. Netzadaption durch intelligentes Pre- und Postprocessing. In *Finite Elemente-Anwendungen in der Baupraxis*, Karlsruhe, 1991. Ernst & Sohn.

[116] E. Rank and O.C. Zienkiewicz. A simple error estimator in the finite element method. *Communications in Applied Numerical Methods*, 3:243–249, 1987.

[117] R. Rannacher. Error control in finite element computations. In H. Bulgak and C. Zenger, editors, *Error control and adaptivity in scientific computing*, NATO Science Series. Kluwer Academic Publishers, 1999.

[118] R. Rannacher and F.T. Suttmeier. A posteriori error estimation and mesh adaption for finite element methods in elasto-plasticity. *Computer Methods in Applied Mechanics and Engineering*, 176:333–361, 1999.

[119] E. Reissner. On the theory of bending elastic plates. *Journal of Mathematics and Physics*, 23:184–191, 1944.

[120] E. Reissner. The effect of transverse shear deformation on the bending of elastic plates. *Journal of Applied Mechanics*, 2(23):69–77, 1945.

[121] J. Riccius. *Adaptive Methoden zur statischen und dynamischen Analyse von Flächentragwerken mit linearen Finiten Elementen*. Dissertation, Institut für Mechanik, Universität Karlsruhe, 1997.

[122] J. Riccius and K. Schweizerhof. Aspects of hierarchical *h*-adaptive dynamic analyses. In B.H.V. Topping, editor, *Third International Conference on Computational Structures Technology*, Budapest, Hungary, 1996. Civil-Comp Press.

[123] D. Scholz, A. Düster, and E. Rank. Model-adaptive structural FEM computations for fluid-structure interaction. In *Proceedings of the Third M.I.T. Conference on Computational Fluid and Solid Mechanics*, Cambridge, USA, 2005.

[124] D. Scholz, E. Rank, M. Glück, M. Breuer, and F. Durst. Fully three-dimensional coupling of fluid and thin-walled structures. In *High Performance Computing in Science and Engineering*. Springer, 2004.

[125] C. Schwab. A-posteriori modeling error estimation for hierarchic plate models. *Numerische Mathematik*, 74:221–259, 1996.

[126] Ch. Schwab. *p- and hp-finite element methods, theory and applications in solid and fluid mechanics*. Oxford University Press, 1998.

[127] H.R. Schwarz. *FORTRAN-Programme zur Methode der Finiten Elemente*. B.G. Teubner, 3rd edition, 1991.

[128] H.R. Schwarz. *Methode der finiten Elemente*. B.G. Teubner, 3rd edition, 1991.

[129] M. Schweingruber-Straten. *Generierung von Oberflächennetzen nach der Gebietsteilungstechnik*. PhD thesis, Fach Numerische Methoden und Informationsverarbeitung, Universität Dortmund, 1999.

[130] J.C. Simo and D.D. Rifai, M.S. Fox. On a stress resultant geometrically exact shell model. Part IV: Variable thickness shells with through-the-thickness stretching. *Computer Methods in Applied Mechanics and Engineering*, 81:91–126, 1990.

[131] E. Stein and S. Ohnimus. Coupled model- and solution-adaptivity in the finite-element method. *Computer Methods in Applied Mechanics and Engineering*, 150:327–350, 1997.

[132] E. Stein and S. Ohnimus. Anisotropic discretization- and model-error estimation in solid mechanics by local Neumann problems. *Computer Methods in Applied Mechanics and Engineering*, 176:363–385, 1999.

[133] E. Stein and M. Rüter. Finite Element Methods for Elasticity with Error-controlled Discretization and Model Adaptivity. In E. Stein, R. de Borst, and T.J.R. Hughes, editors, *Encyclopedia of Computational Mechanics*, volume 2, chapter 2, pages 5–58. John Wiley & Sons, 2004.

[134] E. Stein, M. Rüter, and S. Ohnimus. Adaptive finite element analysis and modelling of solids and structures. Findings, problems and trends. *International Journal for Numerical Methods in Engineering*, 60:103–138, 2004.

[135] B.A. Szabó. Estimation and control of error based on p convergence. In I. Babuška, O.C. Zienkiewicz, J. Gago, and E.R. de A. Olivera, editors, *Accuracy estimates and adaptive refinements in finite element computations*, pages 61–70. John Wiley & Sons, 1986.

[136] B.A. Szabó and I. Babuška. *Finite element analysis*. John Wiley & Sons, 1991.

[137] B.A. Szabó, A. Düster, and E. Rank. The p-version of the Finite Element Method. In E. Stein, R. de Borst, and T.J.R. Hughes, editors, *Encyclopedia of Computational Mechanics*, volume 1, chapter 5, pages 119–139. John Wiley & Sons, 2004.

[138] R. Thomas and I. Gladwell. Variable-order variable-step algorithms for second order systems. part I: The method. *International Journal for Numerical Methods in Engineering*, 26:39–53, 1988.

[139] K. Vemaganti and J.T. Oden. Estimation of local modeling and goal-oriented modeling of heterogeneous materials; part II: A computational environment for adaptive modeling of heterogeneous elastic solids. *Computer Methods in Applied Mechanics and Engineering*, 190:6089–6124, 2001.

[140] R. Verfürth. *A review of a posteriori error estimation and adaptive mesh-refinement techniques*. John Wiley & Sons and B.G. Teubner, 1996.

[141] W.A. Wall, M. Gee, and E. Ramm. The challenge of a three-dimensional shell formulation, the conditioning problem. In *Proceedings of ECCM '99, European Conference on Computational Mechanics*, München, Germany, 1999.

[142] N.-E. Wiberg and F. Abdulwahab. Patch recovery based on superconvergent derivatives and equilibrium. *International Journal for Numerical Methods in Engineering*, 36:2703–2724, 1993.

[143] N.-E. Wiberg and X. Li. A postprocessing technique and an a-posteriori error estimate for the Newmark method in dynamic analysis. *Earthquake Engineering & Structural Dynamics*, 22:465 – 489, 1993.

[144] N.-E. Wiberg and X. Li. A postprocessed error estimate and an adaptive procedure for the semidiscrete finite element method in dynamic analysis. *International Journal for Numerical Methods in Engineering*, 37:3585 – 3603, 1994.

[145] N.-E. Wiberg and X. Li. Superconvergent patch recovery of finite element solution and a-posteriori l_2-norm error estimate. *Communications in Numerical Methods in Engineering*, 10:313 – 320, 1994.

[146] N.-E. Wiberg, L. Zeng, and X. Li. Error estimation and adaptivity in elastodynamics. *Computer Methods in Applied Mechanics and Engineering*, 101:369–395, 1992.

[147] W.L. Wood, M. Bossak, and O.C. Zienkiewicz. An alpha modification of Newmark's method. *International Journal for Numerical Methods in Engineering*, 5:1562–1566, 1981.

[148] P. Wriggers. *Nichtlineare Finite-Element Methoden*. Springer-Verlag, 2001.

[149] H.T.Y. Yang, S. Saigal, A. Masu, and R.K. Kapania. A survey of recent shell finite elements. *International Journal for Numerical Methods in Engineering*, 47:101–127, 2000.

[150] Z. Yosibash and R.M. Kirby. Dynamic response of various von-Kármán non-linear plate models and their 3-D counterparts. *International Journal of Solids and Structures*, 42:2517–2531, 2004.

[151] L. Zeng, N.-E. Wiberg, X. Li, and Y. Xie. A-posteriori local error estimation and adaptive time-stepping for Newmark integration in dynamic analysis. *Earthquake Engineering & Structural Dynamics*, 21:555–571, 1992.

[152] O.C. Zienkiewicz and R.L. Taylor. *The Finite Element Method – Solid Mechanics*, volume 2. Butterworth-Heinemann, 5th edition, 2000.

[153] O.C. Zienkiewicz and Y. Xie. A simple error estimator and adaptive time stepping procedure for dynamic analysis. *Earthquake Engineering & Structural Dynamics*, 20:871–887, 1991.

[154] O.C. Zienkiewicz and J.Z. Zhu. A simple error estimator and adaptive procedure for practical engineering analysis. *International Journal for Numerical Methods in Engineering*, 24:337–357, 1987.

[155] O.C. Zienkiewicz and J.Z. Zhu. The superconvergent patch recovery and a posteriori error estimates. Part 1: The recovery technique. *International Journal for Numerical Methods in Engineering*, 33:1331–1364, 1992.

[156] O.C. Zienkiewicz and J.Z. Zhu. The superconvergent patch recovery and a posteriori error estimates. Part 2: Error estimates and adaptivity. *International Journal for Numerical Methods in Engineering*, 33:1365–1382, 1992.